Radio and Optical Field Effects on Electromagnetically Induced Transparency

A thesis presented by

David McGloin, MSci

to the University of St. Andrews in application for the degree of Doctor of Philosophy

J.F. Allen Physics Research Laboratories
Department of Physics and Astronomy
University of St. Andrews
North Haugh
St. Andrews
Fife
Scotland

October 2000

Declarations

I, David McGloin, hereby certify that this thesis, which is approximately 56,000 words in length, has been written by me, that it is the record of work carried out by me and that it has not been submitted in any previous application for a higher degree.

Date 20/10/00... Signature of candidate

I was admitted as a research student in October 1997 and as a candidate for the degree of PhD in October 1998; the higher study for which this is a record was carried out in the University of St. Andrews between 1997 and 2000.

Date 20/10/00... Signature of candidate

I hereby certify that the candidate has fulfilled the conditions of the Resolution and Regulations appropriate for the degree of PhD in the University of St. Andrews and that the candidate is qualified to submit this thesis in application for that degree.

Date 20/10/00 Signature of supervisor

In submitting this thesis to the University of St. Andrews I understand that I am giving permission for it to be made available for use in accordance with the regulations of the University Library for the time being in force, subject to any copyright vested in the work not being affected thereby. I also understand that the title and abstract will be published, and that a copy of the work may be made and supplied to any bona fide library or research worker.

Date 20/10/00... Signature of candidate

Abstract

Methods by which electromagnetically induced transparency (EIT) can be modified are investigated both experimentally and theoretically.

Specifically it is shown, theoretically, that EIT is best achieved in Doppler broadened systems in the so-called V-scheme configuration in cases where the probe field wavelength is less than that of the coupling field wavelength. This, so-called, up-conversion regime is of importance if short-wavelength inversionless lasers are to be realised and we examine the viability of achieving inversionless gain on a blue line in atomic rubidium. It is found that the observation of inversionless gain should be possible under experimental conditions.

The role of laser linewidth in EIT is also explored. It is shown that EIT and amplification without inversion may still be observed even when the linewidth of either the probe or coupling laser is greater than the homogeneous linewidth of the probe transition. This has implications for the observation of EIT with truly incoherent light sources.

Further EIT is experimentally investigated in the situation where the polarisation of the optical fields involved is altered. We find that there is an optimum polarisation orientation for the observation of EIT.

EIT in multi-level systems is also considered. A general rule for such N-level cascade systems is found. Such systems are also considered when investigating the effect of rf fields on EIT. It is found that the coupling of a rf field into a hyperfine level of the upper coupling field transition level results in the partial destruction of EIT on line centre.

The replacement of an optical coupling field with a microwave field is also discussed. It is found that this is impractical in atomic systems but may be possible in molecules. A novel pump-enhanced optical parametric oscillator, which is single frequency, frequency stable and widely tuneable, is developed with the aim of providing a quantum optical mid-infrared probe source.

This Thesis is dedicated to:

My Grandfathers

William McGloin
(1915 – 1998)
who showed me what true dedication is

and

Patrick Halleran
(1920 – 1992)
who asked me questions,
sometimes even when he didn't know the answers.

Acknowledgements

I have to have your word that if you read the acknowledgements, you'll read the rest of this fine work. Deal?

Before I slip into a more impersonal '*thesis-speak*' let me use my own voice to thank and acknowledge the many people who have made this work possible.

Obviously, I must thank my supervisor, Malcolm Dunn, who has guided me through the PhD process with a steady hand, offered suggestions when required, had the insights I needed when they were just out of my reach and corrected my at times appalling grammar in just about everything I ever wrote while a PhD student.

My thanks too to those who joined me in the study of EIT, Drs (no less) James Boon and Litsa Zekou who both answered the many questions I had in my first year, Graham Turnbull who got me stuck into the experimental work and of course, David Fulton, the prodigal son, who showed up for three months and spurred me on to doing a large portion of the work in this thesis. I also have to thank the cw-OPO group: David Stothard, Alison Carleton, Costas Petridis and the unofficial EIT post-docs, Ian Lindsay and Tom Edwards for their varied help and advice over the years. It's all been much appreciated.

Others that have particularly helped and advised over the years are: Jim Park, Bill Sleat and Dr David Tunstall, who all helped with RF electronics; Dr. Duncan Robertson and Dr. Graham Smith who helped with microwave technology; Professor Geoffrey Duxbury, who advised on all the molecular stuff and all the workshop and office staff who aided and abetted in so many different ways.

Also owed my thanks are my mum and dad, who although they may never have understood what it is I've been doing these past three years, have still supported me and at various times lent me money, put me up (done my washing etc…) and put up with me. The same might be said for Pete and Sue Marshall, whose washing machine (and drier) I've availed myself of over the years. I wouldn't have been half as neat and tidy if it hadn't been for you! Sandy Wilkinson is also owed some debt of gratitude, for driving me to work for a summer, convincing me swimming was a good idea and then spoiling the good work by convincing me beer was a good idea too, it couldn't all be work after all…

My final and most heartfelt thanks are to Vicky Marshall, an inspiration if ever there was one. Her love and support over the years, through both the stresses and strains and the good times has been invaluable and has kept me on course. How can you fail to love someone who doesn't have to read your thesis but still does so (I'll still take the blame for the poor English, mind).

There are, of course, many reasons why I stayed the course and pursued a PhD, but if looking for some inspiration about the validity of Physics I always turn to my elders and betters. That old icon (and iconoclast) Richard Feynman almost inevitably popped up. The one story that sticks in memory is aspirational if nothing else.

"A physicist studying quantum field theory with Murray Gell-Mann at CalTech in the 1950s, before standard textbooks on the subject had become available, discovers unpublished lecture notes by Richard Feynman, circulating samizdat style. He asks Gell-Mann about them. Gell-Mann says no, Dick's methods are not the same as the methods used here. The student asks, well, what are Feynman's methods? Gell-Mann leans coyly against the blackboard and says, Dick's method is this. You write down the problem. You think very hard. (He shuts his eyes and presses his knuckles periodically to his forehead). Then you write down the answer."

I wish I could do that. Maybe if I keep at it, one day I will.

Now read on…

Table of Contents

Pluchra sunt quae videntur
Pluchroria quare scientur
Longe pulcherrima quae ignorantur

Steno (1638-1686)

Beautiful are the things we see,
More beautiful are the things we understand,
Much the most beautiful those we do not comprehend.

Chapter 1

Introduction and Literature Review

1.1 The strange interactions of light and matter

Some of the phenomena displayed by light appear counter-intuitive. Ever since Max Planck introduced the word 'quantum' into the physicists lexicon, new, almost bizarre demonstrations of how light interacts with matter are reported in the literature week after week. In recent years the cooling and trapping of atoms with lasers has had perhaps the greatest impact on atomic physics of any contemporary development. The idea that a laser, a device traditionally associated with ray guns and burning and heating things, can actually *cool* seems to go against common sense. Yet quantum mechanics says that ray guns can cool to temperatures only a little above absolute zero.

Another of the strange interactions of light and matter is the topic of this thesis: Electromagnetically Induced Transparency (EIT). EIT theory says propagate one laser beam through a medium and it will get absorbed; propagate two laser beams through that same medium and neither will be absorbed. A quite literal trick of the light turns an opaque medium into a transparent one. The magic doesn't stop there though. EIT can be used to make media behave in quite unexpected ways, some of which will be investigated in this thesis. One of the main impetuses to work on EIT is another counter-intuitive phenomena called Lasing Without Inversion, a process by which laser action is achieved without the need for the condition, learned in every introductory laser class, of population inversion. In fact Lasing Without Inversion would seem to violate the second law of thermodynamics! Yet it can be achieved, although not without some difficulty.

All such phenomena, of course, are described by theories that describe how light and matter interact. In its simplest sense the processes we shall meet in the course of this work are caused by interference, analogous to that seen in water waves, or in Young's Slits. The difference is that here the interference occurs *within the atoms themselves*. As with experiments in which waves interfere, we will see that coherence plays a large role. We require the light going through a pair of slits to be coherent in order to see a well-defined interference. So too, within the atom, must the properties of coherence come into play, now not of the light wave but of the quantum wave. As such, we require coherent light sources, lasers, to carry out EIT experiments. It has been the development of lasers that has allowed the study of a multitude of light-matter interactions. Of particular interest here are the effects of illuminating atomic vapours with laser light. It is possible to induce optical transitions where the response of the atom retains a distinct phase relationship with the applied optical field. If the atoms are isolated (as in a vapour) then they can

retain this relationship for a length of time approaching the atomic decay time, meaning that coherent phenomena can be observed. EIT is one such process, a result of *quantum interference*.

1.2 Coherent Processes

1.2.1 Rabi Oscillations

Rabi Oscillations are a consequence of coherent excitation of an atom by a monochromatic (or near-monochromatic) light source, resonant with an atomic transition. The effect of constant radiation on a group of atoms, on a time scale much less than the natural lifetime of the excited state, can be seen in figure 1.1. The interesting point to note is that the population all ends up in state 2. This is different from a rate equation approach where the atomic medium would become saturated (half the population could be pumped into the upper level but no more). Instead the population continues to be pumped into level 2. Stimulated emission will then begin to take over and the population will be pumped out of level 2 and back into level 1. This cycle of excitation and de-excitation will repeat, so long as the applied field remains constant. Closer examination of the way in which the populations change show that they oscillate sinusoidally with a constant frequency. This frequency is called the *Rabi frequency.* The Rabi frequency is derived using a quantum mechanical treatment of the atom, based on the probability of a transition taking place at a given time [1-3], rather than the more phenomenological approach used in Einstein's rate equations.

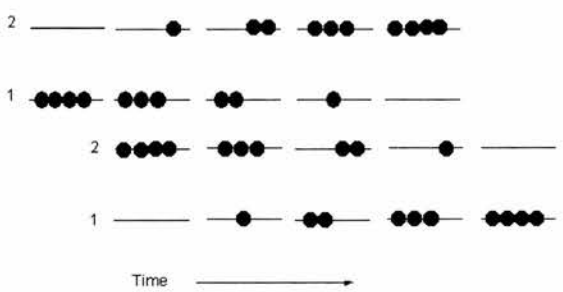

Figure 1.1. *Evolution of the two-level atom with continuous sinusoidal radiation incident upon it – The Rabi atom. Population moves from one level to another until all atoms are in the excited state and then back again. With passing time this pattern repeats sinusoidally.*

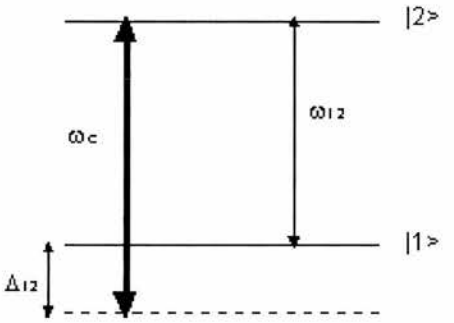

Figure 1.2. *The two-level atom. ω_c is the coupling field (exciting field), ω_{12} is the transition frequency and Δ_{12} denotes the detuning from the transition line centre.*

If we examine a two level atom as shown in figure 1.2 then the Rabi frequency may be expressed as Ω_R:

$$\Omega_R = \sqrt{\Delta_{12}^2 + \left(\frac{\mu_{12}E}{\hbar}\right)^2} \tag{1.1}$$

where Δ_{12} is the detuning (difference between the laser frequency and the transition frequency), μ_{12} is the dipole element for the transition and E is the field strength of the laser. It should be

noted that the Rabi frequency as written is an angular frequency and that as the detuning is increased away from resonance the Rabi frequency will increase and as such the period of Rabi oscillations will decrease. Thus a field far detuned from resonance will have no effect on the atom as we would expect. The Rabi frequency has a ubiquitous presence in quantum optics. Shore [2] outlines a few of its uses: a measure of interaction strength (the role in which it is employed in this thesis), a frequency of population oscillations, a nutation frequency and an optical Larmor frequency among others.

1.2.2 Autler-Townes Effect

In 1955 Autler and Townes demonstrated the ac equivalent of the dc-Stark effect [4]. Using a rf field they split an absorption line in OCS (carbonyl sulphide) into a doublet (figure 1.3a). In order to observe this splitting they probed the rf transition with a microwave frequency field, and observed how the rf field affected the probe. The result is a characteristic doublet absorption trace (figure 1.3b).

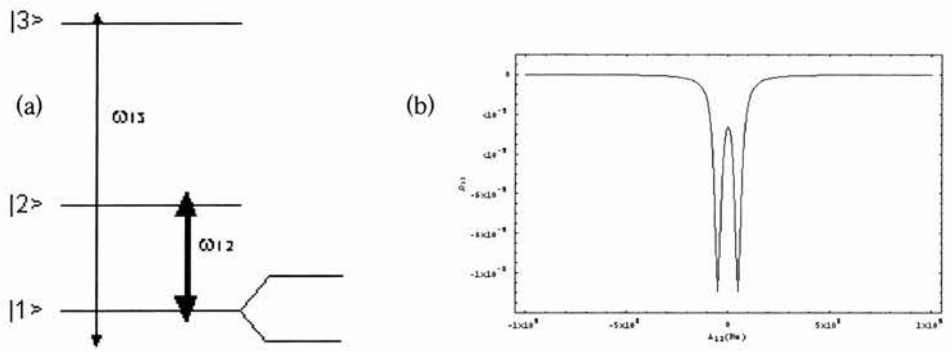

Figure 1.3. *(a) The Autler-Townes experimental set-up is shown. The lower level, |1>, is split by the strong coupling field, ω_{12}. The absorption profile, with the characteristic doublet, of the probe field as it is scanned across level |1> is shown in (b).*

The splitting (also called ac-Stark splitting or dynamic Stark splitting) of the level that occurs is directly related to Rabi frequency. Indeed in a non-Doppler broadened system with the probe field exactly on resonance with the atomic transition the splitting induced by the field equals the Rabi frequency as given by equation (1.1) with $\Delta_{12}=0$. The splitting in this case is symmetric about the resonance point. In cases where the applied field is off-resonance with the transition the splitting will be asymmetric (figure. 1.4).

The importance of Autler-Townes splitting to EIT experiments is that EIT will enhance the depth of the hole that is produced by the Autler-Townes splitting. Quantum interference occurs between the Autler-Townes components and deepens the hole. The two effects work in tandem to make the medium transparent. The ingredient that separates EIT from Autler-Townes splitting is the level of dephasing that the system suffers from. If the dephasing on the unlinked transition (e.g. |2> - |3> in figure 1.3(a) above) is not small enough then Autler-Townes splitting is the effect that is observed and not EIT.

Work on Autler-Townes splitting continues to this day [5-8] with more emphasis on work in the optical regime, which in some cases may be mistaken for EIT. It also has import for work on double resonance spectroscopy [8, 9].

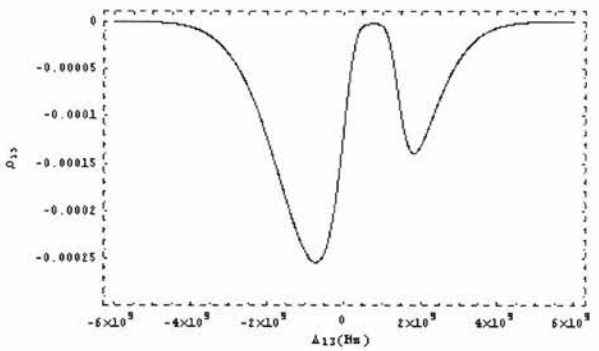

Figure 1.4. *The Rabi splitting is seen to be asymmetric about line centre when the coupling field is not resonant with a transition.*

1.2.3 Fano Interference

The foundations of EIT were laid in an experiment carried out in 1961 by U. Fano [10], which was the first coherence interference experiment. Fano's findings are outlined in figure 1.5.

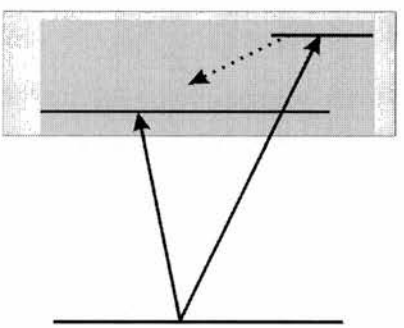

Figure 1.5. *Fano Interference: Two excitation paths to the same ionising state within a continuum leads to a cancellation in absorption as the two paths destructively interfere.*

Excitation takes place between some lower state and a continuum ionising state. It also takes place between the lower state and an autoionised state. Once in the autoionising state the atom relaxes to the ionising state. Hence there are two routes to the final state. Fano found coherent interference between these two routes led to asymmetric peaks in the excitation spectra. Furthermore he found that the 'transition probability vanishes on one side of the resonance'. Coherent interference had turned off the absorption in the medium.

1.2.4 Coherent Population Trapping

The ability to turn off the absorption can also be used to trap population in a particular level, after all if no population is moving from one level to another when under normal circumstances it should, then it can be thought of as being trapped. The extension of Fano's findings to this end led to the idea of coherent population trapping (CPT) [11-13]. This was predicted by Gaspar Orriols and Ennio Arimondo at the University of Pisa in 1976 [14], based on experiments Orriols

and co-workers had done [15], where the elimination of fluorescence from an illuminated sodium cell was observed. They found that using a multimode laser the fluorescence disappeared when the mode spacing was made equal the hyperfine spacing of the excited transitions (figure 1.6 gives a schematic of the atomic system they used). The fluorescence was absent due to the fact that the population had been trapped in a lower lying state, unable to move into the upper state.

Coherent population trapping is commonly carried out in the so-called lambda scheme (see Chapter 2) shown in figure 1.6. The initial atomic state can be thought of as a superposition of the lower two ground states. It is then possible to arrange the fields applied to the system so that the probability amplitude for being in the upper state is zero and hence the population remains trapped in the lower two states. This is due to the destructive interference between the two routes allowed to get to the upper state, e.g. |1>-|3> and |2>-|3>.

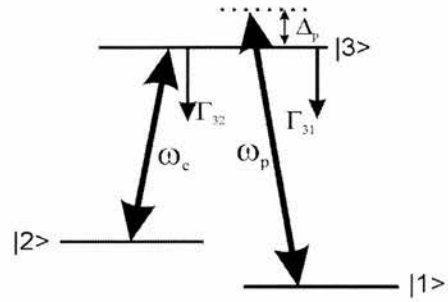

Figure 1.6: *Level Scheme for coherent population trapping (the Lambda Scheme). Typically levels |1> and |2> are hyperfine levels in the same ground state and as such are both populated. Also it is typical that both the applied fields are of similar strength.*

Hence CPT can be explained by considering two of the eigenstates of the Hamiltonian of the atom-field system. These are coherent superpositions of the lower two levels:

$$|coupled\rangle = \frac{\Omega_1}{\Omega_x}|1\rangle + \frac{\Omega_2}{\Omega_x}|2\rangle \tag{1.2}$$

$$|uncoupled\rangle = \frac{\Omega_2}{\Omega_x}|1\rangle - \frac{\Omega_1}{\Omega_x}|2\rangle \tag{1.3}$$

where $\Omega_x = \sqrt{\Omega_1^2 + \Omega_2^2}$. No component of the upper level |3> appears in these equations. One of these happens to be coupled to the upper state through the electric dipole interaction (|*coupled*>) and the other remains uncoupled (a 'dark' state). When the fields strengths (Rabi frequencies) of the coupling fields are set in the appropriate ratios the negative sign that appears in equation (1.3) will result in the dipole moment from the |uncoupled> state to the upper state |3> disappearing (<uncoupled|μ|3>=0). This is CPT and it is this effect which underpins EIT.

CPT was experimentally demonstrated by Orriols' Pisa group [11] and by Carlos Stroud's Group at the University of Rochester, New York [13]. In fact the phenomena as witnessed by the

Rochester group was seen as an adverse effect. They were trying to maximise the population extracted from the ground state. Unfortunately neither group actually examined what happened to light passing through the cell, instead looking either at florescence or populations. This was despite the fact that both groups had predicted that the absorption would be turned off. If they *had* checked then the first observation of EIT would have been made in the 1970's.

1.2.5 Physics of Electromagnetically Induced Transparency

The Coherent Population Trapping Analogy: EIT is essentially a 'subset' of the coherent population trapping phenomenon, the two-effects being very closely related [12]. In CPT the two fields interacting with the atom are close to the same strength and as such the interference effects arise from both fields. In EIT one of the fields is much weaker than the other i.e. $\Omega_1 << \Omega_2$. Thus EIT is due to only to interference effects driven by the stronger of the two fields, the so-called *coupling* field. The weaker field is termed the *probe* field. Using the same lambda scheme for EIT that we used for our CPT explanation we see that the idea is essentially the same. The difference is perhaps in the details. CPT, in general, has the levels |1> and |2> as either Zeeman or hyperfine levels within the ground state of the atom. In EIT these levels are usually discrete electronic states. Thus, in general, one of the levels in EIT will have no population at any time during the process.

Interference between dressed states: A dressed state analysis also leads to the correct EIT result. Here the atom field interaction is considered as a whole so that the Hamiltonian for the system is made up of components including both the bare state atom and the atom field interaction. A dressed state is defined as, 'an eigenstate of the time-independent form of the total Hamiltonian, including interactions' [16]. If we examine the CPT scheme in figure (1.6) then a dressed state analysis leads to the upper two states forming a coherent superposition of states. It is interference between the probe absorption amplitudes to these two states that results in EIT - see figure 1.7. The CPT analogy and the dressed state explanation for EIT can be related to each other, see for example [17].

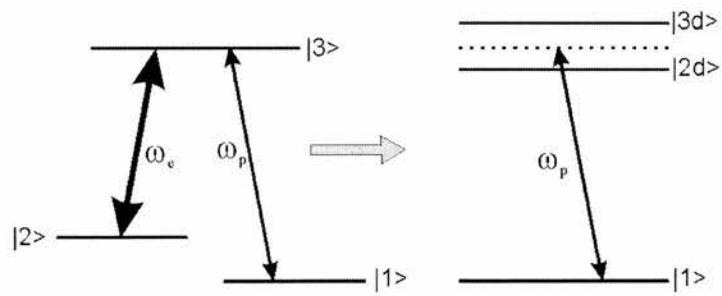

Figure 1.7: *Lambda scheme in dressed basis. The two dressed states are labelled |3d> and |2d>. It is destructive interference between the probe absorption amplitudes that leads to EIT.*

Multiple routes to excitation: Descriptively the simplest explanation, the multiple routes to excitation model of EIT is analogous to the Young's Slits model for interference of light. Here we describe EIT as an interference between two routes to excitation of the upper probe level (e.g level |3> in figure 1.6). The probe can excite population by the |1>-|3> route. An alternative pathway within the atom for population to reach |3> is |1>-|3>-|2>-|3> in which the population is moved between |2> and |3> by the coupling field. We can then think of the two routes to excitation interfering to cancel the original absorption |1>-|3>. Such multi-pathway interferences can also be examined using density matrix perturbation chains, which may also allow additional insight [18].

Other explanations: Other alternatives for explaining the EIT process have been proposed such as the use of Feynman diagrams to represent the interfering processes [19], use of a 3D vector model [20] or methods involving stochastic wavefunction diagrams [21].

1.3 Electromagnetically Induced Transparency

The foundations of EIT were laid by Kocharovskaya and Khanin [22] in 1988 and independently by Steven Harris of Stanford University in 1989 [23]. It is generally the Harris paper that is referenced as the beginning of the EIT literature (mainly because Harris' paper was published in the American *Physical Review Letters* and not the more obscure Russian journal *JETP Letters* that the Kocharovskaya paper appeared in). Both papers addressed a concept known as Lasing Without Inversion (See section 1.4.1). This is a process in which a laser can be made to operate without the usual necessary population inversion by means of atomic coherence. This work was quickly followed by a paper on a similar concept by Marlan Scully of Texas A&M University [24]. EIT was first referred to by name by Harris in a 1990 paper in which another effect based on EIT was proposed, namely the enhancement of nonlinear processes (see section 1.4.2) [25]. The first demonstration of EIT followed in 1991 again by the Harris group [26]. This experiment was carried out in a Lambda scheme in strontium vapour using pulsed lasers, as shown in figure 1.8.

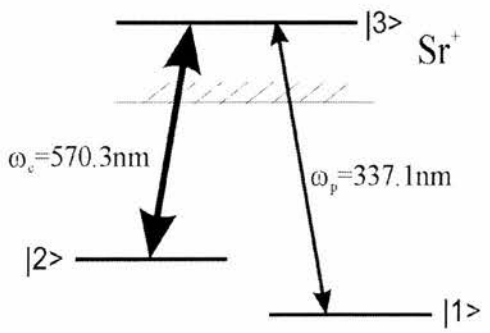

Figure 1.8: *First EIT level set-up in strontium. The coupling field wavelength is 570nm and the probe at 337.1nm.*

The authors were able to able to show that the transmittance of the probe field, which couples between a lower lying state and an autoionising state, could be increased from exp(-20) without

the coupling field to exp(-1) with a coupling field present. They point out the importance of the quantum interference in this increase, if there were no interference process present then the transmittance would only have increased to exp(-7). Another important point to realise is that what is observed is in fact interference and not some sort of hole-burning or saturation effect. One could for instance imagine that if all the population were in some way removed from the lower probe level then obviously there would be a reduction in absorption. But this is *not* what happens as the probe field is kept sufficiently weak so as not to cause significant population movement. This experiment carried out in strontium was followed by a demonstration in a cascade scheme in lead vapour [27]. The work in lead has been expanded by Kasapi [28] as a technique for enhanced isotope discrimination. This works by using EIT to make one isotope of lead transparent to a probe field while another remains opaque. Kasapi showed that 0.03% of Pb-207 could be clearly seen against a background of Pb-208.

Subsequent work by Harris' group examined the dispersive properties of EIT [29]. They showed that since the absorption of the medium is modified the refractive index must be as well. They found that at the point where the absorption is swept through a zero the refractive index varies rapidly with probe frequency (i.e. dispersion) and that this implies a significantly reduced group velocity near the zero probe detuning position. This work laid ground for subsequent ideas about slow light (section 1.4.3.3). In their experiment Harris' group demonstrated a reduced group velocity due to EIT of c/250 but they did not measure the dispersion directly. This experiment was carried out by the Xiao group [30] who measured the dispersion of the medium using a Mach-Zehnder interferometer technique [31]. They observed reduced group velocities of c/13.2.

Other experimental work on EIT includes further work by the Min Xiao group from Arkansas. They have studied continuous-wave EIT in rubidium vapour in work that has close connections with that done at St. Andrews in the past. They have examined the use of EIT as a spectroscopic tool [32] in which an EIT resonance is seen on each of the hyperfine levels that make up the upper coupling field state. This has also been explored by Moseley *et al* in which the technique is compared with two-photon spectroscopy [33]. Further studies have included general investigations of EIT in cascade schemes [34-36] and lambda schemes [37]. The change in EIT as the coupling laser linewidth increases has also been explored [38]. The authors found that as the linewidth of the interacting laser increased the EIT effect degraded due to an increase in the dephasing of the system. This experiment was followed by another looking at the effect of linewidth on the probe field [39]. In this case it was found that only the components of the probe field that were resonant with the probe transition were able to pass through the medium. Off-resonant components were absorbed. More recently this group have looked at building an 'electromagnetically induced grating' [40]. This works by having a strong coupling standing wave, interacting with three-level Lambda-type (or cascade-type) atoms. This can diffract a weak probe field (propagating along a direction normal to the standing wave) into high-order diffractions. By taking advantage of the absorption and dispersion properties of

electromagnetically induced transparency the authors have demonstrated an atomic grating that can fan effectively diffracted light into the first-order direction.. They have also considered EIT and AWI effects in four level N-type medium in Doppler broadened media [41], ideas that are in some part related to the work presented here in chapters 6 and 7.

Work carried out in the St. Andrews group has covered similar ground to that of the Xiao group both independently and at similar times. As has already been mentioned Moseley *et al* [33] investigated uses of EIT for spectroscopy. In the same paper they also clearly showed the nature of the one and two-photon interference effect in EIT. Fulton *et al* [42] showed that EIT is affected by the Zeeman structure of atoms and that EIT resonances can be manipulated once the normal Zeeman level degeneracy is lifted. Further studies of effects due to Zeeman levels in the context of inversionless gain have been carried out by Durrant *et al* [43]. Fulton *et al* [44] also conducted a definitive study of EIT in (cascade, lambda and Vee) three level schemes, showing the roles of, for example, optical pumping in the EIT process. Later work includes investigations into the ability to mismatch the wavelengths of the probe and coupling fields in Doppler broadened EIT both in the case where the probe field wavelength is longer than that of the coupling field [45] and where the probe field has a shorter wavelength than the coupling field (the so-called up-conversion regime) [46], a theme which is further explored in chapter 3. Some of the most impressive work carried out in the St. Andrews group was the discovery of the Electromagnetically Induced Focussing effect [47, 48], in which the spatial variation of the coupling field results in the probe field seeing the coupling field as a lens. This is discussed further in section 1.4.3.2.

Other work has proposed using EIT as a method of eliminating band gaps in resonant optical materials [49]; producing a three-level medium whose quantum mechanical state is a function of position [50]; enhancement of third harmonic generation [51]; generation of a wide spectrum of Raman sidebands while improving propagation through a inhomogeneous medium [52] and the related phenomena of subfemtosecond pulse generation by strong coherences in molecules [53]. EIT can also be used to eliminate self-focussing within an atomic sample [54]; has the potential to utilise optical fields to coherently control Mössbauer spectra [55] and possibly in the measurement of atomic parity nonconversion [56]. Proposals have been made to narrow laser linewidths and improve properties of optical resonators and laser devices by using EIT within the cavities (intracavity EIT) [57]. Along with normal gaseous media EIT has been investigated in RF discharges [58], cold atoms [59, 60] and atomic beams [61].

As can be seen numerous studies have been carried out into EIT, both the process involved and applications of the phenomena. The references given here are to be seen as an introduction to the subject. For an alternative review of the subject area, which deals much more with, for instance pulsed phenomena in EIT, see Jon Marangos' review [17]. The following sections introduce some of the more important areas that result from EIT, including EIT in solids, which is now of

increasing interest, Lasing Without Inversion, enhancement of nonlinear processes, refractive index effects (including slow light) and electromagnetically induced absorption [62].

1.3.1 EIT in solid media

The majority of EIT experiments are carried out in gaseous media, rubidium [44], caesium [63], hydrogen [64] and the like. For many applications, however, the ability to carry out EIT in solid materials would be beneficial (see for example section 1.4.3.3 on slow light) particularly if we wished to take EIT 'into the field'. However in considering solid materials we run into problems. The question can be put as follows: Can EIT be used to realise X-ray vision? The answer is no. The major problem lies in the very broad linewidth transitions and/or the large dephasing rates that occur in solids. In EIT we require a coupling laser field strength rivalling the probe transition linewidth. For this to occur in solids we would require laser strengths that would burn a hole through the material. Not *quite* what we mean by X-ray vision! Some of these problems can be circumvented by cooling the sample down near to absolute zero. This has resulted in the observation of EIT in several solid materials. The first demonstration was carried out in ruby [65] by Zhao *et al* and is also notable for the fact that the coupling field in this experiment was a microwave field rather than an optical field, but this particular experiment has been somewhat disputed. Other similar experiments have been carried out by Ichimura *et al* [66] and by Ham *et al* [67]in Pr^{3+}:Y_2SiO_5. This second group, who are at MIT, have carried out a number of experiments investigating enhancement of four-wave mixing in solids due to EIT [67], the possibility of optical data storage using EIT in solids [68, 69], gain induced by rf fields [70] and line-narrowing effects useful for spectroscopy [71].

Other interesting work on EIT in solids has been carried out by a group at the Australian National University in which they explore EIT effects in a nitrogen-defect centre in diamond. Recently they have shown the dynamic Stark splitting of an EIT resonance [72, 73], in which they split the EIT window into two or more separate lines, a effect similar to that explored in chapters 6 and 7. These effects are slightly different from other EIT experiments in that they are carried out at ESR frequencies rather than at optical frequencies and so further circumvent some of the problems associated with EIT in solid media. As such they have great potential in investigating proof of principle type experiments.

We note that in theory many ion doped crystalline solids may be suitable for EIT. Whether or not they offer any particular advantage over each other is debatable. You always lose out on the dephasing. However some people remain optimistic. A group of Japanese researchers from Toshiba (US Patent 6028873) have recently patented the idea of an inversionless laser (see section 1.4.1) (which uses EIT to work) with a solid medium as the gain material. They list well over 100 possible candidates for the gain medium which makes the patent cover a multitude of potential devices. Somebody is obviously hopeful that one day EIT in solids will become such a practicality that devices will be able to be based upon the idea.

1.3.1.1 EIT in semiconductors

Semiconductor devices may hold the key to applied inversionless laser devices. Since they can be engineered to specific designs there are fewer constraints on semiconductors than in other media. They also have the potential to be used as sensitive detectors in spectral regions where detection is difficult and also to improve existing properties of current semiconductor devices. Various groups have considered EIT-type effects in semiconductors including the Imamoglu group at the University of California, Santa Barbara. They have investigated Fano interference in double quantum well structures [74] similar to the one shown on the right-hand side of figure 1.9 (without the field α). Such schemes make use of quantum tunnelling to couple between the two wells. Schmidt and Imamoglu [75] have also considered using EIT to enhance nonlinearities in semiconductors, with potential in areas such as optical parametric generation or frequency generation. Schmidt and Ram have explored the possibility of creating an all-optical wavelength converter and switch based on EIT [76].

Other work includes that by Pötz [77] who looked at EIT type effects in double well structures where the probe field is controlled by a microwave field. Another recent proposal has been that of Yelin and Hemmer [78] in which EIT in a semiconductor can be used to detect far infrared radiation (around 10microns) by observing a shorter wavelength probe field. The process relies on a four-level system shown in figure 1.9.

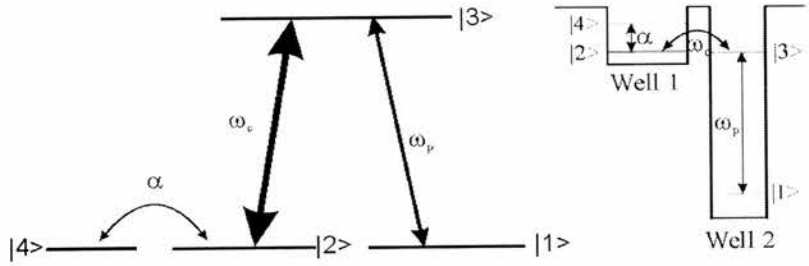

Figure 1.9: *EIT scheme for the detection of long wavelength radiation in a semiconductor. The EIT is set up via the the probe (ω_p) and coupling (ω_c) fields. It can then be destroyed via the application of a third field, α. This third field has a longer wavelength than that of the probe and hence a technologically 'easier' wavelength can be used to monitor the technologically 'hard' wavelength.*

Normal EIT is produced by the coupling field ω_c on the probe field ω_p. Then the EIT can be destroyed, producing a re-absorption of the probe, by the application of a third field α. We can engineer the quantum well structure so that ε lies in the visible region and α in the far infrared. Thus this provides a novel detection technique for the far infrared light. The destruction of EIT in multilevel EIT systems is examined in greater detail in chapter 6.

Other workers have predicted inversionless lasers based on EIT in semiconductors. These include Zhao *et al* [79, 80], who predict LWI effects in a system similar to that shown in figure 1.9

above, and Imamoglu and Ram [81] who predict LWI effects in the absence of a coupling field. They instead rely on the resonance between sub-bands in different quantum wells. This, they show, is identical to the original lambda scheme proposed by Imamoglu and Harris [82].

A more thorough review of experiment and theory of EIT due to quantum tunnelling in semiconductors can be found in [83].

A recent experiment by a group at Imperial College has demonstrated EIT in a quantum well structure for the first time [84]. The energy levels used are two close lying states in the same quantum well (i.e. no tunnelling process is required). The level structure is shown below in figure 1.10.

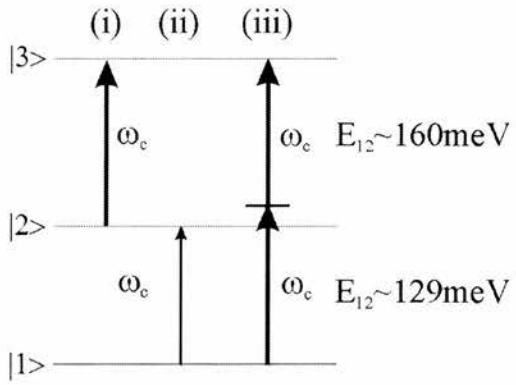

Figure 1.10: *Level structure for observation of EIT in a quantum well cascade scheme. The two transitions are closed spaced in energy allowing for three different coupling regimes: (i) EIT, (ii) Strongly driven two level atom and (iii) phase-locked coherence. The probe field resonant with the |1> -|2> transition is not shown.*

As can be seen the fact that the two transitions are quite closely spaced allows the coupling field to interact with the system in a variety of ways. The first is a normal EIT effect, shown in figure 1.10(i). The second effect is analogous to the strongly driven two-level atom and the third corresponds to an effect the described as 'phase-locked' EIT. This third condition corresponds to the case where the coupling field is two photon resonant with the |1> - |3> transition and was found to produce the biggest EIT effect.

1.4 Applications of EIT

1.4.1 The Inversionless Laser

The concept of an inversionless laser is an intriguing one. If we examine Einstein's rate equation approach of laser theory then it should be impossible to achieve laser action without a population inversion, as Siegman points out [85]:

> 'For laser action to occur, the pumping process must produce not only the excited atoms, but a condition of population inversion...It turns out we may obtain this *essential condition of population inversion* in many ways...'

So counter-intuitively it seems an immediate consequence of EIT that inversionless lasers should be possible. Einstein's rate equation forbids inversionless lasers. A medium will ultimately become saturated when half of the population is in the upper level of the laser transition (and half is in the lower state). Since the medium suffers from stimulated emission as well as stimulated absorption then the medium can never experience laser action without a population inversion, however if the stimulated absorption is turned off, or significantly decreased then it should be possible to have these strange upside down lasers. Such were the proposals by Kocharovskaya and Khanin [22], Harris [23] and Scully [24]. The idea can be examined in the following scheme [86]:

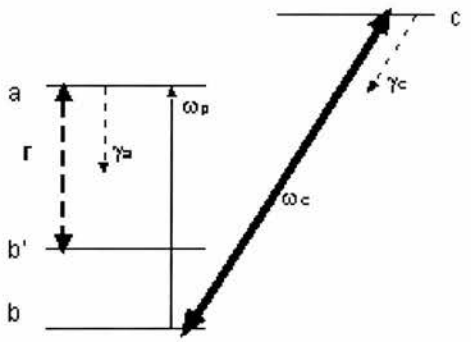

Figure 1.11: *Level scheme for observation of inversionless lasing. The incoherent pump, r, is applied between levels b' and a. Lasing is observed on the a to b transition. Level a is the $5P_{1/2}$ level, level c is the $5P_{3/2}$ level and b and b' correspond to the $5S_{1/2}$ (F=1) and $5S_{1/2}$ (F=2) levels respectively.*

The major difference between a straight EIT scheme and an LWI scheme is the introduction of the *pumping* term r. As with a normal laser, a pump is required to move population into the upper laser level. In the LWI case the pump is generally termed incoherent, as the linewidth is much larger than the linewidth of the atomic transition that it is pumping. It is desirable to use an incoherent pump, as use of a source that interacts coherently with the system under consideration will necessarily upset the coherences generated by the probe and coupling field. For instance Boon examined the possibility of coherently pumping a Vee-scheme [87] and found that an incoherent pump produced more gain.

For many laser wavelengths the effort that would go into building an inversionless laser would be counter productive. For instance there would no specific gain in building an inversionless 633nm laser over a normal He-Ne laser. The main area of interest in the inversionless laser is short-wavelength lasers. Since the Einstein A coefficient increases with frequency:

$$A = B\frac{\hbar\omega^3}{\pi^2 c^3} \tag{1.4}$$

so that the spontaneous emission on transitions with short wavelengths is very rapid this means that the atoms undergoing excitation on such a transition will rapidly decay to a lower state. Hence a population inversion is increasingly difficult to establish as the transition wavelength gets shorter. Inversionless lasers open up the possibility of circumventing this problem. Inversionless lasers themselves, however, have problems of their own, in a particular the difficulties involved in constructing them. So far no inversionless laser of technological importance has been demonstrated.

The first proof of principle inversionless laser was built by the Scully group. The same group had previously reported amplification without inversion in Rb [86] and extended their set-up to demonstrate laser oscillation. The experimental apparatus is shown in figure 1.12

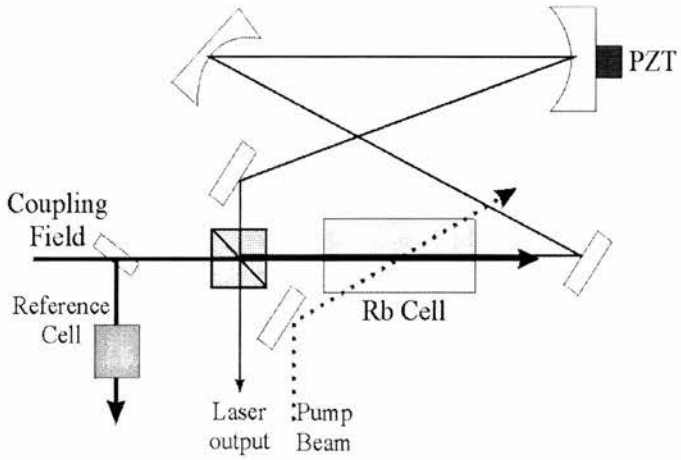

Figure 1.12: *Experimental set-up for observing inversionless lasing in Rb.*

The atomic system is shown in figure 1.11 above. The coupling field is supplied by a single-frequency diode laser resonant with the $5S_{1/2}$-$5P_{3/2}$ transition (the D_2 line). The laser transition is the $5S_{1/2} - 5P_{1/2}$ transition (the D_1 line). The incoherent pump source on the $5S_{1/2} - 5P_{3/2}$ transition is used both to destroy optical pumping due to the strong coupling field and also to act as a pump for the inversionless laser putting a small amount of population into the upper laser transition. A weak magnetic field is used to destroy coherence created by the pump field in the $5S_{1/2}$(F=2) Zeeman levels. When the coupling and pump field come onto resonance, inversionless laser oscillation is observed, the laser field having been built up from cavity noise. The fact that such a system is in fact displaying inversionless gain can be demonstrated by examining the system in the presence of a probe field resonant with the laser transition (the set-up for finding amplification without inversion). In the case where the probe field linewidth is increased so as to become incoherent, the amount of gain decreases significantly indicating that it is a coherent process (i.e inversionless gain) and not a population inversion that accounts for the gain that is

observed. The laser output was approximately 30μW at 794nm. Obviously this is not a practical system.

A number of other proof of principle experiments have been carried out, most notably by Peters and Lange [88], Padmabandu *et al* [89], Sellin *et al* [90] and Jong *et al* [91, 92]. Many others have observed amplification without inversion ([93-95] for example) although none with any significant *wavelength mismatch*. This idea of mismatching the lasing and coupling fields is important in the search for short wavelength inversionless lasers, as ideally we would like a technologically 'easy' laser as the coupling field controlling a short wavelength laser transition. One of the main problems with this idea is that as the wavelengths get further and further apart EIT is increasingly difficult to obtain (although not impossible). A good example of such an EIT experiment was carried out by Boon *et al* [46]. This idea of producing a short wavelength laser using a longer wavelength control field is called 'up-conversion' and is discussed in detail for Doppler broadened systems in [96, 97] and also in Chapter 3 of this thesis. A summary of LWI and AWI experiments is listed in table 1.1.

Type	Authors	Medium	Coupling (nm)	Probe (nm)	R
Pulsed AWI	Nottelmann *et al* [95]	Sm Vapour cell (Λ)	570.68	570.68	1
Pulsed AWI	Fry *et al* [98]	Na Vapour cell (Λ)	589.86	589.86	1
			558.43	558.43	1
Pulsed AWI	van der Veer *et al* [99]	Cd Vapour cell (Λ)	326	479	0.68
CW AWI	Kleinfeld and Streater [100, 101]	K Vapour cell (Vee)	766.5	769.9	1
CW AWI	Zhu *et al* [102, 103]	Rb Vapour cell (Λ)	780	780	1
CW AWI	Sellin *et al* [90]	Ba atomic beam (cascade)	554	821	0.67
CW AWI	Fort *et al* [63]	Cs Vapour cell (Vee)	852	894	0.95
CW AWI	Shiokawa *et al* [104]	Laser-cooled Rb (Λ)	780	780	1
CW AWI	Hollberg *et al* [105]	Laser cooled Rb (Vee)	780	795	0.98
CW LWI	Zibrov *et al* [86]	Rb Vapour cell (Vee)	780	795	0.98
CW LWI	Padmabandu *et al* [89]	Na atomic beam (Λ)	589.76	589.43	1
Pulsed LWI	de Jong *et al* [91]	Cd Vapour cell (Λ)	326	479	0.68
CW LBT	Peters and Lange [88]	Ne Vapour cell (double-Λ)	824.9	611.8	1.35

Table 1.1: *Summary of LWI and AWI experiments to date. CW is continous wave, AWI is amplification without inversion, LWI is lasing without inversion and LBT is lasing below threshold. The value of R is the probe field to coupling field frequency ratio. It is therefore a measure of up-conversion.(see LWI review* [106]*)*

Lasing Without Inversion is not just about short wavelength lasers however. Other aspects of interest include various quantum optical effects, such as the inhibition of spontaneous emission noise in inversionless lasers [107] and the production of squeezed laser light [108, 109]. More recently predictions for producing inversionless gamma ray radiation have been made [110-113].

Inversionless lasers offer tantalising possibilities. Compact short wavelength lasers would be a great boon technologically. But over 10 years after the prediction of such devices no substantial breakthrough has been made. The dearth of experimental work in the field shows, not that the idea is of no interest but that the work is very difficult to achieve despite the wealth of theory papers published ([87, 108, 114-131] for example). The defining experiment is out there just waiting to be performed, but many problems remain. For a more complete discussion of LWI, motivations, different theoretical approaches to the phenomena, experimental realisations and difficulties see the recent comprehensive review by Mompart and Corbalàn [106].

1.4.2 Enhancement of Nonlinear Processes

Many nonlinear processes suffer from re-absorption. That is, if a wave-mixing process results in a frequency being produced on a transition that is not coupled to one of the fields driving the process then any radiation at this frequency stands a chance of being re-absorbed by that transition. Since these types of processes generally produce only a small amount of radiation then the problems are obvious. The fact that EIT can provide transitions that do not re-absorb is therefore very attractive. Indeed this idea was one of the original proposals for EIT [25] in which a four-wave mixing process could be enhanced (i.e. the $\chi^{(3)}$ susceptibility is enhanced). A sample atomic scheme is shown in figure 1.13.

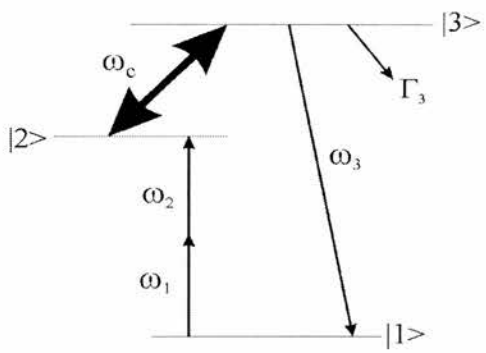

Figure 1.13: *Harris' wave-mixing scheme. The coupling field on the |2> - |3> transition induces transparency on the wave mixing transition |3> - |1> and hence reduces the absorption that the generated field would normally experience.*

The first experimental evidence for enhancement of nonlinearities was by Hakuta *et al* [132]. They demonstrated that a dc field could be used instead of an ac coupling field in certain cases. This first experiment was three wave mixing in hydrogen, which is normally forbidden. The same group then went on to demonstrate four-wave mixing schemes in hydrogen [64], producing light in the UV at 103nm, and also sum-frequency generation in a hydrogen discharge [133]. Work at St. Andrews has looked at similar schemes in sodium [134]. Sum-difference frequency mixing in krypton has been performed by the Marangos group at Imperial college [135-138]. Recent work in this area includes four-wave mixing enhancement in a crystal [71], which opens up possibilities of using EIT for applications such as optical data storage in solids.

Another intriguing application of EIT in the nonlinear regime is the possible development of a broad band optical parametric oscillator with a high efficiency [139]. Such a device has been proposed by Harris and Jain. Lukin *et al* [140] have studied enhancement of parametric processes in which pairs of Stokes and anti-Stokes fields can be generated from very small initial values, e.g. the vacuum field. These ideas have been extended to experimentally produce self-oscillating parametric processes [141] – a mirrorless parametric oscillator. Further studies have investigated the properties of such processes [142, 143]. The idea is that two counter-propagating beams, E_b and E_f, drive a double lambda scheme, shown in figure 1.14.

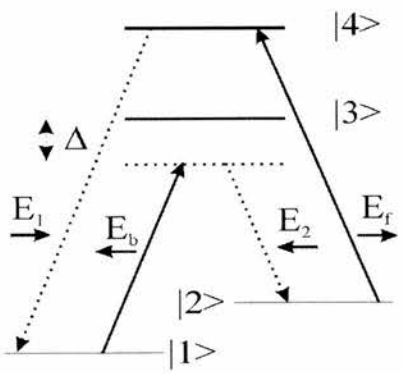

Figure 1.14: *Double lambda scheme used in the mirrorless parametric oscillator scheme. The arrows under the field descriptors (the 'E's) denote the direction of propagation of the fields.*

These fields in turn generate fields (E_1 and E_2) at the Stokes and anti-Stokes frequencies. For an appropriate density length of the medium for a given pump field intensity the system is found to display self-oscillation. Fleischhauer *et al* [142] calculate that such a set-up can be used to produce non-classical photon fields (the photon pairs created in this process are in quantum correlated states resulting in suppression of the intrinsic quantum fluctuations of the light [144]) with very narrow linewidths and low power requirements. This they suggest will be of interest in a number of areas of quantum optics and nonlinear optics.

The enhancement of nonlinear process is the one area of EIT where strong, potentially useful experiments have been carried out. Research in the area continues and it may prove to be that this area of research is the one that benefits the most from quantum interference effects.

1.4.3 Refractive Index Effects

Another topic of interest in quantum interference research is that of the modification of the refractive index properties of a medium. Since the absorption and refractive index of a substance are linked via the Kramers-Kronig relations we see that modification of the absorptive properties of a medium will result in a change in the refractive index properties as well. Examples of uses of this modification are high refractive index media with low absorption (phaseonium), electromagnetically induced focusing and slow light.

In a two level system if we examine the absorption of a probe scanned through the transition we find maximum absorption on line centre. Accompanying this absorption will be a refractive index profile that has a zero coinciding with the maximum absorption. We also see a dispersive element of the refraction (variation of refractive index with frequency) around the maximum absorption point. By moving to a transparent medium we can modify this as shown in figure 1.15. We see that in a transparent medium we have high dispersion (rapidly varying refractive index) and this is the basis for slow light phenomena (section 1.4.3.3) and proposed schemes for magnetometry [145, 146] and line narrowing and frequency stabilisation of lasers [57]. It also allows effects such as Electromagnetically Induced Focussing [47, 48] and optical waveguiding of a probe field [147, 148], discussed below in section 1.4.3.2.

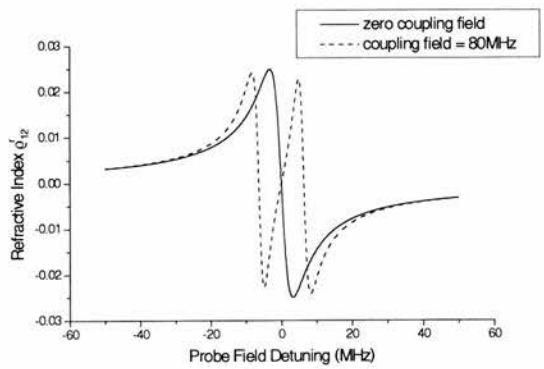

Figure 1.15: *Refractive index as a function of probe field detuning. In the two level case, i.e. no coupling field then we get the classic trace, shown by the solid line. In the case where a coupling field is applied the profile is modified as shown by the dashed line.*

Another refractive index effect due to EIT is that of EIT-induced birefringence. This was first demonstrated by Pavone *et al* [149]. This phenomena is briefly discussed in Chapter 7 when where examine the potential for using EIT-induced birefringence as a method of spectroscopy. Recent work by Patnaik and Agarwal [150] has also shown that birefringent effects in a coherently prepared medium can be used to control magneto-optical rotation.

1.4.3.1 Phaseonium

Phaseonium differs from the highly dispersive media found via EIT in that it is a medium which has a large refractive index with no accompanying probe absorption. It was proposed by Scully [151]. In order to create such a medium (which Scully has called a new state of matter) it is necessary to 'prepare' the medium in some way. This preparation may take the form of incoherent pumping akin to that found in inversionless lasing discussed above. Further theory of enhancement of the refractive index can be found in [152-156]. A proof of principle experiment to observe phaseonium was carried out in rubidium [157]. As expected a region was found in which the absorption vanished accompanied by a large refractive index.

One of the main proposed applications of phaseonium is the development of a high sensitivity magnetometer. If we place a phaseonium medium in the arm of a interferometer then a varying magnetic field will perturb the Zeeman levels of the atomic system. This will detune the probe field slightly and this detuning will alter the refractive index of the medium. This change should be detectable using the interferometer. It is estimated that a magnetometer based on coherently prepared atoms could be 2 orders of magnitude better than a state of the art SQUID magnetometer [158]. Further theory on phaseonium magnetometers can be found in [146] and on other magnetometers based on EIT effects in [159, 160]. Additional advantages in the use of such a magnetometer are that unlike other *optical* magnetometers it can work in the high density – strong field regime potentially allowing a greater signal to noise ratio, and also that it has a larger dynamic range than more conventional devices. Other applications include high-resolution microscopy [158]. The resolution of an optical microscope is given by $n \sin\theta/\lambda$ where n is the refractive index of the lens, θ is the optical collective angle and λ is the wavelength. If we can increase n then obviously the resolution could be increased. The experimental conditions in order to observe such enhancements are difficult to achieve however. A more recent experiment [161] has shown that power broadening of optical resonances can be significantly narrowed in coherently prepared, dense atomic media and that it is possible to observe sub-EIT linewidth effects in such media. Other work on the subject relevant to this thesis has been carried out by Lukin *et al* [162] in which phaseonium can be obtained using so-called *double-dark resonances* with less incoherent pumping than in the case discussed above. Double-dark resonances will be discussed in relation to EIT in multilevel cascade schemes in chapter 6.

1.4.3.2 Electromagnetically Induced Focussing

As we have seen EIT affects both the absorption and the refractive index of a medium. This implies that the stronger the EIT effect, the larger the change in refractive index. We can make use of this fact in normal EIT experiments to develop a new process called Electromagnetically Induced Focussing (EIF). Since laser beams have Gaussian intensity profiles a probe field that has its beam waist matched to the coupling field waist will experience stronger EIT at the centre of the beam than at the edge. The refractive index that the probe experiences will also, therefore, change with the radial intensity of the coupling field. Moseley *et al* showed [47, 48] that this effect implied that the probe field experiences the coupling field as a lens. This is illustrated in figure 1.16.

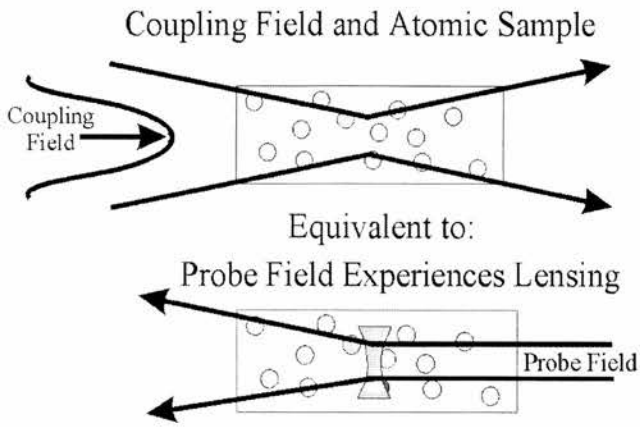

Figure 1.16: *Schematic of Electromagnetically Induced Focussing. The transverse spatial profile of the coupling field results in the probe field experiencing a varying refractive index across its transverse profile. This effect is eqivalent to that of having a lens in the path of the probe field.*

By varying the detuning of the probe field it is possible to have the system act as various types of lenses, e.g. convex or concave. The EIF effect occurs more strongly for tightly focussed beams, where the peak intensity of the coupling field is greater. Therefore when performing such experiments it is important to take into account the EIF effect. Truscott *et al* [163] have used this idea of EIF to produce a waveguide in atomic vapour. Using a Laguerre-Gaussian [164, 165] beam as the coupling field and a normal Gaussian probe field, the probe will experience a high refractive index when it is on line centre with its transition. If the coupling field is red detuned (a negative detuning) it can act so as to guide the probe out of the intense region of the coupling field. If the probe is blue detuned it can act in the opposite way. This results in the probe being waveguided along the Laguerre-Gaussian beam. In essence the refractive profile experienced by the probe is similar to the profile it would experience if it were in an optical fibre. This work has recently been more fully explained by Kapoor and Agarwal using a full density matrix treatment [148].

In this thesis we briefly examine how EIF effects occur in four-level media and how such phenomena lead to the idea of a rf controlled optical lens.

1.4.3.3 Slow Light

The most recent development in EIT research is the idea of 'slow' light. This concept was first demonstrated by the Hau group at the Rowland Institute [166]. EIT is carried out in a Lambda scheme in a sodium Bose-Einstein condensate. Due to the very low coupling field required to induce the transparency (the Doppler broadening in the condensate is almost negligible) the transparency peak is much smaller than the natural linewidth of the transition. The dispersion curve is therefore very steep and this results in light propagating at the probe frequency having a very low group velocity, v_g. This is given by:

$$v_g = \frac{c}{n(\omega_p) + \omega_p \frac{dn}{d\omega_p}} \approx \frac{hc\varepsilon_0}{2\omega_p} \frac{|\Omega_c|^2}{|\mu_{13}|^2 N} \tag{1.5}$$

where $n(\omega_p)$ is the refractive index at the probe frequency ω_p, $dn/d\omega_p$ is the change in refractive index with probe frequency (the dispersion) and N is the atomic density. We see immediately that the higher the dispersion (achieved by EIT) the lower the value for v_g. The Hau group reported group velocities as low as $17ms^{-1}$, hence the name 'slow light'. EIT had been used to slow light down before, with Harris [29] reporting light with speeds of c/250, but it was the huge amount by which the light was slowed that made the Hau experiment so notable.

Two further examples of slow light followed quickly after the first demonstration of the phenomena but this time in 'hot' media [167]. The Scully group performed their experiment in rubidium vapour at around 360K again using EIT in a Lambda configuration. By a careful choice of experimental parameters such as field strength and atomic density a group velocity of $90ms^{-1}$ was observed. It was noted that this was an average velocity as the coupling field is absorbed in the cell and the group velocity decreases with the coupling field power. They also note that the $90ms^{-1}$ is not a lower limit to the group velocity but by further modifications of experimental parameters they could bring the velocity down nearer $10ms^{-1}$. An interesting aside that the authors note is that the Doppler free configuration, where the probe and coupling field counter-propagate, that is necessary for observation of EIT effects in so many experiments (including some of those found in this thesis) is not necessary for the observation of low group velocities.

The second 'hot' gas demonstration of slow light was performed by Budker *et al* [168] again in rubidium. In this case the experiment investigated what happened to the polarisation of the light exiting the gas cell if the polarisation of the input light was changed. The authors show that the process is equivalent to EIT and thus that reduced light group velocity is related to nonlinear magneto-optical effects. Light within the cell suffers from a group delay and as such has a low group velocity, which can be controlled by varying the applied magnetic field. It was found to be of the order of $8ms^{-1}$ in this experiment. This is the lowest published group velocity of light at the time of writing.

Given slow light, what can we do with it? One interesting proposal is that of an optical black hole, an idea put forward by Leonhardt and Piwnicki [169]. The idea is that if light were to interact with a vortex of some sort, e.g. in a Bose-Einstein condensate, then if it were moving slowly enough it would be sucked into the vortex in the same way that matter is sucked into a black hole in space. Thus a black hole that could be built within a laboratory could be possible. This effect arises as light sees a moving dielectric medium as an effective gravitational field. It may be that the vortices recently achieved in Bose-Einstein condensates are too small to work effectively as optical black holes. In that case it may be possible to use Laguerre-Gaussian beams to create a vortex within a sample of hot gas or to carry out EIT within a rotating solid medium.

Many problems exist in all these approaches but a careful experiment in the right medium may well yield results. The analogues between optical black holes and real black holes would then allow black hole and gravitational phenomena, such as Hawking radiation [170], to be studied in the convenience of a laboratory instead of in space.

Leonhardt and Piwnicki have also proposed another possible application of slow light [171], that of a slow light gyroscope. They show that using an optical gyroscope with slow light will increase its sensitivity by anything up to 8 orders of magnitude. Again the problem of observing EIT in solid materials makes this idea that is difficult to realise practically.

Further proposals for uses of slow light include those by Harris [172] in which slow light can be used in ballistic type experiments with atoms and ways in which slow light can be used for nonlinear interactions at very low light levels [173]. Other suggestions include those [174] in which slow light can be used in quantum entanglement experiments and experiments involving other fundamental quantum processes [175].

Slow light remains the most exciting development in the EIT world at the moment. Just over ten years after the original idea was proposed the idea of slow light has given the whole subject area of coherent light matter interactions a boost – asserting that new concepts are there to be found and new uses waiting to be made of them. In another ten years, who's to say, we may have optical black holes sitting in laboratories all over the world in much the same way that Bose-Einstein condensates have become the physics de jour.

1.5 Electromagnetically Induced Absorption

A related effect to EIT is that of electromagnetically induced absorption (EIA) which was first noted by Bergman *et al* [176] in an experiment in NO (Nitrogen Oxide). However the phenomena has been most thoroughly investigated by a group from the Instituto de Physica in Montevidio, Uruguay [62, 177-179]. The effect can be observed in degenerate two level atoms and the Montevideo group has used rubidium in their experiments. The level structure investigated is shown in figure 1.17.

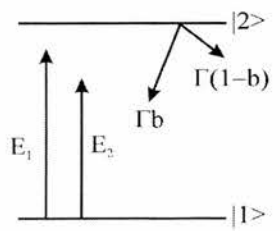

Figure 1.17: *Two level structure for observation of EIA. The two fields are a pump (coupling) and probe field. The parameter b is a branching ratio with b=1 corresponding to a closed transition. The value 1-b corresponds to the probability of level |2> decaying to a level other than |1>.*

Lezama *et al* have shown [62] that EIA can be observed in a degenerate two-level system provided that three conditions are satisfied: (i) That the F number of the ground state is one less that the F number of the excited state; (ii) the transition between the ground and excited state is closed and (iii) the ground state must be degenerate. They also show that the increase in absorption over that of a normal probe absorption trace can exceed 100%. Further, [179] the exact probe absorption spectrum that is observed is dependent on the field polarisations, the magnitude of any applied magnetic field (to lift the level degeneracy) and probe and pump field detunings.

In [177] Akulshin *et al* explain that analogous to the destructive interference effect found in EIT, it is a constructive interference effect that leads to EIA. In [62] Lezama *et al* expand this statement with a theoretical treatment that derives explicit density matrix equations for the degenerate two-level system. It is using this theory that allows the authors to produce the three conditions required for EIA. The underlying physical mechanism for EIA however remains unexplained. Results of a similar nature have also been present by Dancheva *et al* [180] although they too do not offer a explanation for the phenomena. A recent paper by Barreiro and co-workers [181], however, has proposed that the physical mechanism is the spontaneous transfer of light induced coherence from the excited state to the ground state. They show this by considering a four-level N-type system and generalise it to the experiment in [177]. They do not however show that their theory leads to the conditions for EIA outlined above. The assumption that EIA is a constructive interference effect in analogy to EIT remains sound, however.

The EIA effect can also be used to produce media with anomalous dispersion curves. Akulshin *et al* have shown [178] that negative dispersion can be observed which correspond to group velocities of –c/23000. They also noted that a negative dispersion can result in group velocities that are infinitely large (as can be seen by examination of equation 1.5). This they have recently reported [182] can lead to superluminal type effects [183, 184]. Such superluminal experiments have also been reported by Wang *et al* in a media using a Raman gain technique [185] to generate the anomalous dispersion. The possibility of achieving such effects via EIT will be briefly discussed in chapter 6.

1.6 'Old' work on LWI and EIT

Recently a number of papers have been published on the Los Alamos pre-print server regarding LWI and EIT. Many of these are reprints of old Russian articles published in the late 1960s and early 1970s. These papers, many authored by A.K. Popov, purport to predict many of the effects that were later 'discovered' by Western scientists, for example inversionless lasing. These papers along with the references they contain are a reminder that many of the ideas now studied have been looked at in a different light in the past but that it perhaps takes a fresh flash of insight, such as that shown by Harris [23] to ignite research into a discipline. These papers will now probably only be of historical interest as the EIT/LWI community is unlikely refer to them very much. But

they are given here as a nod towards completeness[1]. It is always interesting to note what research occurrs in Eastern Bloc countries that the West never gets to hear about.

1.7 Thesis Précis

The work in this thesis looks at a number of effects related to EIT. We begin, in chapter 2, with an overview of the theoretical models employed in the work found in subsequent chapters. Chapter 3 is primarily concerned with how mismatching the wavelengths of the probe and coupling fields affects both the EIT seen and the amount of inversionless gain that can be observed in the systems. Chapter 4 examines how moving beyond the standard model of EIT, in which we assume that all the laser fields are monochromatic, affects EIT and AWI in a V-scheme. Expressions for the observation of gain in such systems are derived.

The experimental work, in which the affect of changing the probe and coupling field polarisations is examined, begins in chapter 5. We find that EIT can be optimised by appropriately changing the relative polarisations. Chapter 6 looks at EIT in N-level schemes, in particular a four level cascade scheme. We introduce the idea of three photon EIT effects and also the possibility of controlling EIT by using a rf-field to couple two of the four levels as well as using the normal probe and coupling fields. This idea introduces the possibility of rf-controlled electromagnetically induced focussing. We also examine EIT in schemes with N levels and N-1 fields whereby 'higher order' EIT effects can be introduced, potentially by the application of rf fields. We see how EIT can be destroyed and recovered by moving to higher order level manifolds. Chapter 7 is an experimental treatment of some of the theory outlined in chapter 6.

In chapter 8 we examine the effect of not rf fields but microwave fields in EIT experiments, specifically the possibility of using a microwave coupling field. It is shown that microwave induced transparency although possible in atomic systems is exceptionally difficult and may be better achieved in molecular systems. Chapter 9 then details the development of an optical parametric oscillator (OPO) which could be used as the optical probe in a microwave induced transparency experiment. This OPO is also a novel device in its own right and we examine its properties and its potential.

The thesis concludes with chapter 10 and looks forward to work that may be carried out in the future.

The main thrust of this work has led to an examination of EIT in multi-level systems. This resulted from a study of how low frequency fields can be used to control optical fields in the context of EIT. Experimental work has been carried out that shows that rf fields can indeed manipulate optical fields via coherent processes. This work is, in context, rather timely. Now

[1] These papers can be found at the Los Alamos preprint server: http://xxx.lanl.gov/. The specific papers are qu-ph/0005042, qu-ph/0005049, qu-ph/0005060, qu-ph/0005081, qu-ph/0005089, qu-ph/0005094, qu-ph/0005108, qu-ph/0005114 and qu-ph/0005118.

seen emerging in the literature is work which also looks at such multilevel systems. Lukin *et al* [162] have examined processes by which system dynamics can be 'engineered' in multilevel systems, Burkett *et al* [41] have also recently performed experiments investigating optical field effects in multilevel systems as have Gao *et al* [186] in the context of two photon inhibition (something investigated in chapter 5 and 6). The work of Wei and Manson, investigating EIT effects in multilevel systems within ESR transitions [72, 73] is also of relevance to this work.

To summarise the work as a whole, the effect of modifying the fields involved in EIT processes is examined. Examples of these changes include mismatching the wavelengths of the probe and coupling fields, introducing non-monochromatic fields, changing field polarisations or by the use of non-optical fields in EIT. The aim of this thesis is to investigate the role that each of these processes has on EIT in a number of atomic configurations.

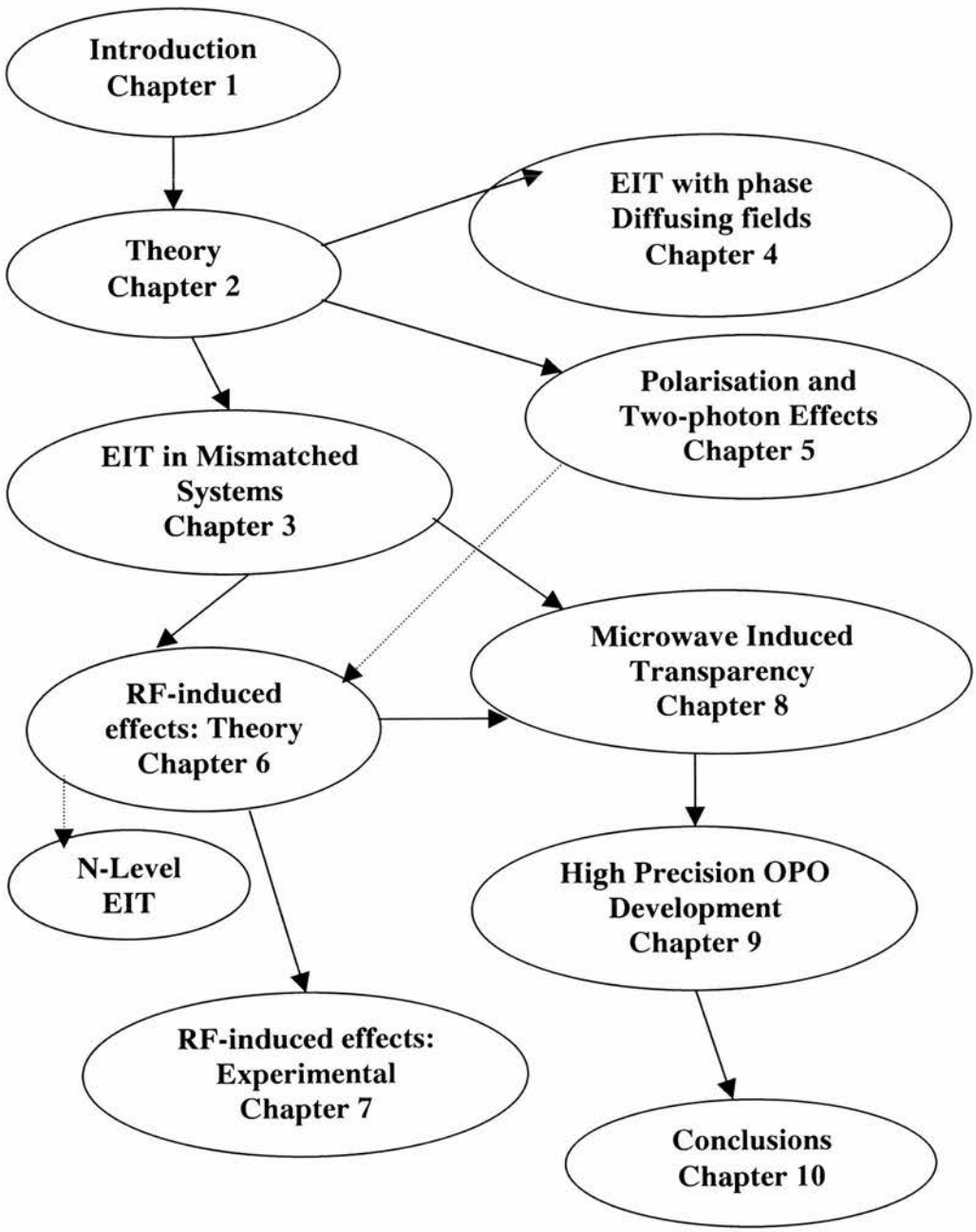

Figure 1.18: *Map outlining the structure of this thesis*

References

[1] **L. Allen and J. H. Eberly**, *Optical Resonance and Two Levels Atoms*. (Dover, New York, 1987).

[2] **B. W. Shore**, *The Theory of Coherent Atomic Excitation*. (Wiley, New York, 1990).

[3] **I. I. Rabi**, "Space Quantization in a Gyrating Magnetic Field," *Physical Review* **51**, 652 (1937).

[4] **S. H. Autler and C. H. Townes**, "Stark Effect in Rapidly Varying Fields," *Physical Review* **100**, 703 (1955).

[5] **K. Nittoh, Y. Yoshida, T. Watanabe and I. Yoguchi**, "Observation of dynamic Stark effect in Zeeman-split absorption lines and determination of dipole moment," *Journal of Physics B-Atomic Molecular and Optical Physics* **31**, 1813-1823 (1998).

[6] **C. J. Wei, D. Suter, A. S. M. Windsor and N. B. Manson**, "ac Stark effect in a doubly driven three-level atom," *Physical Review A* **58**, 2310-2318 (1998).

[7] **C. Delsart and J. C. Keller**, "Observation of the optical Autler-Townes splitting in neon gas with a cascade level scheme," *Journal of Physics B-Atomic Molecular and Optical Physics* **9**, 2769-2775 (1976).

[8] **P. S. Atherton, B. J. Dalton and I. R. Dagg**, "Autler-Townes doublets in the hyperine transitions of $^{14}NH_3$," *Journal of Physics B-Atomic Molecular and Optical Physics* **19**, 277-292 (1986).

[9] **K. Shimoda**, *Double-Resonance Spectroscopy of Molecules by means of Lasers*. in *Laser Spectroscopy of Atoms and Molecules* H. Walther, Eds. (Springer-Verlag, Berlin, 1976).

[10] **U. Fano**, "Effects of configuration interaction on intensities and phase shifts," *Physical Review* **124**, 1866-1878 (1961).

[11] **G. Alzetta, L. Moi and G. Orriols**, "Nonabsorption hyperfine resonances in a sodium vapour irradiated by a multimode dye-laser," *Il Nuovo Cimento* **52B**, 209-218 (1979).

[12] **E. Arimondo**, "Coherent population trapping in laser spectroscopy," *Progress in Optics* **35**, 257-354 (1996).

[13] **H. R. Gray, R. M. Whitley and C. R. Stroud**, "Coherent trapping of atomic populations," *Optics Letters* **3**, 218 (1978).

[14] **E. Arimondo and G. Orriols**, "Nonabsorbing Atomic Coherences by Coherent Two-Photon Transitions in a Three-Level Optical Pumping," *Lettere al Nuovo Cimento* **17**, 333-338 (1976).

[15] **G. Alzetla, L. Gozzini, L. Moi and G. Orriols**, "An Experimental Method for the Observation of R.F. Transitions and Laser Beat Resonances in Orientated Na Vapour.," *Il Nuovo Cimento* **36B**, 5-20 (1976).

[16] **S. M. Barnett and P. M. Radmore**, *Methods in Theoretical Quantum Optics*. (OUP, Oxford, 1997).

[17] **J. P. Marangos**, "Topical review electromagnetically induced transparency," *Journal of Modern Optics* **45**, 471-503 (1998).

[18] **R. R. Moseley**, *Sum Frequency Mixing and Quantum Interference in Three Level Atoms*, PhD thesis, University of St. Andrews (1994).

[19] **J. L. Cohen and P. R. Berman**, "Amplification without inversion: Understanding probability amplitudes, quantum interference, and Feynman rules in a strongly driven system," *Physical Review A* **55**, 3900-3917 (1997).

[20] **A. Kasapi**, "Three-dimensional vector model for a three-state system," *Journal of the Optical Society of America B-Optical Physics* **13**, 1347-1351 (1996).

[21] **J. A. Vaccaro, A. V. Durrant, D. Richards, S. A. Hopkins, H. X. Chen and K. E. Hill**, "Stochastic wavefunction diagrams for electromagnetically induced transparency, inversionless gain and shelving," *Journal of Modern Optics* **45**, 315-333 (1998).

[22] **O. A. Kocharovskaya and Y. I. Khanin**, "Coherent amplification of an ultrashort pulse in a 3-level medium without a population-inversion," *Jetp Letters* **48**, 630-634 (1988).

[23] **S. E. Harris**, "Lasers without inversion - interference of lifetime-broadened resonances," *Physical Review Letters* **62**, 1033-1036 (1989).

[24] **M. O. Scully, S. Y. Zhu and A. Gavrielides**, "Degenerate quantum-beat laser - lasing without inversion and inversion without lasing," *Physical Review Letters* **62**, 2813-2816 (1989).

[25] **S. E. Harris, J. E. Field and A. Imamoglu**, "Nonlinear optical processes using electromagnetically induced transparency," *Physical Review Letters* **64**, 1107-1110 (1990).

[26] **K. J. Boller, A. Imamoglu and S. E. Harris**, "Observation of electromagnetically induced transparency," *Physical Review Letters* **66**, 2593-2596 (1991).

[27] **J. E. Field, K. H. Hahn and S. E. Harris**, "Observation of electromagnetically induced transparency in collisionally broadened lead vapor," *Physical Review Letters* **67**, 3062-3065 (1991).

[28] **A. Kasapi**, "Enhanced isotope discrimination using electromagnetically induced transparency," *Physical Review Letters* **77**, 1035-1038 (1996).

[29] **S. E. Harris, J. E. Field and A. Kasapi**, "Dispersive properties of electromagnetically induced transparency," *Physical Review A* **46**, R29-R32 (1992).

[30] **M. Xiao, Y. Q. Li, S. Z. Jin and J. Geabanacloche**, "Measurement of dispersive properties of electromagnetically induced transparency in rubidium atoms," *Physical Review Letters* **74**, 666-669 (1995).

[31] **R. Schieder**, "Interferometric Nonlinear Spectroscopy," *Optics Communications* **26**, 113-116 (1978).

[32] **S. Z. Jin, Y. Q. Li and M. Xiao**, "Hyperfine spectroscopy of highly-excited atomic states based on atomic coherence," *Optics Communications* **119**, 90-96 (1995).

[33] **R. R. Moseley, S. Shepherd, D. J. Fulton, B. D. Sinclair and M. H. Dunn**, "2-photon effects in continuous-wave electromagnetically-induced transparency," *Optics Communications* **119**, 61-68 (1995).

[34] **Y. Q. Li, S. Z. Jin and M. Xiao**, "Observation of an electromagnetically induced change of absorption in multilevel rubidium atoms," *Physical Review A* **51**, R1754-R1757 (1995).

[35] **Y. Q. Li and M. Xiao**, "Observation of quantum interference between dressed states in an electromagnetically induced transparency," *Physical Review A* **51**, 4959-4962 (1995).

[36] **J. Geabanacloche, Y. Q. Li, S. Z. Jin and M. Xiao**, "Electromagnetically induced transparency in ladder-type inhomogeneously broadened media - theory and experiment," *Physical Review A* **51**, 576-584 (1995).

[37] **Y. Q. Li and M. Xiao**, "Electromagnetically induced transparency in a 3-level lambda-type system in rubidium atoms," *Physical Review A* **51**, R2703-R2706 (1995).

[38] **B. L. Lu, W. H. Burkett and M. Xiao**, "Electromagnetically induced transparency with variable coupling-laser linewidth," *Physical Review A* **56**, 976-979 (1997).

[39] **B. L. Lu, W. H. Burkett and M. Xiao**, "Frequency matching effect in electromagnetically induced transparency," *Optics Communications* **141**, 269-272 (1997).

[40] **H. Y. Ling, Y. Q. Li and M. Xiao**, "Electromagnetically induced grating: Homogeneously broadened medium," *Physical Review A* **57**, 1338-1344 (1998).

[41] **W. H. Burkett, Y. Q. Li and M. Xiao**, "Inhomogeneous broadening-dependent spectral features in a four-level atomic system," *Journal of the Optical Society of America B-Optical Physics* **17**, 293-299 (2000).

[42] **D. J. Fulton, R. R. Moseley, S. Shepherd, B. D. Sinclair and M. H. Dunn**, "Effects of zeeman splitting on electromagnetically-induced transparency," *Optics Communications* **116**, 231-239 (1995).

[43] **A. V. Durrant, H. X. Chen, S. A. Hopkins and J. A. Vaccaro**, "Zeeman-coherence-induced transparency and gain without inversion in laser-cooled rubidium," *Optics Communications* **151**, 136-146 (1998).

[44] **D. J. Fulton, S. Shepherd, R. R. Moseley, B. D. Sinclair and M. H. Dunn**, "Continuous-wave electromagnetically induced transparency - a comparison of v-system, lambda-system, and cascade systems," *Physical Review A* **52**, 2302-2311 (1995).

[45] **S. Shepherd, D. J. Fulton and M. H. Dunn**, "Wavelength dependence of coherently induced transparency in a Doppler-broadened cascade medium," *Physical Review A* **54**, 5394-5399 (1996).

[46] **J. R. Boon, E. Zekou, D. J. Fulton and M. H. Dunn**, "Experimental observation of a coherently induced transparency on a blue probe in a Doppler-broadened mismatched V-type system," *Physical Review A* **57**, 1323-1328 (1998).

[47] **R. R. Moseley, S. Shepherd, D. J. Fulton, B. D. Sinclair and M. H. Dunn**, "Spatial consequences of electromagnetically induced transparency - observation of electromagnetically induced focusing," *Physical Review Letters* **74**, 670-673 (1995).

[48] **R. R. Moseley, S. Shepherd, D. J. Fulton, B. D. Sinclair and M. H. Dunn**, "Electromagnetically-induced focusing," *Physical Review A* **53**, 408-415 (1996).

[49] **G. S. Agarwal and R. W. Boyd**, "Elimination of the band gap of a resonant optical material by electromagnetically induced transparency," *Physical Review A* **60**, R2681-R2684 (1999).

[50] **J. R. Csesznegi and R. Grobe**, "Recall and creation of spatial excitation distributions in dielectric media," *Physical Review Letters* **79**, 3162-3165 (1997).

[51] **S. J. Vanenk, J. A. Zhang and P. Lambropoulos**, "Pump-induced transparency and enhanced 3rd-harmonic generation near an autoionizing state," *Physical Review A* **50**, 3362-3365 (1994).

[52] **S. E. Harris and A. V. Sokolov**, "Broadband spectral generation with refractive index control," *Physical Review A* **55**, R4019-R4022 (1997).

[53] **S. E. Harris and A. V. Sokolov**, "Subfemtosecond pulse generation by molecular modulation," *Physical Review Letters* **81**, 2894-2897 (1998).

[54] **M. Jain, A. J. Merriam, A. Kasapi, G. Y. Yin and S. E. Harris**, "Elimination of optical self-focusing by population trapping," *Physical Review Letters* **75**, 4385-4388 (1995).

[55] **O. Kocharovskaya, R. Kolesov and Y. Rostovtsev**, "Coherent optical control of Mossbauer spectra," *Physical Review Letters* **82**, 3593-3596 (1999).

[56] **A. D. Cronin, R. B. Warrington, S. K. Lamoreaux and E. N. Fortson**, "Studies of electromagnetically induced transparency in thallium vapor and possible utility for measuring atomic parity nonconservation," *Physical Review Letters* **80**, 3719-3722 (1998).

[57] **M. D. Lukin, M. Fleischhauer, M. O. Scully and V. L. Velichansky**, "Intracavity electromagnetically induced transparency," *Optics Letters* **23**, 295-297 (1998).

[58] **F. S. Pavone, M. Artoni, G. Bianchini, P. Cancio, F. S. Cataliotti and M. Inguscio**, "Electromagnetically induced transparency in a RF discharge," *European Physical Journal D* **1**, 85-91 (1998).

[59] **S. A. Hopkins, E. Usadi, H. X. Chen and A. V. Durrant**, "Electromagnetically induced transparency of laser-cooled rubidium atoms in three-level Lambda-type systems," *Optics Communications* **138**, 185-192 (1997).

[60] **H. X. Chen, A. V. Durrant, J. P. Marangos and J. A. Vaccaro**, "Observation of transient electromagnetically induced transparency in a rubidium Lambda system," *Physical Review A* **58**, 1545-1548 (1998).

[61] **G. R. Welch, G. G. Padmabandu, E. S. Fry, M. D. Lukin, D. E. Nikonov, F. Sander, M. O. Scully, A. Weis and F. K. Tittel**, "Observation of V-type electromagnetically induced transparency in a sodium atomic beam," *Foundations of Physics* **28**, 621-638 (1998).

[62] **A. Lezama, S. Barreiro and A. M. Akulshin**, "Electromagnetically induced absorption," *Physical Review A* **59**, 4732-4735 (1999).

[63] **C. Fort, F. S. Cataliotti, T. W. Hansch, M. Inguscio and M. Prevedelli**, "Gain without inversion on the cesium D-1 line," *Optics Communications* **139**, 31-34 (1997).

[64] **R. I. Thompson, B. P. Stoicheff, G. Z. Zhang and K. Hakuta**, "Nonlinear generation of 103 nm radiation with electromagnetically-induced transparency in atomic-hydrogen," *Quantum Optics* **6**, 349-358 (1994).

[65] **Y. Zhao, C. K. Wu, B. S. Ham, M. K. Kim and E. Awad**, "Microwave induced transparency in ruby," *Physical Review Letters* **79**, 641-644 (1997).

[66] **K. Ichimura, K. Yamamoto and N. Gemma**, "Evidence for electromagnetically induced transparency in a solid medium," *Physical Review A* **58**, 4116-4120 (1998).

[67] **B. S. Ham, M. S. Shahriar and P. R. Hemmer**, "Enhanced nondegenerate four-wave mixing owing to electromagnetically induced transparency in a spectral hole-burning crystal," *Optics Letters* **22**, 1138-1140 (1997).

[68] **B. S. Ham, M. S. Shahriar, M. K. Kim and P. R. Hemmer**, "Frequency-selective time-domain optical data storage by electromagnetically induced transparency in a rare-earth-doped solid," *Optics Letters* **22**, 1849-1851 (1997).

[69] **B. S. Ham, S. M. Shahriar and P. R. Hemmer**, "Electromagnetically induced transparency over spectral hole-burning temperature in a rare-earth-doped solid," *Journal of the Optical Society of America B-Optical Physics* **16**, 801-804 (1999).

[70] **B. S. Ham, M. S. Shahriar and P. R. Hemmer**, "Radio-frequency-induced optical gain in Pr3+:Y2SiO5," *Journal of the Optical Society of America B-Optical Physics* **15**, 1541-1544 (1998).

[71] **B. S. Ham, M. S. Shahriar and P. R. Hemmer**, "Enhancement of four-wave mixing and line narrowing by use of quantum coherence in an optically dense double-Lambda solid," *Optics Letters* **24**, 86-88 (1999).

[72] **C. J. Wei and N. B. Manson**, "Observation of the dynamic Stark effect on electromagnetically induced transparency," *Physical Review A* **60**, 2540-2546 (1999).

[73] **C. J. Wei and N. B. Manson**, "Observation of electromagnetically induced transparency within an electron spin resonance transition," *Journal of Optics B-Quantum and Semiclassical Optics* **1**, 464-468 (1999).

[74] **H. Schmidt, K. L. Campman, A. C. Gossard and A. Imamoglu**, "Tunneling induced transparency: Fano interference in intersubband transitions," *Applied Physics Letters* **70**, 3455-3457 (1997).

[75] **H. Schmidt and A. Imamoglu**, "Nonlinear optical devices based on a transparency in semiconductor intersubband transitions," *Optics Communications* **131**, 333-338 (1996).

[76] **H. Schmidt and R. J. Ram**, "All-optical wavelength converter and switch based on electromagnetically induced transparency," *Applied Physics Letters* **76**, 3173-3175 (2000).

[77] **W. Potz**, "Coherent control of light absorption and carrier dynamics in semiconductor nanostructures," *Physical Review Letters* **79**, 3262-3265 (1997).

[78] **S. F. Yelin and P. R. Hemmer**, Sensitive optical detection of mid-infrared radiation based on induced transparency, IQEC Baltimore, (1999),

[79] **Y. Zhao, D. H. Huang and C. K. Wu**, "Electric-field-induced quantum coherence of the intersubband transition in semiconductor quantum-wells," *Optics Letters* **19**, 816-818 (1994).

[80] **Y. Zhao, D. H. Huang and C. K. Wu**, "Lasing without inversion in double quantum wells controlled by a dc field," *Journal of the Optical Society of America B-Optical Physics* **13**, 1614-1618 (1996).

[81] **A. Imamoglu and R. J. Ram**, "Semiconductor-lasers without population-inversion," *Optics Letters* **19**, 1744-1746 (1994).

[82] **A. Imamoglu and S. E. Harris**, "Lasers without inversion - interference of dressed lifetime-broadened states," *Optics Letters* **14**, 1344-1346 (1989).

[83] **H. Schmidt, D. E. Nikonov, K. L. Campman, K. D. Maranowski, A. C. Gossard and A. Imamoglu**, "Quantum interference in semiconductor quantum wells," *Laser Physics* **9**, 797-812 (1999).

[84] **G. B. Serapiglia, E. Paspalakis, C. Sirtori, K. L. Vodopyanov and C. C. Phillips**, "Laser-induced quantum coherence in a semiconductor quantum well," *Physical Review Letters* **84**, 1019-1022 (2000).

[85] **A. E. Siegman**, *Lasers*. (University Science Books, 1996).

[86] **A. S. Zibrov, M. D. Lukin, D. E. Nikonov, L. Hollberg, M. O. Scully, V. L. Velichansky and H. G. Robinson**, "Experimental demonstration of laser oscillation without population-inversion via quantum interference in rb," *Physical Review Letters* **75**, 1499-1502 (1995).

[87] **J. R. Boon**, *Electromagnetically Induced Transparency and Inversionless Lasing*, PhD thesis, University of St. Andrews (1998).

[88] **C. Peters and W. Lange**, "Laser action below threshold inversion due to coherent population trapping," *Applied Physics B-Lasers and Optics* **62**, 221-225 (1996).

[89] **G. G. Padmabandu, G. R. Welch, I. N. Shubin, E. S. Fry, D. E. Nikonov, M. D. Lukin and M. O. Scully**, "Laser oscillation without population inversion in a sodium atomic beam," *Physical Review Letters* **76**, 2053-2056 (1996).

[90] **P. B. Sellin, G. A. Wilson, K. K. Meduri and T. W. Mossberg**, "Observation of inversionless gain and field-assisted lasing in a nearly ideal three-level cascade-type atomic system," *Physical Review A* **54**, 2402-2407 (1996).

[91] **F. B. deJong, A. Mavromanolakis, R. J. C. Spreeuw and H. B. V. vandenHeuvell**, "Synchronously pumped laser without inversion in cadmium," *Physical Review A* **57**, 4869-4876 (1998).

[92] **F. B. deJong**, *Lasing without inversion*, thesis, University of Amsterdam (1998).

[93] **P. Dong, W. M. Man and J. Y. Gao**, "Probe amplification from Raman gain to inversionless gain," *Physics Letters A* **265**, 43-51 (2000).

[94] **W. Lange, A. Nottelman and C. Peters**, "Observation of inversionless amplification in sm vapor and related experiments," *Quantum Optics* **6**, 273-285 (1994).

[95] **A. Nottelmann, C. Peters and W. Lange**, "Inversionless amplification of picosecond pulses due to zeeman coherence," *Physical Review Letters* **70**, 1783-1786 (1993).

[96] **S. F. Yelin, M. D. Lukin, M. O. Scully and P. Mandel**, "Gain without inversion in the frequency up-conversion regime," *Physical Review A* **57**, 3858-3868 (1998).

[97] **V. Ahufinger, J. Mompart and R. Corbalan**, "Lasing without inversion with frequency up-conversion in a Doppler-broadened V-type three-level system," *Physical Review A* **60**, 614-620 (1999).

[98] **E. S. Fry, X. F. Li, D. Nikonov, G. G. Padmabandu, M. O. Scully, A. V. Smith, F. K. Tittel, C. Wang, S. R. Wilkinson and S. Y. Zhu**, "Atomic coherence effects within the

sodium d1 line - lasing without inversion via population trapping," *Physical Review Letters* **70**, 3235-3238 (1993).

[99] **W. E. Vanderveer, R. J. J. Vandiest, A. Donszelmann and H. B. V. Vandenheuvell**, "Experimental demonstration of light amplification without population-inversion," *Physical Review Letters* **70**, 3243-3246 (1993).

[100] **J. A. Kleinfeld and A. D. Streater**, "Observation of gain due to coherence effects in a potassium-helium mixture," *Physical Review A* **49**, R4301-R4304 (1994).

[101] **J. A. Kleinfeld and A. D. Streater**, "Gain and coherence effects induced by strong cw-laser coupling in potassium-rare-gas mixtures," *Physical Review A* **53**, 1839-1853 (1996).

[102] **Y. F. Zhu and J. Lin**, "Sub-Doppler light amplification in a coherently pumped atomic system," *Physical Review A* **53**, 1767-1774 (1996).

[103] **Y. F. Zhu, J. Lin and P. Sanchez**, "Measurement of light amplification in coherently pumped rubidium atoms," *Optics Communications* **128**, 254-261 (1996).

[104] **N. Shiokawa, Y. Torii, T. Hirano and T. Kuga**, Light amplification without population inversion by using laser cooled rubidium atoms, QELS (OSA, (1997),

[105] **J. Kitching and L. Hollberg**, "Interference-induced optical gain without population inversion in cold, trapped atoms," *Physical Review A* **59**, 4685-4689 (1999).

[106] **J. Mompart and R. Corbalan**, "Lasing Without Inversion," *Journal of Optics B-Quantum and Semiclassical Optics* **2**, R7-R24 (2000).

[107] **G. S. Agarwal**, "Inhibition of spontaneous emission noise in lasers without inversion," *Physical Review Letters* **67**, 980-982 (1991).

[108] **Y. F. Zhu, A. I. Rubiera and M. Xiao**, "Inversionless lasing and photon statistics in a V-type atomic system," *Physical Review A* **53**, 1065-1071 (1996).

[109] **X. M. Hu and J. S. Peng**, "Squeezed cascade lasers without and with inversion," *Optics Communications* **154**, 203-216 (1998).

[110] **R. N. Shakhmuratov, G. Kozyreff, R. Coussement, J. Odeurs and P. Mandel**, "Gain without inversion for gamma radiation," *Optics Communications*, (2000).

[111] **R. N. Shakhmuratov**, "Influence of giant nuclear-spin polarisation on resonant gamma-ray absorption and emission," *Australian Journal of Physics* **51**, 339-348 (1998).

[112] **O. Kocharovskaya, R. Kolesov and Y. Rostovtsev**, "Lasing without inversion: a new path to gamma-ray laser," *Laser Physics* **9**, 745-758 (1999).

[113] **R. Kalesoc, Y. Rostovtsev and O. Kocharovskaya**, "Laser control of Mossbauer spectra as a way to gamma-ray lasing," *Optics Communications*, (2000).

[114] **N. A. Ansari and A. H. Toor**, "Quantum theory of non-degenerate inversionless laser: Effects of initial partial coherence," *Journal of Modern Optics* **43**, 2425-2435 (1996).

[115] **J. R. Boon, E. Zekou, D. McGloin and M. H. Dunn**, "Prediction of inversionless gain in a mismatched Doppler-broadened medium," *Physical Review A* **58**, 2560-2566 (1998).

[116] **G. Q. Ge and L. M. Chen**, "Quantum theory of bistable inversionless lasers," *Physical Review A* **58**, 4878-4885 (1998).

[117] **S. Q. Gong, Z. Z. Xu and S. H. Pan**, "The effect of phase fluctuation on electromagnetically induced transparency, inversionless lasing and refractive-index enhancement in a lambda-system," *Journal of Modern Optics* **42**, 1397-1406 (1995).

[118] **S. Q. Gong and Z. Z. Xu**, "Inversionless amplification of a monochromatic-field in a nonresonant 3-level boolean-and medium," *Chinese Science Bulletin* **40**, 84-86 (1995).

[119] **J. B. Khurgin and E. Rosencher**, "Practical aspects of optically coupled inversionless lasers," *Journal of the Optical Society of America B-Optical Physics* **14**, 1249-1253 (1997).

[120] **O. Kocharovskaya, Y. V. Rostovtsev and A. Imamoglu**, "Inversionless amplification in the three-level atoms with and without a hidden inversion in reservoir," *Physical Review A* **58**, 649-654 (1998).

[121] **H. W. Lee**, "Quantum-theory of electromagnetically induced suppression of absorption and inversionless lasing in a 3-level system," *Journal of the Optical Society of America B-Optical Physics* **12**, 449-455 (1995).

[122] **P. Mandel and O. Kocharovskaya**, "Inversionless amplification of a monochromatic-field by a 3-level medium," *Physical Review A* **46**, 2700-2706 (1992).

[123] **P. Mandel and O. Kocharovskaya**, "Inversionless amplification in a multilevel system," *Physical Review A* **47**, 5003-5008 (1993).

[124] **J. Mompart and R. Corbalan**, "Inversionless amplification in three-level systems: dressed states quantum interference and quantum-jump analyses," *Optics Communications* **156**, 133-144 (1998).

[125] **A. K. Popov, S. A. Myslivets, J. Y. Gao, H. Z. Zhang and B. Wellegehausen**, "Inversionless gain in a three-level system driven by a strong field and collisions," *Chinese Physics* **9**, 124-130 (2000).

[126] **F. Silva, V. Ahufinger, J. Mompart and R. Corbalan**, "Inversionless amplification with standing-wave drive," *Laser Physics* **9**, 858-865 (1999).

[127] **G. Vemuri**, "Enhancement of gain in inversionless atomic media using finite bandwidth driving fields," *Quantum Optics* **6**, 305-316 (1994).

[128] **K. Zaheer**, "Gain and diffusion in an inversionless laser," *Physical Review A* **49**, 2914-2921 (1994).

[129] **Y. F. Zhu, O. C. Mullins and M. Xiao**, "Inversionless laser from a closed multilevel system," *Physical Review A* **47**, 602-609 (1993).

[130] **Y. F. Zhu, M. Xiao and Y. Zhao**, "Intensity characteristics of inversionless lasers from induced atomic coherence," *Physical Review A* **49**, 4016-4023 (1994).

[131] **Y. F. Zhu**, "Cascade inversionless and inversion lasers," *Optics Communications* **107**, 499-506 (1994).

[132] **K. Hakuta, L. Marmet and B. P. Stoicheff**, "Electric-field-induced 2nd-harmonic generation with reduced absorption in atomic-hydrogen," *Physical Review Letters* **66**, 596-599 (1991).

[133] **D. W. Tokaryk, G. Z. Zhang and B. P. Stoicheff**, "Nonlinear optical generation in a hydrogen discharge," *Physical Review A* **59**, 3116-3119 (1999).

[134] **R. R. Moseley, S. Shepherd, D. J. Fulton, B. D. Sinclair and M. H. Dunn**, "Interference between excitation routes in resonant sum-frequency mixing," *Physical Review A* **50**, 4339-4349 (1994).

[135] **J. C. Petch, C. H. Keitel, P. L. Knight and J. P. Marangos**, "Role of electromagnetically induced transparency in resonant four-wave-mixing schemes," *Physical Review A* **53**, 543-561 (1996).

[136] **C. Dorman and J. P. Marangos**, "Resonant sum-difference frequency mixing enhanced by electromagnetically induced transparency in krypton," *Physical Review A* **58**, 4121-4132 (1998).

[137] **C. Dorman, J. P. Marangos and J. C. Petch**, "Investigation of vacuum ultraviolet generation in a resonant four-wave mixing scheme in krypton with electromagnetically induced transparency," *Journal of Modern Optics* **45**, 1123-1135 (1998).

[138] **C. Dorman, I. Kucukkara and J. P. Marangos**, "Measurement of high conversion efficiency to 123.6-nm radiation in a four-wave-mixing scheme enhanced by electromagnetically induced transparency - art. no. 013802," *Physical Review A* **6001**, 3802 (5 pages) (2000).

[139] **S. E. Harris and M. Jain**, "Optical parametric oscillators pumped by population-trapped atoms," *Optics Letters* **22**, 636-638 (1997).

[140] **M. D. Lukin, P. R. Hemmer, M. Loffler and M. O. Scully**, "Resonant enhancement of parametric processes via radiative interference and induced coherence," *Physical Review Letters* **81**, 2675-2678 (1998).

[141] **A. S. Zibrov, M. D. Lukin and M. O. Scully**, "Nondegenerate parametric self-oscillation via multiwave mixing in coherent atomic media," *Physical Review Letters* **83**, 4049-4052 (1999).

[142] **M. Fleischhauer, M. D. Lukin, A. B. Matsko and M. O. Scully**, "Threshold and linewidth of a mirrorless parametric oscillator," *Physical Review Letters* **84**, 3558-3561 (2000).

[143] **M. Fleischhauer**, Mirrorless oscillation based on resonantly enhanced 4-wave mixing: All order analytic solutions, qu-ph/9910112

[144] **M. D. Lukin, A. B. Matsko, M. Fleischhauer and M. O. Scully**, "Quantum noise and correlations in resonantly enhanced wave mixing based on atomic coherence," *Physical Review Letters* **82**, 1847-1850 (1999).

[145] **M. O. Scully and M. Fleischhauer**, "High-sensitivity magnetometer based on index-enhanced media," *Physical Review Letters* **69**, 1360-1363 (1992).

[146] **M. Fleischhauer and M. O. Scully**, "Quantum sensitivity limits of an optical magnetometer based on atomic phase coherence," *Physical Review A* **49**, 1973-1986 (1994).

[147] **A. G. Truscott, M. E. J. Friese, N. R. Heckenberg and H. RubinszteinDunlop**, "Optically written waveguide in an atomic vapor (vol 82, pg 1438, 1999)," *Physical Review Letters* **82**, 3561 (1999).

[148] **R. Kapoor and G. S. Agarwal**, "Theory of electromagnetically induced waveguides - art. no. 053818," *Physical Review A* **6105**, 3818 (4 pages) (2000).

[149] **F. S. Pavone, G. Bianchini, F. S. Cataliotti, T. W. Hansch and M. Inguscio**, "Birefringence in electromagnetically induced transparency," *Optics Letters* **22**, 736-738 (1997).

[150] **A. K. Patnaik and G. S. Agarwal**, Controlling magneto-optical rotation via atomic coherence, qu-ph/9911034

[151] **M. O. Scully**, "Enhancement of the index of refraction via quantum coherence," *Physical Review Letters* **67**, 1855-1858 (1991).

[152] **M. O. Scully and S. Y. Zhu**, "Ultra-large index of refraction via quantum interference," *Optics Communications* **87**, 134-138 (1992).

[153] **M. Fleischhauer, C. H. Keitel, M. O. Scully, C. Su, B. T. Ulrich and S. Y. Zhu**, "Resonantly enhanced refractive-index without absorption via atomic coherence," *Physical Review A* **46**, 1468-1487 (1992).

[154] **U. Rathe, M. Fleischhauer, S. Y. Zhu, T. W. Hansch and M. O. Scully**, "Nonlinear-theory of index enhancement via quantum coherence and interference," *Physical Review A* **47**, 4994-5002 (1993).

[155] **M. D. Lukin, S. F. Yelin, A. S. Zibrov and M. O. Scully**, "Enhancement of refractive index with quantum coherence: An overview," *Laser Physics* **9**, 759-772 (1999).

[156] **M. O. Scully and M. Suhail Zubairy**, *Quantum Optics*. (CUP, Cambridge, 1997).

[157] **A. S. Zibrov, M. D. Lukin, L. Hollberg, D. E. Nikonov, M. O. Scully, H. G. Robinson and V. L. Velichansky**, "Experimental demonstration of enhanced index of refraction via quantum coherence in Rb," *Physical Review Letters* **76**, 3935-3938 (1996).

[158] **M. O. Scully**, "From lasers and masers to phaseonium and phasers," *Physics Reports-Review Section of Physics Letters* **219**, 191-201 (1992).

[159] **M. Fleischhauer, A. B. Matsko and M. O. Scully**, Quantum limit of optical magnetometry in the presence of ac-Stark shifts, qu-ph/0001072

[160] **H. Lee, M. Fleischhauer and M. O. Scully**, "Sensitive detection of magnetic fields including their orientation with a magnetometer based on atomic phase coherence," *Physical Review A* **58**, 2587-2595 (1998).

[161] **M. D. Lukin, M. Fleischhauer, A. S. Zibrov, H. G. Robinson, V. L. Velichansky, L. Hollberg and M. O. Scully**, "Spectroscopy in dense coherent media: Line narrowing and interference effects," *Physical Review Letters* **79**, 2959-2962 (1997).

[162] **M. D. Lukin, S. F. Yelin, M. Fleischhauer and M. O. Scully**, "Quantum interference effects induced by interacting dark resonances," *Physical Review A* **60**, 3225-3228 (1999).

[163] **A. G. Truscott, M. E. J. Friese, N. R. Heckenberg and H. RubinszteinDunlop**, "Optically written waveguide in an atomic vapor," *Physical Review Letters* **82**, 1438-1441 (1999).

[164] **M. J. Padgett and L. Allen**, "The angular momentum of light: optical spanners and the rotational frequency shift," *Optical and Quantum Electronics* **31**, 1-12 (1999).

[165] **L. Allen, M. J. Padgett and M. Babiker**, "The orbital angular momentum of light," *Progress in Optics* **39**, 291-372 (1999).

[166] **L. V. Hau, S. E. Harris, Z. Dutton and C. H. Behroozi**, "Light speed reduction to 17 metres per second in an ultracold atomic gas," *Nature* **397**, 594-598 (1999).

[167] **M. M. Kash, V. A. Sautenkov, A. S. Zibrov, L. Hollberg, G. R. Welch, M. D. Lukin, Y. Rostovtsev, E. S. Fry and M. O. Scully**, "Ultraslow group velocity and enhanced nonlinear optical effects in a coherently driven hot atomic gas," *Physical Review Letters* **82**, 5229-5232 (1999).

[168] **D. Budker, D. F. Kimball, S. M. Rochester and V. V. Yashchuk**, "Nonlinear magneto-optics and reduced group velocity of light in atomic vapor with slow ground state relaxation," *Physical Review Letters* **83**, 1767-1770 (1999).

[169] **U. Leonhardt and P. Piwnicki**, "Relativistic effects of light in moving media with extremely low group velocity," *Physical Review Letters* **84**, 822-825 (2000).

[170] **S. M. Hawking**, "Black Hole Explosions?," *Nature* **248**, 30 (1974).

[171] **U. Leonhardt and P. Piwnicki**, Ultrahigh sensitivity of slow-light gyroscope, physics/0003092

[172] **S. E. Harris**, Electromagnetically Induced Transparency in Atoms and Molecules, IQEC San Francisco, (2000), QWJ1.

[173] **S. E. Harris and L. V. Hau**, "Nonlinear optics at low light levels," *Physical Review Letters* **82**, 4611-4614 (1999).

[174] **M. D. Lukin and A. Imamoglu**, "Nonlinear optics and quantum entanglement of ultraslow single photons," *Physical Review Letters* **84**, 1419-1422 (2000).

[175] **Y. Rostovtsev, O. Kocharovskaya and M. O. Scully**, Freezing light via atomic coherence, qu-ph/0001058v2

[176] **A. Kuhn, S. Steuerwald and K. Bergmann**, "Coherent population transfer in NO with pulsed lasers: the consequences of hyperfine structure, Doppler broadening and electromagnetically induced absorption," *European Physical Journal D* **1**, 57-70 (1998).

[177] **A. M. Akulshin, S. Barreiro and A. Lezama**, "Electromagnetically induced absorption and transparency due to resonant excitation of quasidegenerate levels in Rb vapor," *Physical Review A* **57**, 2996-3002 (1998).

[178] **A. M. Akulshin, S. Barreiro and A. Lezama**, "Steep anomalous dispersion in coherently prepared Rb vapor," *Physical Review Letters* **83**, 4277-4280 (1999).

[179] **A. Lezama, S. Barreiro, A. Lipsich and A. M. Akulshin**, "Coherent two-field spectroscopy of degenerate two-level systems - art. no. 013801," *Physical Review A* **6001**, 3801 (11 pages) (2000).

[180] **Y. Dancheva, G. Alzetta, S. Cartaleva, M. Taslakov and C. Andreeva**, "Coherent effects on the Zeeman sublevels of hyperfine states in optical pumping of Rb by monomode diode laser," *Optics Communications* **178**, 103-110 (2000).

[181] **A. V. Taichenachev, A. M. Tumaikin and V. I. Yudin**, "Electromagnetically induced absorption in a four-state system - art. no. 011802," *Physical Review A* **6001**, 1802 (4 pages) (2000).

[182] **S. Barreiro, A. Lipsich, A. Lezama and A. M. Akulshin**, Optical propagation with slow and negative group velocity in Rb vapor, QELS 2000 San Francisco, (2000), 137.

[183] **R. Y. Chiao, E. Bolda, J. Bowie, J. Boyce, J. C. Garrison and M. W. Mitchell**, "Superluminal and parelectric effects in rubidium vapor and ammonia gas," *Quantum and Semiclassical Optics* **7**, 279-295 (1995).

[184] **M. W. Mitchell and R. Y. Chiao**, "Causality and negative group delays in a simple bandpass amplifier," *American Journal of Physics* **66**, 14-19 (1998).

[185] **L. J. Wang, A. Kuzmich and A. Dogarlu**, "Gain-assisted superluminal light propagation," *Nature*, (2000).

[186] **J. Y. Gao, S. H. Yang, D. Wang, X. Z. Guo, K. X. Chen, Y. Jiang and B. Zhao**, "Electromagnetically induced inhibition of two-photon absorption in sodium vapor - art. no. 023401," *Physical Review A* **6102**, 3401 (3 pages) (2000).

Chapter 2

Theory and experimental overview

2.1 Modelling EIT

In order to investigate EIT it is necessary to examine how coherent light interacts with an atomic system. For incoherent light it is possible to use Einstein's rate equation approach but this is not valid when the light is coherent. We may, however, use a semi-classical approach in which the atom is a quantum object and the light is described by a classical field. Such a model allows us to examine the populations of the atomic levels involved and the coherences established between those levels. It is possible to relate atomic susceptibilities to these coherences and thus inspect the absorption and dispersion of the light incident on the atoms. For the sake of brevity we will examine only the simple atomic systems relevant to EIT and the main theoretical tool used in this thesis: the density matrix. Any other theoretical methods employed in later chapters will be introduced when required. The interested reader is directed to other works for a fuller introduction to the theory of EIT [1-9].

2.2 Semi-classical atom-light interactions: The Density Matrix

It is not always possible to know the state vector $|\psi\rangle$ for a given system. This is the case when we deal we an ensemble of atoms such as those encountered in the EIT experiments described in this thesis. This poses a problem if we wish to extract information about the system. Normally we would use the expectation value of the corresponding expectation operator:

$$\langle A \rangle = \langle \psi | A | \psi \rangle \tag{2.1}$$

where $|\psi>$ can be expanded in terms of an orthonormal basis set $\{\phi\}$:

$$|\psi\rangle = \sum_{i=1}^{n} c_i |\phi_i\rangle \tag{2.2}$$

where c_i is the probability amplitude of being in a state $|\phi_i\rangle$. For example if we take the unperturbed states of a three level atom the wavefunction may be written:

$$|\psi\rangle = c_1|1\rangle + c_2|2\rangle + c_3|3\rangle \tag{2.3}$$

We then introduce the density operator [2, 10, 11]:

$$\rho = |\psi\rangle\langle\psi| \tag{2.4}$$

which can be written in terms of a n x n density matrix (n being the number of wavefunctions that describe the system. An element of the density matrix may be written:

$$\rho_{ij} = \langle \phi_i | \rho | \phi_j \rangle = \langle \phi_i | \psi \rangle \langle \psi | \phi_j \rangle = c_i c_j^* \tag{2.5}$$

using (2.3) and (2.4).

The matrix elements can be related to observable quantities, $|c_i|^2$ is the probability for the atom being in state $|i\rangle$, which lies between 0 and 1 since the system is closed. The off diagonal matrix elements $c_i c_j^*$ are called the coherences since they depend on the phase difference between c_i and c_j. These can be related to the macroscopic properties of the atomic medium (see section 2.2.1). Using (2.4) we are able to re-express the expectation value in (2.1):

$$\begin{aligned} \langle A \rangle &= \left\langle \sum_i c_i \phi_i \middle| A \middle| \sum_j c_j \phi_j \right\rangle = \sum_{i,j} c_i^* c_j \langle \phi_i | A | \phi_j \rangle \\ &= \sum_{i,j} \rho_{ji} A_{ij} = \sum (\rho A)_{jj} = Tr(\rho A) \end{aligned} \tag{2.6}$$

which now depends solely on the matrix element A and the probability amplitudes c_i. Since the operator ρ defines an n x n matrix in which the off diagonal elements are complex we have n^2 real elements which define our matrix and hence our system. We can remove one of these degrees of freedom by using the trace normalisation property of the density matrix:

$$Tr(\rho) = \sum_{i=1}^{n} \rho_{ii} = 1 \tag{2.7}$$

which ensures the conservation of probability (and hence population) and allows us to remove the equation for ρ_{11}, since:

$$\rho_{11} = 1 - \sum_{i=2}^{n} \rho_{ii} \tag{2.8}$$

leaving us with a set of n^2-1 linear real equations which describe our entire system. We can then use a linear algebra package to solve this matrix and extract the information we require.

We may now derive the equation of motion for the density matrix, staring from the Schrödinger equation:

$$|\dot{\psi}\rangle = -\frac{i}{\hbar} H |\psi\rangle \tag{2.9}$$

We then differentiate equation (2.4) with respect to time:

$$\dot{\rho} = |\dot{\psi}\rangle\langle\psi| + |\psi\rangle\langle\dot{\psi}| \tag{2.10}$$

then using (2.9) to substitute for $|\dot{\psi}\rangle$ and $\langle\dot{\psi}|$ we end up with:

$$\dot{\rho} = -\frac{i}{\hbar}[H, \rho] \tag{2.11}$$

which is the Liouville equation, the density matrix equation of motion. Thus the ijth element of the density matrix is given by:

$$\dot{\rho}_{ij} = -\frac{i}{\hbar}\sum_{k=1}^{n}(H_{ik}\rho_{kj} - \rho_{ik}H_{kj}) \tag{2.12}$$

Strictly, for our ensemble of atoms we must use an average value for the expectation value <A> [12]:

$$\langle A\rangle = \sum_{\psi} P_{\psi}\langle\psi|A|\psi\rangle \tag{2.13}$$

where P_ψ is the probability that the system is in state $|\psi>$. Hence we define a general density operator as:

$$\rho = \sum_{\psi} P_{\psi}|\psi\rangle\langle\psi| \tag{2.14}$$

Following a similar procedure as above we arrive at equation (2.11).

The Hamiltonian in the atom-field interaction can be defined as:

$$H = H_0 + H_{\text{int}} \tag{2.15}$$

where H_0 is the bare state Hamiltonian and H_{int} is an interaction term comprised of the electric dipole interactions induced within the atom due to the applied electric field. Thus we can write H as:

$$H = H_0 - \mu_{ij}E \tag{2.16}$$

where E is the electric field strength and μ_{ij} is the electric dipole matrix element. The matrix element for a particular transition will define whether a transition is allowed or not. Obviously the matrix elements $\mu_{ii} = 0$ but the values for the other elements will determine the type of system we are dealing with, e.g Cascade, Lambda or Vee (see section 2.3). For a simple two level atom the Hamiltonians may be expressed as [13]:

$$H_0 = \hbar\omega_1|1\rangle\langle 1| + \hbar\omega_2|2\rangle\langle 2| \tag{2.17}$$

and

$$H_{\text{int}} = -\mu_{ij} E(|2\rangle\langle 1| + |1\rangle\langle 2|) \tag{2.18}$$

2.2.1 Spontaneous Decay Terms

Our system of equations now describes the interaction of the light field with the atom but does not take into account the effects of spontaneous decay and atomic dephasing along with incoherent pumping. It is possible to add these terms phenomenologically. Decay terms are added such that they either remove or add population to the levels under consideration. For example spontaneous decay from level j to level i is included by adding a term of the form $-\Gamma_{ji}\rho_{ji}$ to the density matrix equation for ρ_{jj}. A corresponding positive term will be added to the ρ_{ii} term to conserve population (assuming a closed system). Hence we will have:

$$\dot{\rho}_{jj} = -\frac{i}{\hbar}[H,\rho]_{jj} - \Gamma_{ji}\rho_{jj} \tag{2.19}$$

2.2.2 Incoherent Pumping Terms

Incoherent pump sources can be thought of in a similar way. We make use of pump sources to investigate inversionless gain within a system. *Incoherent* sources are used in preference to coherent sources because they are simpler to deal with and also because as was pointed out in Chapter 1 coherent pump sources act to diminish the gain/EIT in the system, at the points of interest, and hence may destroy the quantum optical effects we are interested in. If we couple our laser between levels i and j in our atom the density matrix equations of motion are modified thus:

$$\dot{\rho}_{ii} = -\frac{i}{\hbar}[H,\rho]_{ii} + R_{ij}\left(\rho_{jj} - \rho_{ii}\right) \tag{2.20}$$

with a similar negative R_{12} term for the $\dot{\rho}_{jj}$ term. The pumping term R_{ij} is related to the strength of the incoherent field.

2.2.3 Decoherence Decay Rates

As we have seen we must introduce decay terms to account for the spontaneous emission processes occurring within the atom. We must also take account of the decay processes associated with the other matrix terms, the so-called *dephasing* rates. Such decays act to destroy the coherences set-up within the system. These are given by:

$$\gamma_{ij} = \frac{1}{2}\left(\sum_k \Gamma_{ik} + \sum_l \Gamma_{jl}\right) + \gamma_{deph} \tag{2.21}$$

where k denotes all the levels into which population from level i may decay and l denotes all the levels into which population from level j may decay. The extra term γ_{deph} includes any extra dephasing that the system may suffer from, for example collisional dephasing, not accounted for

by the decay rate dephasing. In general the work in this thesis has no extra dephasing ($\gamma_{deph} = 0$).

2.2.4 Alternative Decay Rate Method: Relaxation Matrix

It is possible to incorporate both dephasing and decay terms into the density matrix by means of a relaxation matrix Γ [2], defined by:

$$\langle i|\Gamma|j\rangle = \gamma_i \delta_{ij} \tag{2.22}$$

We may then modify the equation of motion for the density matrix (2.11) to:

$$\dot{\rho} = -\frac{i}{\hbar}[H,\rho] - \frac{1}{2}\{\Gamma,\rho\} \tag{2.23}$$

where $\{\Gamma,\rho\} = \Gamma\rho + \rho\Gamma$. Thus the ijth element of the matrix becomes:

$$\dot{\rho}_{ij} = -\frac{i}{\hbar}\sum_k \left(H_{ik}\rho_{kj} - \rho_{ik}H_{kj}\right) - \frac{1}{2}\sum_k \left(\Gamma_{ik}\rho_{kj} + \rho_{ik}\Gamma_{kj}\right) \tag{2.24}$$

However this approach is slightly different to that discussed above in that the decay rates are all lumped together via the γ_i terms. Also there is no mechanism for adding decay terms that add population to a level, rather than leaving it. This method is perhaps not as physically helpful as phenomenologically adding the terms, the method used for the derivation of matrix elements in this work.

2.2.5 Decay Rates and Unit Definitions

The issue of decay rates is not always a clear cut one. This is due to the differing definitions of the Einstein A coefficient/decay rates that can occur. Unfortunately when authors quote decay rates in papers they rarely cite where they come from and this can lead to confusion, particularly over whether the units are in true megahertz or whether they are in angular units e.g the megaradian/s. In previous work by this group this distinction was left somewhat ambiguous. Indeed the units of many of the variables used in the model discussed above can take either angular or linear values, e.g. the Rabi frequency, the frequency itself and frequency detuning. Previous work from this group has not made these distinctions and so strictly some of that work is incorrect. However since this work was not used to make estimates on real experimentally verifiable values, e.g. absorption or refractive index then the mistakes that were made were simply scaling errors. In the work that follows it is the intention to be clear which units are being used. Therefore all values quoted in MHz, will be in true megahertz. Some values will be quoted thus: $x = 40/2\pi$ MHz, meaning that the value x is expressed in megahertz but the number in the numerator is in Mrads^{-1} i.e. it is left in an angular form, i.e. the value of x is 40Mrad/s. Where appropriate other values will be quoted in megaradians/s.

Quoted values of A coefficients of transitions of interest are given in table 2.1, where:

$$\Gamma_{ji}(MRads^{-1}) = A_{ji}(MRads^{-1}) \tag{2.25}$$

	$A_{ji}(x\ 10^6 s^{-1})$				
Transition	λ(nm) [14]	Heavens [15]	Lingard [16]	Wiese [17]	Theodosiou [18]
$5P_{3/2} - 5S_{1/2}$	780	37.5	37.73	37.0	38.9
$5D_{5/2} - 5P_{3/2}$	776	2.70	2.29	-	-
$6P_{1/2} - 5S_{1/2}$	420	2.43	3.346	1.5	8

Table 2.1: *Published values for Einstein A coefficients in rubidium for transitions of interest to experimental and theoretical work carried out in this thesis.*

2.2.6 Relating the Density Matrix Elements to Atomic Susceptibilities

We have already mentioned that density matrix elements may be related to measurable quantities such as population, absorption and refractive index. This can be quantified when it is seen that the density matrix elements can be related to macroscopic susceptibilities. The induced polarisation of the medium can be expressed in terms of the off-diagonal density matrix ρ_{ij} [19]:

$$P(t) = N\mu_{ij}\rho_{ij} \tag{2.26}$$

where μ_{ij} is the dipole matrix element for the transition from level i to level j and N is the number of atoms within our system. This equation is valid so long as the dipole-dipole interaction between the atoms themselves can be ignored. If this weren't the case then local field effects would need to be considered. Moseley *et al* [20] have shown that such effects are negligible in the types of EIT experiments considered in this work. Equation (2.26) can now be equated to the macroscopic polarisation equation:

$$\begin{aligned} P(t) &= \varepsilon_0 \chi E \\ &= \varepsilon_0 (\chi' - i\chi'') E \end{aligned} \tag{2.27}$$

where ε_0 is the permittivity of free space, χ is the electric susceptibility and E is the optical field strength inducing the polarisation. The real part of the susceptibility, χ' is related to the refractive index of the medium; the complex part, χ'' is related to the absorption the electric field experiences in the medium. These two quantities are related by the Kramers-Kronig relations [19] and as such we can now see that modification of the absorption, for instance in a medium undergoing EIT, will modify the refractive index as well.

Equating equations (2.26) and (2.27) allows macroscopic quantities to be related to the numbers produced by the density matrix:

$$\chi' = \frac{N\mu_{ij}^2 \,\mathrm{Re}(\rho_{ij})}{2\hbar\varepsilon_0\Omega_{ij}} \tag{2.28}$$

$$\chi'' = -\frac{N\mu_{ij}^2 \,\mathrm{Im}(\rho_{ij})}{2\hbar\varepsilon_0\Omega_{ij}} \tag{2.29}$$

where 'Re' and 'Im' stand for the real and imaginary parts and we define the half-Rabi (angular) frequency as:

$$\Omega_{ij} = \frac{\mu_{ij} E}{2\hbar} \tag{2.30}$$

2.2.7 Dressed States

It is also possible to consider the atomic system in terms of the so-called dressed states. These states are the eigenstates of the atom-field Hamiltonian, instead of the bare atom itself, and can often give insight into how coherent processes occur. Indeed, as has been pointed out in chapter 1 EIT can be thought of as interference between excitation to dressed states. We briefly use dressed states in chapter 5 to examine some of the properties of an atomic system and the method for their calculation is outlined in section (5.7.3.1). References to dressed states can be found in [1, 2, 13, 21] for example.

2.3 Three Level Systems

Modelling of EIT is achieved by considering three level atomic systems. Despite the fact that most real atomic manifolds are made up of a multiple of levels, often far removed from the idealised three levels, a good approximation of what happens in real experiments can be made. The three most common models are discussed briefly in the following section: the cascade (or ladder), the Lambda and the V schemes. We examine the cascade model in a little more detail than the other two systems as an illustration of the EIT effects that we investigate in later chapters.

2.3.1 The Cascade Scheme

The cascade scheme consists of three levels one on top of the other as shown in figure 2.1. Two fields interact with the system, the probe field denoted E_p and the coupling field denoted E_c. These fields have angular frequencies ω_p and ω_c respectively. Optical field detunings are denoted by Δ_i.

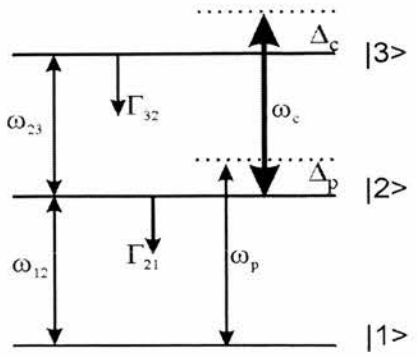

Figure 2.1: *Three Level Cascade Scheme with the coupling field applied between levels |2> and |3> and the probe field between levels |1> and |2>.*

The density matrix for the system is derived by setting the dipole matrix element for the $|1\rangle - |3\rangle$ transition to zero, i.e. it is electric dipole non-allowed. The detunings are defined (in the homogeneously broadened cased) as:

$$\Delta_p = \omega_p - \omega_{12} \tag{2.31}$$

$$\Delta_c = \omega_c - \omega_{23} \tag{2.32}$$

We now examine how EIT may come about using our theoretical model. If we base the system shown in figure 2.1 upon levels found in atomic rubidium we have for level |1> the $5S_{1/2}$ state, for level |2> the $5P_{3/2}$ state and for the upper state we have the $5D_{5/2}$ level. The decay rates for these transitions are approximately Γ_{21}=6 MHz and Γ_{32}=0.4 MHz. First we see what happens in the case where only the probe laser is applied to the atoms, hence we set the probe field Rabi frequency $\Omega_p = 1$ MHz and the coupling field Rabi frequency $\Omega_c = 0$ MHz. The resulting trace, details the homogeneous linewidth of the probe transition as we would expect (Doppler broadening will be introduced in section 2.4.3) and is shown in figure 2.2(a).

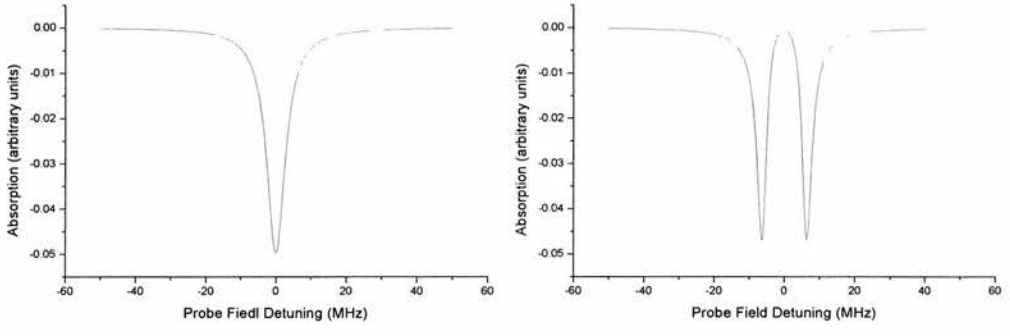

(a) (b)

Figure 2.2: *Absorption profiles for the cascade scheme. (a) The case where $\Omega_c = 0$ MHz, a normal absorption profile. (b) $\Omega_c = 13$ MHz, an EIT profile. The 'arbitrary units' refer to the value of the appropriate density matrix element, proportional to absorption in this case.*

We see that the absorption profile is markedly changed when we introduce a finite coupling field. Figure 2.2(b) shows the profile when Ω_c=13MHz. The absorption profile is clearly split two components, the signature feature of EIT. The corresponding traces for the refractive indices, the real part of ρ^{12} are plotted in figure 2.3(a) and 2.3(b). Further we can examine how the populations of the atomic levels look in the steady state. These are shown in figure 2.4. It can be seen that most of the population is in |1> and some of the population is in |3>, essentially no population is in |2>, which is indicative of the interference effect that occurs in EIT.

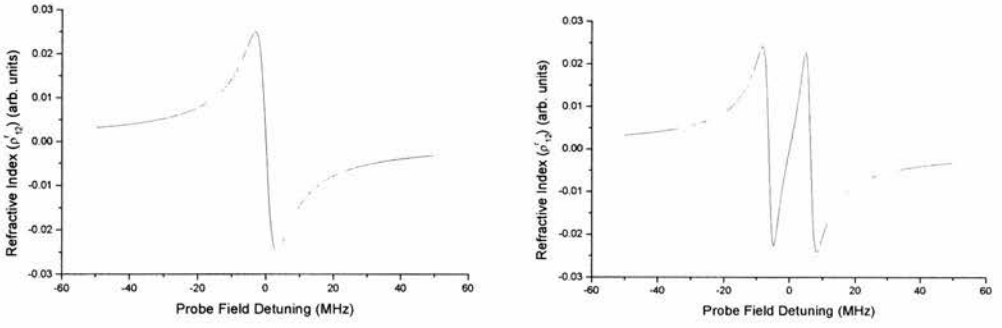

(a) (b)

Figure 2.3: *Index of refraction profiles for the cascade scheme. (a) The case where* $\Omega_C = 0$ *MHz, a normal absorption profile. (b)* $\Omega_C = 80$ *MHz, with a steep dispersion around line centre.*

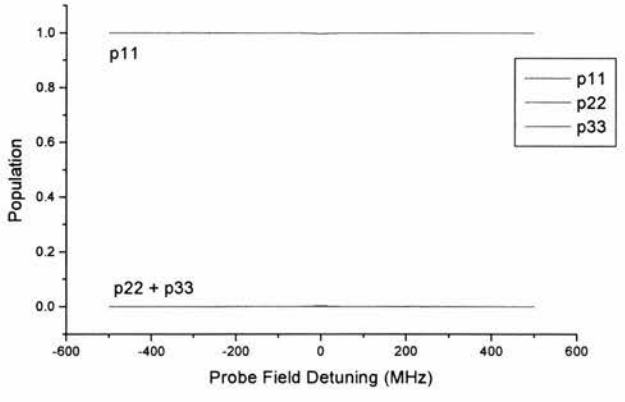

Figure 2.4: *Population distribution in steady state cascade scheme EIT. The majority of the population is found in the ground state, while only a small amount of the population is in the upper two levels (ρ_{22} and ρ_{33} are both very small and nearly equal). Hence EIT is not a saturation effect since nearly all the population is trapped in the lower level.*

We can see how this occurs in the cascade scheme by examining density matrix equations as derived by Gea-Banaloche *et al* [22]:

$$\rho_{21} = -\frac{i\Omega_p}{\gamma_{21} - i\Delta_p + \dfrac{\Omega_c^2/4}{\gamma_{31} - i(\Delta_p + \Delta_c)}} \tag{2.33}$$

Examination of this equation gives us some idea of how the coupling field affects the absorption, although a number of approximations have to be made in deriving the equation and modelling with a full density matrix gives a far more accurate result. When the coupling field is turned off we will observe a maximum in absorption in the resulting trace for a zero probe field detuning. However with a coupling field present this maximum will be shifted to a value where the probe field detuning equals the coupling field Rabi frequency (provided the coupling field detuning is equal to zero). We also see another important feature, that the system can make use of a Doppler free situation when the probe and coupling fields counterpropagate and are of roughly equal wavelength, in essence setting $\Delta_p + \Delta_c \approx 0$. This is examined in more detail in reference [23] and in section 2.4.3 below. By expanding equation (2.33) it is possible to show that so long as the following inequality holds:

$$\Omega_c^2 \geq \sqrt{\Gamma_{21}\Gamma_{32}} \tag{2.34}$$

then zero (or near to zero) absorption will be found when the probe detuning is zero. Equations (2.33) and (2.34) are only strictly valid with a weak probe field approximation. As Wielandy and Gaeta have pointed out [24] when the probe field strength begins to approach that of the coupling field strength then the situation becomes slightly more complicated and constructive interference effects as well as destructive interference effects can take place. These effects mirror those examined by Agarwal [25] in which constructive type processes are predicted for an inverted cascade scheme (i.e. the probe field is stronger than the coupling field).

An alternative for examining the EIT process in the cascade scheme is to examine the ρ_{12} term without any approximation which is what is done in this work. Instead of a simplified equation such as (2.32), the full equation found by solving the density matrix is used.

2.3.2 The Lambda Scheme

The Lambda (Λ) scheme is broadly the same as the cascade scheme and is shown in figure 2.5. This time it is the transition between the two lower states, |1> - |2>, that is dipole non-allowed.

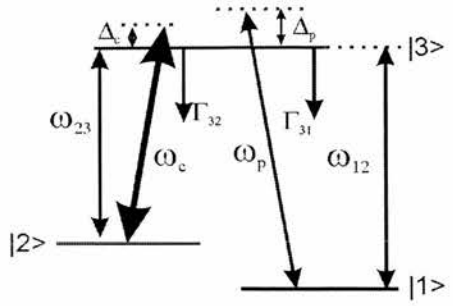

Figure 2.5: *Three Level Lambda Scheme with the coupling field applied between levels |2> and |3> and the probe field between levels |1> and |3>.*

The lambda scheme is particularly important in quantum coherence experiments as it is relatively simple to achieve by using ground state hyperfine levels as the lower two levels and is also the basis for Coherent Population Trapping. As such it is well studied [1, 2, 26-28] for example. We can see traces of EIT in the lambda scheme in figure 2.6.

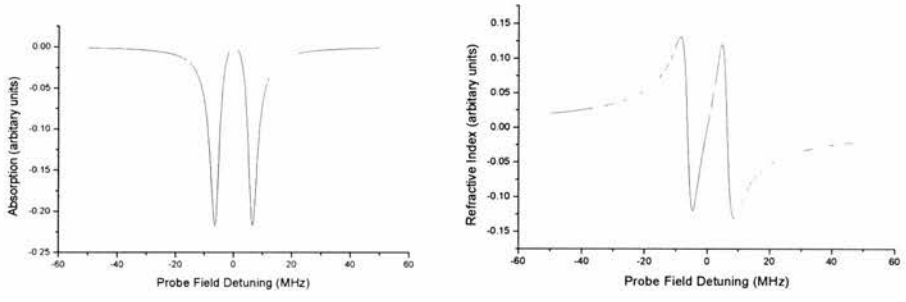

(a) (b)

Figure 2.6: *Three Level Lambda Scheme (a) Absorption profile and (b) Refractive index profile with the coupling field, Ω_c=13MHz, applied between levels |2> and |3>.*

2.3.3 The V-Scheme

The V scheme is a little different from the cascade and lambda schemes in that both the probe and coupling fields interact with the same ground state, see figure 2.7.

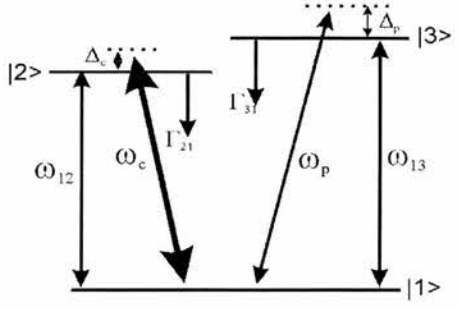

Figure 2.7: *Three Level Vee Scheme with the coupling field applied between levels |1> and |2> and the probe field between levels |1> and |3>.*

This time the non-allowed transition is between the two upper states, |2> - |3>. By a simple symmetry considerations the positions of the probe and coupling fields are interchangeable in a Vee scheme. The fact that the strong coupling field interacts directly with the ground state means that the Vee scheme suffers from optical pumping more than the cascade scheme (the lambda scheme also has optical pumping problems) and as such is more difficult to implement experimentally. The probe absorption in a EIT Vee scheme is shown in figure 2.8

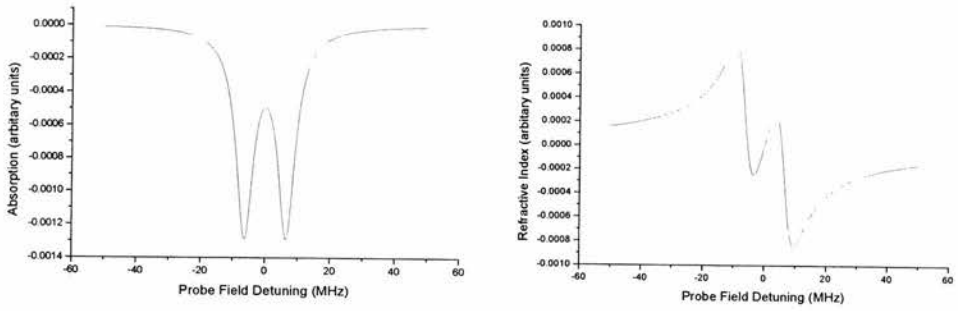

(a) (b)

Figure 2.8: *Three Level Vee Scheme (a) Absorption profile and (b) Refractive index profile with the coupling field, Ω_c=13MHz, applied between levels |1> and |2>.*

The main difference in the EIT traces in the three schemes is the width of the EIT hole. This width is determined by the dephasing on the unlinked transition within the system. In the presence of radiative dephasing alone the lambda scheme has the sharpest hole as it suffers from no radiative dephasing on its unlinked transition. The cascade scheme will only have a contribution to the unlinked dephasing from the decay rate on the coupling transition while the Vee scheme will have contributions from the probe and coupling transition decay rates and hence all being equal it has the largest EIT width. A comparison of EIT and amplification without inversion in all three schemes can be found in chapter 3.

2.3.4 Derivation of Density Matrices: Moseley's N Level Rules

We can derive a density matrix from first principles using the techniques outlined above. This however can become time consuming and tedious (prone to error) if the matrix moves beyond a three level system. As such Richard Moseley developed a set of rules [3] that may be used to derive a density matrix for many N-level systems. The rules are based on patterns which appear within the density matrices themselves. They allow a matrix to be written down directly without making use of the Liouville equation. This does however have some limitations (as it stands). It cannot for instance deal with situations where more than one field couples to a single transition. The rules are found to be a powerful and useful method for dealing with multilevel systems.

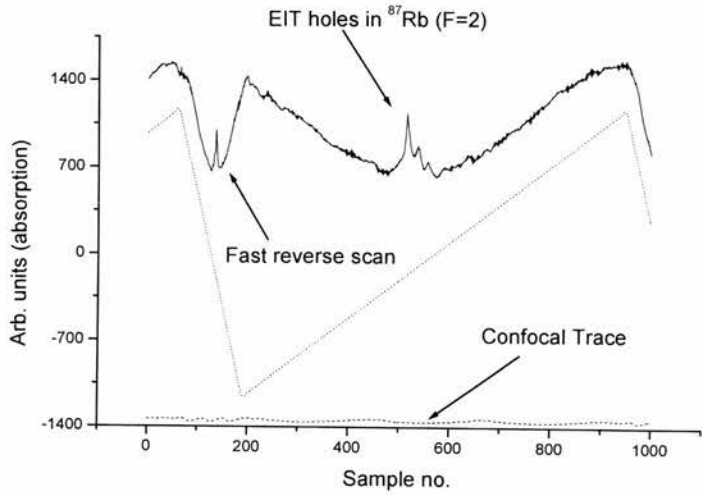

Figure 2.10: *Typical experimental EIT trace. The solid line is the rubidium absorption trace, the dotted line the probe laser frequency scan and the dashed line the scanning confocal marker. The first absorption dip is the fast reserves scan of the probe laser and the second longer scan is the one of real interest. The multiple peaks that can be seen on this trace are due to the hyperfine structure of the upper coupling field level in rubidium.*

2.4.1 Atomic Rubidium

The EIT experiments in this thesis are carried out in atomic rubidium and as such it is appropriate to outline some of its important properties, relevant to what follows. We will examine its level structure, including hyperfine and Zeeman structure. Atomic decay rates have been discussed in section 2.2.5 above.

2.4.1.1 Level Structure

Rubidium is an alkali metal with two natural isotopes ^{85}Rb and ^{87}Rb. Each isotope has a ground state with two hyperfine levels which gives rise to a four peak absorption spectrum. For the 85 isotope the nuclear spin, I=5/2 and for the 87 isotope I=3/2. Combined with the J quantum number the nuclear spin gives the F quantum number (F=I+J) which determines the number of hyperfine levels and the number of degenerate Zeeman levels, m_F=2F+1 for a particular state. This results in a hyperfine structure for the particular fine structure of interest that is displayed in figure 2.11(a), (b) and (c).

2.4 Experimental EIT

To observe EIT we need several ingredients. We need a medium in which to carry out experiments and laser sources with which to probe it. The medium we require must have a number of relatively simple transitions that are accessible with contemporary laser wavelengths. Rubidium is ideal as it fulfils both these criteria; it is discussed further in section 2.4.1. The laser sources that we use are a modified Schwarz Ti:Sapphire laser as the coupling field and a Microlase Ti:Sapphire laser as the probe laser. Both lasers are argon-ion pumped.

The Schwarz laser is passively stable and can be tuned via both etalon control and by tuning a set of Brewster plates and has a linewidth of <5MHz [29]. It can deliver up to 1W of power at around 700-1000nm. The Microlase laser is actively stabilised and can be locked to a given frequency by means of a side of fringe locking mechanism. It can be scanned over a 40GHz range using a microprocessor control system and has a linewidth of around 100kHz. It too can deliver up to 1W at around 700-1000nm. A typical experimental configuration is shown in figure 2.9. In order to improve signal to noise ratio the probe field is modulated by means of an optical chopper and is detected using phase sensitive detection. A frequency marker is obtained by using a 300MHz low finesse etalon. The Ti:sapphire wavelengths are set using a wavemeter [30]. A typical experimental trace is shown in figure 2.10.

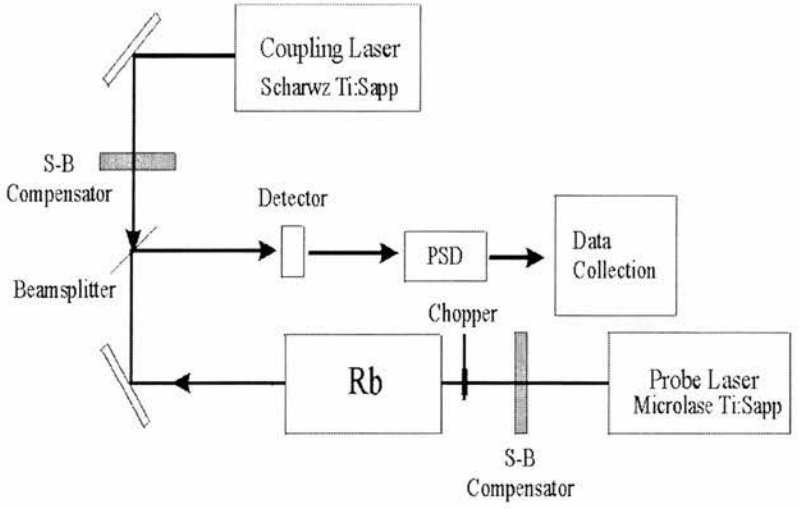

Figure 2.9: *Typical experimental set-up for observation of EIT. S-B compensator stands for Soliel-Babiney compensator. These are used to control the polarisation of the probe and coupling fields.*

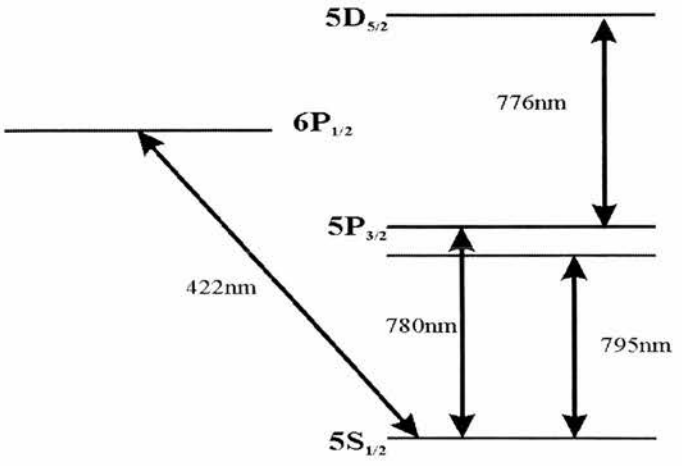

Figure 2.11(a): *Atomic rubidium level structure of relevance to the work carried out in this thesis.*

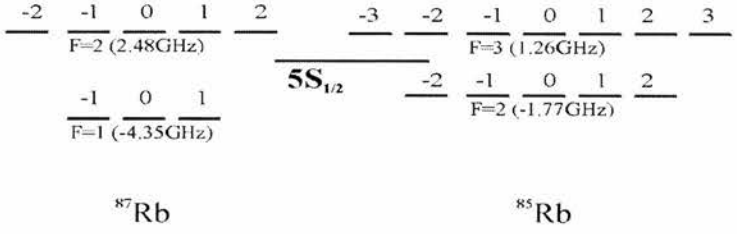

Figure 2.11(b): *Hyperfine structure of the $5S_{1/2}$ state in ^{87}Rb and ^{85}Rb.*

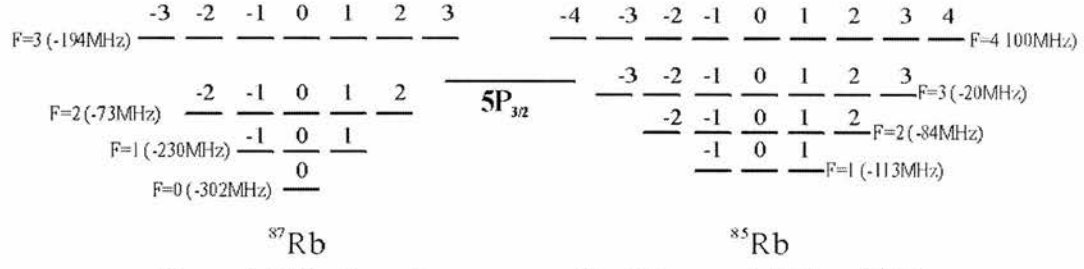

Figure 2.11(c): *Hyperfine structure of the $5P_{1/2}$ state in ^{87}Rb and ^{85}Rb.*

The hyperfine structure of the $5D_{5/2}$ state in ^{87}Rb will be detailed in Chapter 5 when it becomes relevant for the observation of EIT. More detailed examinations of the level structure of rubidium can be found in [4, 5].

2.4.2 Doppler Broadening

In an ideal experimental system we would be able to ignore Doppler broadening. Physically this would correspond to experiments carried out in either a 'cold' atomic sample (Bose Einstein condensate, optical trap) or in an atomic beam. In an experiment carried out in a gas cell, for example, we must also include the effects of Doppler broadening. This may be introduced by integrating the density matrix element of interest over the Maxwellian velocity distribution of the atoms under consideration. This is given by:

$$N(v) = \frac{N_0}{u\sqrt{\pi}} \exp[-\frac{v^2}{u^2}] \tag{2.35}$$

where v is the atomic velocity, N_0 is the atomic density and u is the average atomic velocity given by:

$$u = \sqrt{\frac{2k_B T}{M}} \tag{2.36}$$

T is the temperature in Kelvin and M is the atomic mass. Thus the Doppler broadened profile is given by:

$$\mathrm{Im}[\rho_{ji}] = \frac{N_0}{u\sqrt{\pi}} \int_{-\infty}^{\infty} \mathrm{Im}[\rho_{ji}(v)] \exp[-\frac{v^2}{u^2}] dv \tag{2.37}$$

We must also introduce Doppler contributions into the field detunings. For example we modify the detunings in equations (2.31) and (2.32) as follows:

$$\Delta_p = \omega_p - \omega_{12} - k_p V_z \tag{2.38}$$

$$\Delta_c = \omega_c - \omega_{13} - k_c V_z \tag{2.39}$$

where k_p and k_c are the wavevectors for the probe and coupling field ($k = 2\pi/\lambda$) and V_z is the velocity of a particular atomic velocity group. Hence $k_p V_z$ gives the Doppler shift contribution to the detuning of the probe field.

A Doppler broadened EIT profile is shown in figure 2.12. As we would expect the Doppler broadened lineshape is much broader than that of the homogeneous lineshape. Doppler broadening will act to destroy any EIT within a given system because the EIT at each velocity group will act to mask the EIT at line centre. EIT can still be observed in Doppler broadened systems however, but it requires a larger coupling field Rabi frequency than in the non-Doppler broadened case to see any effect.

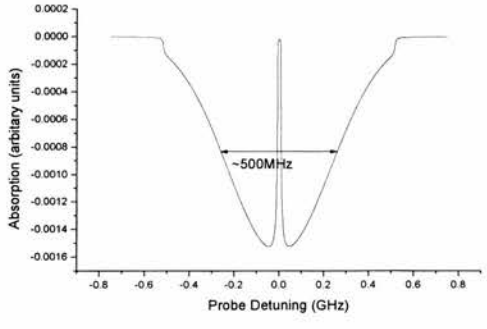

Figure 2.12: *Doppler broadened EIT profile for a cascade scheme. The probe field is at 780nm and the coupling field at 776nm. The coupling field strength is 600MHz. The profile is much broader than that in the non-Doppler case shown in figure 2.2(a).*

2.4.3 Beam Geometries and EIT

In non-Doppler broadened schemes the beam geometry of the probe and coupling fields is unimportant. In a Doppler broadened system however it is important to take the relative directions of the beams into account since the Doppler shift seen by a particular beam is proportional to its wavenumber. This is since in order to *observe* EIT we must have a condition of two-photon resonance:

$$\Delta_p \pm \Delta_c = 0 \tag{2.40}$$

where the + sign corresponds to the cascade scheme and the – to the lambda and vee schemes. This implies, to best deal with Doppler effects, that in the case of a cascade scheme the probe and coupling field should counter-propagate and in the lambda and vee schemes they should co-propagate. In the case where the probe and coupling field wavelengths are the same we can operate in a Doppler free regime, i.e. all the velocity groups experience EIT at the same probe frequencies. But if the wavelengths are different, each velocity group will experience EIT at a different probe frequency. Then the EIT at line centre will be either completely or significantly masked in the integration process described in 2.4.2 above. Thus the beam geometry of the probe field relative to the coupling field is particularly important in Doppler broadened systems. These effects will be discussed in more detail in Chapter 3.

References

[1] **S. Alam**, *Lasers without inversion and electromagnetically induced transparency*. (SPIE Press, Washington, 1999).

[2] **M. O. Scully and M. Suhail Zubairy**, *Quantum Optics*. (CUP, Cambridge, 1997).

[3] **R. R. Moseley**, *Sum Frequency Mixing and Quantum Interference in Three Level Atoms*, PhD thesis, University of St. Andrews (1994).

[4] **D. J. Fulton**, *Quantum Interference Effects: Electromagnetically Induced Transparency and Focussing*, PhD thesis, University of St. Andrews (1996).

[5] **J. R. Boon**, *Electromagnetically Induced Transparency and Inversionless Lasing*, PhD thesis, University of St. Andrews (1998).

[6] **E. Zekou**, *Atomic Coherence Effects: Electromagnetically Induced Transparency and Inversionless Lasing*, PhD thesis, University of St. Andrews (1998).

[7] **J. P. Marangos**, "Topical review electromagnetically induced transparency," *Journal of Modern Optics* **45**, 471-503 (1998).

[8] **S. E. Harris**, "Electromagnetically induced transparency," *Physics Today* **50**, 36-42 (1997).

[9] **M. H. Dunn**, *Electromagnetically Induced Transparency*. in *SUSSP 47: Laser Sources and Applications*Eds. 1995) pp. 411-446.

[10] **M. Sargent, M. O. Scully and W. E. Lamb**, *Laser Physics*. (Addison Wesley, Reading, Mass., 1974).

[11] **L. D. Landau and E. M. Liftshitz**, *Quantum Mechanics*. (2nd ed.) (Pergamon Press, London, 1959).

[12] **P. Meystre and M. Sargent**, *Elements of Quantum Optics*. (3rd ed.) (Springer-Verlag, Berlin, 1999).

[13] **S. M. Barnett and P. M. Radmore**, *Methods in Theoretical Quantum Optics*. (OUP, Oxford, 1997).

[14] **C. E. Moore**, "Atomic Energy Levels - As derived from the analyses of optical spectra," *Circular of the National Bureau of Standards*, 467 (1952).

[15] **O. S. Heavens**, "Radiative transition probabilities of the lower excited states of the alkali metals," *Journal of the Optical Society of America* **51**, 1058-1061 (1961).

[16] **A. Lingard and S. E. Neilsen**, *Atomic Data and Nuclear Data Tables*. (Academic Press, New York and London, 1977).

[17] **W. L. Wiese and G. A. Martin**, *A Physicist's Desk Reference*. (American Institute of Physics, 1989).

[18] **C. E. Theodosiou**, "Lifetime of alkali-metal-atom Rydberg states," *Physical Review A* **30**, 2881 (1984).

[19] **A. Yariv**, *Quantum Electronics*. (3rd ed.) (John Wiley & Sons, Singapore, 1989).

[20] **R. R. Moseley, B. D. Sinclair and M. H. Dunn**, "Local-field effect in the 3-level atom," *Optics Communications* **108**, 247-252 (1994).

[21] **C. Cohen-Tannoudji, J. Dupont-Roc and G. Grynberg**, *Atom-Photon Interactions*. (Wiley-Interscience, New York, 1998).

[22] **J. Geabanacloche, Y. Q. Li, S. Z. Jin and M. Xiao**, "Electromagnetically induced transparency in ladder-type inhomogeneously broadened media - theory and experiment," *Physical Review A* **51**, 576-584 (1995).

[23] **R. R. Moseley, S. Shepherd, D. J. Fulton, B. D. Sinclair and M. H. Dunn**, "2-photon effects in continuous-wave electromagnetically-induced transparency," *Optics Communications* **119**, 61-68 (1995).

[24] **S. Wielandy and A. L. Gaeta**, "Investigation of electromagnetically induced transparency in the strong probe regime," *Physical Review A* **58**, 2500-2505 (1998).

[25] **G. S. Agarwal**, "Nature of the quantum interference in electromagnetic-field-induced control of absorption," *Physical Review A* **55**, 2467-2470 (1997).

[26] **H. R. Gray, R. M. Whitley and C. R. Stroud**, "Coherent trapping of atomic populations," *Optics Letters* **3**, 218 (1978).

[27] **A. Imamoglu, J. E. Field and S. E. Harris**, "Lasers without inversion - a closed lifetime broadened system," *Physical Review Letters* **66**, 1154-1156 (1991).

[28] **M. O. Scully, S. Y. Zhu and A. Gavrielides**, "Degenerate quantum-beat laser - lasing without inversion and inversion without lasing," *Physical Review Letters* **62**, 2813-2816 (1989).

[29] **S. Shepherd**, *Use and Development of a CW Titanium Sapphire Laser for Nonlinear Optics*, PhD thesis, University of St. Andrews (1993).

[30] **D. M. Kane**, *Atomic Spectroscopy in the UV and Visible*, PhD thesis, University of St. Andrews (1983).

Chapter 3

EIT in Wavelength Mismatched Systems

3.1 Introduction

Much of the early work on EIT and LWI was proof of principle type work [1-3]. The experiments carried out, particularly in the continuous wave regime, used probe and coupling fields whose wavelengths were more or less the same, i.e. they were *matched.* However, for many of the useful applications of EIT, such as short wavelength inversionless lasing and enhancement of nonlinear processes it is desirable to use a longer wavelength coupling field, one which is more technologically attainable, to control a shorter wavelength probe field. Such experiments require the use of *mismatched* wavelengths. Previous work in this group by Boon *et al.* has demonstrated mismatched continuous wave EIT in rubidium [4]. In this experiment an infrared coupling field at 780nm was used to control a blue probe field at 422nm. The scheme employed is shown below in figure 3.1.

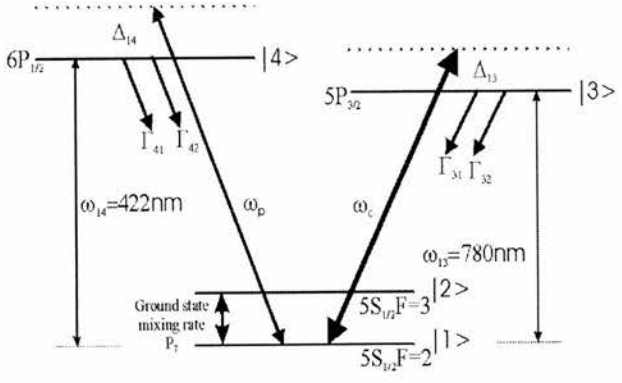

Figure 3.1: *Level scheme for the observation of EIT on a blue line in rubidium.*

The significance of this work is that it demonstrated for the first time that mismatched EIT in a Doppler broadened medium, where the probe wavelength is shorter than the coupling field by a significant margin, was possible and thus opened up the possibility of inversionless lasing in such regimes. In such a mismatched system the main difficulties to overcome are due to Doppler broadening. In a matched wavelength system the experimental beam geometry can be altered, in effect, to cancel out the Doppler broadening of the atomic medium, the so-called Doppler-free configuration. In mismatched systems this is no longer the case as the two-photon Doppler width will be much larger due to the wavevectors for the two beams being of unequal magnitude. In order to observe EIT it is necessary to split beyond this two-photon width and as this increases with mismatching wavelength it becomes correspondingly harder to observe EIT.

The experiment was also notable for two other reasons: firstly it was possible to observe EIT with no noticeable optical pumping effects, which is not usually the case in V-schemes. This was

explained by the proposal that the coupling field was strong enough to interact with both hyperfine levels in the ground state and thus mixing them, overcoming the optical pumping. A fuller treatment of this experiment is given in [4-6]. Secondly it was shown that EIT in a Doppler broadened system could be carried out with coupling field Rabi frequencies of less than the Doppler width of the probe transition. This was contrary to what was previously thought. This was due to the fact that the experiment was carried out in a Vee-scheme. The advantage that is inherent in the Vee scheme, namely the rapid reduction of the two photon absorption as the coupling field is detuned from resonance, is discussed below.

In this chapter the work carried out by Boon *et al* [4] and Shepherd *et al* [7] on mismatched systems is extended. Boon *et al* examined experimentally the case where the probe field wavelength was shorter than the coupling field wavelength, in a Vee-scheme. Shepherd examined, again experimentally, the case with matched wavelengths and where the probe field wavelength was longer than the coupling field wavelength. This was carried out in a cascade scheme. We examine, theoretically, two situations, (1) a comparison of EIT in the standard cascade, lambda and Vee-schemes under conditions of matched and mismatched wavelengths and (2) whether it is possible to see inversionless gain in mismatched Doppler broadened systems. We introduce a diagrammatic representation which is particularly valuable in providing insight into the limiting processes involved in the different level configurations.

3.2 Comparison of Mismatched Systems

3.2.1 Basis of Comparison

In order to fairly compare the three basic schemes for EIT (cascade, lambda and Vee) it is necessary to deal with hypothetical level structures. This is necessary to ensure that decay rates and probe and coupling field wavelengths can be directly compared. This would obviously not be the case if we used a real atomic system for each case. Here we assume the three closed level systems shown in figure 3.2.

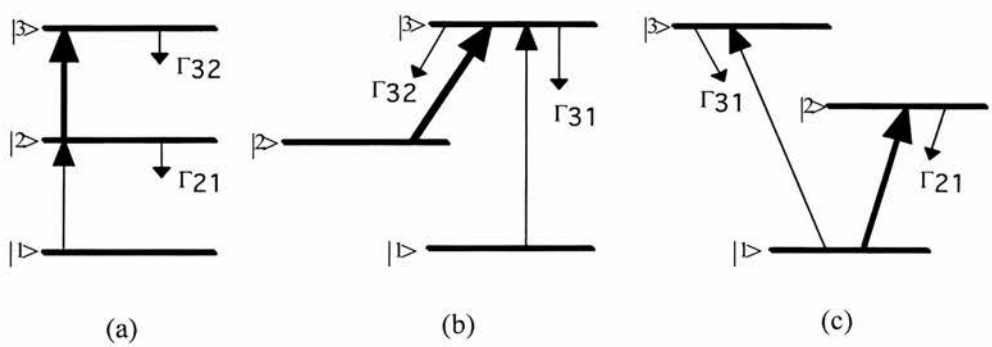

Figure 3.2: *Energy level configurations under consideration (a) Cascade (b) Lambda and (c) Vee. The thick solid line represents the coupling field, the thin solid line the probe field.*

All the decay rates are set to $40x10^6 s^{-1}$ and the dephasing on the unlinked transition is set to $40x10^6 s^{-1}$ as well. This latter value corresponds to the maximum dephasing that would occur due to level lifetime effects alone, e.g for $\Gamma_{ij}=40x10^6 s^{-1}$, and the dephasing for the ij^{th} transition given by:

$$\gamma_{ij} = \frac{1}{2}\left(\sum_k \Gamma_{ik} + \sum_l \Gamma_{jl}\right) + \gamma_{deph} \tag{3.1}$$

where γ_{deph} is any dephasing other than that due to level lifetime effects (e.g collisions) and k indicates all the levels into which population may decay from level i (k<i).The subscript l denotes all the levels in to which population may decay from level j (l<j), the condition is:

$$\gamma_{ij} \leq 40\times10^{-6} s^{-1} \tag{3.2}$$

These values are chosen as they are loosely based on decay rate parameters found in atomic rubidium. In order to directly compare the absorption profiles in each case we keep the wavelength of the probe field constant at 800nm and allow the coupling field to vary, with values of 400nm, 800nm and 1600nm. This leads to a total of nine different considered schemes, three for each of the cascade, lambda and Vee manifolds in the wavelength regimes $\lambda_c<\lambda_p$, $\lambda_c=\lambda_p$ and $\lambda_c>\lambda_p$. We use a probe field Rabi frequency of 100kHz, which is weak compared to the coupling field and also will not significantly alter the population in the lower state of the probe transition. The Rabi frequency of the coupling field is set at half the value of the Doppler width of the probe transition. These values are 250MHz and 500MHz respectively. The Doppler width is calculated assuming that the probe is interacting with rubidium vapour at 40°C, which would allow significant absorption in the infrared. This is based on past experience of experimental work in rubidium [7-9]. The systems under question are then analysed using the density matrix formalism outlined in chapter 2 (section 2.2).

3.2.2 Autler-Townes Components

The application of a strong field to an atomic transition will result in the levels comprising that transition splitting into two components. When this transition is probed by another field, coupling one of the split levels to another unconnected level, the probe absorption profile is seen to display the Autler-Townes splitting shown in figure 1.3. We term the two split components seen in the probe absorption the *Autler-Townes components*. The positions of the components will depend on the strength of the strong coupling field and its detuning from its transition.

The positions of the Autler-Townes components are calculated for the Cascade scheme and for the Lambda and Vee schemes using the following two equations respectively:

$$\Delta_{probe} = k_1 V_z - \frac{1}{2}\left(\Delta_{coupling} + k_2 V_z\right) \mp \frac{1}{2}\left(\sqrt{\Omega_c^2 + \left(\Delta_{coupling} + k_2 V_z\right)^2}\right) \tag{3.3}$$

$$\Delta_{probe} = k_1 V_z + \frac{1}{2}\left(\Delta_{coupling} - k_2 V_z\right) \pm \frac{1}{2}\left(\sqrt{\Omega_c^2 + \left(\Delta_{coupling} - k_2 V_z\right)^2}\right) \tag{3.4}$$

where Δ_{probe} and $\Delta_{coupling}$ refer to the detuning of the zero velocity group in the lab frame (we subsequently refer to this as the "manual detuning"), k_1 and k_2 are the wavevectors of the probe and coupling fields respectively, V_z is the atomic velocity, and Ω_c is the coupling field Rabi frequency. In equation (3.3) and (3.4) we have assumed co-propagating beams in the Lambda and Vee-type schemes and counter-propagating beams in the Cascade system. Differences in the nature of the energy level configurations are counterbalanced by selecting these beam geometries so that the Autler-Townes components and absorption resonances occur in the same positions for all three schemes, for a given set of probe and coupling wavelengths. Inspecting Eqs. (3.3) and (3.4) confirms this for the limiting case of zero manual detuning of the coupling field (i.e. $\Delta_{coupling}$ =0). The positions of the absorption resonances for all three schemes are given, for the single and two-photon absorptions respectively, by:

$$\Delta_{probe} = k_1 V_z \tag{3.5}$$

$$\Delta_{probe} = k_1 V_z - k_2 V_z + \Delta_{coupling} \tag{3.6}$$

where we assume $\Delta_{coupling}$ =0. Although, in this limiting case, the positions of the Autler-Townes components and absorption resonances are the same for all schemes; crucially, significant differences are manifested in the magnitudes of the Autler-Townes components for the different configurations.

3.2.3 Theoretical Results

The calculated absorption profiles for the three systems are plotted in figure 3.3. Figures 3.4, 3.5 and 3.6 provide two-dimensional displays of the Autler-Townes absorption components and the single and two photon resonance positions as a function of probe field detuning and atomic velocity for the different schemes. The results presented here can be explained by the fact that the change in absorption with atomic velocity is different in each of the threes schemes and for each of the wavelength regimes. Figure 3.4, 3.5 and 3.6 follow a similar display technique used by Townes and Schawlow [10], in that we plot, as a function of probe field detuning, the individual contributions made by different velocity groups across the Doppler profile to the absorption of the probe in the presence of the coupling field. A horizontal line taken across the diagram refers to a particular velocity group. The points at which such an horizontal line intersects the two plotted curves gives the field detunings corresponding to the locations of the Autler-Townes components for that particular velocity group. The thickness of the plotted curve at each point of intersection gives the absorption associated with that particular Autler-Townes component as experienced by the probe field. The absorption is calculated using a density matrix analysis, with allowance made for the relative population of atoms in the particular velocity group as well as for the effects of detuning. It is important to note that the thickness of the line should be read

along a normal to the tangent at the given point on the curve. This avoids ambiguities at the turning point on some of the curves. If a vertical line is drawn on the diagram corresponding to a particular probe field detuning, the locations of its intersection(s) with the plotted curves identify the velocity group or groups (predominantly) responsible for the absorption experienced by the probe field. Further, the sum of the thicknesses of the two curves at these intersection points indicates the total absorption experienced by the probe field at such a detuning. These plots thus contain all the information necessary to explain the presence or lack of a transparency in the associated absorption profile. In producing the curves we assume a Doppler-free type configuration – by selecting such beam geometries to achieve this situation differences in the nature of the three schemes are counterbalanced so that the Autler-Townes components and absorption resonances are at the same positions in each of the three schemes for a given set of probe and coupling wavelengths.

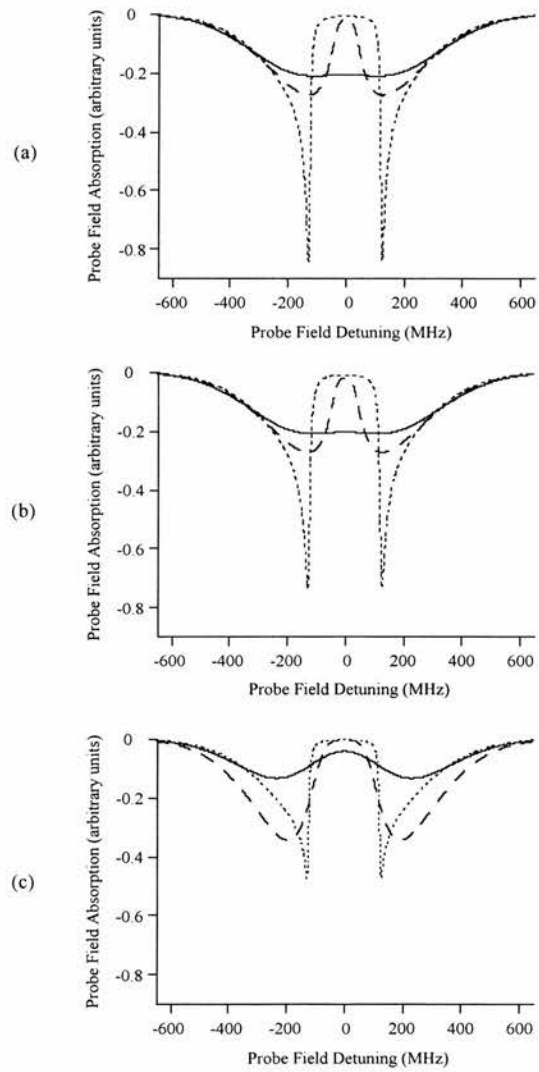

Figure 3.3: *Absorption profiles for (a) Cascade (b) Lambda and (c) Vee-schemes. In each case the dotted line represents the $\lambda_c<\lambda_p$ regime, the dashed line the $\lambda_c=\lambda_p$ regime and the solid line the $\lambda_c>\lambda_p$ regime.*

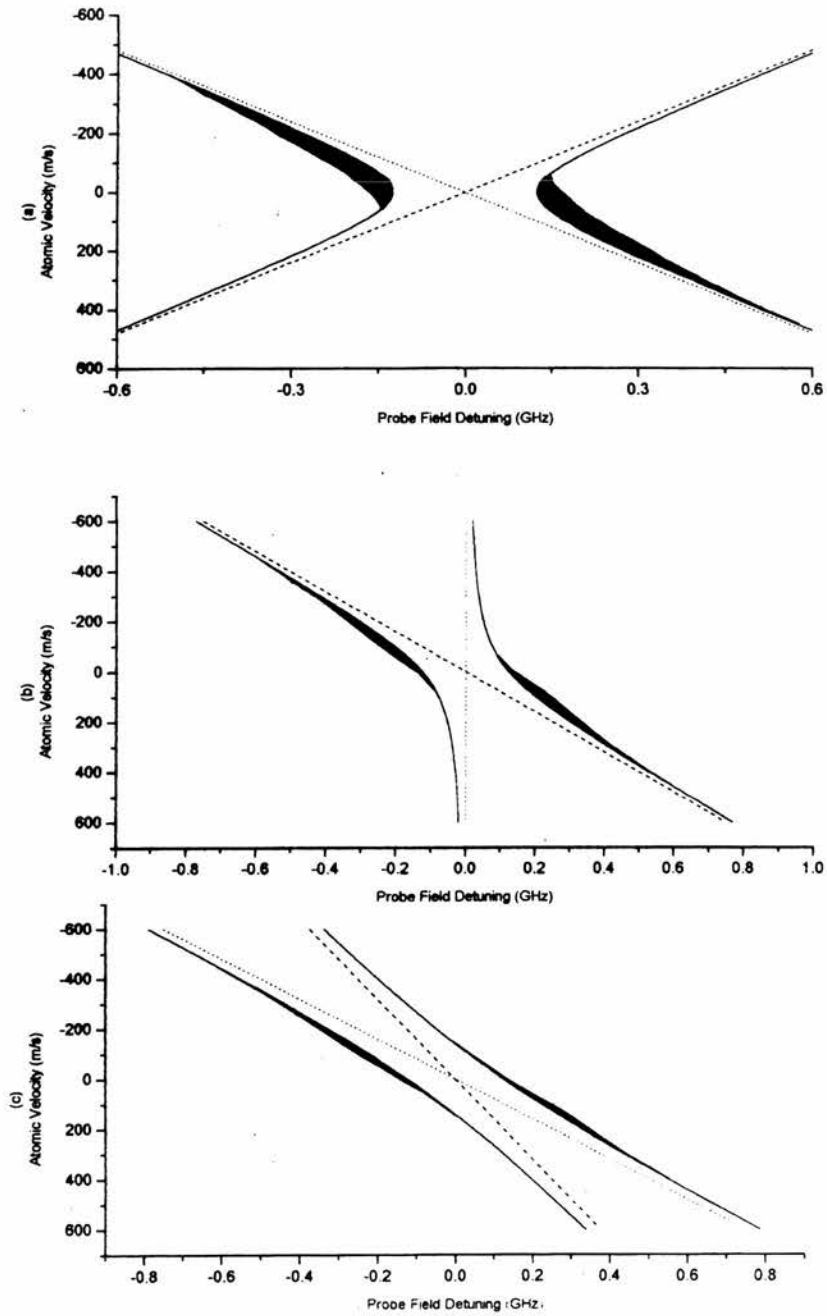

Figure 3.4: *Plots of the Autler-Townes and absorption resonance positions as a function of atomic velocity and probe field detuning for the cascade scheme. Three wavelength regimes are displayed (a) $\lambda_c<\lambda_p$, (b) $\lambda_c=\lambda_p$, and (c) $\lambda_c>\lambda_p$. The magnitude of the Autler-Townes components is indicated, in each plot, by the thickness of the lines read in the direction of the normal to the tangent to the Autler-Townes components at a given atomic velocity. The thickness of these lines is proportional to the absorption coefficient for the atomic velocity specified. The positions of the Autler-Townes components are shown by solid lines, the single photon resonance by a dashed line, and the two-photon resonance by a dotted line.*

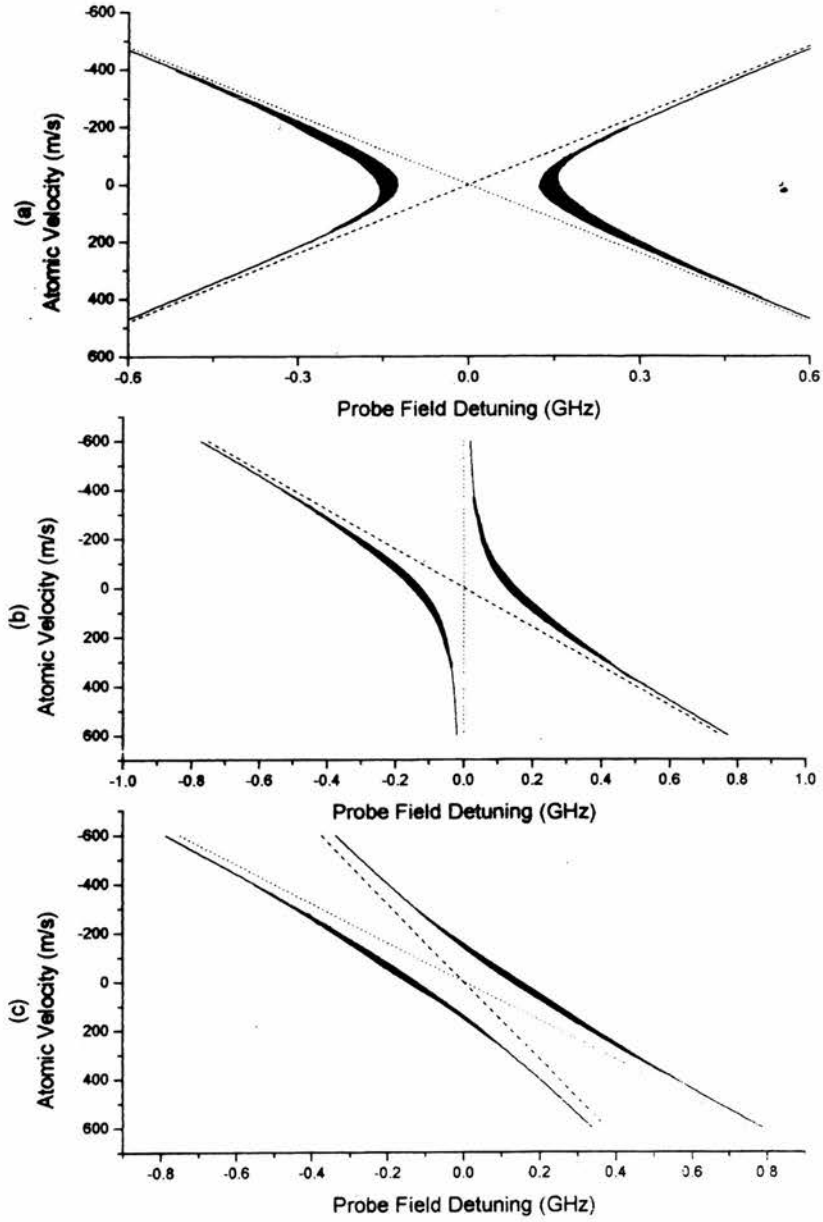

Figure 3.5: *Plots of the Autler-Townes and absorption resonance positions as a function of atomic velocity and probe field detuning for the lambda scheme. Three wavelength regimes are displayed (a) $\lambda_c<\lambda_p$, (b) $\lambda_c=\lambda_p$, and (c) $\lambda_c>\lambda_p$. The magnitude of the Autler-Townes components is indicated, in each plot, by the thickness of the lines read in the direction of the normal to the tangent to the Autler-Townes components at a given atomic velocity. The thickness of these lines is proportional to the absorption coefficient for the atomic velocity specified. The positions of the Autler-Townes components are shown by solid lines, the single photon resonance by a dashed line, and the two-photon resonance by a dotted line.*

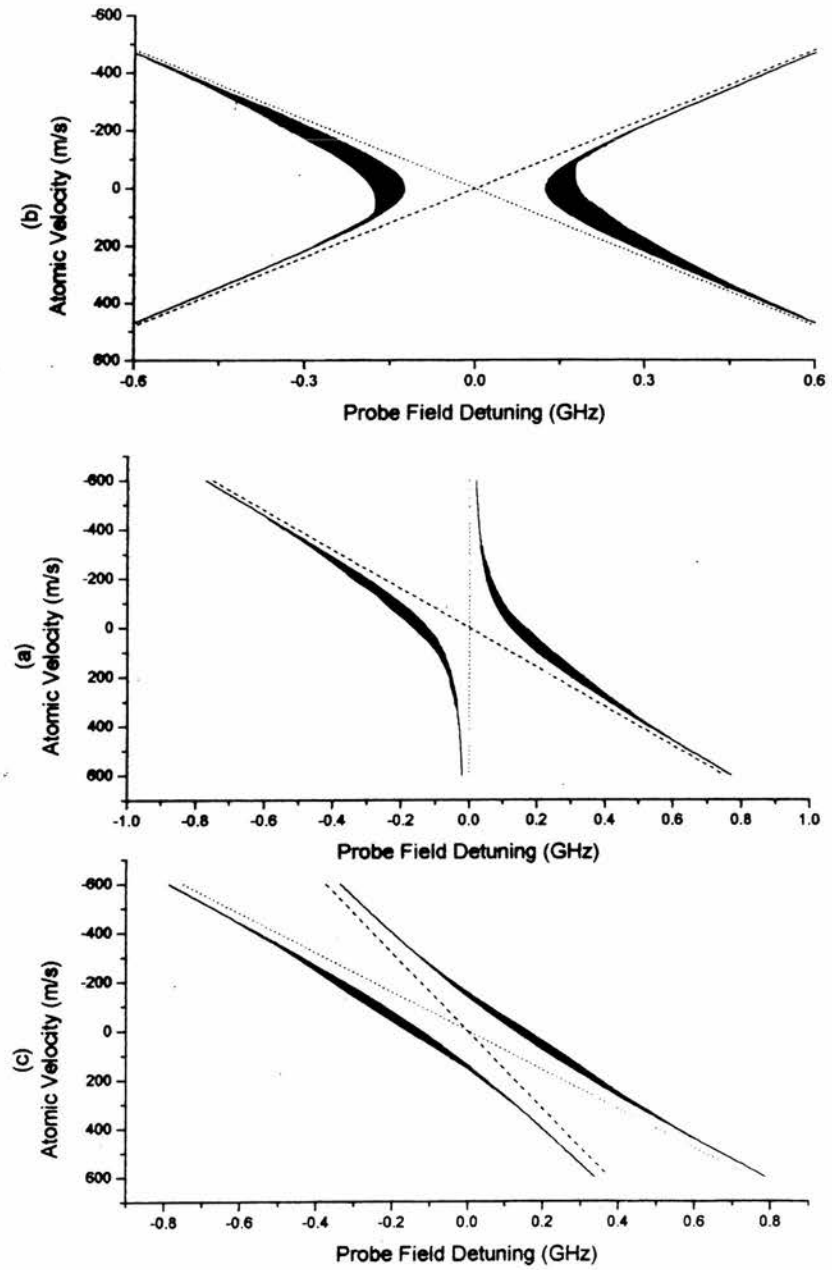

Figure 3.6: *Plots of the Autler-Townes and absorption resonance positions as a function of atomic velocity and probe field detuning for the Vee-scheme. Three wavelength regimes are displayed (a) $\lambda_c<\lambda_p$, (b) $\lambda_c=\lambda_p$, and (c) $\lambda_c>\lambda_p$. The magnitude of the Autler-Townes components is indicated, in each plot, by the thickness of the lines read in the direction of the normal to the tangent to the Autler-Townes components at a given atomic velocity. The thickness of these lines is proportional to the absorption coefficient for the atomic velocity specified. The positions of the Autler-Townes components are shown by solid lines, the single photon resonance by a dashed line, and the two-photon resonance by a dotted line.*

In the zero velocity group the Autler-Townes components are symmetric about the zero coupling field detuning point. When the coupling field is detuned, however, the components are asymmetric. Use of the appropriate beam geometries ensures that the locations of the two components for a given velocity group are the same in each of the schemes for a given probe field, coupling field wavelength ratio. Only the magnitude of the absorption differs in each of the three schemes for each wavelength regime. In section 3.2.4 we distinguish between the two Autler-Townes components for any given system by noting that for high velocities the components split further apart and that one follows the position of the single photon resonance and the other follows the two-photon resonance position. The component that follows the single photon resonance is referred to as the *primary* Autler-Townes component while the other component is the *secondary* Autler-Townes component. These are shown in figure 3.7

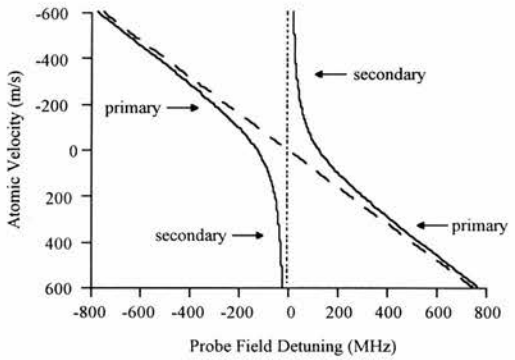

Figure 3.7: *Plot of the Autler-Townes and absorption resonance positions as a function of atomic velocity and probe field detuning. The primary and secondary Autler-Townes components are labelled.*

3.2.4 Discussion

We can see by inspection of figure 3.3 that EIT is always worse in the case where the probe wavelength is less than the coupling field wavelength. EIT is improved, however, compared to the case where the wavelengths are equal, when the probe field wavelength is greater than the coupling field wavelength. In the Vee-type scheme we can see how this happens by considering the two routes to excitation model of EIT. A single probe photon can be absorbed exciting the atom from state |1> to state |2>. Alternatively the atom may reach state |2> by absorbing a coupling field photon, moving to state |3>, moving back to |1> and then absorbing a probe photon to take it to level |2>. This is illustrated in figure 3.8. By considering the one and two photon resonance positions in figures 3.4, 3.5 and 3.6 we can see that the two pathways to absorption are only coincident for the zero velocity group at zero probe field detuning. The absorption process associated with a given velocity group is not limited to a discrete velocity group but covers the homogeneously broadened lineshape centred on the positions indicated in figures 3.4, 3.5 and 3.6. EIT can therefore occur at any point where the one and two photon absorption lineshapes overlap to this extent. In the case where the magnitudes of the absorption routes are equal, for a given frequency, full cancellation may take place. If, at a specific frequency, the magnitudes of

the absorptions are unequal only a partial reduction in absorption will be seen. In the case where the absorption resonances for a given velocity group are separated by more than the homogeneous linewidth EIT does not occur, and increasingly it is important to make sure that the associated (Autler-Townes split) absorption components do not obscure the transparency that is created on resonance for other velocity groups.

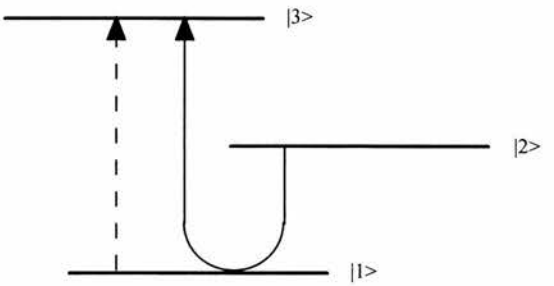

Figure 3.8: *One and two photon routes in a Vee scheme.*

The best transparency occurs when the coupling field wavelength is shorter than that of the probe field (a down conversion process) because the Doppler detuning (the Doppler-shifted contribution to the coupling field detuning) is greatest in this case. The Doppler shift in the frequency of the coupling field is proportional to the frequency of the coupling field itself (i.e. to $k_c V_z$) and will therefore increase in magnitude if we decrease the coupling field wavelength. So, Autler-Townes splitting, which is dependent on detuning, will also increase as the coupling wavelength decreases. In the $\lambda_c<\lambda_p$ regime the Autler-Townes components for the non-zero velocity atoms are split further apart and therefore further away from resonance. Thus, EIT created at line centre for the zero velocity group is better preserved in this mismatched wavelength regime because the Autler-Townes components of the non-zero velocity atoms are Doppler detuned away from resonance and do not overlap with the transparency. Part (a) of figures 3.4, 3.5, and 3.6 clearly show the Autler-Townes splitting increasing with the modulus of the velocity so that coincidence of the single and two-photon resonances (the point for which maximum EIT occurs) at line centre is not obscured.

As we increase the coupling wavelength relative to the probe wavelength the magnitude of the Doppler detuning decreases relative to the Doppler width of the absorption profile, which is fixed by the probe wavelength. The Autler-Townes splitting for the non-zero velocity atoms will tend towards that for the zero velocity atoms and the associated Autler-Townes absorptions will start to overlap with the line centre transparency. The matched wavelength regime represents the special case when the Doppler shifts of the probe and coupling fields are equal and exactly cancel, ensuring that the two-photon resonance position is fixed for all velocity groups. This is the so-called Doppler free situation and is routinely employed in EIT experiments to negate the effects of Doppler broadening. The result is that the non-zero velocity, secondary, Autler-Townes absorptions only partially obscure the on-resonance transparency. The extent to which the transparency can be maintained in this regime depends largely on the dephasing. If dephasing is

increased the linewidth of the Autler-Townes absorption components close to resonance will increase and further encroach on the transparency window.

In the $\lambda_c>\lambda_p$ regime figures 3.4(c), 3.5(c), and 3.6(c) show that the Autler-Townes components overlap completely with line centre. Following the argument through from the $\lambda_c>\lambda_p$ and $\lambda_c=\lambda_p$ cases we would expect the transparency created on resonance to be obscured and this is exactly what happens in the Lambda and Cascade systems. However, in the Vee-type scheme the transparency window is maintained to a greater extent. This can be explained by considering the magnitude of the Autler-Townes components close to resonance. Careful inspection of the traces depicted in figures 3.4, 3.5, and 3.6 reveals that while the positions of the Autler-Townes components are the same in each energy level scheme, for a given set of wavelengths, the magnitudes are different (denoted by the line thicknesses). For high positive and negative velocities the primary and secondary Autler-Townes components separate and closely follow the single and two-photon resonance positions. In this regime the magnitude of each component is determined predominantly by the particular absorption resonance associated with it. The single photon absorption defines the magnitude of the primary Autler-Townes component and the two-photon absorption determines the magnitude of the secondary component. It is the secondary Autler-Townes components that overlap with the on-resonance transparency in the $\lambda_c>\lambda_p$ regime. In a Vee-type system the magnitude of these secondary components falls off very rapidly as velocity increases and consequently the transparency at line centre is not destroyed to the same extent as it is in the Cascade and Lambda schemes.

In all three schemes it is also apparent that the magnitude of these secondary Autler-Townes components falls off more rapidly with increasing velocity when the coupling wavelength is lower. This trend occurs because, as has been pointed out above, the Doppler shifted contribution to the coupling field detuning, for a given velocity, is greater for a higher coupling field frequency. Consequently, the coupling field detuning changes and the two-photon resonance moves further from the intermediate atomic level as the coupling field wavelength is decreased. Since the magnitude of the secondary Autler-Townes components are dependent on the strength of the two-photon process they reduce as the two-photon resonance moves away from simultaneous resonance with the intermediate state. This diminution of the secondary Autler-Townes components always occurs as velocity increases in a given system. Importantly, it occurs more rapidly when coupling wavelength is lower and the Doppler shift is consequently greater for a given velocity.

The preceding argument applies to all three considered schemes but the Vee configuration exhibits a more sudden reduction in the magnitude of the secondary Autler-Townes components. The explanation for this lies in the nature of the two-photon process. In a Vee scheme the two-photon absorption route begins in the upper level of the coupling transition and therefore relies on that level being significantly populated. When the coupling field is detuned by the Doppler shift

associated with non-zero velocity atoms the population excited into the upper level of the coupling transition rapidly falls off. Consequently, the reduction in the magnitude of the two-photon absorption is markedly more rapid in a Vee scheme with increasing atomic velocity and the secondary Autler-Townes components that overlap with line centre are of such a low magnitude that the transparency may still be observed.

To illustrate how the two-photon process differs in each scheme we examine how the two-photon absorption changes as we detune the coupling field. Figure 3.9 shows a series of traces, for each energy level scheme, in which the coupling field is manually detuned. EIT diminishes as the manual detuning of the coupling laser is increased because the two-photon and single photon resonances no longer coincide at line centre. This detuning also shows the two-photon nature of the EIT process itself. EIT is destroyed as the one and two photon resonances are separated. Gradually the single and two-photon processes are resolved as distinct absorption peaks. The resolved two-photon peak in the Vee scheme is seen to quickly disappear, while it persists for the Lambda and Cascade systems.

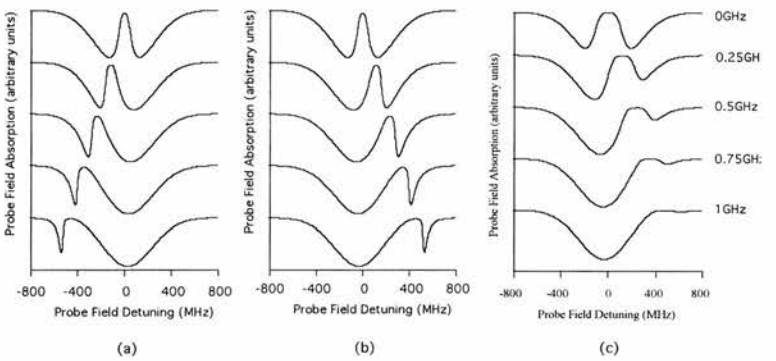

Figure 3.9: *Absorption traces for (a) Cascade, (b) Lambda and (c) Vee-schemes as the coupling field is detuned. The uppermost trace shows the absorption with zero coupling field detuning, i.e. perfect EIT. Successive traces show the two-photon feature being detuned away from the one photon resonance point. This is illustrative of the one and two photon interference process that leads to EIT*

Due to the fortuitous nature of the two-photon process in the Vee scheme, which we term the *Vee-scheme advantage*, the induced transparency is better than in a Cascade or Lambda scheme for each of the wavelength regimes. Indeed, comparison of the transparency induced in the mismatched ($\lambda_c > \lambda_p$) Vee scheme and the matched ($\lambda_c = \lambda_p$) Cascade and Lambda systems indicates that while the transparency is slightly deeper in the latter case it is broader in the former. Direct comparison of the absorption profiles in the mismatched, $\lambda_c > \lambda_p$, regime for all schemes shows that transparency is present in the Vee scheme while completely destroyed in the Cascade and Lambda systems, for our selected coupling field Rabi frequency. Figure 3.10 indicates the on-resonance absorption as a function of coupling field Rabi frequency. We can of course recover

EIT in the mismatched Lambda and Cascade by increasing the coupling field Rabi frequency to split the overlapping Autler-Townes components away from line centre by more than the Doppler width. However, importantly, transparency is achieved in the Vee scheme for a coupling field Rabi frequency significantly lower than the Doppler width (approximately 500MHz), which means that we can carry out these type of experiments at relatively low coupling field powers.

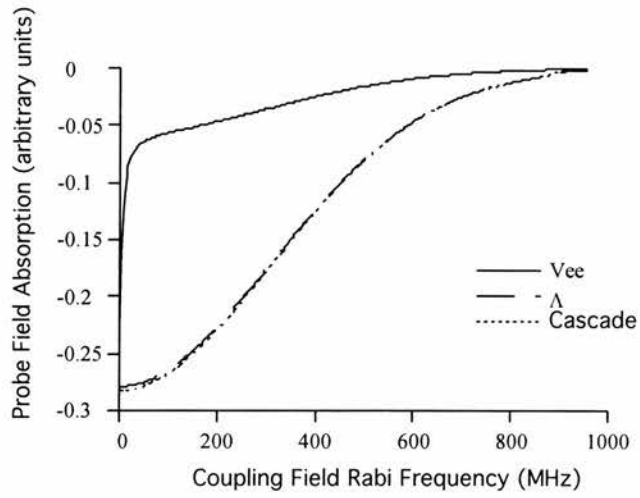

Figure 3.10: *On-resonance transparency plotted as a function of the coupling field Rabi frequency. The solid line depicts the Vee-scheme, the dashed line the Lambda scheme and the dotted line the Cascade scheme.*

3.2.5 Further Theoretical Considerations

The main results of the presented analysis have been discussed. We now consider some further points of interest that arise from the theoretical model. Firstly, in figures 3.4, 3.5, and 3.6 we see that as the coupling wavelength increases so does the range over which absorption may be observed in all three schemes. This increase in bandwidth occurs because the two-photon process persists for higher velocity atoms due to the reduction in the magnitude of the Doppler shift for a given atomic velocity. There is a corresponding reduction in the peak predicted absorption because the total number of absorbing atoms remains constant. The total integrated absorption is always the same regardless of the choice of probe and coupling wavelengths.

Secondly, if we compare the magnitudes of the Autler-Townes components of the Cascade and Lambda schemes we notice, for example, that while the absorption profiles for the matched wavelength systems are identical in figure 3.3 the Autler-Townes absorptions in figures 3.4 and 3.5 are of a lower magnitude in the Lambda scheme. This apparent discrepancy is due to linewidth effects. Referring back to figure 3.2, we see that for the Lambda scheme both the decay rates, Γ_{31} and Γ_{32}, describe population movement out of the upper level of the probe transition. The total decay from this level in the Lambda scheme, which determines the linewidth, is therefore twice the value for the Cascade and Vee-type systems. Consequently, the absorption profile of each individual Autler-Townes component is spread out in wavelength and reduced in

peak magnitude, with no change in the total absorption. When we integrate over all atomic velocities we therefore get the same 'net' absorption profile in the Cascade and Lambda schemes for the matched wavelength case.

So far, we have failed to take into account the effect of coupling field saturation. The cynic may claim that the difference in the three energy level schemes is a result of population transfer due to this effect rather than EIT. It is true to say that coupling field saturation plays its part in reducing the absorption as it does in any system based on a Vee scheme, but it is not the presence of this effect which allows us to observe transparency in the $\lambda_c > \lambda_p$ regime, rather the absence of it. Coupling field saturation occurs in a Vee scheme because the coupling field is connected to the ground state and therefore excites a fraction of the population from that state into the upper level of the coupling field transition. The exact proportion of the population excited in this way will depend upon the strength of the coupling field. There is of course an upper limit that occurs when the coupling field transition is saturated and the populations in the upper and lower levels are equalised. In a Doppler-broadened system this process is velocity selective. While the velocity group of atoms for which the coupling field is on-resonance will quickly become saturated, other velocity groups for which the coupling field is detuned will not. In the latter case, the effects of coupling field saturation are minimal.

Coupling field saturation is inextricably linked to EIT since the latter effect relies on the interference of single and two-photon absorption, and the magnitude of the two-photon absorption is dependent on the population in the upper level of the coupling transition. If we consider Figs. 3.4, 3.5, and 3.6 we see that the lack of a reduction in absorption in the Cascade and Lambda schemes is not due to a lack of induced transparency for the zero velocity group at line centre. In fact, EIT still takes place for atoms at rest, but it is masked by the secondary Autler-Townes absorptions of the higher velocity groups. In the Vee scheme, we still observe the transparency that is induced at line centre in the normal way, because the secondary Autler-Townes components - associated with the high velocity groups - that overlap with line centre are very small in magnitude. As discussed earlier, these Autler-Townes components are reduced in magnitude because the two-photon process is greatly diminished when the coupling field is detuned from resonance, i.e. when the coupling field saturation effect is negligible. It is therefore the lack of coupling field saturation for high velocity atoms that allows us to observe transparency in the Vee-type scheme for probe frequencies higher than the coupling field frequency. It is of course the case that absorption is halved by coupling field saturation of the zero velocity group atoms, but EIT effects reduce absorption well beyond this limit.

3.2.6 Extending the Wavelength Mismatch

The results discussed in section 3.2 can be broadly applied to any mismatched Doppler-broadened system. We have chosen to mismatch the wavelengths by varying the coupling field frequency while that of the probe is constant. In a real experimental scheme it would be more likely that the coupling field remained in the visible region of the spectrum while a higher

frequency was sought on the probe transition. However, it is the case that the level of transparency achievable in a system is the same for the same ratios of both coupling field to probe field wavelengths and driving Rabi frequency to Doppler width, regardless of the actual wavelengths involved. One further point to note is that the transition decay rates will also affect the level of observed transparency.

For the Vee scheme we have seen that in the $\lambda_c > \lambda_p$ regime significant transparency is predicted for a driving frequency that is half the Doppler width. In this system, the ratio of coupling and probe wavelengths is 2:1. We can therefore expect that a 200nm coupling transition driving a 100nm probe transition will induce that same level of transparency if the coupling field Rabi frequency is adjusted to be half the new Doppler-width and the transition decay rates are unchanged. If we further increase the ratio of coupling and probe fields then we would expect the induced transparency to degrade. In order to investigate this we have selected a Vee-scheme in which the coupling field is in the visible (500nm) and kept constant while the probe field wavelength is reduced, decay rates are the same as before. The ratios considered are approximately 2:1, 4:1, 8:1 and 16:1 and the results are shown in Fig. 3.11. As the probe field is changed the coupling field strength is altered to maintain the coupling field Rabi frequency at half the probe field Doppler-width in each case, if the Rabi frequency were not changed in this way we would expect the transparency to degrade more significantly. This takes the probe field down to 30nm, well into the VUV (Vacuum Ultraviolet). As can be seen, once the ratio increases to 8:1 (the probe at 60nm) there is no transparency window. There is, however, a reduction in absorption due to the presence of the coupling field beyond that expected from coupling field saturation alone. This reduction does manifest itself as a EIT window as the absorption reduction is spread out over the entire Doppler lineshape function.

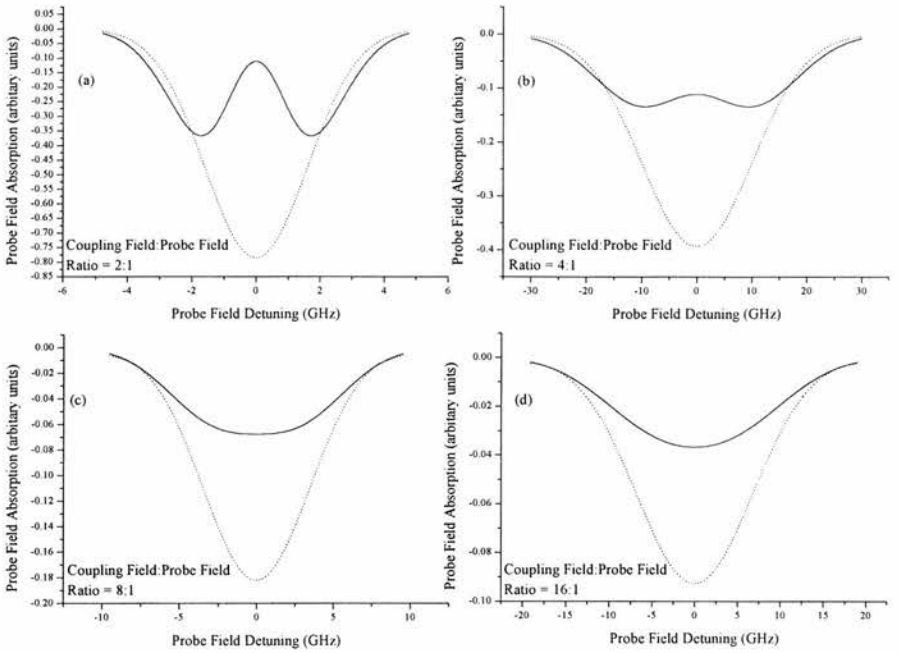

Figure 3.11 *EIT in mismatched Vee schemes. Plots detail probe field absorption in the absence (dotted line) and presence (solid line) of a coupling field. In (a) the probe field is 250nm, (b) 125nm, (c) 60nm, (d) 30nm. In all cases the coupling field wavelength is 500nm. The transparency window is seen to degrade as the probe field wavelength decreases.*

The implication is that EIT can be induced, in cases where the Rabi splitting is half the Doppler-width, for coupling field-probe field wavelength ratios of approximately 4:1 or less. In moving to higher ratios the Vee-scheme advantage is lost and Rabi splitting comparable or greater than the Doppler-width is required. Such results are important when practical inversionless lasing systems are under consideration. They are also important in schemes where a radio frequency field acts as the coupling field [11], indicating that a large amount of power will be required to induce transparencies on an optical transition (see also chapter 8).

The result that EIT is strongest for the mismatched $\lambda_c<\lambda_p$ wavelength regime in a Cascade scheme has been demonstrated to apply to all three energy level configurations. We have also highlighted the robust nature of the Vee-type system that results from the unique form of the two-photon process. While the induced transparency is more pronounced when the coupling field frequency is higher than that of the probe, induced transparency it is still realisable for high frequency probe systems in a Vee-type scheme. Indeed, the transparency induced in the mismatched Vee configuration ($\lambda_c>\lambda_p$) compares favourably with that induced in the matched Cascade and Lambda systems. While we have not employed a real atomic system in this analysis we have clearly shown that EIT can be realised in a probe field twice the frequency of the coupling field for a sub-Doppler width Rabi frequency. These results imply that the exploitation of quantum coherence effects are not confined to matched wavelength systems in Doppler-

broadened media, and that the Vee scheme provides the best potential level of transparency in a system subject to Doppler effects, particularly for configurations in which the probe frequency is far in excess of the coupling field frequency. These results may also have wider implications for other inhomogeneously broadened media such as quantum wells.

3.3 Prediction of Inversionless Gain in a Mismatched Doppler Broadened V-Scheme

We now move from general EIT in mismatched Doppler broadened systems to look at the possibility of observing inversionless gain in a specific system based on the experiment carried out by Boon *et al* [4] in which EIT on a blue line using an infrared coupling field was demonstrated. As is shown above the best prospect for achieving EIT in the frequency up-conversion regime is a Vee-scheme. So it seems sensible that we choose such a system to investigate whether we can exploit the Vee-scheme advantage.

3.3.1 Comparison of Matched and Mismatched Schemes

Once more, in order to compare fairly matched and mismatched schemes we must use artificially constructed systems. As in the comparison of EIT schemes we loosely base our systems on atomic rubidium. The schemes we compare are depicted in figure 3.12. We consider a matched and mismatched Vee-scheme. The mismatched scheme corresponds to real transitions in rubidium. The probe field is resonant with the $5S_{1/2}$-$6P_{1/2}$ transition, with a wavelength of 422nm. The coupling field has a wavelength of 780nm and is resonant with the $5S_{1/2}$-$5P_{3/2}$ transition. We ignore the hyperfine structure of the $5S_{1/2}$ state and use an idealised three level system. The matched system is also based on rubidium now with the coupling field resonant with the $5S_{1/2}$-$6P_{1/2}$ transition and has a wavelength of 422nm. The probe field remains the same as in the mismatched case. We make the systems exactly the same except for the wavelengths and we must use some arbitrary values for the decay rates, in order to make a realistic comparison. Thus the decay rate for the $6P_{3/2}$ state is altered from its true value. If we were to use this real value then, in the matched case, the amount of gain predicted actually reduces.

We assume that the rubidium gas is inside a cell heated to 130°C. This temperature corresponds to an experimentally measured absorption at the probe transition (422nm) of approximately 80%.

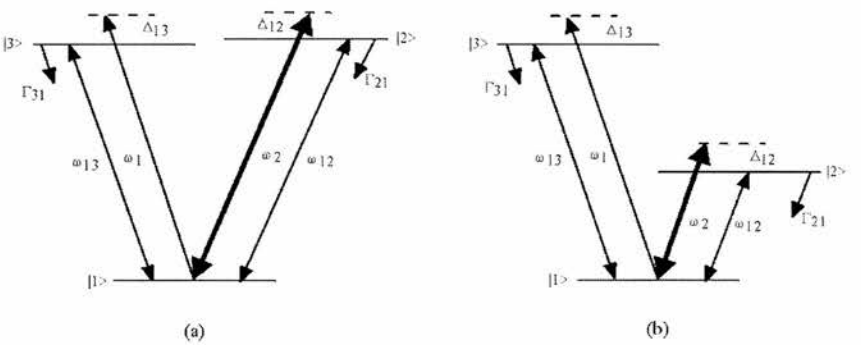

Figure 3.12: *(a) Matched and (b) mismatched Vee-schemes under consideration*

The two systems are modelled using the density matrix equations for a closed three level Vee-scheme:

$$\dot{\rho}_{11} = i\Omega_c(\tilde{\rho}_{21} - \tilde{\rho}_{12}) + i\Omega_p(\tilde{\rho}_{31} - \tilde{\rho}_{13}) + R_{13}(\rho_{33} - \rho_{11}) + \Gamma_{21}\rho_{22} + \Gamma_{31}\rho_{33} \quad (3.7a)$$

$$\dot{\rho}_{22} = i\Omega_c(\tilde{\rho}_{12} - \tilde{\rho}_{21}) - \Gamma_{21}\rho_{22} \quad (3.7b)$$

$$\dot{\rho}_{33} = i\Omega_p(\tilde{\rho}_{13} - \tilde{\rho}_{31}) - \Gamma_{31}\rho_{33} - R_{13}(\rho_{33} - \rho_{11}) \quad (3.7c)$$

$$\dot{\rho}_{12} = -i(\Delta_{12} - i\gamma_{12})\tilde{\rho}_{12} + i\Omega_c(\rho_{22} - \rho_{11}) + i\Omega_p\tilde{\rho}_{32} \quad (3.7d)$$

$$\dot{\rho}_{13} = -i(\Delta_{13} - i\gamma_{13})\tilde{\rho}_{12} + i\Omega_p(\rho_{33} - \rho_{11}) + i\Omega_c\tilde{\rho}_{23} \quad (3.7e)$$

$$\dot{\rho}_{12} = -i(\Delta_{12} - \Delta_{12} - i\gamma_{23})\tilde{\rho}_{23} + i\Omega_c\tilde{\rho}_{13} - i\Omega_p\tilde{\rho}_{21} \quad (3.7f)$$

where the subscripts refer to the three levels as in figure 3.12. The R_{13} term is a incoherent pumping rate used to establish gain in the system. The detunings are defined as:

$$\Delta_{13} = \omega_1 - \omega_{13} - k_1 V_z \quad (3.8)$$

$$\Delta_{12} = \omega_2 - \omega_{12} - k_2 V_z \quad (3.9)$$

The other symbols have their usual meanings. The decay rates are given by Γ_{21}=6.4MHz and Γ_{31}=1.3MHz in both systems and the coherence decay rates are given by:

$$\gamma_{12} = \frac{1}{2}(\Gamma_{21} + R_{13}) \quad (3.10)$$

$$\gamma_{13} = \frac{1}{2}(\Gamma_{31} + 2R_{13}) \quad (3.11)$$

$$\gamma_{23} = \frac{1}{2}(\Gamma_{21} + \Gamma_{31} + R_{13}) \quad (3.12)$$

The incoherent nature of the pumping term means it contributes to the dephasing of one or other of the states |1> and |3>. Hence using arbitrarily large pumping rates will result in either reduced amounts of gain, or no gain at all.

3.3.2 Absorption

Since we wish to compare the amount of gain, a real number, and not just the values of the density matrix elements we need to relate the appropriate density matrix element to the absorption coefficient:

$$\gamma(\omega) = \frac{3A_{ji}N\lambda^2\,\mathrm{Im}(\rho_{ij})}{32\pi n\Omega_{ij}} \quad (3.13)$$

where the amplitude of the optical field varies exponentially with distance z, according to exp[(γ/2)z], the Einstein A coefficient and the wavelength λ are that of the specific transition in

question |j>-|i>, N is the total atomic population per cubic metre, n the refractive index of the medium and Ω_{ij} is the half-Rabi frequency defined in equation (2.26). The validity of equation (3.13) is discussed further in [5].

In applying equation (3.13) we must take into account the degeneracy of the levels involved. Since we are dealing with a quasi-real system we also take into account the fact that rubidium has four ground state hyperfine levels, two each corresponding to the two naturally occurring isotopes. If we consider the $5S_{1/2}$ (F=3)-$6P_{1/2}$ transition (the probe field transition) we can calculate the percentage absorption we would expect using the equation:

$$\%Absorption = 100 \times [1 - Exp(-\gamma L)] \tag{3.14}$$

where L is the length of the cell we are using. For the probe wavelength of 422nm and a cell temperature of 130°C the absorption coefficient is calculated to be $73m^{-1}$. This implies absorption of 77% in a 2cm cell. This is in good agreement with experimental results.

3.3.3 Theoretical Results

The peak 'on-resonance' absorption as a function of the coupling field Rabi frequency is shown in figure 3.13. We see that a deeper transparency is found in the matched system than in the mismatched system, for a given coupling field Rabi frequency, as we would expect from the argument in section 3.2. We also see that significant transparency is predicted for coupling field Rabi frequencies less than the inhomogeneous linewidth (approximately 1GHz in this case).

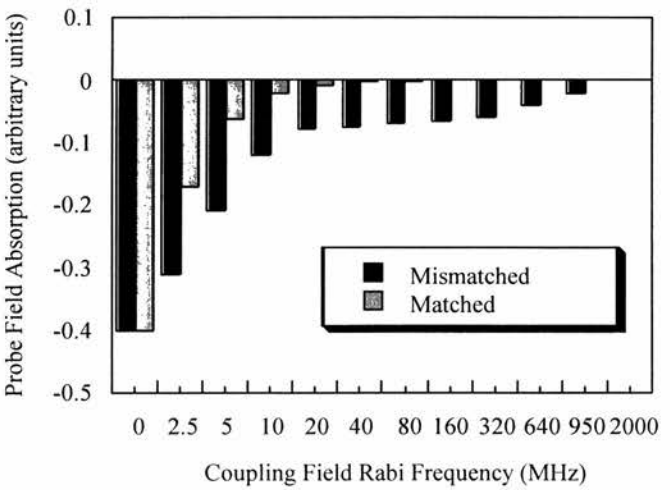

Figure 3.13: *On-resonance absorption in matched and mismatched cases over a range of Rabi frequencies.*

Figure 3.13 along with results for inversionless gain found in tables 3.1 and 3.2 give the principal results for comparison in the matched and mismatched cases. Values for the density matrix element relating to the absorption or gain, ρ^{i}_{13} are given along with the diagonal density matrix elements, related to the relative populations of the three atomic levels |1>, |2> and |3>. A value for the gain bandwidth, the range of frequencies over which gain can be found, is also given. The

column titled 'ρ^{i}_{13} peak' gives the highest value of ρ^{i}_{13}, since as we will see, in the case of inversionless gain it is possible to find more gain if we detune the probe slight from exact resonance with the |1>-|3> transition. The calculated percentage absorption or gain values are based on a 2cm cell at 130°C. Also listed for comparison purposes are the values of absorption of the probe field in the absence of a coupling field. In the cases where we observe gain the incoherent pumping rate R_{13} is 1.6MHz ($10x10^{6}s^{-1}$) in both the matched and mismatched systems.

The absorption predicted in both systems in the absence of the coupling field is identical, as we would expect, but as we turn the coupling field on we see that the absorption is reduced significantly, and by different amounts, in both schemes. This is more pronounced in the matched system (i.e. better EIT) but is still present in the mismatched system. The populations also begin to change as we increase the Rabi frequency and the upper coupling field level comes close to saturation as Ω_c is made larger.

The peak gain predicted in the matched case exceeds that of the mismatched case by nearly five times when the coupling field is set at 20MHz over a similar gain bandwidth. As the coupling field is increased, the total net gain also increases along with the bandwidth over which it is produced. The magnitude of predicted peak gain reaches a maximum for a specific Rabi frequency because for higher Rabi frequencies the gain bandwidth increases and this acts to reduced the peak gain. Interestingly for higher Rabi frequencies the gain peak is seen to split into two components and thus the peak gain value is found at some probe detuning. Hence the on-resonance gain and peak gain are given in tables 3.1 and 3.2. From the population values we see that the gain we produce is inversionless as the population in the lower probe level is always greater than in the upper probe level. However for the high Rabi frequency value of 950MHz the total population in the upper probe and coupling field levels is greater than that in the ground state but we still see no population inversion on the probe transition.

Matched	Rabi Frequency (MHz)	ρ^{i}_{13} resoance	ρ^{i}_{13} peak	ρ_{11}	ρ_{22}	ρ_{33}	Absorption %	Gain %	Gain Bandwidth (MHz)
Absorption	Ω_c=0	-0.0004	-0.0004	1	0	0	64	-	-
Transparency	Ω_c=20	-0.00002	-0.00002	0.9823	0.0177	0	5	-	-
Transparency	Ω_c=160	-0.000001	-0.000001	0.875	0.125	0	0.3	-	-
Transparency	Ω_c=950	0	0	0.62	0.38	0	0	-	-
Gain	Ω_c=20	0.000082	0.000082	0.634	0.014	0.352	-	24	18
Gain	Ω_c=160	0.000025	0.000102	0.58	0.099	0.321	-	0.233	108
Gain	Ω_c=950	0.000001	0.000033	0.451	0.299	0.25	-	0.033	648

Table 3.1: *Overview of the principal results from the modelling for the matched system. Values shown are the density matrix elements relating to the absorption, gain and atomic populations for various coupling field Rabi frequencies in both the absence and presence of incoherent pumping. In the cases where pumping is applied the value of R_{13} is 1.6MHz. For the calculation of percentage absorption and gain, a 2cm cell at 130°C is assumed.*

Mismatched	Rabi Frequency (MHz)	ρ^{i}_{13} resoance	ρ^{i}_{13} peak	ρ_{11}	ρ_{22}	ρ_{33}	Absorption %	Gain %	Gain Bandwidth (MHz)
Absorption	Ω_c=0	-0.0004	-0.0004	1	0	0	64	-	-
Transparency	Ω_c=20	-0.000084	-0.000084	0.968	0.032	0	19	-	-
Transparency	Ω_c=160	-0.000062	-0.000062	0.799	0.201	0	15	-	-
Transparency	Ω_c=950	-0.00002	0.00002	0.552	0.448	0	5	-	-
Gain	Ω_c=20	0.000018	0.000018	0.627	0.025	0.348	-	5	27
Gain	Ω_c=160	0.0000315	0.0000315	0.541	0.159	0.3	-	8	108
Gain	Ω_c=950	0.000012	0.000012	0.418	0.351	0.231	-	3	324

Table 3.2: Overview of the principal results from the modelling for the mismatched system. Values shown are the density matrix elements relating to the absorption, gain and atomic populations for various coupling field Rabi frequencies in both the absence and presence of incoherent pumping. In the cases where pumping is applied the value of R_{13} is 1.6MHz. For the calculation of percentage absorption and gain, a 2cm cell at 130°C is assumed.

Figure 3.14 shows the absorption profiles for the two systems with the coupling field Rabi frequency set at 160MHz. Traces are shown for zero pumping field and for R_{13}=1.6MHz. The splitting of the gain feature can clearly be seen in the matched case.

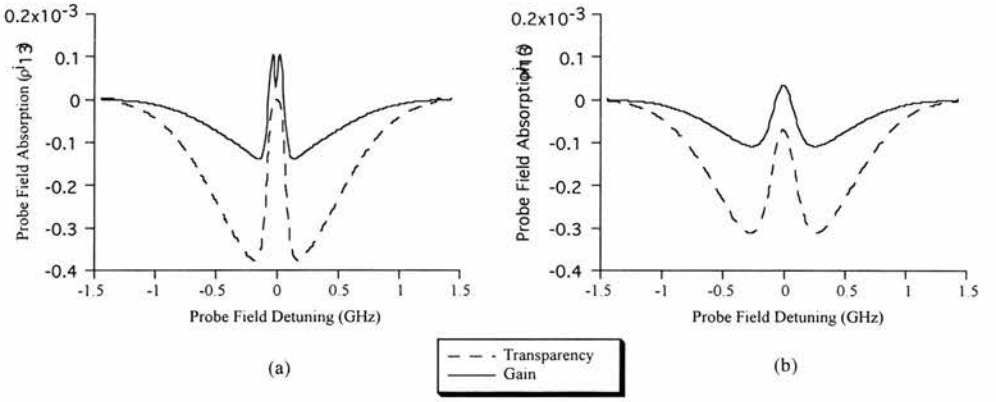

Figure 3.14: *Absorption and gain profiles: (a) matched and (b) mismatched systems. The solid lines represent the system in which incoherent excitation has been introduced and hence display gain while the dashed lines display the absorption profiles in the absence of incoherent pumping.*

3.3.4 Discussion

The main significance of these results is that inversionless gain is predicted in a system where the probe field frequency is much higher than that of the coupling field used to induce transparency in a Doppler broadened, wavelength mismatched medium. It is also possible to achieve this with Rabi frequencies below the Doppler width of the probe transition. While it is well accepted that AWI and EIT can be produced in a Doppler broadened system by Autler-Townes splitting beyond the Doppler width of the probe field [12] it is shown here that this is not a limiting case in the Vee-scheme. This allows us to work at much lower coupling field powers and hence places us well within the continuous-wave laser range.

The reason for this can be found by referring to the argument found in section 3.2.4 above. In the matched scheme the EIT feature is resolved from the Doppler-broadened absorption profile since the position of the two-photon resonance is fixed, independent of the atomic velocity, so that the transparency created at line centre, for the zero velocity group, remains visible. This can be confirmed by examining equations (3.4)-(3.6). In the mismatched scheme the Doppler free situation is not observed and so the two-photon resonance position will be different for each velocity group. For the cases considered in tables 3.1 and 3.2, that of Δ_c=0 the Autler-Townes positions are plotted in figure 3.6(b) (matched case) and figure 3.6(c) (mismatched case). It is therefore the Vee-Scheme advantage that we discussed above that allows inversionless gain to be predicted even in the mismatched case. If we examine the cascade and lambda schemes in figures 3.4(c) and 3.5(c) we find that the EIT is obscured in the mismatched wavelength case and hence

we will see no inversionless gain. It is the nature of the two-photon process in the Vee scheme that provides the advantage.

How far can we push the wavelength mismatch? If we wish to generate useful inversionless lasers, a large mismatch is obviously advantageous. In figure 3.15 we plot the on-resonance absorption coefficient as a fraction of the absorption coefficient in the absence of the coupling field as a function of probe wavelength, for a range of coupling field Rabi frequencies. In this in instance we consider only transparency (and not gain). The probe wavelength is varied while the coupling field is held constant at 780nm. The vertical dashed lined indicates the mismatched situation discussed here. By plotting the logarithm of the absorption we see that in the mismatched case a coupling field of around 950MHz can reduce the absorption by more than an order of magnitude. We also see that a region of constant transparency is predicted for wavelengths greater than about 600nm with a coupling field Rabi frequency of 950MHz. This is due to the fact that this Rabi frequency rivals the Doppler width of the probe field at these wavelengths. We see quite clearly that as the wavelength mismatch increases the level of transparency drops. But even at the UV wavelength of 200nm approximately 60% transparency is predicted for a coupling field Rabi frequency of 950MHz.

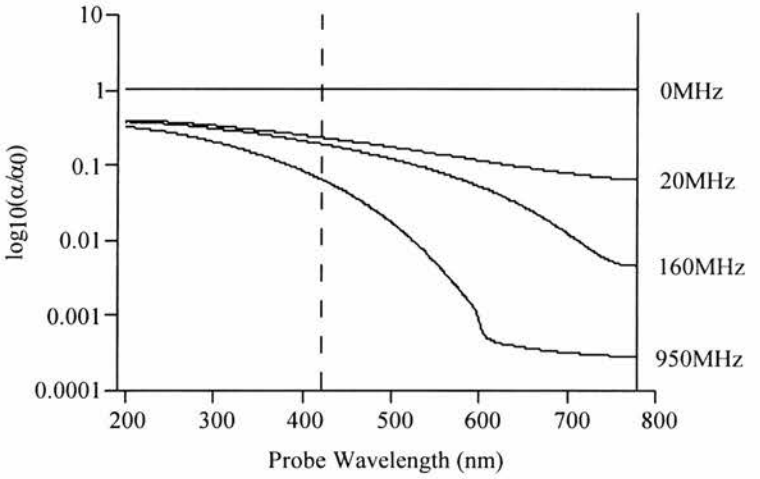

Figure 3.15: *Logarithm of the ratio of absorption coefficient in the presence and absence of a coupling field as a function of probe field wavelength. The dashed vertical line indicates our mismatched system probe field wavelength. The magnitude of coupling field Rabi frequency used to generate each plot is listed on the right hand side.*

3.3.5 Gain Splitting

We now investigate the splitting feature that is seen in the gain profile of the wavelength matched case. This is again due to the Doppler detuning effect. In the Vee-scheme it turns out that if we consider a homogeneously broadened system then the maximum gain that such a system displays will not be found when the coupling field is on resonance but when it is detuned. This is shown in figure 3.16 below. So in the matched wavelength case it will such that the superposition of EIT

profiles for each velocity group will result in a gain profile that has two sidebands that correspond to the two velocity groups which display the maximum gain. In the mismatched wavelength case this splitting feature is not seen, due to the fact that the two Autler-Townes components, associated with the two-photon resonance, of the non-zero velocity group overlap with the gain dip at line centre thus obscuring it.

The reason for the maximum in gain away from line centre is not fully explained. It would appear, however, that the phenomenon results due to a trade off between one and two photon loss processes and the two-photon gain process. So as the coupling field is detuned, the effectiveness of the two-photon gain stays high but at those points the loss introduced by the absorption of the probe field is decreased as it is no longer resonant with the probe transition. A full explanation of this phenomena would probably require treatment via the quantum jump formalism [13], and requires a dressed state analysis, which would allow the analysis of each of the processes involved and to eliminate the unfavourable ones, but we do not consider that here. Similar types of effects are discussed in [14-19].

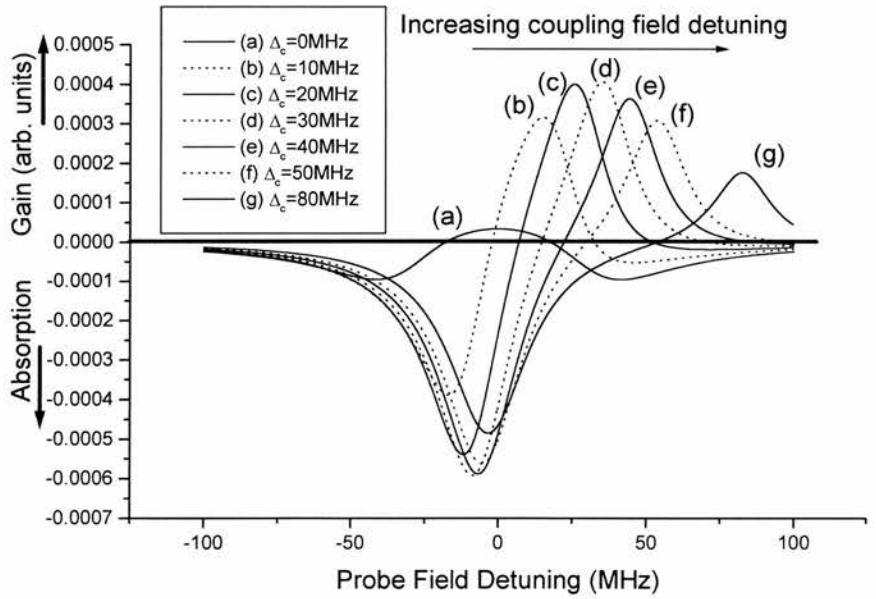

Figure 3.16: *Gain profiles in a homogeneously broadened media as a function of probe frequency detuning. Each trace has a different coupling field detuning, shown in the caption. The incoherent rate is 16MHz.*

3.3.6 Practical Considerations

So could we use our mismatched system to see inversionless gain in an experiment? We have predicted that for a 2cm cell heated to 130°C and a coupling Rabi frequency of 160MHz 8% gain can be observed. This calculation involves a incoherent pumping rate of 1.6MHz and the amount of gain compares favourably with gains found in experimentally demonstrated inversionless lasers and AWI experiments[1, 20, 21].

However we have neglected to include a number of factors that will affect any real experiment. These factors include collisional dephasing, which will act to reduce the quantum interference. In an experiment this can be controlled by changing the particle density via temperature or cell length. Another problem may be the variation of the coupling field Rabi frequency over the interaction length along the cell. So if we were to observe a drop at of Rabi frequency at some point within the cell we would see some of the probe field absorbed and thus the EIT effect would be lessened. The level of gain that we can observe scales exponentially with temperature, so it may be that adjustment of various system parameters can circumvent any potential problems that we may encounter. So it seems that our system may very well be a practical candidate for an inversionless laser. Indeed a recent experiment by Jong *et al* [22] has possibly demonstrated inversionless gain in our infrared-blue system. Incoherent blue SHG light is used as the pump source, so it is not necessarily a practical system. Also the result is still in some doubt, and remains unpublished. It differs slightly from our system as it is performed Doppler free in an atomic beam.

3.3.7 Incoherent pumping Issues

In order to pump an inversionless laser we need an incoherent pump source. In the proof of principle experiments demonstrating inversionless gain and lasing the incoherent pump is a broad linewidth laser which has a wavelength either exactly the same or very close to that of the probe field. Obviously for a practical system this is not of any use and an alternative pumping mechanism must be used. In the above argument we have assumed an incoherent pump on the probe transition. We would normally assume this to be some sort of optical field but it needn't necessarily be so. We could for instance envisage an electron collision pumping mechanism, for example by rf or dc excitation, whereby population from the ground state is excited to many higher lying levels and thus we provide incoherent pumping on the probe field. This sort of mechanism would allow a practical source of say, blue light, to be developed.

Other types of pumping mechanism are possible, such as pumping from the upper coupling field level to the upper probe field level. This is shown in figure 3.17. With this method of pumping the mismatched wavelength case in fact shows an advantage over the matched system. Zekou found [6] that in the matched case no gain is found via a R_{23} pumping mechanism but that gain in the mismatched system is unaffected. Indeed pumping via the upper coupling field level means the system is more 'inversionless' than pumping via level $|1\rangle$ since no extra population is moved out of the ground state. The problem with this type of pumping is that is requires the $|2\rangle$-$|3\rangle$ transition to be dipole allowed, which we initially assumed it was not. It may, therefore, have a decay rate Γ_{32} that will act to further dephase the system.

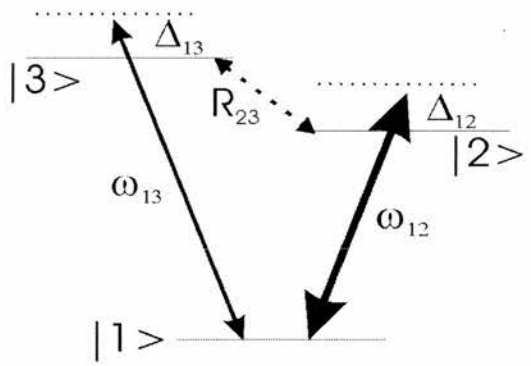

Figure 3.17: *Diagram showing an alternative method of incoherent pumping via the uper level of the coupling field to the upper probe field level.*

3.4 Conclusions

In this chapter we have examined the effects of mismatching the probe and coupling wavelengths in EIT and for observation of inversionless gain in Doppler broadened systems. We have seen that it is not necessary to work in the Doppler free situation of having probe and coupling field wavelengths matched and that EIT can be readily produced in a situation where the probe wavelength is some fraction of the coupling field wavelength. In examining EIT in mismatched systems we have seen that the induced transparency is always better in the case where $\lambda_p > \lambda_c$ and always worse in the case where $\lambda_p < \lambda_c$. This is found to be because of the Doppler detuning effect that effectively detunes the coupling field away from resonance when a non-zero velocity group (within a Doppler broadened atomic system) is considered. We also find that the Vee-scheme has a inherent advantage when it comes to observing EIT in the $\lambda_p < \lambda_c$ regime due to the nature of the two-photon process within the system.

We go on to show that this advantage enables us to predict inversionless gain in mismatched wavelength Vee-schemes and thus opens up the opportunity of building compact, practical inversionless lasers. We predict 8% gain in a system where the probe field has a wavelength of 422nm and the coupling field is resonant with a 780nm transition using only a modest amount of incoherent pumping. This value of gain compares favourably with previous experimentally observed values of inversionless gain and thus indicates that a experimental blue inversionless laser could be developed.

References

[1] **A. S. Zibrov, M. D. Lukin, D. E. Nikonov, L. W. Hollberg, M. O. Scully and V. L. Velichansky**, "Experimental demonstration of continuous-wave amplification without inversion via quantum interference in rb," *Laser Physics* **5**, 553-555 (1995).

[2] **G. G. Padmabandu, G. R. Welch, I. N. Shubin, E. S. Fry, D. E. Nikonov, M. D. Lukin and M. O. Scully**, "Laser oscillation without population inversion in a sodium atomic beam," *Physical Review Letters* **76**, 2053-2056 (1996).

[3] **E. S. Fry, X. F. Li, D. Nikonov, G. G. Padmabandu, M. O. Scully, A. V. Smith, F. K. Tittel, C. Wang, S. R. Wilkinson and S. Y. Zhu**, "Atomic coherence effects within the sodium d1 line - lasing without inversion via population trapping," *Physical Review Letters* **70**, 3235-3238 (1993).

[4] **J. R. Boon, E. Zekou, D. J. Fulton and M. H. Dunn**, "Experimental observation of a coherently induced transparency on a blue probe in a Doppler-broadened mismatched V-type system," *Physical Review A* **57**, 1323-1328 (1998).

[5] **J. R. Boon**, *Electromagnetically Induced Transparency and Inversionless Lasing*, PhD thesis, University of St. Andrews (1998).

[6] **E. Zekou**, *Atomic Coherence Effects: Electromagnetically Induced Transparency and Inversionless Lasing*, PhD thesis, University of St. Andrews (1998).

[7] **S. Shepherd, D. J. Fulton and M. H. Dunn**, "Wavelength dependence of coherently induced transparency in a Doppler-broadened cascade medium," *Physical Review A* **54**, 5394-5399 (1996).

[8] **D. J. Fulton, S. Shepherd, R. R. Moseley, B. D. Sinclair and M. H. Dunn**, "Continuous-wave electromagnetically induced transparency - a comparison of v-system, lambda-system, and cascade systems," *Physical Review A* **52**, 2302-2311 (1995).

[9] **R. R. Moseley, S. Shepherd, D. J. Fulton, B. D. Sinclair and M. H. Dunn**, "2-photon effects in continuous-wave electromagnetically-induced transparency," *Optics Communications* **119**, 61-68 (1995).

[10] **C. H. Townes and A. L. Schawlow**, *Microwave Spectroscopy*. (McGraw-Hill, London, 1955).

[11] **S. F. Yelin, M. D. Lukin, M. O. Scully and P. Mandel**, "Gain without inversion in the frequency up-conversion regime," *Physical Review A* **57**, 3858-3868 (1998).

[12] **M. D. Lukin, M. O. Scully, G. R. Welch, E. S. Fry, L. Hollberg, G. G. Padmabandu, H. G. Robinson and A. S. Zibrov**, "Lasing without inversion: The road to new short-wavelength losers," *Laser Physics* **6**, 436-447 (1996).

[13] **C. Cohen-Tannoudji, B. Zambon and E. Arimondo**, "Quantum-jump approach to dissipative processes: application to amplification without inversion," *Journal of the Optical Society of America B-Optical Physics* **10**, 2107 (1993).

[14] **J. Mompart, R. Corbalan and R. Vilaseca**, "Lasing without inversion in the V-type three-level system under the two-photon resonance condition," *Optics Communications* **147**, 299-304 (1998).

[15] **J. Mompart and R. Corbalan**, "Inversionless amplification in three-level systems: dressed states quantum interference and quantum-jump analyses," *Optics Communications* **156**, 133-144 (1998).

[16] **J. Mompart, V. Ahufinger, F. Silva, R. Corbalan and R. Vilaseca**, "Quantum interference and quantum-Zeno effect in amplification without inversion," *Laser Physics* **9**, 844-857 (1999).

[17] **G. Grynberg, M. Pinard and P. Mandel**, "Amplification without population inversion in a V three-level system: A physical interpretation," *Physical Review A* **54**, 776-785 (1996).

[18] **F. B. deJong, R. J. C. Spreeuw and H. B. V. vandenHeuvell**, "Quantum Zeno effect and V-scheme lasing without inversion," *Physical Review A* **55**, 3918-3922 (1997).

[19] **J. Mompart and R. Corbalan**, "Lasing Without Inversion," *Journal of Optics B-Quantum and Semiclassical Optics* **2**, R7-R24 (2000).

[20] **C. Peters and W. Lange**, "Laser action below threshold inversion due to coherent population trapping," *Applied Physics B-Lasers and Optics* **62**, 221-225 (1996).

[21] **C. Fort, F. S. Cataliotti, T. W. Hansch, M. Inguscio and M. Prevedelli**, "Gain without inversion on the cesium D-1 line," *Optics Communications* **139**, 31-34 (1997).

[22] **F. B. de Jong**, *Lasing without inversion*, thesis, University of Amsterdam (1998).

Chapter 4

EIT with phase diffusing fields

4.1 Introduction

It is usual to consider the sources that interact with atoms in many quantum optical experiments as having an arbitrarily small linewidth, which in practice is rarely the case. Linewidth can have a significant effect in an EIT experiment, since a finite linewidth will add to the overall dephasing of the system. As an example the Schwarz Ti:sapphire laser used in the EIT experiments described in this thesis has a linewidth of up to ~5MHz which rivals the decay rate of some of the rubidium transitions into which it couples. Hence laser linewidth plays its role.

In this chapter we consider the case of EIT in a homogeneously broadened 3-level V scheme with a phase diffusing coupling or probe field and an incoherent pump source. We investigate the possibility of performing EIT experiments with a truly incoherent probe field, i.e. a probe other than a laser source. We also show that it is possible to create inversionless gain in such a system with a broad linewidth coupling field. Further we investigate the fact that the atomic model considered here indicates that with the coupling field on resonance inversionless gain is best achieved in systems where the probe and coupling field decay rates wavelength are mismatched.

Schemes that have included phase fluctuating and even chaotic fields have been considered before. Anontha Lakshmi and Swain [1] looked at how laser linewidths effected the efficiency in enhancement of sum-frequency mixing using EIT. Sultana and Zubairy [2] investigated coupling field linewidth effects in cascade schemes, as did Gea-Banaloche *et al* [3] when considering the theory to explain their EIT experiment in atomic rubidium. Gong *et al* have examined both Λ [4] and V schemes [5]. They have shown for instance the degradation of EIT in schemes with finite coupling field linewidths [6] and that a non-inversion laser may turn into an inversionless laser [5] by inclusion of linewidth effects. Vermuri *et al* [7] considered a cascade scheme with both phase fluctuating and chaotic (and hence genuinely incoherent) coupling fields and showed that LWI is achievable with both, with the amount of gain decreasing as the incoherence of the coupling laser increased. Kofman [8] has also examined EIT in cascade and lambda schemes with phase diffusing and chaotic fields showing that EIT can still be observed even with large linewidth fields. Our scheme differs from that of Gong *et al* [5] in that we include an incoherent pump in our model to create gain on the lasing transition and leave the transition between the upper two levels as non-dipole allowed as is seen in many atomic schemes [9]. This is a significant difference, in that the Gong scheme relies more heavily on the direct modification of atomic parameters along with the coherence of the coupling field, whereas we can modify gain properties, in the main, by modifying the coupling field strength and linewidth.

4.2 Model System and Equations of Motion

We consider a closed three level V scheme as shown in figure 4.1. The probe field ω_p interacts with the |1> - |3> transition and the coupling field ω_c interacts with the |1> - |2> transition. The probe and coupling transitions have decay rates Γ_{31} and Γ_{21} respectively. An incoherent pump moves population from |1> to |3> and is denoted R_{13}. Probe and coupling field detunings are given by $\Delta_{13} = \omega_p - \omega_{13}$ and $\Delta_{12} = \omega_c - \omega_{12}$, where ω_{13} and ω_{12} are the transition frequencies.

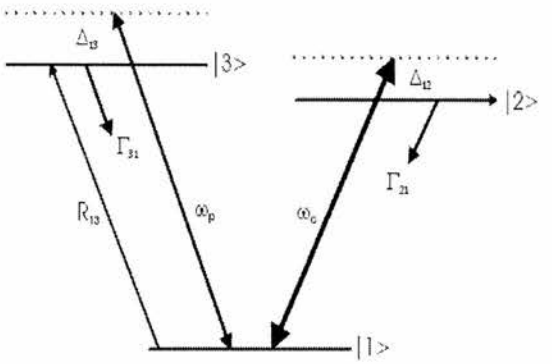

Figure 4.1: *Vee scheme with incoherent pumping.*

The equations of motion for such a system are given by:

$$\dot{\rho}_{11} = i\Omega_c(\tilde{\rho}_{21} - \tilde{\rho}_{12}) + i\Omega_p(\tilde{\rho}_{31} - \tilde{\rho}_{13}) + R_{13}(\rho_{33} - \rho_{11}) + \Gamma_{21}\rho_{22} + \Gamma_{31}\rho_{33} \tag{4.1a}$$

$$\dot{\rho}_{22} = i\Omega_c(\tilde{\rho}_{12} - \tilde{\rho}_{21}) - \Gamma_{21}\rho_{22} \tag{4.1b}$$

$$\rho_{33} = i\Omega_p(\tilde{\rho}_{13} - \tilde{\rho}_{31}) - \Gamma_{31}\rho_{33} - R_{13}(\rho_{33} - \rho_{11}) \tag{4.1c}$$

$$\dot{\tilde{\rho}}_{12} = -i(\Delta_{12} - i\gamma_{12})\tilde{\rho}_{12} + i\Omega_c(\rho_{22} - \rho_{11}) + i\Omega_p\tilde{\rho}_{32} \tag{4.1d}$$

$$\dot{\tilde{\rho}}_{13} = -i(\Delta_{13} - i\gamma_{13})\tilde{\rho}_{13} + i\Omega_p(\rho_{33} - \rho_{11}) + i\Omega_c\tilde{\rho}_{23} \tag{4.1e}$$

$$\dot{\tilde{\rho}}_{23} = -i(\Delta_{12} - \Delta_{13} - i\gamma_{23})\tilde{\rho}_{23} + i\Omega_c\tilde{\rho}_{13} - i\Omega_p\tilde{\rho}_{21} \tag{4.1f}$$

where the $\tilde{\rho}_{ij}$ terms are introduced to remove the optical frequency oscillations of ρ_{ij} and the Rabi frequencies are given by:

$$\Omega_p = \frac{\mu_{13}E_p}{2\hbar} \tag{4.2a}$$

$$\Omega_c = \frac{\mu_{12}E_c}{2\hbar} \tag{4.2b}$$

(μ_{ij} are transition dipole matrix elements and E_p and E_c are the probe and coupling field strengths) and the dephasings are given by:

$$\gamma_{12} = \frac{1}{2}(\Gamma_{21} + R_{13}) \tag{4.3a}$$

$$\gamma_{13} = \frac{1}{2}(\Gamma_{31} + 2R_{13}) \tag{4.3b}$$

$$\gamma_{23} = \frac{1}{2}(\Gamma_{21} + \Gamma_{31} + R_{13}) \tag{4.3c}$$

By solving the equations (4.1a-f) for the steady state condition, substituting in real and imaginary parts for the appropriate density matrix elements and by assuming a closed system we can derive an 8x8 density matrix to describe this system.

We can introduce the effects of laser linewidth using a phase described by the Wiener-Levy stochastic process [10]. We take the phase fluctuations of the coupling field to be described by:

$$\Omega_c = \Omega_{c0} \exp[i\phi(t)] \tag{4.4}$$

where the phase ϕ(t) is a Gaussian process (with zero average):

$$\langle \phi(t) \rangle = 0 \tag{4.5}$$

The derivative of such a diffusion process gives a white noise:

$$\langle \dot{\phi}(t)\dot{\phi}(t') \rangle = 2R_L \delta(t - t') \tag{4.6}$$

where the laser linewidth is given by $2R_L$.

To introduce the effect of laser linewidth into our model we redefine the variables ρ_{12} and ρ_{23} as follows:

$$\tilde{\rho}_{23} = \tilde{\rho}'_{23} e^{i\phi} \tag{4.7}$$

$$\tilde{\rho}_{12} = \tilde{\rho}'_{12} e^{i\phi} \tag{4.8}$$

Using these new variables we modify equations (4.1d) and (4.1f),

$$\dot{\tilde{\rho}}'_{12} = -i(\Delta_{12} - i\gamma_{12})\tilde{\rho}'_{12} + i\Omega_{c0}(\rho_{22} - \rho_{11}) + i\Omega_p \rho'_{32} - i\dot{\phi}(t)\rho'_{12} \tag{4.9}$$

$$\dot{\tilde{\rho}}'_{23} = -i(\Delta_{12} - \Delta_{13} - i\gamma_{23})\tilde{\rho}'_{23} + i\Omega_{c0}\tilde{\rho}'_{13} - i\Omega_p \tilde{\rho}_{21} - i\dot{\phi}(t)\tilde{\rho}'_{23} \tag{4.10}$$

We can now derive a set of equations of motion for the stochastic averaged density matrix elements (4.1a-f). Dropping the primes and using the relations which are obtained by an integration of equations (4.9) and (4.10) [5],

$$i\left\langle \dot{\phi}(t)\tilde{\rho}_{12}\right\rangle = R_L\left\langle \tilde{\rho}_{12}\right\rangle \tag{4.11}$$

$$i\left\langle \dot{\phi}(t)\tilde{\rho}_{23}\right\rangle = R_L\left\langle \tilde{\rho}_{23}\right\rangle \tag{4.12}$$

we find (dropping the equation for $\dot{\rho}_{11}$):

$$\left\langle \dot{\rho}_{22}\right\rangle = i\overline{\Omega}_c\left(\left\langle \tilde{\rho}_{12}\right\rangle - \left\langle \tilde{\rho}_{21}\right\rangle\right) - \Gamma_{21}\left\langle \rho_{22}\right\rangle \tag{4.13}$$

$$\left\langle \dot{\rho}_{33}\right\rangle = i\overline{\Omega}_p\left(\left\langle \tilde{\rho}_{13}\right\rangle - \left\langle \tilde{\rho}_{31}\right\rangle\right) - \Gamma_{31}\left\langle \tilde{\rho}_{23}\right\rangle - R_{13}\left(\left\langle \rho_{33}\right\rangle - \left\langle \rho_{11}\right\rangle\right) \tag{4.14}$$

$$\left\langle \dot{\tilde{\rho}}_{12}\right\rangle = -i\left(\Delta_{12} - i\gamma_{12}\right)\left\langle \tilde{\rho}_{12}\right\rangle + i\overline{\Omega}_c\left(\left\langle \tilde{\rho}_{22}\right\rangle - \left\langle \tilde{\rho}_{11}\right\rangle\right) + i\overline{\Omega}_p\left\langle \tilde{\rho}_{32}\right\rangle - R_L\left\langle \rho_{12}\right\rangle \tag{4.15}$$

$$\left\langle \dot{\tilde{\rho}}_{13}\right\rangle = -i\left(\Delta_{13} - i\gamma_{13}\right)\left\langle \tilde{\rho}_{13}\right\rangle + i\overline{\Omega}_p\left(\left\langle \rho_{33}\right\rangle - \left\langle \rho_{11}\right\rangle\right) + i\overline{\Omega}_c\left\langle \tilde{\rho}_{23}\right\rangle \tag{4.16}$$

$$\left\langle \dot{\tilde{\rho}}_{23}\right\rangle = -i\left(\Delta_{12} - \Delta_{13} - i\gamma_{23}\right)\left\langle \tilde{\rho}_{23}\right\rangle + i\overline{\Omega}_c\left\langle \tilde{\rho}_{13}\right\rangle + i\overline{\Omega}_p\left\langle \tilde{\rho}_{21}\right\rangle - R_L\left\langle \rho_{23}\right\rangle \tag{4.17}$$

where $\overline{\Omega}_c$ and $\overline{\Omega}_p$ are the steady-state values of the Rabi frequencies. Again solving for the steady state and substituting real and imaginary parts we can derive the density matrix which completely describes our model system. Using a symbolic computer package (Mathematica) we can solve for the matrix element of interest. We can therefore see by examination of equation (4.15) and (4.17) that the introduction of the phase diffusing field is to modify the appropriate dephasings:

$$\gamma_{12} \rightarrow \gamma_{12} + R_L \tag{4.18}$$

$$\gamma_{23} \rightarrow \gamma_{23} + R_L \tag{4.19}$$

So our model can now be simply applied to any system we wish to add linewidth effects to. Immediately we can predict that if EIT experiments are able to withstand dephasing effects, i.e. collisions, then they can withstand finite linewidths. From the above we can see that our model reduces to that for a monochromatic coupling field in the limit where $R_L = 0$. A similar approach is used to model linewidth effects in the probe beam.

4.3 Linewidth Effects on EIT

When we put a finite linewidth into the coupling field we see that EIT is slowly destroyed as the linewidth is made larger (fig 4.2). We would expect this both as the linewidth 'smears' out across the transition line width and hence dephases the system. The destruction of EIT comes about mainly due to this dephasing but EIT can be seen even when the linewidth exceeds the decay rate of the probe transition. So long as the coupling Rabi frequency is large enough, EIT should be recoverable for any coupling field linewidth.

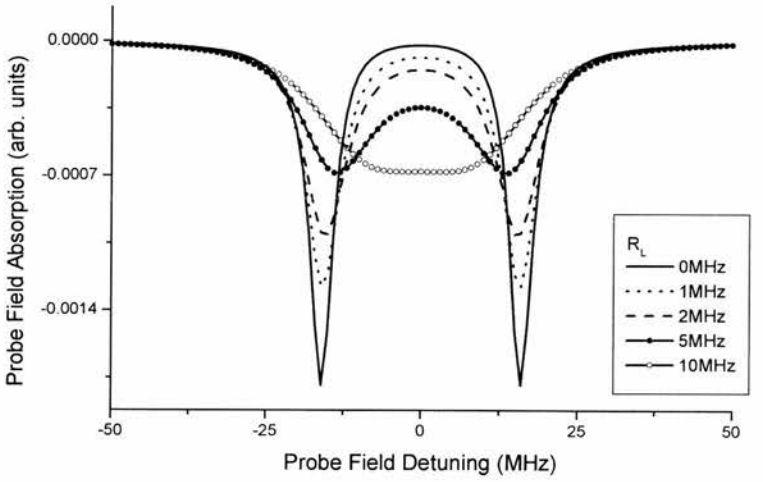

Figure 4.2: *Probe field absorption as a function of probe field detuning for a range of different coupling field linewidths.*

The intrinsic symmetry of the V scheme naturally suggests that EIT can survive linewidth effects on the probe field also. This is indeed found to be the case (fig 4.3). Here we see that EIT is again preserved even when the homogeneous linewidth of the probe transition is less than the probe field linewidth. This is again due to the size of the coupling field Rabi frequency, which should be able to preserve EIT provided it is larger than the finite linewidths of the fields. As we would also expect the dispersion in a medium interacting with phase diffusing fields is adversely affected. It is possible that this regime where the probe field linewidth is larger than the transition decay rate may have a practical application. Many short wavelength transitions are inaccessible to EIT experiments due to a lack of laser sources.

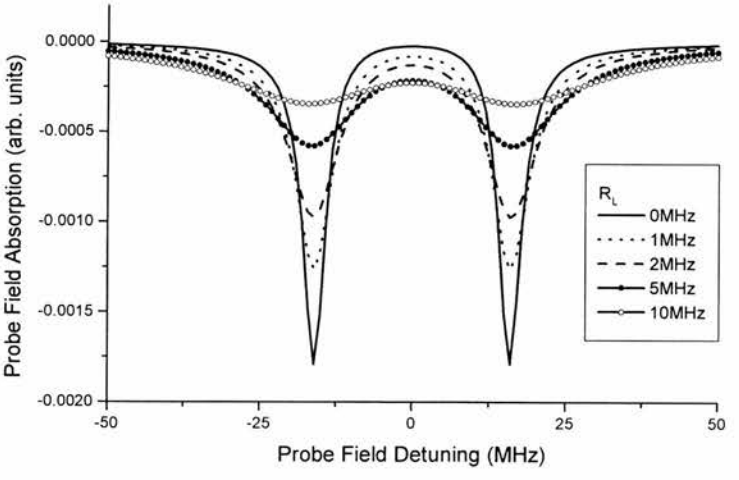

Figure 4.3: *Probe field absorption as a function of probe field detuning for a range of probe field linewidths.*

Here we envisage an experiment as shown in figure 4.4, a double helium beam experiment. Helium has transitions attractive for EIT, primarily the 58nm transition coupled, in a lambda scheme, to a 2.06 micron transition, shown in figure 4.5. If a laser probe with a finite linewidth can be used in an EIT experiment, then conceivably an excited emission source such as 58nm emission from a helium beam could be used as a probe source. This could provide a new source for EIT probe beams. Obviously emission from a laser is different to emission from a helium beam, but the possibility remains.

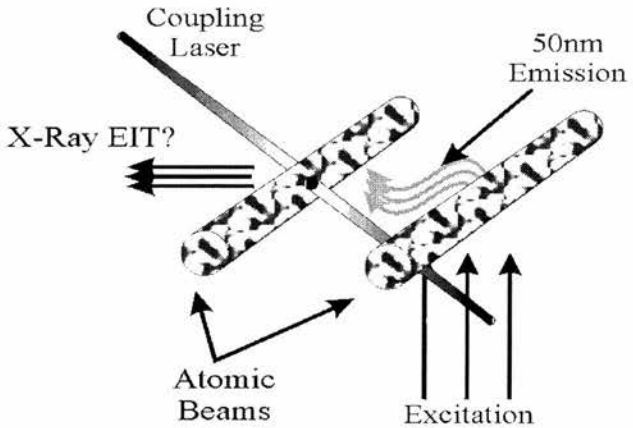

Figure 4.4: *Possible experimental set-up for the observation of EIT with an incoherent probe field at 58nm.*

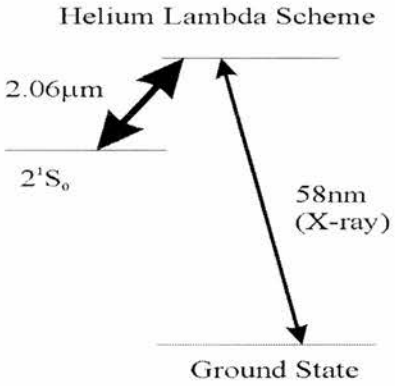

Figure 4.5: *Lambda system with potential for observing EIT in the X-ray regime.*

4.4 EIT with Two Phase Diffusing Fields

We now briefly examine what happens in the case where both fields have finite linewidths. From what we have observed above we would still expect EIT to be preserved but to die away more quickly than in the cases where only one field is phase diffusing. The on-resonance absorption is shown as a function of both probe and coupling field linewidth in figure 4.6. The on-resonance absorption is seen to drop more quickly with coupling field linewidth than with probe linewidth consistent with figures 4.2 and 4.3.

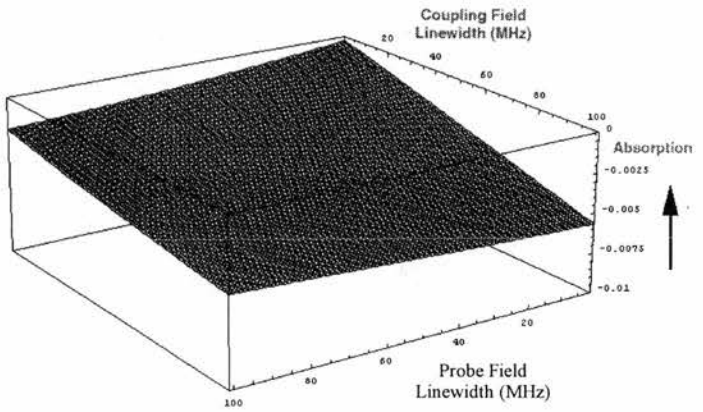

Figure 4.6: *On resonance probe field absorption as a function of probe and coupling field linewidth. Both linewidths are in MHz.*

4.5 Decay rate considerations and AWI

We will consider primarily the gain and absorption when the coupling field is resonant with the |1> - |2> transition, i.e. when $\Delta_{12} = 0$, this helps us to analyse some of the analytical solutions to the density matrix equations more simply. We do this despite the maximum gain being found when the coupling field is detuned from resonance (section 3.3.5 and [11]). For the following argument it is immaterial if the coupling field is detuned or not. We begin by establishing bounds for achieving gain with a monochromatic driving field. In the first instance we will assume that the coupling and probe field transitions are equal, i.e. that the decay rates are the same, $\Gamma_{21} = \Gamma_{31} = 6.4MHz$. Zhu [12] showed that the condition for AWI with on resonance fields is:

$$R_{13} > \frac{\Gamma_{31}{}^2}{\Gamma_{21} - \Gamma_{31}} \tag{4.20}$$

which is never satisfied for matched decay rates (and implicitly matched wavelengths) as seen in figure 4.7. No gain whatsoever is seen until Γ_{31}=4MHz, with Ω_c=5Γ_{21}.

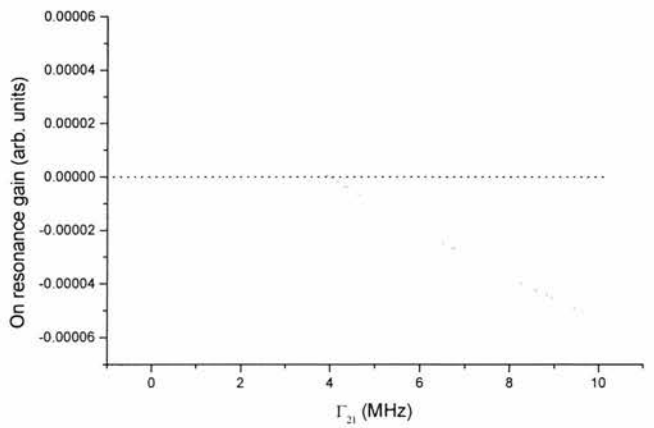

Figure 4.7: *Gain, with the probe field on resonance, as a function of probe field decay rate (Γ_{21}) The dotted line marks the crossover point from absorption to gain.*

Normally this condition is seen as a restriction on the production of short wavelength lasers by means of AWI. Recently however Mompart *et al* [13] have shown that this condition for the 3 level V-scheme can be relaxed in the case of detuned fields. We note however that rubidium appears to be anomalous in this respect in that the decay rates decrease as the wavelength of the transitions decreases. We also note that LWI offers the possibility of long-wavelength laser sources (down conversion), for instance in the mid-infrared. An experiment of this nature has been carried out by Peters and Lange [14]. Some atomic systems (such as neon) have transitions appropriate for down conversion, as do numerous molecules. As we would expect, the amount of gain increases as the decay rate on the probe decreases, shown clearly for a range of decay rates in figure 4.7. Using this information we set $\Gamma_{31}=0.2\Gamma_{21}$. These decay rates roughly correspond to the decay rates in the infrared-coupled blue-probe EIT scheme we have looked at previously [9].

4.6 Coupling Field Linewidth Effects on AWI

We now examine the effect that increasing coupling field linewidth has on the observed gain. This is most easily shown in a general way by examining a plot of gain versus linewidth and pumping (figure 4.8(a) and (b)). We see for $\Omega_c=5\Gamma_{21}$ and the parameters given above that gain is observed even if the linewidth exceeds 100MHz i.e.$R_L=16\Gamma_{21}$. We can therefore say that even with appreciable phase diffusing fields the AWI condition is still conserved.

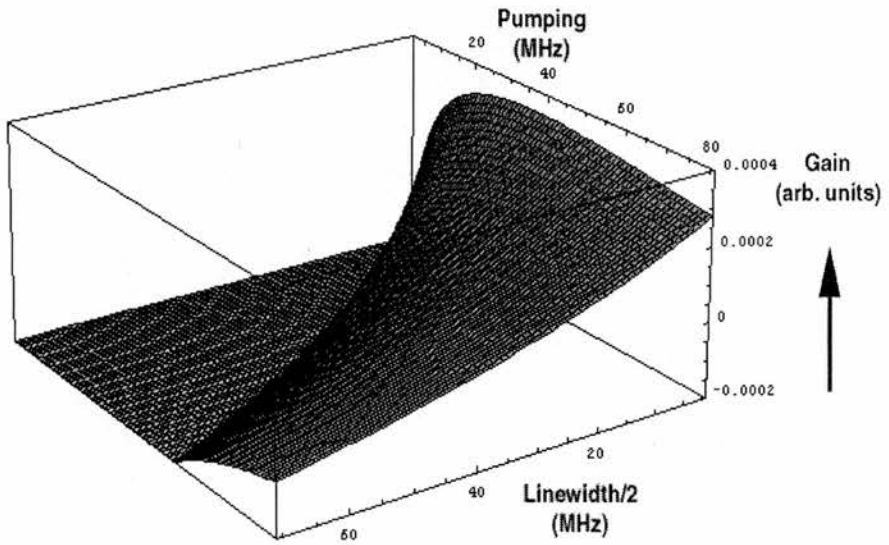

Figure 4.8(a): *Gain/absorption on probe field resonance as a function of coupling field linewidth and incoherent pumping rate.*

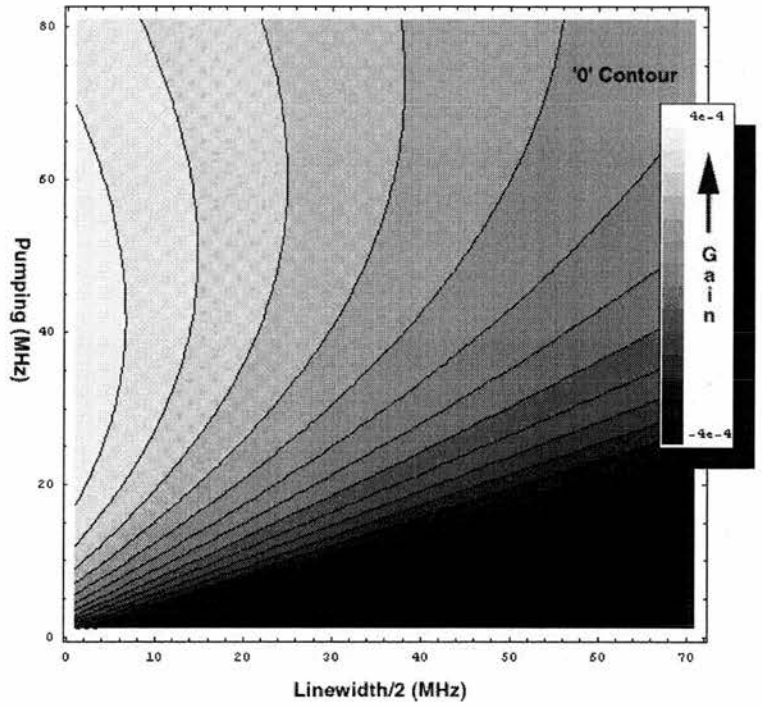

Figure 4.8(b): Contour *plot corresponding to figure 4.8(a) above. The darker regions correspond to lower values of gain/absorption, i.e. the dark region in the bottom right of the figure correspond to the 'plain' at the upper bottom left in figure 4.8(a). The '0' contour, the region of zero absorption is given as a reference.*

By deriving conditions for gain in our system we are able to examine the effect increasing linewidth has on the gain more explicitly. We solve the density matrix equations (4.1a-f) in the steady state (assuming $\Omega_c >> \Omega_p$) for the zeroth order of the probe for ρ_{22}, ρ_{33} and ρ_{12} and to all orders of the probe for the other matrix elements. Then we extract the expression for the probe field gain, Im(ρ_{13}). For the system to display any gain Im(ρ_{13})>0, and using this inequality we generate an inequality for the magnitude of incoherent pumping to produce gain:

$$R_{13} > \frac{1}{\Gamma_{21}\Gamma_{31}}\left(\begin{array}{l} -4R_L\Gamma_{21}\Gamma_{31} - {\Gamma_{21}}^2\Gamma_{31} - \frac{\Gamma_{21}{\Gamma_{31}}^2}{2} + 2\Gamma_{21}\Omega_c^2 - 2\Gamma_{31}\Omega_c^2 - \\ \sqrt{(\frac{{\Gamma_{21}}^2{\Gamma_{31}}^4}{4} - 16R_L{\Gamma_{21}}^2\Gamma_{31}\Omega_c^2 - 4\Gamma_{21}^3\Gamma_{31}\Omega_c^2 + 2\Gamma_{21}^2\Gamma_{31}^2\Omega_c^2 - \\ 2\Gamma_{21}\Gamma_{31}^3\Omega_c^2 + 4\Gamma_{21}^2\Omega_c^4 - 8\Gamma_{21}\Gamma_{31}\Omega_c^4 + 8\Gamma_{31}^2\Omega_c^4)} \end{array}\right) \quad (4.21)$$

which is rather complicated to analysis by inspection. We therefore make the simplification:

$$R_{13} > \frac{1}{\Gamma_{21}\Gamma_{31}}\left(-4R_L\Gamma_{21}\Gamma_{31} - \alpha - \sqrt{\beta - 16R_L\Gamma_{21}^2\Gamma_{31}\Omega_c^2}\right) > 0 \quad (4.22)$$

where

$$\alpha = \Gamma_{21}{}^2\Gamma_{31} + \frac{\Gamma_{21}\Gamma_{31}{}^2}{2} - 2\Gamma_{21}\Omega_c^2 + 2\Gamma_{31}\Omega_c^2 \tag{4.23}$$

and

$$\beta = \frac{\Gamma_{21}^2\Gamma_{31}^4}{4} - 4\Gamma_{21}^3\Gamma_{31}\Omega_c^2 + 2\Gamma_{21}^2\Gamma_{31}^2\Omega_c^2 - 2\Gamma_{21}\Gamma_{31}^3\Omega_c^2 + 4\Gamma_{21}^2\Omega_c^4 - 8\Gamma_{21}\Gamma_{31}\Omega_c^4 + 8\Gamma_{31}^2\Omega_c^4 \tag{4.24}$$

First, considering the case where $R_L = 0$ for simplicity, we examine the gain conditions. We see that there are two possible ranges of values for α, positive and negative. If α is positive this implies that $\Gamma_{31} > \Gamma_{21}$ (assuming that $\Omega_c >> \Gamma_{21}, \Gamma_{31}$) and AWI is not found to occur under such conditions, thus we can concentrate on the situation where $\alpha<0$. For $\alpha<0$ to occur we require $\Gamma_{21} > \Gamma_{31}$. This is in broad agreement with both the modelling and Zhu's result [12] shown in equation (4.21). We also see that gain is found when $-\alpha > \sqrt{\beta}$ which is true for very high coupling fields and for the α condition $\Gamma_{21} > \Gamma_{31}$. We can verify this derivation numerically. For a monochromatic driving field with a Rabi frequency of $5\Gamma_{21}$, (Γ_{21}=6.4MHz) and $\Gamma_{31}=0.2\Gamma_{21}$ the value of pumping that will result in $\mathrm{Im}(\rho_{13})=0$ is approximately 0.4MHz. We then model this and the graph is seen to confirm our prediction (figure 4.9), as expected gain is seen to occur with a slight increase in the pumping.

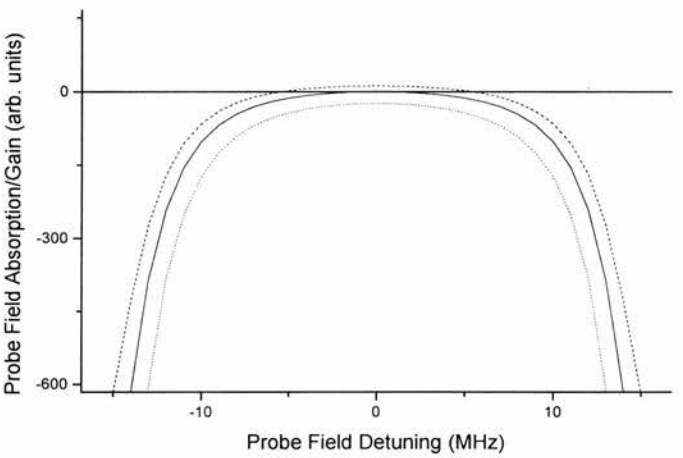

Figure 4.9: *Verifying the gain condition. We calculate a pumping rate of 0.4MHz to give us exactly zero absorption in the presence of a coupling field Rabi frequency of $5\Gamma_{21}$ and a probe field decay rate of $0.2\Gamma_{21}$. We see that for zero pumping we do not achieve perfect EIT and that gain is observed if we increase the pumping rate slightly to 0.8MHz.*

We do not derive explicit expressions for the population differences but we can see the gain is inversionless by examining the populations predicted by the density matrix (figure 4.10). Interestingly we do not see the behaviour predicted by Gong *et al* [5] by which a non-inversion laser moves into an inversionless regime with the addition of linewidth. This is attributed to the different pumping and decay processes their model employed in comparison to the models used

here. We also find that if we modify our model to include an incoherent pump from the |2> - |3> levels we do not recover the results of of Gong *et al.* We conclude that the pumping mechanisms discussed here do not allow for the same movement of population as when the laser action is created by spontaneous decay alone.

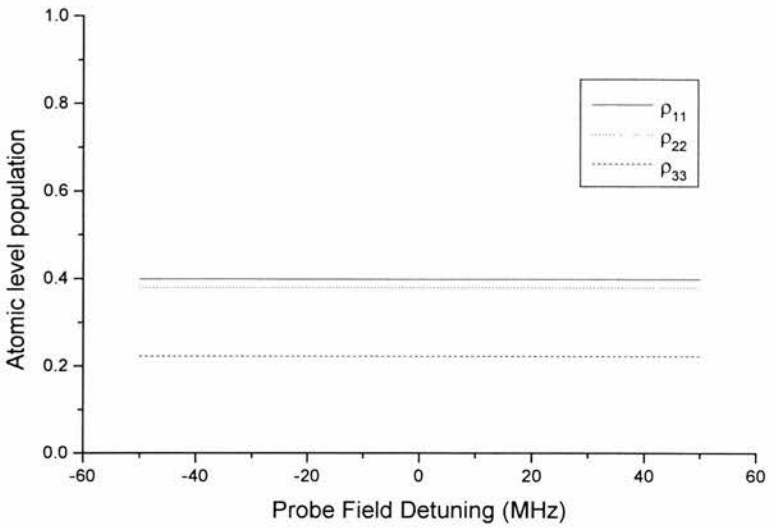

Figure 4.10: *Atomic populations in an incoherently pumped Vee-scheme. The pumping rate is 1.6MHz and $\Gamma_{31}=0.2\Gamma_{21}$. It can be seen that the gain is inversionless since the upper state of the probe has less population (~half) than the ground state.*

When we move into the regime where there is a finite linewidth coupling field we see that from equation (4.22) the value of R_L has little effect on β, so by examining how it affects α we can determine that increasing R_L reduces gain in a incoherently pumped 3 level V-scheme. We see now that the inequality, after some manipulation,

$$4R_L\Gamma_{21}\Gamma_{31}+\alpha<0 \tag{4.25}$$

which gives:

$$\Omega_c^2 > \frac{\Gamma_{21}\Gamma_{31}}{2}\left(\frac{4R_L+\Gamma_{21}-\Gamma_{31}/2}{\Gamma_{21}-\Gamma_{31}}\right) \tag{4.26}$$

which must be true for gain. Thus increasing the linewidth of the coupling field makes it hard for the gain condition to be satisfied. An increase in R_L can be over come by both modifying decay rates or more simply by increasing the coupling field Rabi frequency.

4.7 Conclusions

Normal EIT and LWI theory assumes that the interacting fields are perfectly monochromatic. Experimentally this is not always the case. We have shown that an incoherently pumped three V-scheme, one of the standard atomic system used in quantum optics, can display inversionless gain even in the situation where the coupling field is partially incoherent. We have examined the

conditions under which this system may exhibit gain and found them to be similar to those found by Zhu [12]. We have extended these conditions to take into account our phase diffusing coupling field. We show graphically how the gain in a V-scheme varies over varying pump and linewidth values. We see, as expected, that for high linewidths the dephasing of the coherences that takes place destroys all the gain. However the system is relatively robust and can withstand linewidths of the order of 10 times greater than the coupling field linewidth. We have also discussed the possibility of long wavelength inversionless lasers and the anomalous properties of rubidium that make it an ideal candidate for short wavelength inversionless lasers. The linewidth effects that we observe on the coupling laser have been investigated for the case where the probe laser is made incoherent. We find due to the symmetry of the V-scheme that a broad linewidth probe supports EIT in the same way that a broad coupling field does. This has potentially important consequences for producing EIT on transitions where no probe laser source exists. We propose an experimental scheme in helium that could make use of such an effect to produce a 58nm inversionless laser.

References

[1] **A. Anantha Lakshmi and S. Swain**, "Effect of laser linewidth on nonlinear optical parametric processes exploiting electromagnetically induced transparency," *Journal of Modern Optics* **38**, 2031-2041 (1991).

[2] **S. Sultana and M. S. Zubairy**, "Effect of finite bandwidth on refractive-index enhancement and lasing without inversion," *Physical Review A* **49**, 438-448 (1994).

[3] **J. Geabanacloche, Y. Q. Li, S. Z. Jin and M. Xiao**, "Electromagnetically induced transparency in ladder-type inhomogeneously broadened media - theory and experiment," *Physical Review A* **51**, 576-584 (1995).

[4] **S. Q. Gong, Z. Z. Xu and S. H. Pan**, "The effect of phase fluctuation on electromagnetically induced transparency, inversionless lasing and refractive-index enhancement in a lambda-system," *Journal of Modern Optics* **42**, 1397-1406 (1995).

[5] **S. Q. Gong, Z. Z. Xu, Z. Q. Zhang and S. H. Pan**, "Change from an inversion laser to a noninversion laser due to a phase-fluctuation effect," *Physical Review A* **52**, 4787-4790 (1995).

[6] **S. Q. Gong and Z. Z. Xu**, "The effect of phase fluctuation on absorption and dispersion in a v-medium," *Optics Communications* **115**, 65-70 (1995).

[7] **G. Vemuri, K. V. Vasavada and G. S. Agarwal**, "Lasing without inversion in the absence of a coherent coupling field," *Physical Review A* **52**, 3228-3230 (1995).

[8] **A. G. Kofman**, "Electromagnetically induced transparency with coherent and stochastic fields," *Physical Review A* **56**, 2280-2291 (1997).

[9] **J. R. Boon, E. Zekou, D. J. Fulton and M. H. Dunn**, "Experimental observation of a coherently induced transparency on a blue probe in a Doppler-broadened mismatched V-type system," *Physical Review A* **57**, 1323-1328 (1998).

[10] **M. O. Scully and M. Suhail Zubairy**, *Quantum Optics*. (CUP, Cambridge, 1997).

[11] **J. Mompart and R. Corbalan**, "Inversionless amplification in three-level systems: dressed states quantum interference and quantum-jump analyses," *Optics Communications* **156**, 133-144 (1998).

[12] **Y. F. Zhu**, "Lasing without inversion in a closed 3-level system," *Physical Review A* **45**, R6149-R6153 (1992).

[13] **J. Mompart, R. Corbalan and R. Vilaseca**, "Lasing without inversion in the V-type three-level system under the two-photon resonance condition," *Optics Communications* **147**, 299-304 (1998).

[14] **C. Peters and W. Lange**, "Laser action below threshold inversion due to coherent population trapping," *Applied Physics B-Lasers and Optics* **62**, 221-225 (1996).

Chapter 5

Polarisation and Two-Photon Effects in EIT

5.1 Two-Photon Effects in EIT

The nature of two-photon processes in EIT was investigated by Moseley *et al* [1], and was shown to be an intrinsic part of the EIT mechanism. It is this process which we examine in further detail in this chapter. Two different phenomena are discussed: the first is the how the two photon imprint in EIT is changed by the polarisation of the probe and coupling fields. In doing so we provide a comprehensive investigation in the role of polarisation and spectral lineshapes in cascade scheme EIT. The second phenomena is a process suggested by Agarwal and Harshawardham [2] in which EIT is used to inhibit two-photon absorption, or in some cases to enhance it. Examined are the properties of a similar type of scheme to that in [2] except that a four level V-manifold is investigated instead of a four level Y-manifold. Interesting properties are found to occur such as a medium that displays multiple dark states.

5.2 Polarisation Effects on EIT in a Cascade Scheme

The effect that probe and coupling field polarisation have on EIT has been little studied, except when it is explicitly important in experiments dealing with, for example, Zeeman splitting [3]. Of late there has been some interest, however, particularly in coherent control of polarisation [4], where EIT is used to change the polarisation state of the probe field, thus turning the atomic medium into a waveplate. Interest has also fallen on the use and enhancement of magneto-optical effects [5, 6] where EIT effects coupled with non-degenerate magnetic sublevels can produce enhancement of magneto-optical rotation and even produce a magneto-optical switch. Studies by Durrant *et al.*[7] have examined the role of polarisation in EIT in a Lambda scheme within a MOT. In this chapter the effect of changing field polarisation in a situation where the magnetic sublevels are degenerate is studied. We calculate transition probabilities for photons of either linear or circular polarisation in a cascade scheme in rubidium and examine the predicted EIT curves. By using EIT to examine the hyperfine structure of the upper coupling field transition we can then compare our theory with experimental data. We also examine how EIT can be improved or degraded by changing field polarisation.

More specifically we examine the 'two-routes to excitation' model of EIT and show that the strength of the two-photon absorption results in enhancement or degradation of EIT depending on the probe and coupling field polarisation. In our cascade scheme it is also possible to resolve the hyperfine structure of the upper coupling field transition using EIT [1], and we show how polarisation affects this method of atomic spectroscopy.

5.3 Theoretical Considerations

5.3.1 Two-photon Effects

The experimental atomic system is shown on the left hand side of figure 5.1. It is in essence a simple three level cascade scheme used in a number of experiments [8, 9].

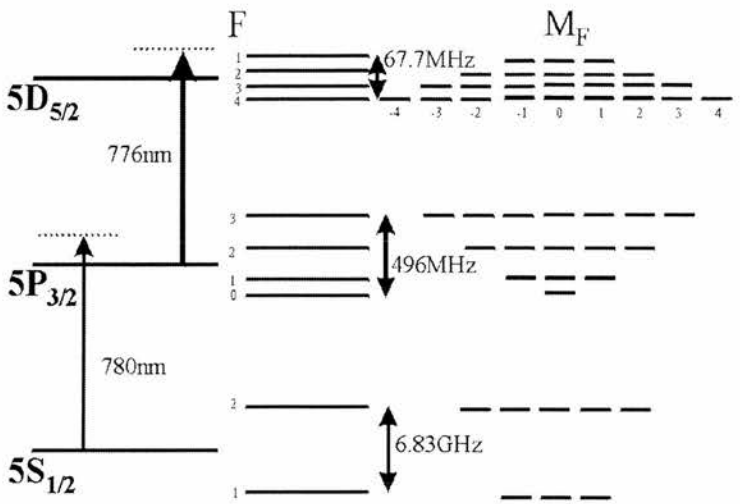

Figure 5.1: *Level structure (^{87}Rb) under consideration for observation of polarisation effects on EIT.*

However, rubidium has a much more complicated structure due to its intrinsic nuclear spin, therefore in order to examine fully the two-photon effects we must take into account all the sublevels. Note in this chapter we only consider the $5S_{1/2}$(F=2) - $5P_{3/2}$(F'=1,2,3) - $5D_{5/2}$(F''=1,2,3,4) transitions of ^{87}Rb but our arguments are valid for any of the rubidium isotopes or ground state F levels. Previously, it has been shown what role two-photon interference plays in EIT [1]. Extending this work by calculating the two-photon transition probabilities for the $5S_{1/2}$ - $5P_{3/2}$ - $5D_{5/2}$ transition we are able to predict the relative magnitudes of EIT features for various probe and coupling field polarisation orientations. The transition amplitude for an atomic transition between two m_F levels is given by [10]:

$$< IJFm_F \left| d_q \right| IJ'F'm'_F > = (-1)^{F-m_F} \begin{pmatrix} F & 1 & F' \\ -m_F & q & m'_F \end{pmatrix} x(-1)^{I+J+F+1} \sqrt{(2F+1)(2F'+1)} \begin{Bmatrix} J & 1 & J' \\ F' & I & F \end{Bmatrix} \left\langle J \| d \| J' \right\rangle \tag{5.1}$$

where I is the nuclear spin (I = 3/2 for Rb^{87}), J is the angular momentum, F the total angular momentum and m_F the magnetic sublevels of F states. Each F states has (2F+1) degenerate m_F values. The primes on the quantum numbers (e.g. J') correspond to the initial state in which the atom resides. The value d_q is the dipole operator and the value of q is polarisation dependent, with:

$$q = m_F - m'_F = 0 \tag{5.2}$$

for linearly polarised light, and:

$$q = m_F - m'_F = \pm 1 \tag{5.3}$$

for circularly polarised light. The value $\left(J\|d\|J'\right)$ is the reduced matrix element as defined by Shore [10], and can be left unevaluated if one is considering only the relative dipole matrix strengths, as is the case in this work. The values in the (...) denote standard 3j symbol notation and similarly the values in the {...} denote standard 6j symbols [10, 11]. Here they are evaluated via a mathematical algebra package.

We can then easily calculate the relative transition strengths, without evaluating the reduced matrix element $\left(J\|d\|J'\right)$, using:

$$S_q = \left| < IJFm_F \left| d_q \right| IJ'F'm'_F > \right|^2 \tag{5.4}$$

We then normalise the relative transition strengths for each transition for given initial values of F and q (polarisation). The normalised transition strengths are then treated as the probability value for excitation and by appropriate addition and multiplication we are able to calculate the probability of starting in a given F, m_F level and ending up in any other F, m_F level. As such we are able to predict values for the two photon transition strengths and hence the strength of observed EIT features.

In examining the EIT in our cascade system we use nine combinations of field polarisation, with π representing linearly polarised light, σ^+ right-handed circularly polarised light and σ^- left hand circularly polarised light. We see that there are a number of possible transition routes to the upper state each with its own weighted probability. By multiplying probabilities for the two transitions $5S_{1/2} - 5P_{3/2}$ and $5P_{3/2} - 5D_{5/2}$ we end up with a two-photon transition probability for each allowed m_F to m_F level. Then summing over all allowed transitions we arrive at a transition probability between F states. The full set of probabilities can be seen in table 5.1, below. The values for the case where both optical fields have π polarisation have been included in figure 5.2.

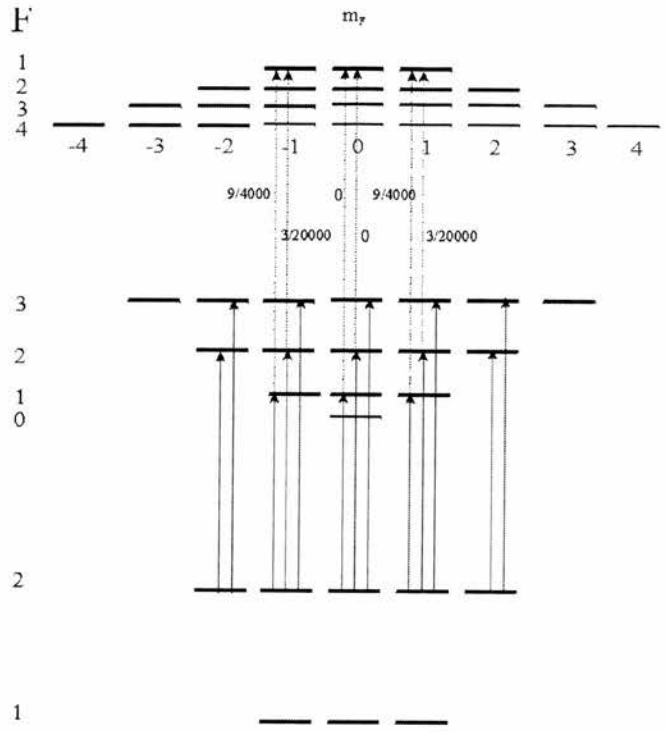

Figure 5.2: *Transition routes and probabilities in the case where probe and coupling field have linear (π) polarisation.*

It should be noted that for our system we can legitimately multiply and add across the relevant dipole transitions because each system is independent of the others. An examination of figure 5.2 highlights this fact. In order to end up in the $5D_{5/2}$ (F=1) upper state an atom may interact with the applied optical fields and arrive in this state via either the $5P_{3/2}$ (F=1) or $5P_{3/2}$ (F=2) intermediate state. The choice of which route is employed by the atom is dependent on its relative velocity. This velocity component selects which intermediate level the atom is Doppler shifted into resonance with, and hence which route it employs to the upper level. If the situation had been that a particular atom had a certain probability of employing one route as opposed to the other then the route to the upper state would be more complicated. It would involve calculating the coherent superposition of two separate wavefunctions and therefore we would be unable to simply add and multiply across the normalised transition probabilities.

Probe Polarisation	Coupling Polarisation	Peak I F''=4	Peak II F''=3	Peak III F''=2	Peak IV F''=1
π	π	3600	1232	1160	168
π	σ^+	2700	2044	695	231
π	σ^-	2700	2044	695	231
σ^+	σ^+	5400	1848	690	252
σ^+	σ^-	900	1428	1165	147
σ^+	π	2700	2044	695	231
σ^-	σ^-	5400	1848	690	252
σ^-	σ^+	900	1428	1165	147
σ^-	π	2700	2044	695	231

Table 5.1: *Two-photon transition probabilities for $5S_{1/2}(F=2)$ - $5P_{3/2}(F'=1,2,3)$ - $5D_{5/2}(F''=1,2,3,4)$ route in rubidium. The values are expressed as parts of 35,000.*

Shown in table 5.2 are the two-photon transition probabilities of ending up in the F=4 state of the $5D_{5/2}$ level, normalised against the largest value. This gives us a measure of the relative amount of EIT we expect for each combination of field polarisations.

Probe Polarisation	Coupling Polarisation	Peak I
π	π	0.69
π	σ^+	0.48
π	σ^-	0.45
σ^+	σ^+	1
σ^+	σ^-	0.16
σ^+	π	0.48
σ^-	σ^-	0.97
σ^-	σ^+	0.16
σ^-	π	0.51

Table 5.2: *Two-photon transition probabilities for ending up in the F=4 state of the $5D_{5/2}$ level. The values are normalised against the largest value.*

5.3.2 Observation of Doppler free EIT

To conclude our theory section we briefly look at the conditions for observing sub-Doppler EIT. EIT is a two photon resonance process [1]. The location of an EIT resonance in the cascade system is given by.

$$\Delta_1 + \Delta_2 = 0 \tag{5.5}$$

where Δ_1 is the probe field detuning (figure 5.1) and Δ_2 the coupling field detuning. Therefore, the location of an EIT resonance is independent of the structure and position of the intermediate level. It is the energy separation of the lower and upper levels, relative to the photon energies of the applied optical fields that is the important parameter. However, for the EIT effect to be physically observed it is required that the probe field falls within the absorption linewidth of the $5S_{1/2}$ - $5P_{3/2}$ probe transition. The individual detunings can be written in terms of the Doppler

shift, kV_z on a transition for an atom with velocity component V_z in the direction of the beam propagation:

$$\Delta_1 = \Delta_1^0 + k_1 V_z \tag{5.5}$$

$$\Delta_2 = \Delta_2^0 + k_2 V_z \tag{5.6}$$

where Δ_1^0 is the detuning of the applied field from the atomic transition and k_i is the wavenumber of the applied light. In order to observe sub-Doppler effects on the probe field it is necessary to reduce the two photon residual linewidth below that of the single photon probe field Doppler width. The residual Doppler width of the two-photon transition is:

$$\Delta\nu = \left|(k_1 + k_2)u\right| \tag{5.7}$$

where:

$$u = \sqrt{2k_B T / M} \tag{5.8}$$

T being the temperature of the gas and M the atomic mass. The first requirement to minimise the residual Doppler width is to choose a system which employs optical fields of nearly equal wavelengths i.e. $|k_1| \approx |k_2|$. If the two input fields then counterpropagate the frequency shifts on the individual transitions will be in the opposite direction and the residual Doppler width will be low, similar to the situation occurring in Doppler free two photon spectroscopy [12]. For the cascade system being considered in this work the co-propagating two photon width is 536 MHz while with counter-propagating fields this value reduces to only 1.38 MHz, at 320K. These values compare with the single photon probe Doppler width of 528 MHz. Therefore, the fact that the probe and coupling field wavelengths are closely matched can be used, in effect, to cancel out the masking effects of Doppler broadening on the probe transition that would normally act to obscure the observation of EIT.

5.4 Experimental Set-up

The experimental set-up used to investigate these effects is shown in figure 5.3. We make use of two single frequency continuous wave Ti:Sapphire lasers, one a Microlase MBR- 110 which is employed as the probe field. It generates light at around 780nm for interaction with the $5S_{1/2}$ - $5P_{3/2}$ transition and is tuneable across this atomic transition. It has a linewidth of <100kHz. The coupling laser is a modified Schwarz Electro-Optic Titan CW and provides radiation at around 776nm for interaction with the $5P_{3/2}$ - $5D_{5/2}$ transition. The coupling laser is passively stable and it is possible to manually tune it by employing a solid etalon and a set of Brewster plates. It has a linewidth of <5MHz. We estimate that the coupling field Rabi frequency is approximately 30MHz. The rubidium cell used is 2cm long and is heated to approximately 60°. The coupling field is unfocussed through the cell and the probe is only weakly focussed in order to keep its

spatial profile within that of the coupling field. So as to minimise power broadening effects we do not employ further focusing of the beams. The absorption traces are monitored by a photodiode placed after the cell and phase sensitive detection is used to improve the signal to noise ratio. In order to control the polarisation of the fields a Soleil-Babinet compensator is placed in the path of both the probe and coupling fields before they enter the cell. Both fields are linearly polarised in the same sense before propagation through the compensators. It should be noted that if the polarisation of the probe and coupling field are set to be in the same circular polarisation then the atomic sample will 'observe' the polarisation of both fields as though they are circularly polarised in the opposite sense since the beams are counter-propagating.

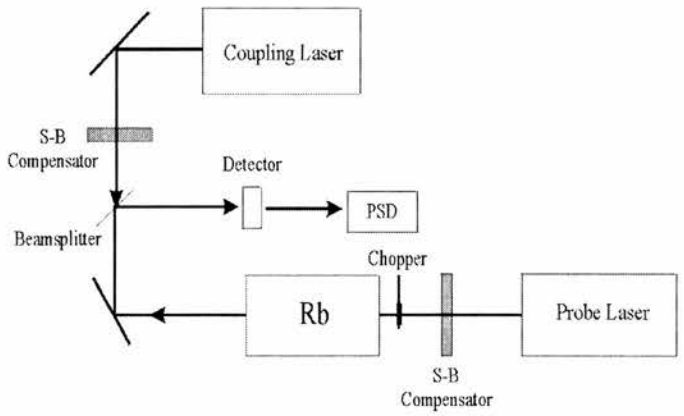

Figure 5.3: *Experimental Set-up for investigation of beam polarisation effects on EIT.*

We must also take into account the axis of quantisation for the system. This effectively determines how we apply the selection rules and also how we treat the polarisation of the fields. For instance if we choose a quantisation axis that is perpendicular to a field with linear polarisation it will mean that the field should be treated as a superposition of left and right handed circularly polarised light. This would obviously complicate our treatment somewhat. It turns out, however, that we are able to choose an arbitrary quantisation axis in the case we are dealing with (i.e. two light fields with no applied magnetic field) [10] and this enables us to proceed in the manner described above. In the case that we discuss in chapter 6, where a magnetic field is also applied we must treat the problem with more care.

5.5 Experimental Results

The experimental traces corresponding to the rows VI, IV and V of table 5.1 have been reproduced in figures 5.4(a), (b) and (c) respectively. It can be seen that each of the absorption profiles are broadly similar, each consisting of three resolvable EIT peaks. In all the traces there should in fact be a fourth peak, corresponding to the F=1 state in the $5D_{5/2}$ level, however the relative dipole strengths of the two-photon routes terminating in this state are so weak these peaks can not be resolved. The relative depths of each of these peaks can be seen to depend on the relative polarisation orientations of the applied optical field as predicted. Figure 5.5 compares directly the situation outlined in row IV and V of table 5.1. It can clearly be seen that the depth of EIT feature in the σ^+-σ^+ case is much greater than in the σ^+-σ^- case.

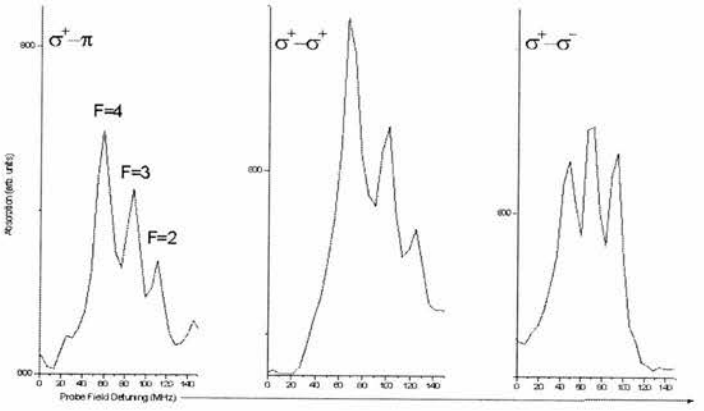

Figure 5.4: *Experimental traces for the (a) σ^+-π, (b) σ^+-σ^+, and (c) σ^+-σ^- cases.*

In general EIT experiments upper state hyperfine structure would not be observed due to power broadening effects. This is due to the fact that high powered coupling fields are normally employed and both fields are also usually focused within the cell in order to obtain better spatial profile matching of the beams. The combined effect is to induce coupling field Rabi frequencies much closer to the single photon Doppler width of the probe field (i.e. $>>\Delta\nu_D$) and hence power broadening effects become significant. In this experiment by choosing not to focus the optical fields we are able to resolve the hyperfine levels in the upper transition as shown in the experimental traces figures 5.4 and 5.5.

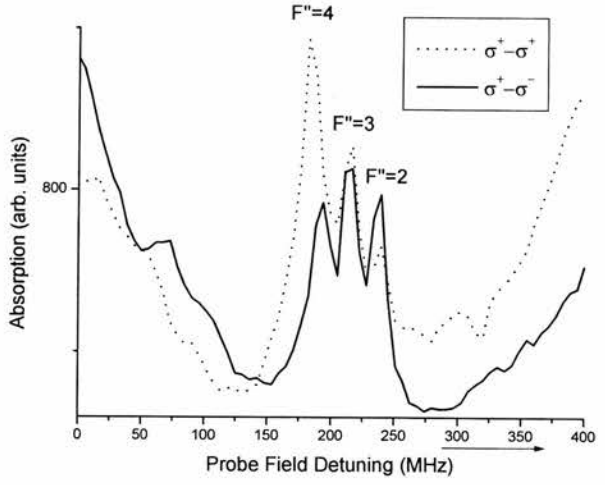

Figure 5.5: *Comparing the depth of EIT in two different polarisation configurations. We clearly see that better EIT is observed in the σ^+-σ^+ case than in the σ^+-σ^-.*

It is well known that the two-photon absorption route is fundamental to the EIT process. It is the interference between the one and two photon routes to the upper probe level that is of

fundamental importance in EIT. This has clearly been shown by Moseley *et al* [1]. Therefore, the greater the probability of a two-photon transition within a particular system then the greater the EIT feature we would expect to observe. Thus as the two-photon transition probability changes, which will happen as the probe and coupling field polarisations are changed, we expect the EIT to change aswell. EIT is the imprint of the two-photon process on the probe field absorption. This is exactly what we observe, as outlined in figure 5.5. In the case of σ^+-σ^+ polarisation we expect a two-photon probability of 0.22 of being in the $5D_{5/2}$ level; compare this to the probability of 0.11 of being in the $5D_{5/2}$ level with σ^+-σ^- polarisation. We see in figure 5.4 that the overall amount of EIT does indeed change from one polarisation orientation to the next, explained quite simply by the two-photon transition probabilities.

We now examine the EIT traces showing the structure in the upper coupling field level. Consider the three traces shown in figure 5.4. It can be seen that there is a significant difference between traces when the circular polarisation of the applied fields is in the same or in the opposite sense (as experienced by the atomic sample). Relative to the σ^+-σ^+ field orientation it can be seen that in the σ^+-σ^- case the F=4 peak is significantly reduced, to such an extent that the F=3 peak is larger. These results are readily explained when the two-photon probabilities are examined, see table 5.1. However we cannot directly compare the EIT in each of the polarisation cases. This is due to the fact that rotation of the Soleil-Babinet compensators shifts the probe and coupling beams slightly changing their overlap. Also the drift of the coupling field changes the exact position of the peaks and hence exactly where their height should be measured from. We can however examine how our theory compares with experiment in each individual case. In figure 5.4 (a), the σ^+-π case, we predict a ratio of peak depths (F=4:F=3:F=2) of 1.32:1:0.34. We observe a ratio of 1.2:1:0.6, in reasonably good agreement with our predictions. For the σ^+-σ^+ case (figure 5.4 (b)), we predict a ratio of 2.92:1:0.37 and observe a ratio of 1.62:1:0.46, which implies we did not resolve the F=4 peak well enough. In the final case of σ^+-σ^-, (figure. 5.4 (c)), we predict a ratio of 0.63:1:0.82 and observe a slightly worse ratio of 0.83:1:0.88. So our predictions are in broad agreement with our observations and the general trends in relative peak sizes are all correct. We also see from table 5.1 that in fact the optimum orientation for observing EIT. is when the field orientations are circularly polarised in the same sense as seen by the atom. The prediction of the two effects whereby the EIT is maximised in the σ^+-σ^+ case and the fact that the F=3 hole is larger than the F=4 hole in the σ^+-σ^- case (which is not an obvious result) implies that our theory is largely correct.

Such findings have potential use when using EIT as a method of spectroscopy [1]. We can envisage a situation where hyperfine structure is unable to be resolved, for example due to power broadening effects of the coupling field. If we can change polarisation orientation to enhance the EIT we can bring down the required coupling field power and therefore begin to resolve the structure. We note that such effects in other schemes; e.g. Lambda and V-scheme may also be of interest [6].

5.6 Polarisation Effects Conclusions

In conclusion, we have shown that the polarisation of the optical fields plays an important role in electromagnetically induced transparency experiments. EIT can be enhanced or degraded by the appropriate choice of polarisation for the probe and coupling fields. We have shown that this phenomenon is a direct result of the relative probability of the two-photon transition from the ground state to the upper state connected by the coupling field.

By taking into account all of the degenerate magnetic hyperfine levels it was possible to explore and explain the cases where EIT may be used as a method of spectroscopy to examine the hyperfine structure of this upper coupling field state. Again it was seen that polarisation orientation effects were evident. EIT absorption profiles can be significantly altered by use of appropriate polarisation orientations of the optical fields. If EIT is to be employed as a method of spectroscopy this must be taken into account. A second area of relevance where these effects should be considered is in experiments to study EIT effects where a magnetic field is applied to a medium in order to lift the magnetic sublevel degeneracy i.e. in magneto-optical effects

5.7 EIT Effects in a Four Level Vee-Scheme

We will now examine a number of EIT related effects in a four-level Vee scheme. Specifically we investigate the system shown in figure 5.6. The third applied field is able to control the coupling field and hence some interesting effects are found in exploring such a system including the inhibition of two-photon absorption. We will also see effects analogous to those that will be examined in greater detail in the context of N-Level cascade schemes in Chapter 6.

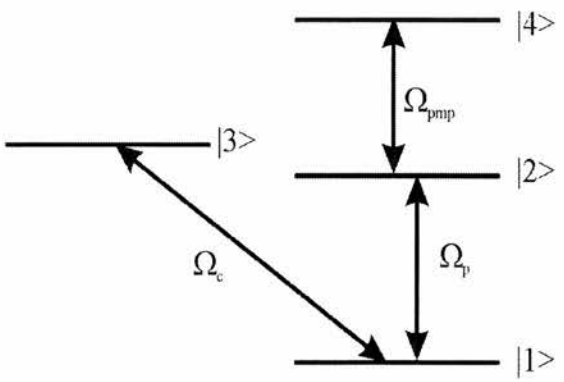

Figure 5.6: *Four level Vee-Scheme. Decay rates are not shown but each level can decay to any other except from |3> - |2> or |4> - |1>.*

The idea that two-photon absorption can be suppressed in four level systems via coherent effects was proposed by Agarwal and Harshawardhan [2]. They examined a Y scheme shown in figure 5.7. The two photon process from the ground state to state |3> will occur as normal until the control field (coupling field) is applied. Effectively what happens when the coupling field is applied is that the probe transition between |1> and |2> is made transparent and hence the two-photon absorption is by necessity reduced. It can also be argued that transparency is induced on the |2> - |3> transition by the coupling field. This will act to further suppress the two-photon

process. Recently Gao *et al* [13] have shown that this inhibition is possible. Making use of a Y scheme in sodium vapour they demonstrated a 60% reduction in two-photon absorption.

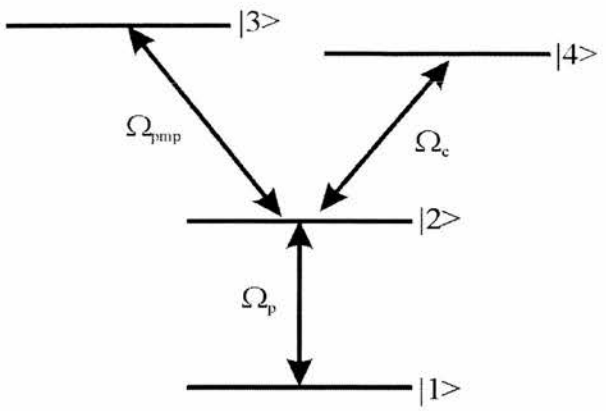

Figure 5.7: Y-scheme considered by Agarwal and Harshawardhan. The two-photon route is |1> -|2> - |3> and can be controlled via the coupling field, Ω_c on the |2> - |4> route.

In the four level system considered here the system dynamics are slightly different to those in the Y scheme and depending exactly what type of effect we wish to see we can change which of the fields acts as the coupling field (by changing the appropriate field strengths). For examination of two-photon inhibition we make the field applied to the |1> - |2> transition the coupling field. This will allow the absorption on the |1> - |3> transition to be modified and hence the two-photon absorption from the |1> - |4> route to be inhibited. Our system is also different in that the coupling field is applied to the ground state and will therefore play a role in reducing two-photon absorption via a saturation process.

To examine two-photon absorption we monitor the coherence ρ_{44} which gives a measure of the population of the upper level of the two photon transition, level |4>. We make the two fields involved in the two-photon process weak and monitor what happens when we increase the strength of the control (coupling) field. We would expect that as the control field becomes strong enough to induce transparency on the |1> - |2> transition the two-photon absorption will reduce. This is what we see in figure 5.8. For high control fields we can reduce the two-photon absorption to almost zero. We can envisage, for instance, an experimental realisation of this type of system in rubidium with the |1> - |2> and |1> - |3> transitions being either of the D lines and the |2> - |4> transition being the 776nm, $5D_{5/2} - 5P_{3/2}$ transition.

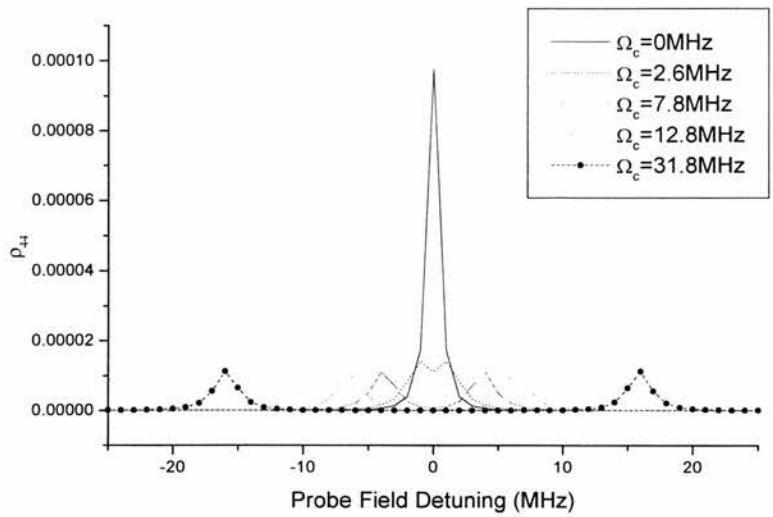

Figure 5.8: *Change in two-photon absorption (displayed as population in level |4>) with coupling field Rabi frequency as a function of probe field detuning.*

We can also drive the four level system in other ways. We first examine how the absorption on the |1> - |2> transition is altered by having the other two fields act as coupling fields. In the first instance we set the field strength of the coupling field on the |2> - |4> transition to 3.2MHz and vary the other coupling field on the |1> - |3> transition. We observe the probe absorptions shown in figure 5.9.

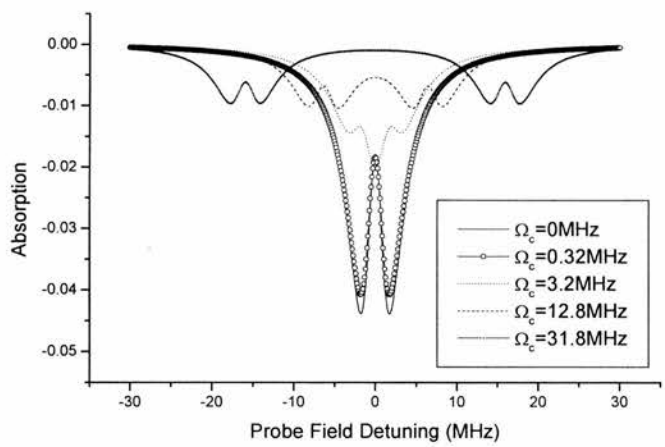

Figure 5.9: Probe absorption as a function of probe field detuning. The applied coupling field strength is varied while Ω_{pmp} = 3.2MHz.

As we increase the strength of the coupling field we see that EIT is induced. When we match the strength of the two coupling fields, i.e. both fields have a Rabi frequency of 1.6MHz we observe a triplet structure. As the field strength of the coupling field is increased beyond 1.6MHz we observe an EIT structure where the main Autler-Townes peaks are themselves split into two

components. We see that the system can be driven into states that can be said to be 'dark'. For instance the splitting of the individual Autler-Townes peaks produce areas of lower absorption than their surroundings. By judicious choice of decay rates and Rabi frequencies we can make these areas darker, that is less absorbing, than the central EIT point. Such systems have multiple dark states and are examined further in chapter 6 and by Lukin *et al* [14].

Next we consider the case where the field on the |1> - |3> transition is kept fixed with a Rabi frequency of 3.2MHz and the other coupling field strength is varied. We see the results in figure 5.10. This time the splitting of the Autler-Townes peaks is much less pronounced and is slightly asymmetric. Again, we see a triplet structure when the two coupling field strengths are matched. If we increase the strength of the field on the |1> - |3> transition to 15.9MHz and then vary the strength of the other coupling field we see the absorption profiles shown in figure 5.11.

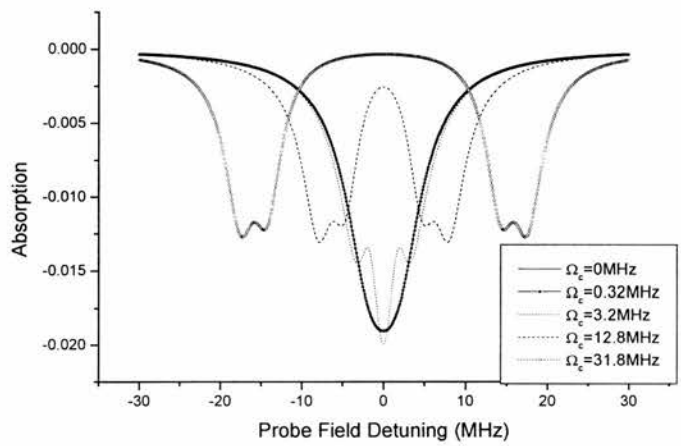

Figure 5.10: *Probe absorption profiles as a function of probe field detuning. In this case the value of Ω_{pmp} is varied while Ω_c is kept constant at 3.2MHz. Note that the curves for Ω_{pmp} = 0MHz and Ω_{pmp} = 0.32MHz overlap.*

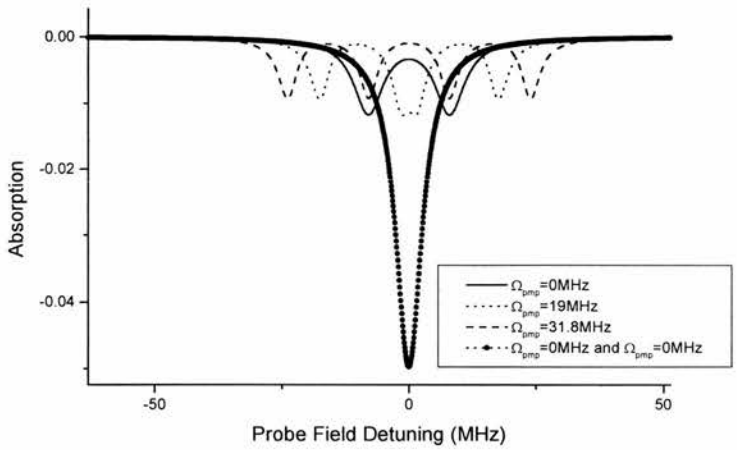

Figure 5.11: *Probe absorption profiles as a function of probe field detuning. In this case the value of Ω_{pmp} is varied while Ω_c is kept constant at 15.9MHz. We now see multiple dark states appearing. A plot when both Ω_{pmp} and Ω_c are both zero is shown for comparison.*

We now see that we drive the system into areas with multiple dark regions and also that when the field strengths of the two coupling fields are matched the triplet that we observe results in a significant destruction of EIT on line-centre. We also see by comparing the triplet structure with the lineshape in the absence of either of the coupling fields that the on-resonance part of the triplet has a narrower linewidth that the bare probe absorption. So our system also results in some line-narrowing.

To confirm the idea that matching the coupling field strengths results in a triplet structure we match both field strengths and then vary them. The resulting probe absorption is plotted in figure 5.12. A triplet structure is indeed found in all cases except when the coupling field strength is very low (not big enough to induce any splitting of the levels).

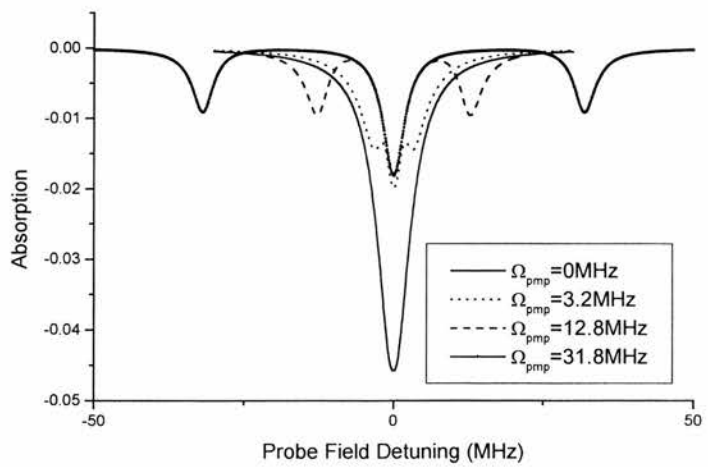

Figure 5.12: *Probe absorption profiles as a function of probe field detuning with $\Omega_{pmp} = \Omega_c$.*

5.7.1 Absorption profile discussion

Why does this four level system display these absorption profiles? The results can be explained in a number of ways. The first is the one we discussed above for the control of two-photon absorption, namely that we have two competing routes to EIT. We see that one of the coupling fields is the dominant in the EIT process and the other merely perturbs the dominant EIT process. The form of this perturbation is to produce a splitting in the Autler-Townes components of the main EIT profile proportional to the second coupling field's Rabi frequency.

We can also consider the process to be a multiphoton phenomena much in the same way that normal EIT is an interplay between a one and two photon pathway to excitation. We can in fact 'detune' out the one, two and three photon absorptions that make up the EIT processes in the four level system and this is shown in figure 5.13. However the actual pathways that are involved in the Vee scheme are rather more difficult to visualise than in the cascade systems we discuss in chapter 6, so we will investigate the absorption profiles in terms of induced Autler-Townes splittings as this is the simplest visual model.

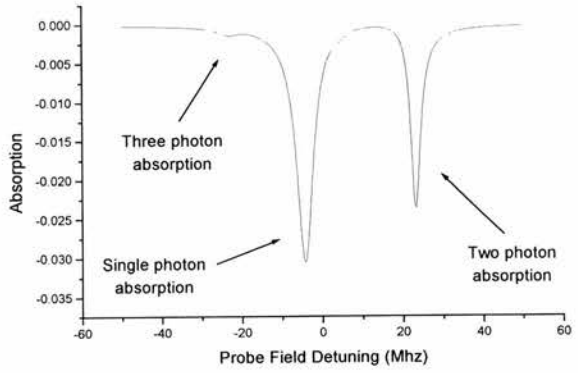

Figure 5.13: *Probe field absorption with the coupling and pump fields detuned. This allows us to see the underlying one, two and three photon absorptions that lead to the quantum interference effects. The detunings are Δ_{pmp}=-10MHz and Δ_c=-10MHz. The field strengths are Ω_{pmp}=25.5MHz and Ω_c=15.9MHz.*

The splitting of a level induced by the application of a field is shown below (figure 5.14) for both a resonant and detuned field. We see that in the resonant case the level is split symmetrically about the position of the level. For instance if we then probe such a two-level atom while it is being driven by a strong coupling field, we observe a triplet structure, called the Mollow Triplet[1] [15, 16], illustrated in figure 5.15. We can therefore immediately see why we observe a triplet structure in the case where the Rabi frequencies of the two driving fields are the same. We create the same splitting on the lower level of the probe transition as on the upper level and hence a triplet structure.

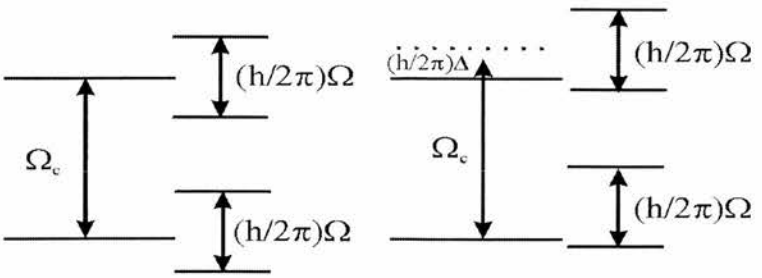

Figure 5.14: *Aulter-Townes splitting of a strongly driven two level atom. On the left the case where the field is on resonance, and on the right, where the field is detuned. The coupling field Rabi frequency is given by Ω_c and the generalised Rabi frequency* $\Omega = \sqrt{\Omega_c^2 + \Delta^2}$.

The other probe absorptions that we observe are therefore the result of a mismatch in the amount of splitting of the lower and upper levels of the probe transition. The case where the splitting of the lower level is greater than that of the upper level is shown in figure 5.16. The opposite case will obviously be similar in nature. Effectively this means that we can treat the four level system as a two level atom such as that shown in figure 5.15 in which the splitting of the upper and lower level can be independently controlled. This is qualitatively the same as if we considered the system in a dressed state basis.

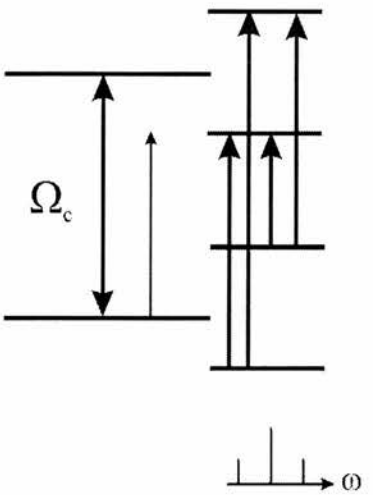

Figure 5.15: *Probing a strongly driven two level atom – Mollow Triplet structure.*

[1] The Mollow Triplet actually refers to a spectrum seen in emission rather than absorption but the principle is the same.

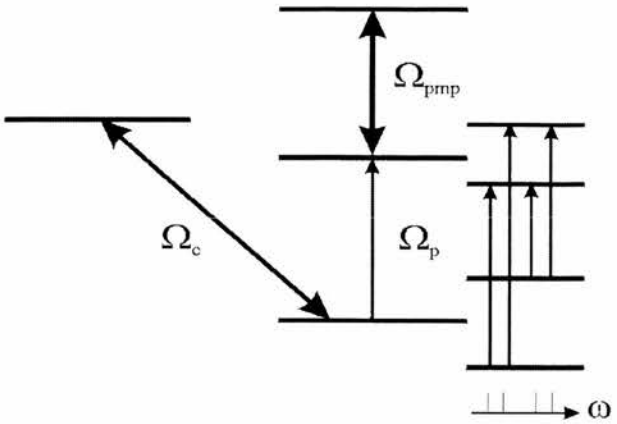

Figure 5.16: *State splitting in the four level Vee-scheme. Here the Rabi frequency of the lower coupling field $\Omega_c > \Omega_{pmp}$. The absorptions leading to the observed profile are shown on the right.*

If we examine the equation that governs the probe absorption we can see what role the inclusion of a third field plays:

$$\rho_{12}^{i} = \frac{\Omega_p(\rho_{22} - \rho_{11}) - \Delta_{12}\rho_{12}^{r} - \Omega_{pmp}\rho_{14}^{r} + \Omega_p\rho_{23}^{r}}{\gamma_{12}} \tag{5.9}$$

In the case where no third field is applied, i.e. either Ω_c or Ω_{pmp}=0, then the system will behave as a normal cascade or Vee-scheme respectively. For instance in the case where Ω_{pmp}=0 then we see that probe absorption is controlled by the ρ_{23} coherence (that of the unlinked transition) as we would expect for normal EIT. Where we have a finite Ω_{pmp} then we see that a competing coherence, ρ_{14} comes into play and it is the interaction of these two 'unlinked' transition coherences that results in the lineshapes that we observe. We can also say, therefore, that the process we observe are coherent processes driven by the interaction of the unlinked transition coherences. This is akin to the phenomena described by Lukin *et al* [14] which they describe as interacting dark resonances.

5.7.2 Coherently driven Four Level Vee-Scheme

We now examine the case where the probe field is resonant with the |1> - |3> transition and two strong fields couple the |1> - |2> and |2> - |4> transitions respectively. The effects on the probe absorption in such a system are less obvious than in the cases considered above. We may expect to observe gain in this configuration since the decay from level |4> can be used to populate the upper probe transition. If we set the lower coupling field, |1> - |2>, at 15.8MHz and then examine what happens as the upper coupling field is increased, we see an absorption profile like that shown in figure 5.17. We see that as we increase the pump field Rabi frequency we drive the system into a state where gain is possible and then ultimately destroy the gain. In fact what we are observing here is the coherent pump field inducing transparency on the coupling field. So ultimately the probe field sees little effect due to either of the other applied fields (expect maybe

a slight reduction in overall absorption due to some residual coupling field population movement). As has been noted by Fulton [17] and Boon [18], the gain observed is improved when an incoherent pump is used instead of a coherent one.

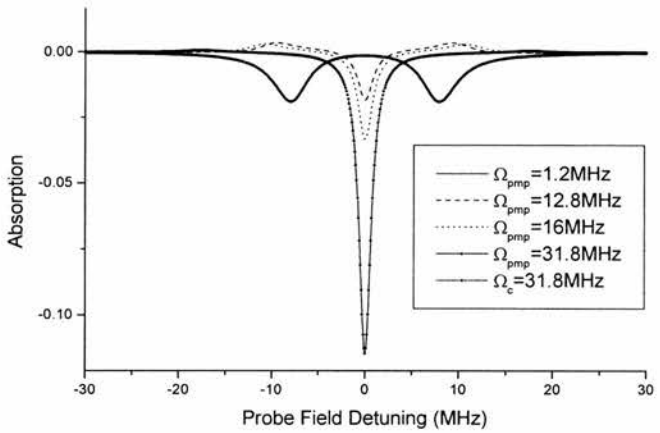

Figure 5.17: *Coherent pumping of four level Vee-scheme. Probe absorption/gain is shown as a function of probe field detuning. Each trace represents a different pump field Rabi frequency.*

5.7.3 The Dressed State basis

We can also examine the probe field absorption in the dressed state [19]. This allows us to easily see the effect of the driving field(s) have on the system, including the mechanism by which interference comes about.

5.7.3.1 Two-Photon Inhibition case

We begin by looking at the case in which we inhibit the two photon absorption (|1>-|2>-|4> route) via the coupling field on the |1>-|3> transition. The Hamiltonian for the Vee-scheme may be written as:

$$\begin{aligned} H = \hbar\Delta_1 |2\rangle\langle 2| + \hbar(\Delta_1 + \Delta_2)|4\rangle\langle 4| + \hbar(\Delta_1 + \Delta_1)|3\rangle\langle 3| \\ -\hbar\left(\Omega_{pmp}|2\rangle\langle 4| + \Omega_c|1\rangle\langle 3| + \Omega_p|1\rangle\langle 2| + H.c\right) \end{aligned} \tag{5.10}$$

which can be written as the matrix:

$$H = \begin{pmatrix} 0 & -\Omega_p & -\Omega_c & 0 \\ -\Omega_p & \Delta_1 & 0 & -\Omega_{pmp} \\ -\Omega_c & 0 & \Delta+\Delta_1 & 0 \\ 0 & -\Omega_{pmp} & 0 & \Delta_1+\Delta_2 \end{pmatrix} \tag{5.11}$$

We make the assumption that the probe and pump fields are much weaker than the coupling field and so we can set Ω_p=Ω_{pmp}=0. We also assume two-photon resonance and set Δ=Δ_1=-Δ_2. In such a case we have two relevant eigenfrequencies:

$$\omega_{\pm} = \Delta \pm \sqrt{\Delta^2 + \Omega_c^2} \tag{5.12}$$

The corresponding (normalised) eigenstates, the dressed states of the system, are:

$$|\pm\rangle = \frac{\omega\pm}{\Omega_c\left(1+\left[\frac{\omega\pm}{\Omega_c}\right]^2\right)^{1/2}}|1\rangle + \frac{1}{\left(1+\left[\frac{\omega\pm}{\Omega_c}\right]^2\right)^{1/2}}|3\rangle \tag{5.15}$$

We now see how the two photon absorption can be inhibited. There are two routes that the excitation can take, |+>-|2>-|4> or |->-|2>-|4>. This is shown in figure 5.18.

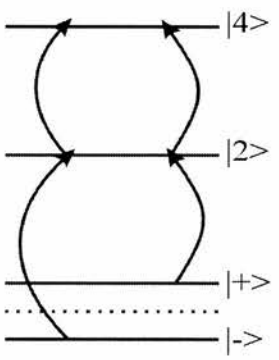

Figure 5.18: *Two photon inhibition in the dressed state basis. The states |+> and |-> are the result of the strong coupling field on the |1> - |3> transition in the bare state basis. It is the fact that we have two independent routes that are able to interfere that leads to the inhibition of the two photon absorption.*

5.7.3.2 The Doubly-driven System

We now look at what happens in the system where the probe field is resonant between the |1> - |2> transition and the other two fields are strong in comparison. In this case, with the probe field detuning equal to zero we find that there are four dressed states given by:

$$|\pm_1\rangle = \frac{1}{\sqrt{1+\left(\omega_{\pm_1}/\Omega_c^2\right)}}\frac{\omega_{\pm_1}}{\Omega_c}|1\rangle + \frac{1}{\sqrt{1+\left(\omega_{\pm_1}/\Omega_c^2\right)}}|3\rangle \tag{5.16}$$

$$|\pm 2\rangle = \frac{1}{\sqrt{1+\left(\omega_{\pm_2}/\Omega_{pmp}^2\right)}}\frac{\omega_{\pm 2}}{\Omega_{pmp}}|2\rangle + \frac{1}{\sqrt{1+\left(\omega_{\pm_2}/\Omega_{pmp}^2\right)}}|4\rangle \tag{5.17}$$

with the eigenfrequencies:

$$\omega_{\pm 1} = \frac{\Delta}{2} \pm \frac{\sqrt{\Delta^2 + 4\Omega_c^2}}{2} \tag{5.18}$$

$$\omega_{\pm 2} = \frac{\Delta}{2} \pm \frac{\sqrt{\Delta_2^2 + 4\Omega_{pmp}^2}}{2} \tag{5.19}$$

This leads to a level configuration shown in figure 5.18.

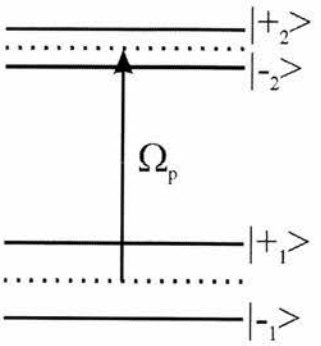

Figure 5.18: *Doubly driven probe transition in the dressed state basis. A double doublet structure is evident, similar to that shown in figure 5.16. As the probe tunes across the transitions it is interference between dressed states that leads to points of transparency. Hence in such a system multiple dark states are possible.*

So we see that the application of two strong fields results in a probe field linked to two doublets. The doublet structure is controlled by the strength of the appropriate Rabi frequency. This is equivalent to the qualitative discussion of the system given in 5.7.1. Inclusion of a probe field detuning term in the above analysis leads to equations for the dressed states of a similar form to those in (5.16) and (5.17) but with slightly more complicated eigenfrequencies.

We see from the dressed state equations that quantum interference is apparent in the doubly driven system due to the mixture of the states |1> and |3> or |2> and |4>. It is also more immediately apparent where the triplet structure and double dark features come from when we consider how the probe tunes across the dressed states and hence where the points of quantum interference occur.

5.7.4 Refractive Index Effects.

We do not explicitly examine the change in refractive index in our four level system but we can conclude from the examination of such changes in a multilevel cascade scheme in chapter 6 that the modification of the probe absorption we observe will result in a modified refractive index profile. Some of the sharp absorption resonances observed will result in a large value of $dn/d\upsilon$ and could have applications in, for instance, slow light production.

5.8 Conclusions

In this chapter we have examined the role of two-photon processes and polarisation of probe and coupling field in EIT experiments. We have shown the role that polarisation plays in either enhancing or degrading the observed EIT, in doing so we have identified the optimum polarisations for EIT in the $5S_{1/2}$ - $5P_{3/2}$ - $5D_{5/2}$ cascade scheme in rubidium. Polarisation will be important, for instance, in experiments where the amount of EIT observed is required to be maximised.

We have also examined the properties of a four level Vee-scheme in which a probe field is affected by two other fields, either strong or weak. We have seen that this system can be used to inhibit two-photon absorption, produce multiple dark states and under the right conditions inversionless gain.

References

[1] **R. R. Moseley, S. Shepherd, D. J. Fulton, B. D. Sinclair and M. H. Dunn**, "2-photon effects in continuous-wave electromagnetically-induced transparency," *Optics Communications* **119**, 61-68 (1995).

[2] **G. S. Agarwal and W. Harshawardhan**, "Inhibition and enhancement of two-photon absorption," *Physical Review Letters* **77**, 1039-1042 (1996).

[3] **D. J. Fulton, R. R. Moseley, S. Shepherd, B. D. Sinclair and M. H. Dunn**, "Effects of zeeman splitting on electromagnetically-induced transparency," *Optics Communications* **116**, 231-239 (1995).

[4] **S. Wielandy and A. L. Gaeta**, "Coherent control of the polarization of an optical field," *Physical Review Letters* **81**, 3359-3362 (1998).

[5] **D. Budker, D. F. Kimball, S. M. Rochester and V. V. Yashchuk**, "Nonlinear magneto-optics and reduced group velocity of light in atomic vapor with slow ground state relaxation," *Physical Review Letters* **83**, 1767-1770 (1999).

[6] **A. K. Patnaik and G. S. Agarwal**, Controlling magneto-optical rotation via atomic coherence, qu-ph/9911034

[7] **A. V. Durrant, H. X. Chen, S. A. Hopkins and J. A. Vaccaro**, "Zeeman-coherence-induced transparency and gain without inversion in laser-cooled rubidium," *Optics Communications* **151**, 136-146 (1998).

[8] **D. J. Fulton, S. Shepherd, R. R. Moseley, B. D. Sinclair and M. H. Dunn**, "Continuous-wave electromagnetically induced transparency - a comparison of v-system, lambda-system, and cascade systems," *Physical Review A* **52**, 2302-2311 (1995).

[9] **S. Z. Jin, Y. Q. Li and M. Xiao**, "Hyperfine spectroscopy of highly-excited atomic states based on atomic coherence," *Optics Communications* **119**, 90-96 (1995).

[10] **B. W. Shore**, *The Theory of Coherent Atomic Excitation.* (Wiley, New York, 1990).

[11] **M. Weissbluth**, *Atoms and Molecules, Student Edition.* (Academic Press Inc., London, 1978).

[12] **V. S. Letokhov and V. P. Chebotayev**, *Nonlinear Laser Spectroscopy.* (Springer-Verlag, Berlin, 1977).

[13] **J. Y. Gao, S. H. Yang, D. Wang, X. Z. Guo, K. X. Chen, Y. Jiang and B. Zhao**, "Electromagnetically induced inhibition of two-photon absorption in sodium vapor - art. no. 023401," *Physical Review A* **6102**, 3401 (3 pages) (2000).

[14] **M. D. Lukin, S. F. Yelin, M. Fleischhauer and M. O. Scully**, "Quantum interference effects induced by interacting dark resonances," *Physical Review A* **60**, 3225-3228 (1999).

[15] **B. R. Mollow**, "Absorption and Emission Line-Shape Functions for Driven Atoms," *Physical Review A* **5**, 1522-1527 (1972).

[16] **B. R. Mollow**, "Power Spectrum of Light Scattered by Two-Level Systems," *Physical Review* **188**, 1969-1975 (1969).

[17] **D. J. Fulton**, *Quantum Interference Effects: Electromagnetically Induced Transparency and Focussing*, PhD thesis, University of St. Andrews (1996).

[18] **J. R. Boon**, *Electromagnetically Induced Transparency and Inversionless Lasing*, PhD thesis, University of St. Andrews (1998).

[19] **S. M. Barnett and P. M. Radmore**, *Methods in Theoretical Quantum Optics*. (OUP, Oxford, 1997).

Chapter 6

RF induced EIT effects: Theory

6.1 Introduction

EIT is normally considered as a three level, two-field process. In many cases this is for simplicity, often due to available computing power and in many cases because although the atomic system being examined is multilevel it can be accurately modelled as a three level scheme. We have already seen some of this simplification in chapter 3. But now that many of the basic ideas concerning EIT are well understood theorists are turning to multilevel systems, e.g. [1-3] and to multi-field arrangements. In many cases this allows theorists to develop 'designer' systems, with tailored properties suitable to a specific problem of interest. This interest is now being turned into experimental work examining such phenomena as two-photon inhibition [4] and enhancement [5]. We have examined some of these type of systems in chapter 5.

In this chapter we outline some of the theory pertaining to multilevel systems and in particular to a N-level cascade manifold with N-1 fields applied. We examine how EIT resonances can be manipulated by the applications of external fields and how potentially interesting new phenomena can result from such systems. We then examine a system where, in a four level cascade, the third applied field is in the radio frequency regime which leads us to the possibility of rf control of optical effects within rubidium. We then make use of our N level model to examine the rubidium scheme in more detail. Some of these effects are then demonstrated in chapter 7. We conclude with a look at how an rf field in a four level model can be used to control electromagnetically induced transparency – an rf-controlled optical lens.

6.2 EIT in N level systems with N-1 fields

Despite many of the experimental systems in which EIT is investigated involving more than three levels, essential features can be adequately explained using a three-level approximation. Increasingly, however, schemes in which multilevel effects are seen are being examined. Schmidt and Imamoglu [6] have proposed a four level scheme in which giant Kerr nonlinearities may be obtained, as have Rebic et al [7] in a four level scheme within a single atom. Burkett et al [8] have examined inversionless gain profiles in four level media. Manson and Wei [9, 10] have done some elegant experiments into how EIT profiles can be modified by the application of extra fields within an ESR (electron spin resonance) context. Xia et al have looked at EIT in atoms with hyperfine structure [11]. Agarwal and Harshawardhan have shown that two-photon absorption can be inhibited and enhanced using EIT in a four level scheme [1], discussed in Chapter 5, and this has been experimentally demonstrated by Gao et al [4]. Harris and Yamamoto have examined a four-level scheme that will absorb two-photons but not one [3] which could be used

as an optical switch. Harris and Hau [12] have studied a similar system for use with slow light [13]. Of particular relevance to the effects outlined in this chapter is work done by Lukin et al [2] in which the idea of 'double-dark resonances' has recently been proposed. An EIT profile is split into two 'dark' components with a re-absorption of light on line-centre. This effect was also predicted by Sandhya and Sharma [14] in which they discussed the possibility of destruction of EIT using a rf field and thus allowing the observation of sub-natural linewidths.

In this section (section 6.2) we examine EIT in cascade schemes with N levels and N-1 applied fields. We show that, for manifolds with an odd number of levels, transparency is observed on line centre and N-2 dark states are present, and that for manifolds with an even number of levels transparency is destroyed on line centre (i.e. we see absorption of the probe field) but that there are still N-2 dark states. We also examine the possibility of realising such schemes in atomic rubidium where a six level cascade scheme can be found with some of the levels being hyperfine levels in the manifold of the upper coupling field.

To allow further examination of the systems considered here the density matrix for a six level cascade system is printed in appendix A. By setting appropriate driving frequencies to zero the matrix can be reduced to that for a five level, or four level etc system.

6.2.1 Three level system

The theory of EIT within a three level cascade scheme is well-established [15, 16]. If we apply a weak probe field between levels |1> and |2> and a stronger coupling field between levels |2> and |3>, as we have considered before, then the absorption of the probe on line-centre will be cancelled due to a quantum interference process that results from interfering pathways to level |2>. The system may be completely described by a density matrix under steady state conditions and thus the probe absorption may be examined. The probe absorption (proportional to $\mathrm{Im}[\rho_{21}]$) in such a scheme is given by [16]:

$$\mathrm{Im}[\rho_{21}] = -\mathrm{Re}\left[\frac{\Omega_p}{\gamma_{21} - i\Delta_{12} + \dfrac{\Omega_c^2}{\gamma_{31} - i(\Delta_{12} + \Delta_{23})}}\right] \tag{6.1}$$

where the symbols have their usual meaning We therefore see that for zero coupling field a minimum is found in $\mathrm{Im}[\rho_{21}]$ when the probe field detuning is zero as we would expect (i.e maximum absorption). When the coupling field is introduced we find that that minimum is shifted by a value equal to the coupling field Rabi frequency. On line centre we find that the value of the $\mathrm{Im}[\rho_{21}]$ is much more than in the zero coupling field. This minimum in absorption on line centre (for zero coupling field detuning) is the induced transparency effect.

6.2.2 Four Level System

We now turn to what happens to the probe absorption in a four level cascade scheme as shown in figure 6.1. This is the system studied by Sandhya and Sharma [14]. Again by analysing the

density matrix equations for the system, it is possible to obtain an expression for the probe absorption:

$$\mathrm{Im}[\rho_{21}] = -\mathrm{Re}\left[\frac{\left(\gamma_{31} - i(\Delta_{23}+\Delta_{12}) + \Omega_{rf}^2/\alpha\right)\Omega_p}{\Omega_c^2 + (\gamma_{21} - i\Delta_{12})(\gamma_{31} - i(\Delta_{23}+\Delta_{12})) + \Omega_{rf}^2(\gamma_{21} - i\Delta_{12})/\alpha}\right] \quad (6.2)$$

where $\alpha = \gamma_{41} - i(\Delta_{12}+\Delta_{23}+\Delta_{34})$.

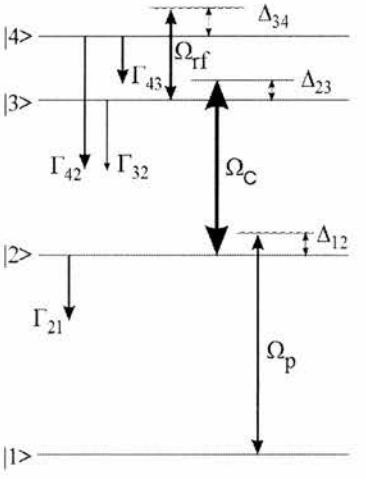

Figure 6.1: *Four level cascade scheme. The upper field, resonant with the |3> - |4> transition is assumed to be an rf field with the |3> and |4> levels F states in the same state.*

Equation (6.2) reduces to equation (6.1) when we reduce Ω_{rf} to zero. Equation (6.2) is also immediately more complicated to analyse than equation (6.1) but we note that an extra term in the denominator appears proportional to Ω_{rf}^2, in a similar manner to the term proportional to Ω_c^2 that appears in the expression for three level EIT. (Although we refer to the third applied field as Ω_{rf} it should be noted that it need not be an rf field, this is merely a convenience for the discussion we have below in section 6.2.5). So we might logically expect the point of minimum absorption to shift. Indeed that is what we find as shown in figure 6.2. Here we see that the EIT dip in the absorption that is found in a three level manifold is split into two different components and that on line centre we see a sharp feature signifying re-absorption.

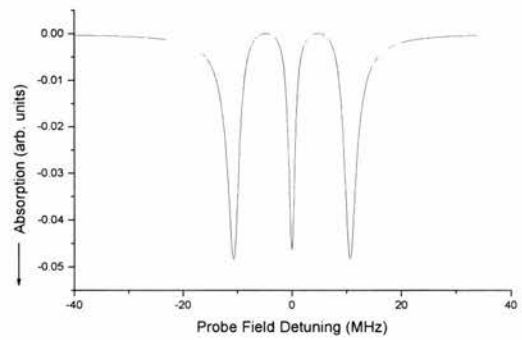

Figure 6.2: *Probe absorption as a function of probe field detuning in a four level cascade. $\Omega_p \approx 300kHz$, $\Omega_c \approx 20MHz$, and $\Omega_{rf} \approx 10MHz$.*

The EIT feature has been split into two and destroyed on line centre. This process is analogous to the interference between one and two photon routes found in a three level cascade [17]. We can see this by examining what happens if we detune the three fields from resonance. In figure 6.3(a) we detune the coupling field and the third field from line centre. We see that each of the one, two and three photon peaks can be resolved. We now see in figure 6.3(b) the result if we tune the coupling field back on to resonance with the one photon absorption – we see EIT. Now if we tune the three photon resonance back to line centre we find that the EIT is destroyed at line centre and the EIT feature is split. This splitting is the double-dark feature noted in [2]. The addition of an extra level and field to our cascade scheme has changed the problem we investigate from a one and two photon absorption to one with a three photon component as well.

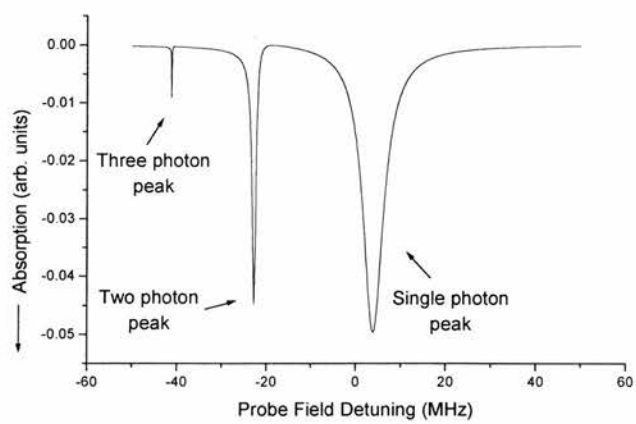

Figure 6.3(a): *Probe absorption trace in the four level cascade scheme with the coupling and rf fields detuned so as to display the one, two and three photon absorption peaks. Interference of these processes leads to EIT and the destruction of EIT. $\Omega_p \approx 300kHz$, $\Omega_c \approx 20MHz$, $\Omega_{rf} \approx 10MHz$, $\Delta_p = 20MHz$ and $\Delta_c = 20MHz$.*

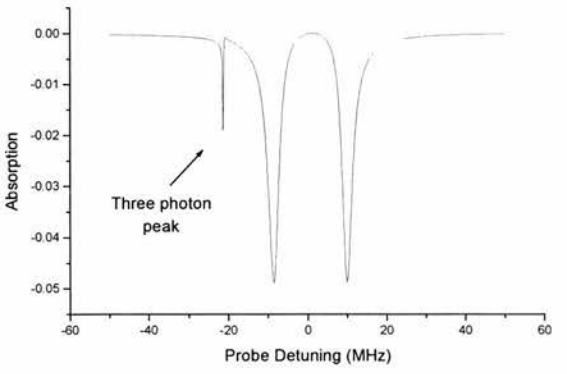

Figure 6.3(b): *Probe absorption trace in the four level cascade scheme with the rf field detuned so as to display the three photon absorption peak and the EIT due to interference of one and two photon absorption routes.* $\Omega_p \approx 300kHz$, $\Omega_c \approx 20MHz$, $\Omega_{rf} \approx 10MHz$ *and* $\Delta_{34}=20MHz$.

6.2.3 Five Level System

In a five level cascade scheme we find that with four applied fields the destruction of EIT on line centre seen in a four level system is reversed resulting once again in a transparency region. This is shown in figure 6.4. We also see that we have once again split the central feature to produce three dark states, or areas of minimum absorption, in the absorption profile. The reason for the transparency point on line centre is again analogous to the reason we see EIT in a three level system. We now have one, two, three and four photon routes that interfere destructively to give a transparency. We can see this by detuning each of the fields away from resonance to observe the individual photon absorptions, shown in figure 6.5. If we were to tune the fields back onto resonance one by one we would see normal EIT, four level EIT and finally five level EIT. This process is now 'multi-photon' EIT and will be generally true for any odd numbered cascade scheme.

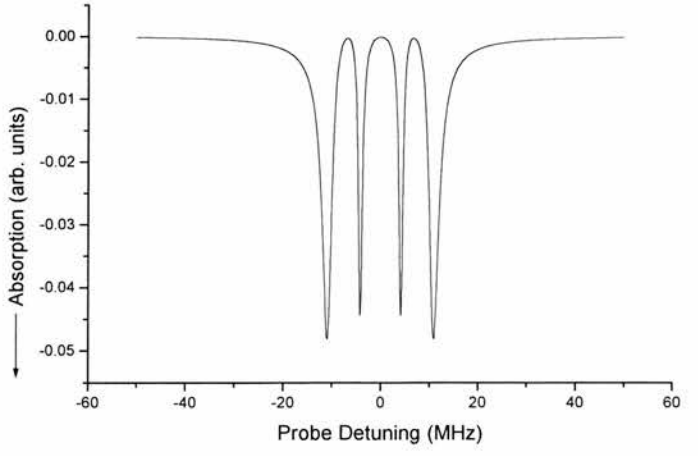

Figure 6.4: *Probe absorption in 5 level system.* $\Omega_p \approx 300kHz$, $\Omega_c \approx 20MHz$, $\Omega_{rf} \approx 10MHz$ *and* $\Omega_{45} \approx 10MHz$

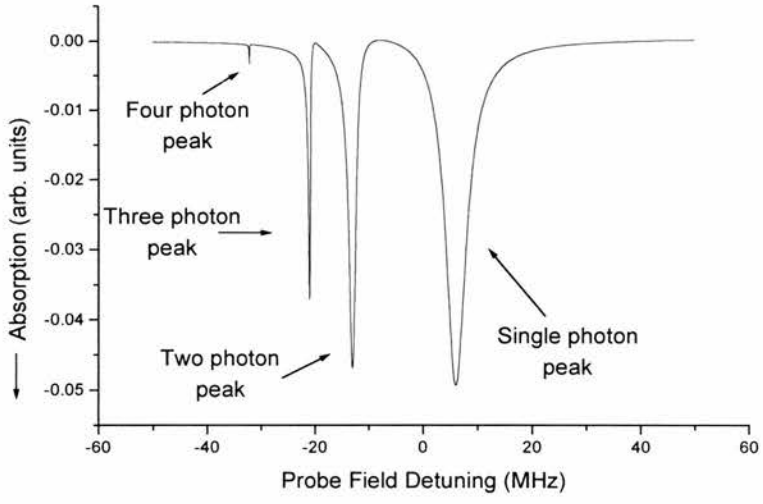

Figure 6.5: *Detuned 1,2,3,4 photon processes in the five level cascade scheme.* $\Omega_p \approx 300kHz$, $\Omega_c \approx 20MHz$, $\Omega_{rf} \approx 10MHz$, $\Omega_{45} \approx 10MHz$ *and* $\Delta_{23}=\Delta_{34}=\Delta_{45}=20MHz$.

6.2.4 Six Level System

We finally turn to a six level cascade scheme to test our predictions. Having examined what happens by adding an extra level and an extra field from N=3 to N=5 we assume that once again the central feature found in the five level cascade will split and we will be left with a destruction of transparency (absorption) on line centre. This is what we observe in figure 6.6.

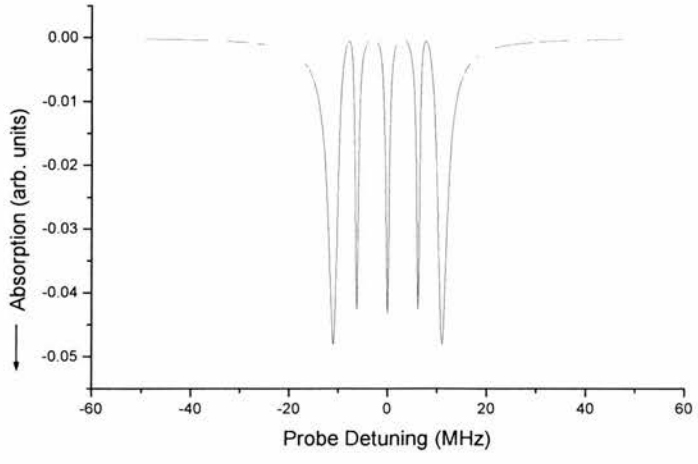

Figure 6.6: *Probe absorption in six level system.* $\Omega_p \approx 300kHz$, $\Omega_c \approx 20MHz$ *and* $\Omega_{rf}=\Omega_{45}=\Omega_{56} \approx 10MHz$.

We also see that we now have 4 areas of minimum absorption. We are now able to make a generalisation about N level cascade schemes. We find that for N is even then on line centre we will observe a region of high absorption on line centre e.g. N=2, normal absorption, N=4 destruction of EIT on line centre etc. We also find for N even and N>2 that we have N-2 dark states or areas of low absorption. For cascades where N is odd we see EIT effects (absorptive minima on line centre). This is just a manifestation of multiphoton interference within the atomic system. We also find that we see N-2 dark states in odd numbered cascades as well as in even numbered ones. As has been pointed out by Lukin *et al* [2] it is possible to engineer atomic responses in a four level medium and this should also be possible in higher order manifolds.

6.2.5 Possible Experimental Realisations

In discussing N Level cascade schemes we have not fully addressed the type of transitions that we are considering. In principle all the transitions can be in the optical regime, or indeed in any wavelength regime that is desired. That is because these effects are general to any arbitrary system. However in practice the effects presented are unlikely to be observed in any arbitrary system. This is mainly due to either decay rate considerations, power of applied fields (e.g microwave fields [18] and Chapter 8) and Doppler broadening effects. For instance, it may be difficult to find a five level optical cascade scheme, and such a scheme would not be Doppler free in the same way that we can have a Doppler free three level cascade [17]. One possible scheme for achieving a six level cascade is that shown in figure 6.7. In this system (found in atomic rubidium) the fourth, fifth and sixth levels are found in the hyperfine structure of the upper state of the coupling transition. Based on our models we predict that the destruction of EIT and splitting of EIT features could be observed in such a system.

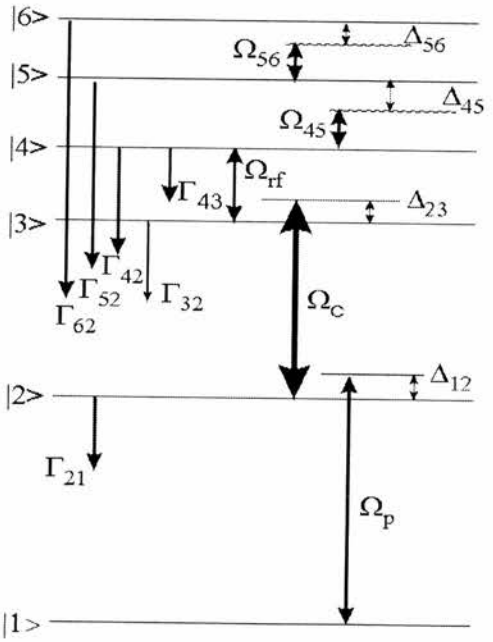

Figure 6.7: *Possible Six level cascade scheme in Rb.*

However, there are associated problems in working in such a system, namely detuning effects. Since the hyperfine states are quite close together in frequency space, a field interacting with one of the levels is likely to interact with at least one of the other levels. This gives rise to more complicated lineshapes than we have predicted above. We examine the case in ^{87}Rb in which the probe is resonant with the $5S_{1/2}(F=2) - 5P_{3/2}(F=3)$ transition and the coupling field is resonant with the $5P_{3/2}(F=3) - 5D_{5/2}(F=4)$ transition. The rf fields are applied to the $5D_{5/2}(F=4)$ - $5D_{5/2}(F=3)$, $5D_{5/2}(F=3)$ - $5D_{5/2}(F=2)$ and $5D_{5/2}(F=2)$ - $5D_{5/2}(F=1)$ transitions respectively. We ignore polarisation effects (Chapter 5) and the fact that as the probe field tunes through resonance two-photon resonance [17] will be achieved on each of the $5D_{5/2}$ F states, and concentrate on the probe absorption due to EIT on the $5D_{5/2}(F=4)$ state in a Doppler free situation. The spacing of the three hyperfine transitions are 29MHz, 23MHz and 16MHz respectively. We see from figure 6.8 what sort of lineshape we would expect, if we apply a field resonant with levels |3> and |4> that can also couple to the |4> - |5> and |5> - |6> transitions. The rf field is therefore detuned from the |4>-|5> transition by 6MHz and from the |5>-|6> transition by 13MHz.

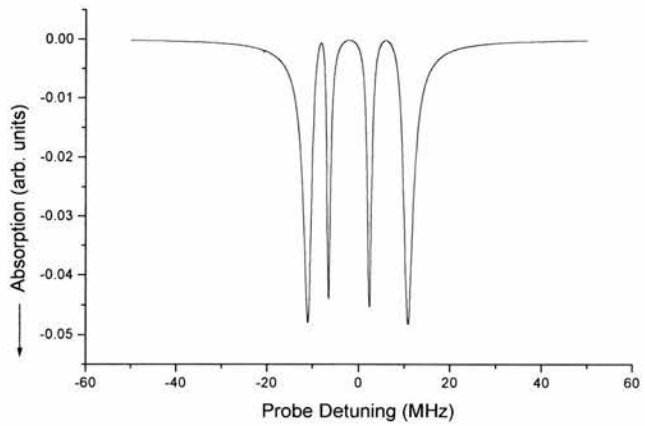

Figure 6.8: *Probe absorption in six level system based on atomic Rb. Here the rf field interacts with the three upper transitions but is only resonant with the |3> - |4> transition and is detuned from the |4> - |5> and |5> - |6> transitions.* $\Omega_p \approx 300kHz$, $\Omega_c \approx 20MHz$, $\Omega_{rf}=\Omega_{45}=\Omega_{56} \approx 10MHz$. *The detunings are* $\Delta_{45}=6MHz$ *and* $\Delta_{56}=13MHz$.

We do not see the type of absorption profile predicted in figure 6.6 because the last transition in the cascade, |5> - |6>, is detuned from resonance by a significant amount and since it is a five photon feature it is very weak and so it does not have a significant effect. Instead we get a profile more akin to that predicted in a five level system (figure 6.4). We see that the system has three dark states, not the four we have predicted above. Therefore we see that when we have closely spaced upper levels in our ladder, we predict slightly different effects than for a general arbitrarily spaced cascade scheme. We could of course have three individual fields applied to the upper three transitions in which the detunings could be controlled independently. The effect this would have is the equivalent of having three detuned fields interacting with each level, with one

of the fields being quite far detuned from one of the levels and having little effect. Thus much the same effect as shown in figure 6.8 would be observed.

Obviously if we have arbitrarily large field strengths as well as arbitrarily detuned fields then a much more complicated structure would appear, which we do not consider here as this would be far more difficult to realise experimentally. If we could observe the lineshapes shown in figure 6.8 then we could hope to build rf controlled lenses (discussed below) and investigate rf control of EIT.

Our density matrix model will not work for the case where a single probe and coupling field pair can be two photon resonant with a number of hyperfine levels, i.e. we cannot predict the lineshapes shown in figure 5.4, for instance, very easily. In order to try to predict the sort of lineshapes we should see if we carried out an rf-controlled EIT experiment we need to take a slightly different tack. We imagine the six level system shown in figure 6.6 with a probe and coupling field applied, along with a single rf field resonant with the |3> - |4> transition. We can then model the system by treating it as a discrete set of 5 levels for each of the four state F levels. For instance, we consider the level structure for each F state as shown in figure 6.9.

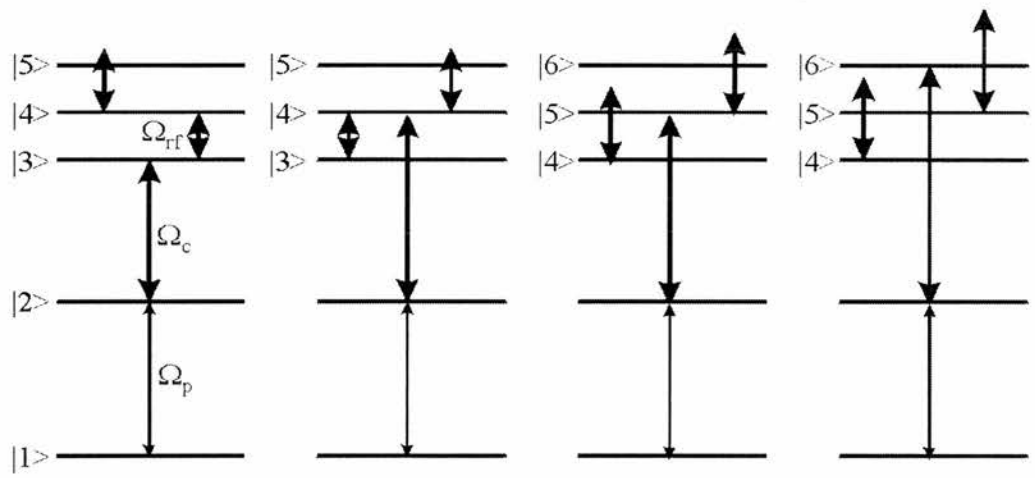

Figure 6.9: *Level structures for consideration of EIT in six level model. In each system the coupling field is resonant with a different transition, corresponding to a different F state.*

We can ignore the sixth level in each case as the rf field will be detuned from this level and, as we have seen, this five photon absorption effect will be very small. We can then plot the absorption expected for each F state, shifted by the appropriate frequency (i.e. the F=4 peak is 28.8MHz away from the F=3 peak). We also take into account the two-photon probabilities calculated in chapter 5 to scale the absorptions appropriately. This leads to an absorption profile such as the one shown in figure 6.10.

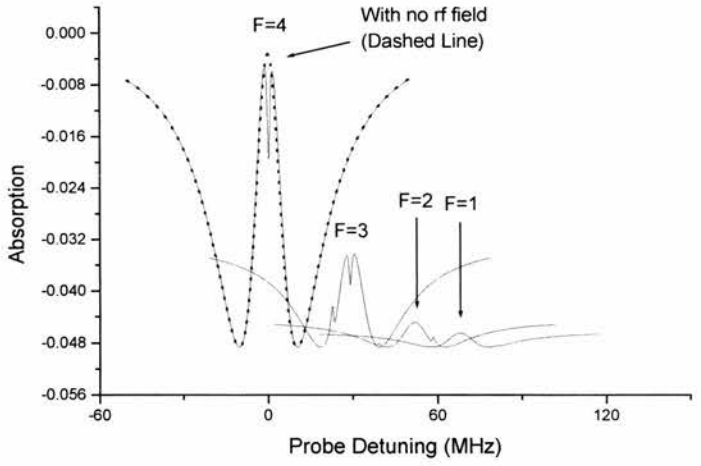

Figure 6.10: *F state absorption profiles for the $5D_{5/2}$ level in ^{87}Rb due to EIT. Each peak is calculated via an individual density matrix calculation and the plot is appropriately scaled and displaced to give a final trace. The F=4 trace with no applied rf field is also shown (dashed line) for reference. Field strengths are: $\Omega_p \approx 300kHz$, $\Omega_c \approx 20MHz$, and $\Omega_{34}=\Omega_{45}=\Omega_{56} \approx 2.2MHz$*

However the change in absorption of the EIT peaks themselves is predicted to be quite small for many applied rf field strengths, so it may be possible that the change in EIT is hard to detect directly. Experimentally we can overcome this problem by modulating any applied rf field and using PSD detection to observe the change in the probe field due to the rf field. This is essentially the same as taking the difference trace between the case where no rf field is applied and where an rf field is applied. When the difference traces are created from our model we see, for example, the trace shown in figure 6.11.

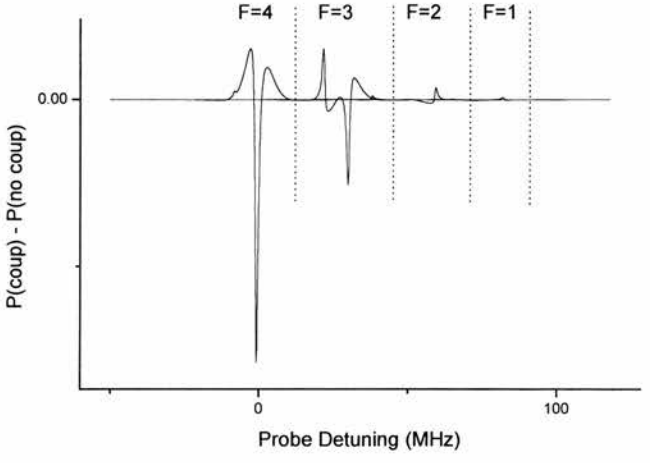

Figure 6.11: *RF 'difference' trace. The plot shows the difference in the EIT trace with a RF field applied and no RF field applied. The peaks associated with each F state are divided by the dotted lines.*

We will examine this model and its predictions when we consider the experimental results in chapter 7.

6.2.6 Two Photon Inhibition

We note the role EIT has in two-photon inhibition in multilevel cascade schemes. The population in state |3> gives a measure of the two-photon emission from the two-photon route |1>-|2>-|3>. In a four level scheme with no third field applied and with the probe and coupling field both made weak fields (Rabi frequencies of 1MHz) the population in state three is at a maximum on line centre (shown in figure 6.12). This is what we would expect - maximum two-photon emission when both probe and coupling fields are resonant. But we can then reduce this maximum by applying our third field at some Rabi frequency greater than that of the probe and coupling field. This effect, also shown in figure 6.12, occurs simply because we are, in effect, inducing EIT on the intermediate level, |2>-|3>, by applying the third field, and hence we reduce the two-photon emission from level |3>. This effect is similar to that predicted by Agarwal and Harshawardhan [1] and observed by Gao *et al* [4] in a Y four level configuration.

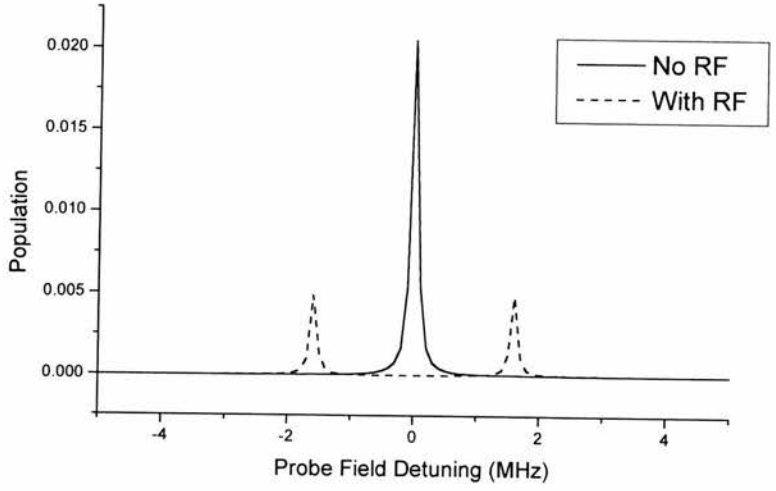

Figure 6.12: *Two photon inhibition trace in a four level cascade scheme. The solid line shows the population in the third level (a measure of two-photon absorption) with no third (RF) field applied Here $\Omega_p=\Omega_c\approx300kHz$. The dashed line is the population in the third level with a third field applied. In this case: $\Omega_p=\Omega_c\approx300kHz$ and $\Omega_{34}\approx20MHz$.*

6.3 Electromagnetically Induced Focussing Effects in Four level media

We now turn our attention to the possibility of producing an rf controlled optical lens. This is a possible use of a four level system with a rf field resonant with the |3> - |4> transition. We start by examining how the refractive index changes in the N-level cascade system and what those changes may imply.

6.3.1 Refractive Index Changes

The modification to the EIT profiles in multi-level cascades will affect the refractive index profiles of the medium. Since the features that appear in these EIT profiles are very sharp and have smaller linewidths than that of the normal EIT profiles, we expect sharper refractive index changes in higher level cascade schemes. Such profiles for N-level systems with N=3,4,5 and 6 are plotted in figure 6.13. We see that with larger N change in refractive index will be sharper.

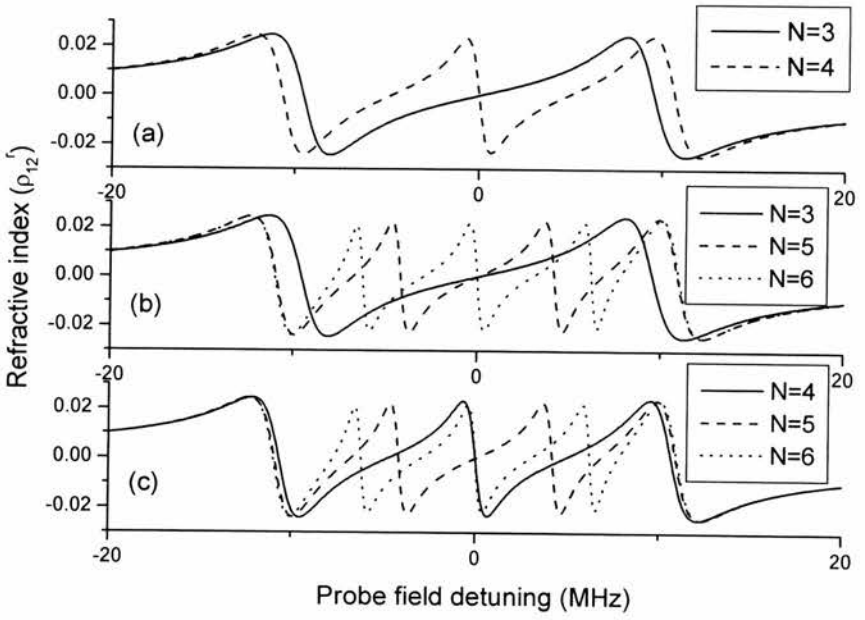

Figure 6.13: *Refractive index profiles (ρ^r_{12}) in N-level cascade schemes. In each of (a), (b) and (c) the Rabi frequencies are $\Omega_{12}\approx 300kHz$, $\Omega_{23}\approx 20MHz$ and $\Omega_{34}=\Omega_{45}\ldots\Omega_{56}\approx 10MHz$. (a) Comparison between the N=3 and N=4 cases. (b) Comparison between the N=3,4 and 5 cases. (c) Comparison between the N=4,5 and 6 cases. The same graphs are plotted more than once to allow comparisons to be more easily made.*

This has potential uses in phaseonium type media [19] and possibly in production of slow light. Lukin *et al* [2] have shown that phaseonium can be created in four level media and so should be apparent in media with a greater numbers of levels. We can see the potential effect on the production of slow light by comparing the gradients of the refractive index curves. This gradient is the important parameter in the value of the group velocity of the light given by equation (1.5). Figure 6.14 shows the gradients for the cases where N=3,4,5 and 6. In comparison to the N=3 curve the first thing that is evident is that there are only a few regions where the dispersion is greater than in the N=3 cases. So we may not actually be able to slow the light down much more than in the three level case. However if we compare the maximum positive value of the coherence in the N=6 case to that in the N=3 case we find that the dispersion ($dn/d\omega$, or $d\rho^r_{12}/d\omega$) is four times larger in the N=6 case. Perhaps of more interest is the fact that the dispersion can become significantly more negative in the N>3 cases. This could be useful in producing media in which pulses travel with negative group velocities [20, 21]. By considering the relationship

between ρ^{r}_{12} and the susceptibility of the medium we can make an estimation of how the group velocity can be affected by using multi-level cascade systems. We use equation (2.24) to make this connection and the relation [22]:

$$n \approx 1 + \frac{\chi'}{2} \tag{6.3}$$

to relate the susceptibility χ' to the refractive index.

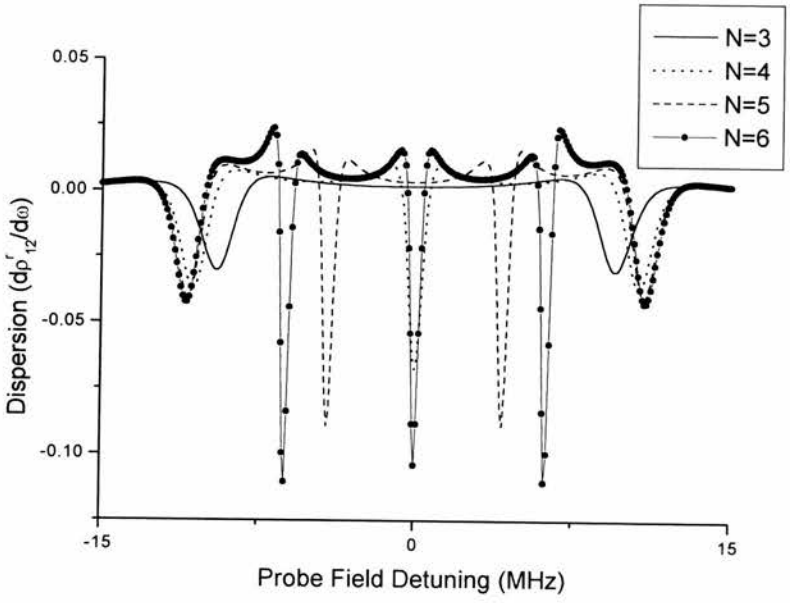

Figure 6.14: *Derivative of the refractive index profiles for N=3,4,5 and 6 shown in figure 6.13. Parameters are the same as quoted in figure 6.13 above.*

Thus we can write the group velocity as:

$$v_g = \frac{c}{1 + \frac{N|\mu_{ij}|^2}{4\varepsilon_0 \hbar \Omega_{12}} \left(\rho^r_{ij} + \omega_p \frac{d\rho^r_{ij}}{d\omega} \right)} \tag{6.4}$$

We will assume that the constant before the brackets in equation (6.4) is 1 for convenience, since it will not change in moving between any of the schemes. Further we will assume that the factor within the brackets is significantly different than 1 and hence we can reduce the equation to:

$$v_g \propto \frac{c}{\rho^r_{ij} + \omega_p \frac{d\rho^r_{ij}}{d\omega}} \tag{6.5}$$

which allows us to calculate order of magnitude changes in the group velocity due to changes in the atomic model, if not calculate group velocities exactly. Exact calculations depend, of course, on the exact experimental parameters; these will be considered later. The simplest situation to start with is the case where the probe field is on resonance i.e. $\rho^r_{12}=0$. In the case of N being odd this is also absorption free but in the case where N is even then there will be absorption at this point. In the three level system v_g is $1000c/\omega_p$, but in the four level system this has changed to -15 c/ω_p. The five level system is roughly the same as the three level scheme at this point but the in the six level manifold the group velocity has changed to -10 c/ω_p.

So if we imagine EIT in a rubidium cascade scheme with the probe field on the $5S_{1/2}$-$5P_{3/2}$ transition, then we can calculate the dipole strength of the transition using [23]:

$$\left|\mu_{ij}\right|^2 = \frac{3\pi\varepsilon_0\hbar c^3 A_{ji}}{g_1\omega_0^3} \tag{6.6}$$

where g_1 is the degeneracy and is equal to 1 in this instance. For the 780nm rubidium transition, the dipole strength is ~7.5D. We take the probe field Rabi frequency as 1kHz and the atomic density as $N=1x10^{12}cm^{-3}$, which is appropriate for a Doppler free system (e.g. an atomic beam). For the N=3 system this implies a group velocity of v_g~c/815. For the N=4 system however this leads to a value of v_g=-c/28500 and v_g=-c/40750. We shall return to the idea of a negative group velocity in section (6.3.1.1) below. In the N=6 case with a probe detuning of ~7MHz we can observe a group velocity of c/4077, so we can slow light down further by moving to higher order manifolds, and detuning slightly. This value is lower than can be achieved in the N=3 case at value of detuning, which can be seen by examination of figure (6.13) and (6.14), with these particular atomic and optical field parameters.

We also note the possibility that refractive index changes in such media can give rise to electromagnetically induced focussing effects [24, 25]. The possibility exists for the third field in a three level medium to control the focussing properties of the probe field. This leads to the idea of a rf controlled optical lens. With the fine frequency control available at rf frequencies this would allow unprecedented manipulation of the lensing action on the probe.

6.3.1.1 Negative Group Velocities

We have seen that it is possible to have negative group velocities using the anomalous dispersion found via EIT processes. This type of dispersion is well known and is described by Sommerfeld [26]. Light moving through such a medium will have shorter wavelengths refracted less than longer ones. In allowing anomalous dispersion we find that negative group velocities are possible, as we have seen. The group velocity can also, in such circumstances, become larger than c. Jackson [27] notes that when negative group velocities are encountered the concept of group velocity becomes meaningless. However in a recent experiment, Wang *et al* [21] have shown that a negative group velocity produced by a region of anomalous dispersion leads to

apparent superluminal behaviour. In this experiment a group velocity of v_g=-c/310 was measured, resulting in a pulse of light travelling through a caesium gas cell being detected 62ns before it entered the cell! Based on the data presented in the Wang paper, if the light entered a medium with a group velocity of v_g=-c/40750 then the pulse delay would be approximately 8μs. The main difference between the Wang experiment and the one suggested here is that the Wang scheme is based on a Raman type process far from an atomic resonance and as such the propagating pulse experiences the anomalous dispersion in a region of low absorption. The areas of high, negative group velocity in the EIT scheme may fall in areas of probe absorption, hence the pulse may not propagate through the cell whilst still retaining its initial shape. Such an absorption makes the phenomena more difficult to study.

.

As Wang *et al* point out a negative group velocity can be counter intuitive, indeed potentially nonsensical. This is a problem that was first pointed out by Wien [28], who noted that the new (at the time) theory of relativity was at odds with the effects of anomalous dispersion. Sommerfeld [28] suggests that the true speed at which a pulse propagates should be defined differently as the frontal, or initial velocity of step-function pulse signal which doe not exceed c. How this definition relates to the Wang experiment has yet to be analysed [21]. Wang and co-workers explain the phenomena in terms of a propagation time. In vacuum a pulse will propagate over a distance d in a time t=d/c but for a medium of length d this time will become $t=d/v_g$. The time difference for the two distances is:

$$\Delta t = \frac{d}{v_g} - \frac{d}{c} = \left(n_g - 1\right)\frac{d}{c} \tag{6.7}$$

where:

$$n_g = n(\omega) + \omega\frac{dn}{d\omega} \tag{6.8}$$

when n_g is negative, the time delay Δt is negative and hence the light can appear to have travelled through a anomalously dispersive medium before it could have travelled through a similar distance in vacuum. Furthermore it is possible that Δt can become larger than the vacuum transit time d/c, hence the pulse can be detected exiting the medium before it has entered it. This Wang *et al* maintain can be described via the wave nature of light. It may be possible that the increases in negative group velocity achievable by moving to multilevel cascade schemes could aid these superluminal effect experiments, by providing a mechanism to achieve more larger pulse advancements than are possible than in normal three level systems.

6.3.2 RF-controlled lensing

The spatially varying field strength of the coupling field gives rise to the EIF effect. By having a different Rabi frequency acting upon the probe at the centre and edge of the coupling field we produce a probe which experiences a varying refractive index across its profile and hence the

coupling field acts like a lens. To demonstrate this we consider the simple model of EIF outlined by Moseley *et al* [24]. First we assume that the probe and coupling fields are left on resonance. Then we model the dispersion due to two different Rabi frequencies, a lower value of 0.3MHz corresponding to the outer edge of the coupling field and a higher one of 6.4MHz corresponding to the centre of the coupling field. The difference in the dispersion produced by these two Rabi frequencies gives a measure of the lensing action, if any, that is produced. The resulting trace is shown in figure 6.15. The variation of the refractive index as the RF field is detuned from line centre is indicative of lensing.

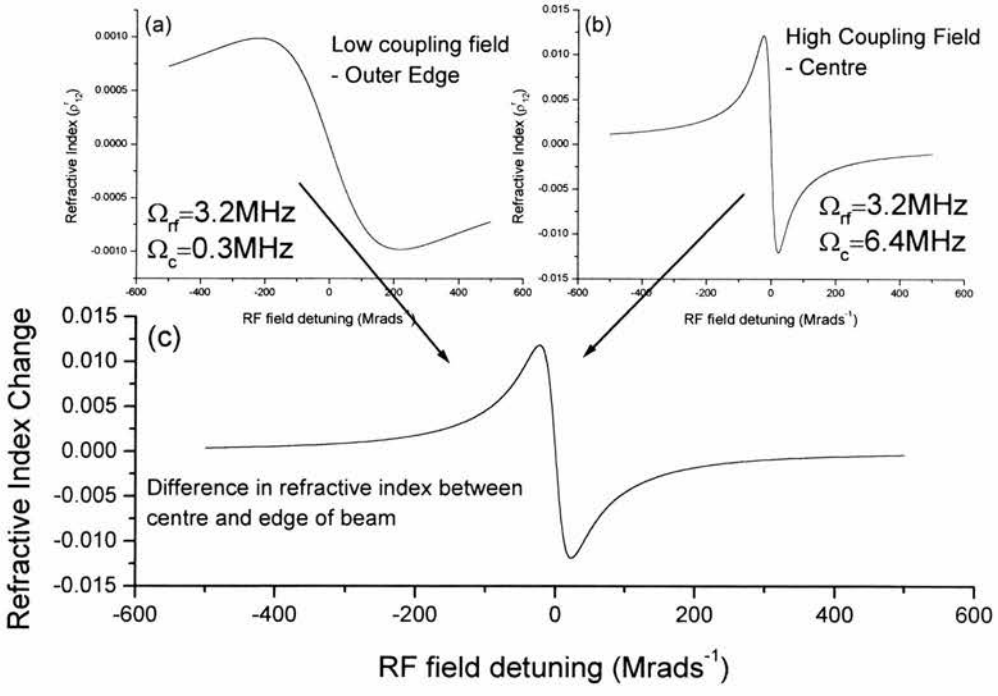

Figure 6.15: *Demonstration of the possibility of RF-induced EIF. (a) and (b) show the refractive index (ρ'_{12}) change of the probe as a function RF detuning. In both (a) and (b) the RF Rabi frequency is 3.2MHz. In (a) the coupling field Rabi frequency is 0.3MHz and in (b) it is 6.4MHz. This, therefore, corresponds to the case where the probe field completely overlaps with the coupling field.*

We can also consider a case where the Rabi frequency of the outer edge of the coupling field (as experienced by the probe) is closer to the central Rabi frequency than in the situation shown in figure 6.15. This would correspond to a case where the probe field is more tightly confined within the coupling field than in figure 6.15. This case is shown in figure 6.16. Thus we see that a number of different lensing regimes may be reached via this approach.

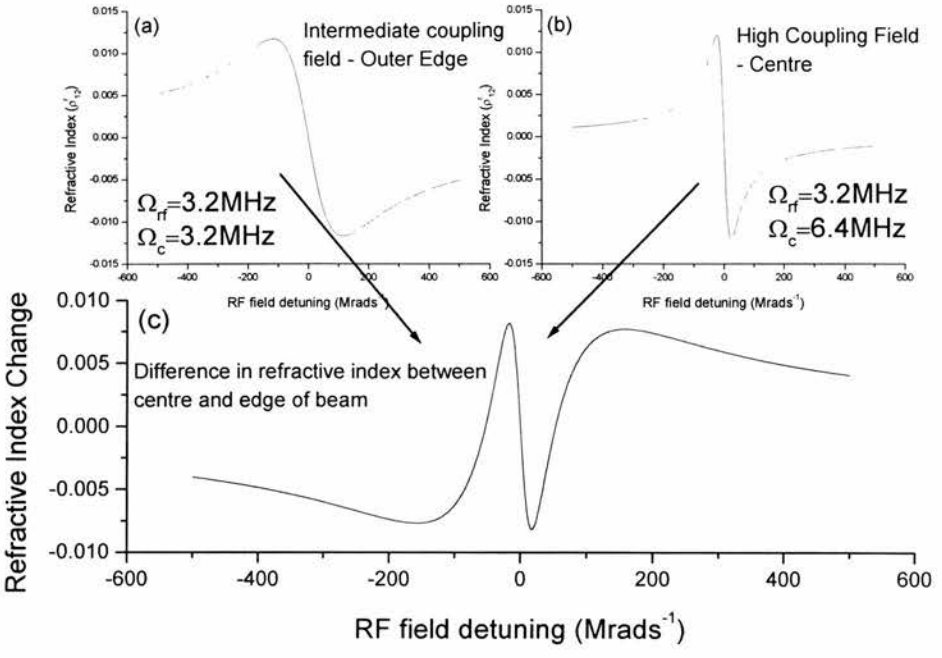

Figure 6.16: *Refractive index change due to RF modified EIT. (a) and (b) show the refractive index (ρ'_{12}) change of the probe as a function RF detuning. In both (a) and (b) the RF Rabi frequency is 3.2MHz. In (a) the coupling field Rabi frequency is 3.2MHz and in (b) it is 6.4MHz. This, therefore, corresponds to the case where the probe field is contained with the probe field and does not completely overlap it.*

We can also envisage lensing action in higher order cascade manifolds, where more complex lensing profiles are found. This is shown in figure 6.17.

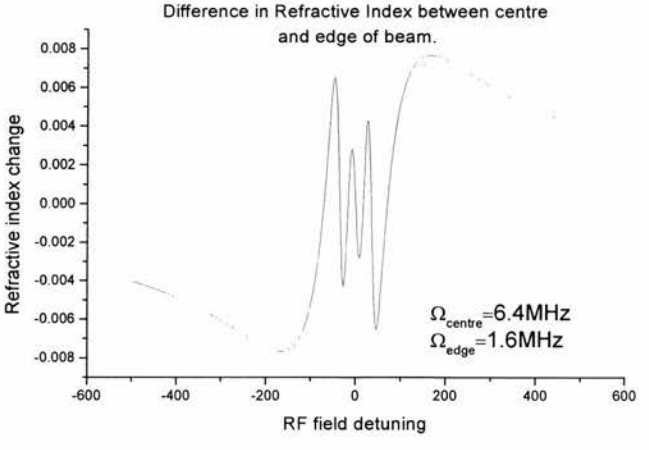

Figure 6.17: *Change of refractive index between the outer and inner edge of the coupling field as a function of RF detuning for a five level cascade scheme. The central Rabi frequency is 6.4MHz and the edge Rabi frequency is 1.6MHz.*

The high-resolution control of RF and microwave sources that is available would allow a very fine control of the focussing properties of the probe beam. It should be noted, however that the lensing action that is predicted in the four level cascade scheme differs from that we have studied previously in the three level cascade scheme. In the three level scheme the fact that the probe is undergoing EIT means that the lensing action takes place with no resulting absorption of the probe, this is not the case in the four level cascade. As the third field is brought onto resonance with the upper level the EIT is destroyed allowing the system probe to be absorbed and consequently allowing elimination of Doppler broadening, if it exists, on the probe [29]. Hence the focussing that we see is not accompanied by a zero in absorption as can be seen in figure 6.18 (this can be rectified by moving to the five level system discussed above). So in principle the destruction of EIT that we observe in a four-level cascade can be used to allow RF control of the focussing of an optical field.

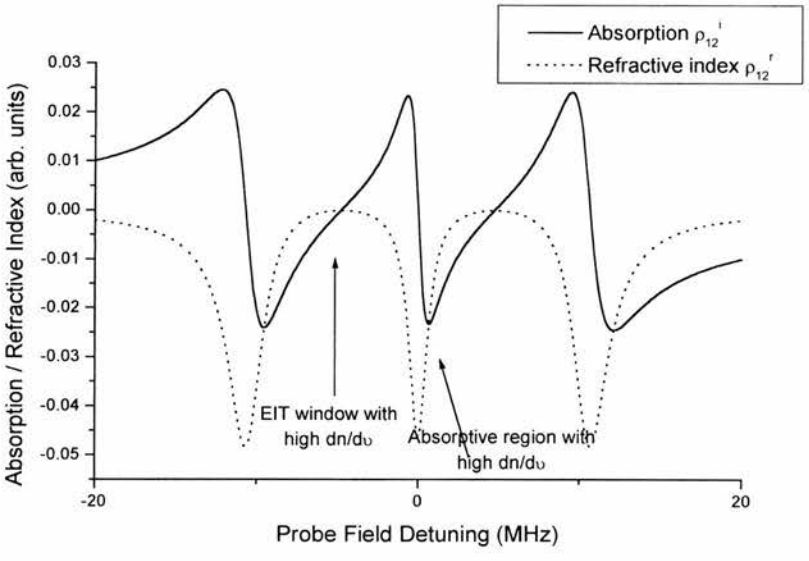

Figure 6.18: *Refractive index profile with overlaid absorption profile for N=4.*

6.4 Conclusions

In considering how rf fields may modify EIT we have examined EIT in multilevel cascade schemes. We have shown that for cascades with an odd number of levels there is a transparency effect on line centre due to the quantum interference in the system. Likewise in a system with an even number of states the probe field is significantly absorbed on line centre. This is due to coherent processes in which an N photon effect interferes with the N-1 process which leads to transparency. In effect we see multiphoton EIT effects in such systems. We also find that N level cascades with N-1 applied fields have N-2 'dark' states or areas of low absorption. We have examined other properties of such systems including refractive index profiles and inhibition of two-photon absorption. We have examined the possible experimental realisation of a six level cascade scheme in rubidium using the hyperfine states in the upper coupling field level as the fourth, fifth and sixth level. Hence we examine the rf modification of EIT resonances and outline

the main deviations of our proposed scheme from the ideal theory, that of the transition frequencies being very close together. By using rf transitions we eliminate Doppler broadening problems that would be evident in all optical schemes.

References

[1] **G. S. Agarwal and W. Harshawardhan**, "Inhibition and enhancement of two-photon absorption," *Physical Review Letters* **77**, 1039-1042 (1996).

[2] **M. D. Lukin, S. F. Yelin, M. Fleischhauer and M. O. Scully**, "Quantum interference effects induced by interacting dark resonances," *Physical Review A* **60**, 3225-3228 (1999).

[3] **S. E. Harris and Y. Yamamoto**, "Photon switching by quantum interference," *Physical Review Letters* **81**, 3611-3614 (1998).

[4] **J. Y. Gao, S. H. Yang, D. Wang, X. Z. Guo, K. X. Chen, Y. Jiang and B. Zhao**, "Electromagnetically induced inhibition of two-photon absorption in sodium vapor - art. no. 023401," *Physical Review A* **6102**, 3401 (3 pages) (2000).

[5] **N. Mulchan, D. G. Ducreay, R. Pina, M. Yan and Y. F. Zhu**, "Nonlinear excitation by quantum interference in a Doppler-broadened rubidium atomic system," *Journal of the Optical Society of America B-Optical Physics* **17**, 820-826 (2000).

[6] **H. Schmidt and A. Imamoglu**, "Giant Kerr nonlinearities obtained by electromagnetically induced transparency," *Optics Letters* **21**, 1936-1938 (1996).

[7] **S. Rebic, S. M. Tan, A. S. Parkins and D. F. Walls**, "Large Kerr nonlinearity with a single atom," *Journal of Optics B-Quantum and Semiclassical Optics* **1**, 490-495 (1999).

[8] **W. H. Burkett, Y. Q. Li and M. Xiao**, "Inhomogeneous broadening-dependent spectral features in a four-level atomic system," *Journal of the Optical Society of America B-Optical Physics* **17**, 293-299 (2000).

[9] **C. J. Wei and N. B. Manson**, "Observation of the dynamic Stark effect on electromagnetically induced transparency," *Physical Review A* **60**, 2540-2546 (1999).

[10] **C. J. Wei and N. B. Manson**, "Observation of electromagnetically induced transparency within an electron spin resonance transition," *Journal of Optics B-Quantum and Semiclassical Optics* **1**, 464-468 (1999).

[11] **H. Xia, S. J. Sharpe, A. J. Merriam and S. E. Harris**, "Electromagnetically induced transparency in atoms with hyperfine structure," *Physical Review A* **56**, R3362-R3365 (1997).

[12] **S. E. Harris and L. V. Hau**, "Nonlinear optics at low light levels," *Physical Review Letters* **82**, 4611-4614 (1999).

[13] **L. V. Hau, S. E. Harris, Z. Dutton and C. H. Behroozi**, "Light speed reduction to 17 metres per second in an ultracold atomic gas," *Nature* **397**, 594-598 (1999).

[14] **S. N. Sandhya and K. K. Sharma**, "Atomic coherence effects in four-level systems: Doppler-free absorption within an electromagnetically-induced-transparency window," *Physical Review A* **55**, 2155-2158 (1997).

[15] **D. J. Fulton, S. Shepherd, R. R. Moseley, B. D. Sinclair and M. H. Dunn**, "Continuous-wave electromagnetically induced transparency - a comparison of v-system, lambda-system, and cascade systems," *Physical Review A* **52**, 2302-2311 (1995).

[16] **J. Geabanacloche, Y. Q. Li, S. Z. Jin and M. Xiao**, "Electromagnetically induced transparency in ladder-type inhomogeneously broadened media - theory and experiment," *Physical Review A* **51**, 576-584 (1995).

[17] **R. R. Moseley, S. Shepherd, D. J. Fulton, B. D. Sinclair and M. H. Dunn**, "2-photon effects in continuous-wave electromagnetically-induced transparency," *Optics Communications* **119**, 61-68 (1995).

[18] **D. McGloin and M. H. Dunn**, "Simple theory of microwave induced transparency in atomic and molecular systems," *Journal of Modern Optics* **In press**, (2000).

[19] **M. D. Lukin, S. F. Yelin, A. S. Zibrov and M. O. Scully**, "Enhancement of refractive index with quantum coherence: An overview," *Laser Physics* **9**, 759-772 (1999).

[20] **E. L. Bolda, R. Y. Chiao and J. C. Garrison**, "Two Theorems for the group velocity in dispersive media," *Physical Review A* **48**, 3890-3894 (1993).

[21] **L. J. Wang, A. Kuzmich and A. Dogarlu**, "Gain-assisted superluminal light propagation," *Nature*, (2000).

[22] **M. H. Dunn**, *Laser Physics 2 lecture notes, University of St. Andrews*. (1997).

[23] **R. Louden**, *The Quantum Theory of Light*. (2nd ed.) (OUP, Oxford, 1983).

[24] **R. R. Moseley, S. Shepherd, D. J. Fulton, B. D. Sinclair and M. H. Dunn**, "Spatial consequences of electromagnetically induced transparency - observation of electromagnetically induced focusing," *Physical Review Letters* **74**, 670-673 (1995).

[25] **R. R. Moseley, S. Shepherd, D. J. Fulton, B. D. Sinclair and M. H. Dunn**, "Electromagnetically-induced focusing," *Physical Review A* **53**, 408-415 (1996).

[26] **A. Sommerfeld**, *Optics*. Lectures on Theoretical Physics (Academic Press, London, 1949), vol. 4.

[27] **J. D. Jackson**, *Classical Electrodynamics*. (1st ed.).

[28] **L. Brillouin**, *Wave Propagation and Group Velocity*. (Academic Press, London, 1960).

[29] **A. K. Popov and V. M. Shalaev**, "Elimination of Doppler broadening at coherently driven quantum transitions," *Physical Review A* **59**, R946-R949 (1999).

Chapter 7

RF induced EIT effects: Experiment

7.1 Introduction

In the last chapter we discussed how an rf field may be used to manipulate EIT. We examined a six level scheme in rubidium in which the upper four levels were all F states of the $5D_{5/2}$ state. We saw that EIT could be manipulated by the application of a single rf field resonant with the |3> - |4> transition and which we consider to be detuned from the |4> - |5> and |5> - |6> transitions. In this chapter we show that EIT can indeed be manipulated in this way. Although with the level structure under consideration we find that the results are not as clean as those predicted in chapter 6. We begin however by taking the opportunity to compare EIT using a diode laser as the probe field to that when using a Ti:Sapphire. The relevance of these experiments to the observation of rf modified EIT will be discussed below.

7.2 RF modification of EIT resonances

As outlined in chapter 5, EIT can be used to probe the hyperfine structure of the upper level of the coupling field transition. In this section we examine how this may be carried out experimentally. The basic set-up as can be imagined involves normal cascade-scheme EIT. There needs to be a third field, an rf field, applied between the F=4 and F=3 states in the $5D_{5/2}$ state (the upper coupling field transition level). To create this field (~29MHz) we use a coil wound around the rubidium cell in a Helmholz pair geometry. To allow impedance matching of the coil to the rf amplifier we use a tuning circuit as shown in figure 7.1. The impedance matching is very important to ensure that power transfer from the amplifier to the cell is maximised. If impedance matching is poor then the power dissipated in the amplifier can cause it to burn out and the power dissipated in the coils will have a large heating effect and thus will change the absorption of the probe field in the rubidium cell. The output from the rf oscillator is passed through a pre-amp before being fully amplified. The amplifier (RTXAMP from Hands Electronics) used is rated variable up to 15W and provides up to 37dB of gain and can be tuned over the range 1.8-30MHz. The rf oscillator can also be easily tuned over this range. A diagram of the experimental set-up is shown in figure 7.2.

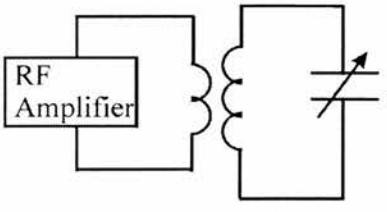

Figure 7.1: *Tuned circuit set-up for producing rf field in the rubidium cell. The cell sits in the set of coils connected to the variable capacitor.*

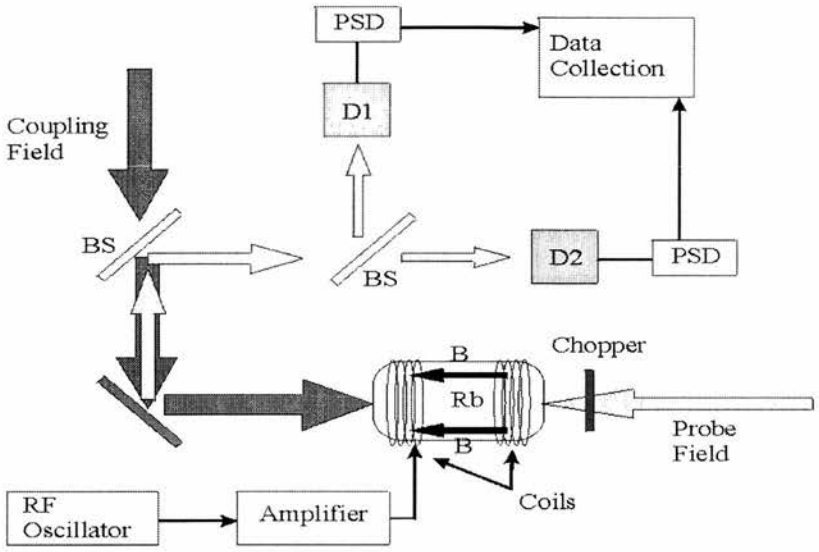

Figure 7.2: *Schematic of the experimental Set-up. D1 and D2 are photodetectors, BS is beamsplitter and B denotes the magnetic field. One of the PSDs detects the chopper modulated probe and the other detects the rf modulated probe.*

Initially the hyperfine structure of the upper level of the coupling field transition is resolved via EIT in a similar manner to that described in chapter 5. Then the rf field is applied so as to be resonant between the F=4 and F=3 levels, as depicted in figure 6.7. If we take a simple four level cascade model, then we would expect, with a reasonable rf field strength applied to see a splitting of the EIT profile and a re-absorption of the probe at line centre. Examination of figure 7.3, which shows an EIT trace both without and with the rf applied shows that no such splitting of the EIT feature was observed.

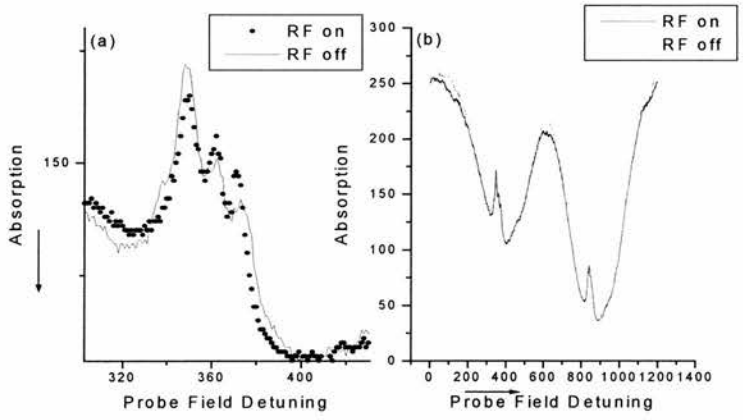

Figure 7.3: *EIT in the presence and absence of the RF field. Trace (a) shows that differences are small and difficult to compare directly – notice the slight differences in overlapping the traces. (b) shows the complete traces used to overlap the EIT features. The good overlap of (b) indicates that the coupling field has drifted very slightly, producing a slight shift in the overlap in (a).*

It was possible to suggest that the EIT feature had been degraded, but with no great certainty. In the EIT experiments carried out in this thesis it is normal to modulate the probe field by using an optical chopper. This allows a phase sensitive detection method to be used to detect the probe, which results in a much improved signal to noise ratio than without the modulation. In a similar way we can modulate the rf field via AM modulation (modulation frequency ~ 2kHz with up to 100% modulation depth). If the PSD is used to recover the signal at the modulation frequency of the rf field then we are able to detect the changes in the probe field that are due only to the application of the rf field. We can also set up the system to take simultaneous traces of the probe absorption and the rf-affected probe absorption. The modulation of the rf field technique is a very sensitive method for detection of changes in the probe absorption and it overcomes the limitations of directly detecting small changes in the probe absorption. A typical dual trace is shown in figure 7.4 and the difficulties in observing differences between the normal EIT absorption traces are illustrated in figure 7.3, above.

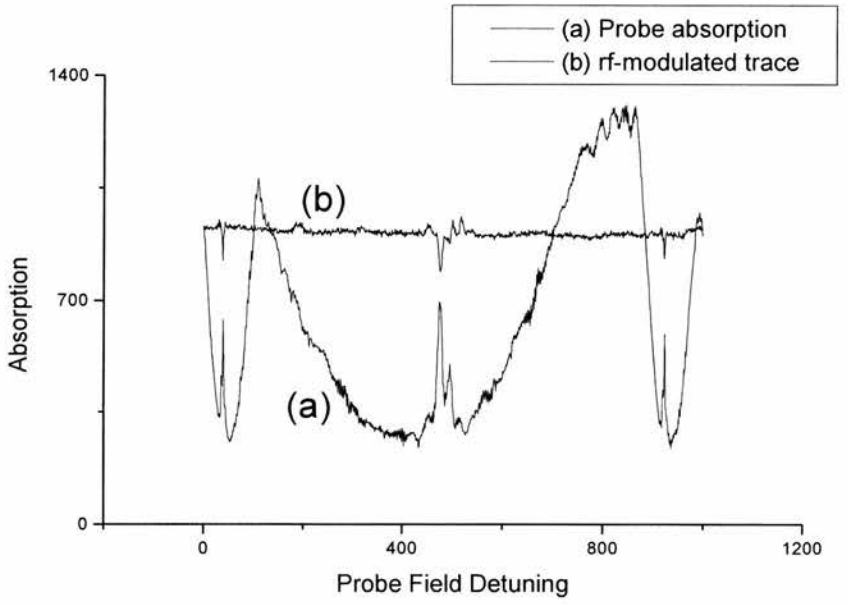

Figure 7.4: *Typical dual trace EIT profiles. (a) is the normal probe absorption trace, and (b) is the change in probe absorption due to the presence of the rf field.*

In carrying out this experiment two sets of main results were taken. These are similar in overall trends but differ in their details. The difference is in the polarisations of the probe and coupling fields. The complications that arise in multilevel systems such as the one considered here due to polarisation effects are discussed in section 7.2.3 below.

7.2.1 Initial Results

In the initial run of the experiment the probe and coupling field had oppositely circular polarisations. The rf modulated probe signal looked like that shown in figure 7.5. This is a

characteristic trace with an initial number of peaks in the positive direction followed by two distinct downward peaks followed by a couple of positive peaks.

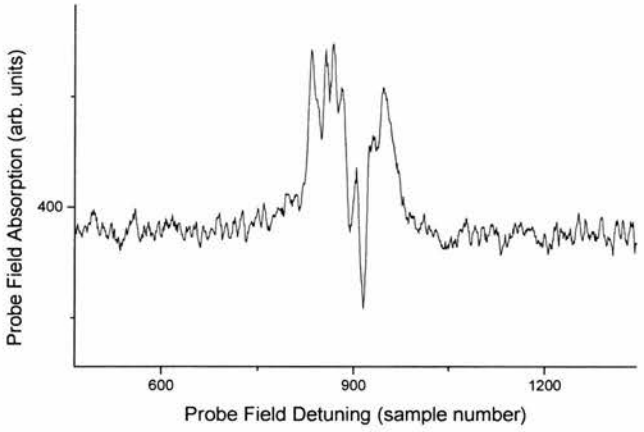

Figure 7.5: *Probe field absorption trace due to the application of a RF field (of ~29MHz). The x-axis is uncalibrated, being left as a computer sample number.*

Straightaway we see that the presence of the rf field has an effect on the probe field, if there is no rf field applied then the trace in figure 7.5 above would be a flat line. The relation of this trace to the actual EIT peaks becomes clearer by examining a dual trace, where the probe absorption and rf modified absorption are recorded simultaneously. Such a trace is shown in figure 7.6

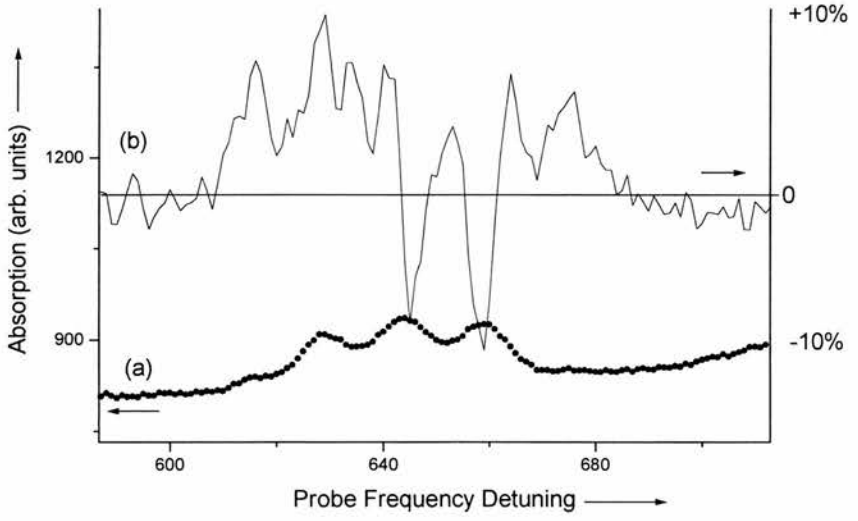

Figure 7.6: *Dual EIT trace with the (a) normal probe absorption (b) the rf modulated trace. On the right hand axis the change in absorption, from the zero line, of the rf modulated trace is shown as a percentage of the total absorption of the probe field. The rf field frequency is 29MHz*

It can now be seen that the initial change in absorption occurs *before* the initial EIT peak and that the first EIT peak also has an absorption change associated with it. The second and third EIT peaks also have clear rf-induced features associated with them. There is also evidence of a rf-induced feature after the third EIT peak. These results are typical and were readily reproducible.

We can further explore this phenomena by tuning the rf field off the F=4 to F=3 transition. If we tune it to 25MHz, this moves it more into resonance with the F=3 to F=2 transition and the resulting trace is shown in figure 7.7.

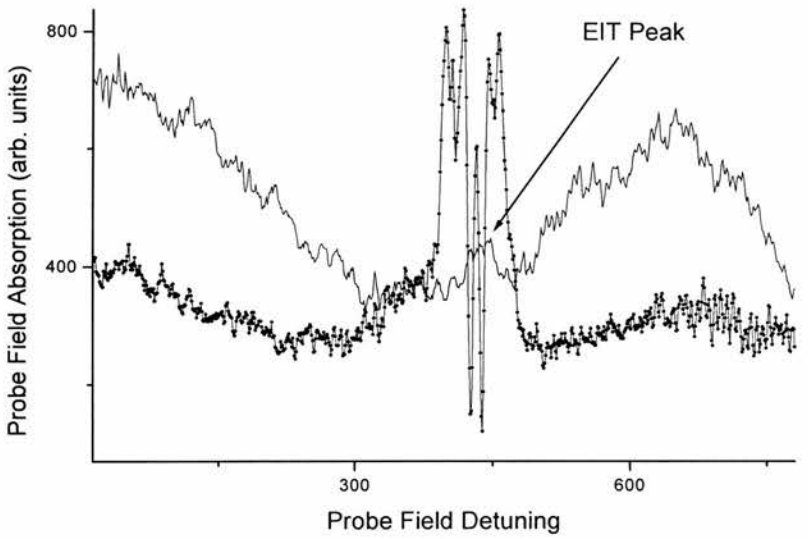

Figure 7.7: *Dual EIT trace for an rf field of 25MHz and 15W. Here the rf noise is worse than in the 29MHz case and hence the EIT peaks are less easily resolvable.*

It is clear to see that in changing frequency in this manner the rf trace becomes more 'symmetric' i.e. the initial positive change and the subsequent positive change are of more equal height as are the two negative peaks of equal depth. Due to the increased rf noise at this frequency the EIT peaks themselves are more difficult to resolve and hence the trace is a little more difficult to interpret.

There is further evidence that the rf-induced changes are indeed modification of the EIT resonances if we look at the ^{85}Rb (F=3) peak, shown in figure 7.8. Comparison with figure 7.9 shows how the rf-modulation may be used as a sensitive detection of EIT.

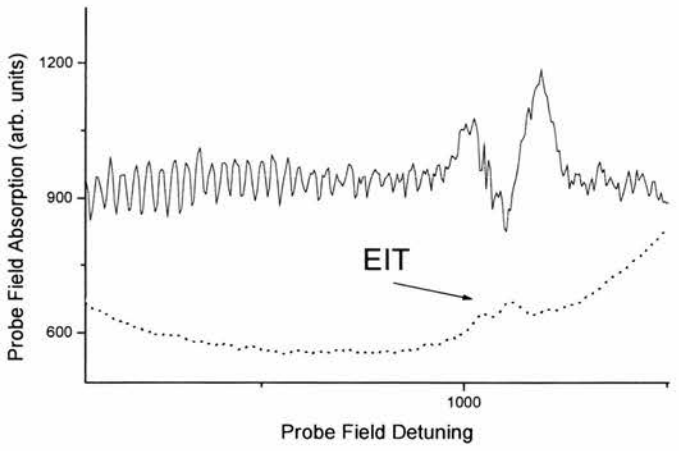

Figure 7.8: *EIT and rf-modulated EIT on the ^{85}Rb (F=3) peak. Here the structure is less complicated and potentially less well resolved than in the ^{87}Rb case.*

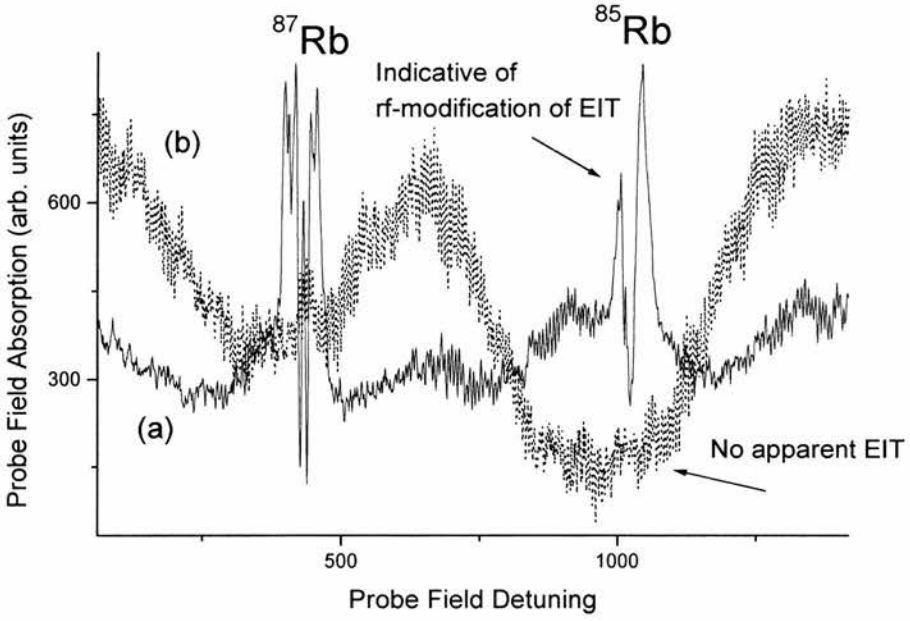

Figure 7.9: *EIT traces with the rf field detuned to 25MHz and an rf power of 15W. (a) is the rf-modulated trace and (b) the normal probe absorption trace. Here in the ^{85}Rb case we can see no clear indication of any EIT however the rf-modulated trace indicates that EIT is indeed occurring and that it is merely masked by broadening and noise processes in the normal absorption trace. Hence this rf-modulated technique can be used as a sensitive method of EIT detection.*

7.2.2 Latter Results

The second set of results was taken with both the probe and coupling field having the same circular polarisation. This as we have seen in chapter 5 will result in a differing EIT probe absorption profile than in the case where the polarisations are of opposite circular polarisation so

we might expect the rf-modulated profile to differ as well. A particular advantage is the dominance of the first EIT peak in this case (see chapter 5). A typical trace for these polarisation orientations is shown in figure 7.10.

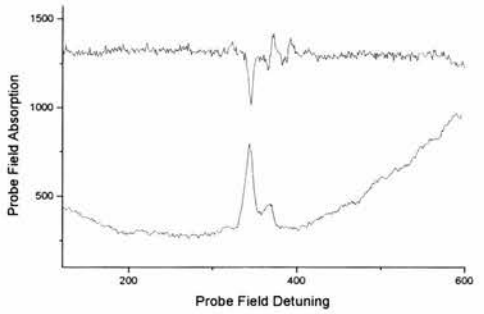

Figure 7.10: *Typical dual EIT trace: both fields have the same circular polarisation*

Now we see a somewhat different behaviour in the rf-modulated trace. We still have a positive peak just before any of the EIT peaks but we now have two negative dips that roughly correspond to the first two EIT peaks followed by some more positive peaks that lie outside the EIT region. This behaviour differs somewhat from that displayed in section 7.2.1 above.

In this case we examine what happens when the power of the rf field is reduced, the results being show in figure 7.11

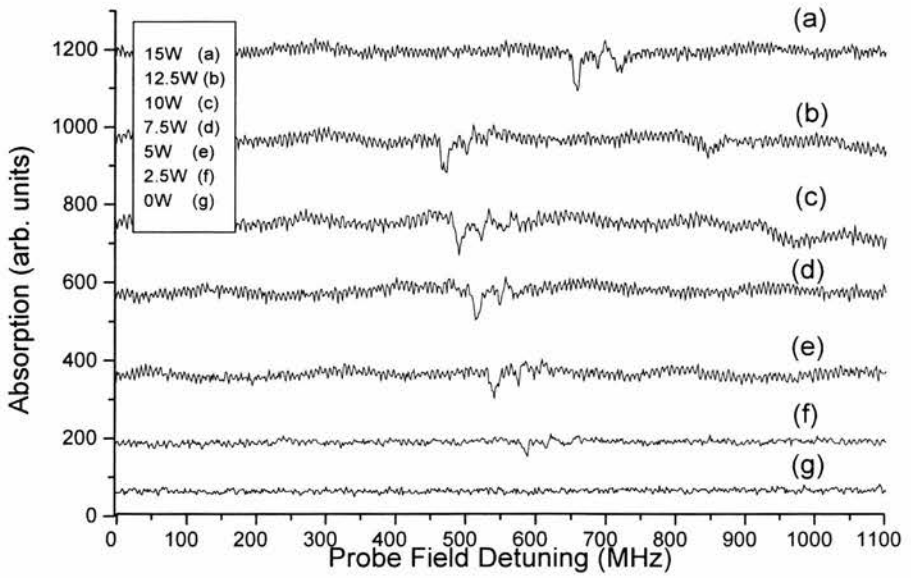

Figure 7.11: *Variation in rf-modulated probe absorption with rf power. The displacement of the peaks on each of the traces is due to the computer scans being started at different points in the probe absorption. The peaks themselves appear at roughly the same point in the normal EIT probe absorption trace.*

The variation with power is quite clear, the rf-induced change to the EIT falls off with decreasing power. This is as we would expect; as the Rabi frequency of the rf field drops so does the effect it has. With no rf field present there is no effect. We can also examine the effect of detuning the rf field from the F=4 to F=3 transition. Due to limitations on the rf amplifier used, significant detuning is only possible below 29MHz (the amplifier is only rated to 30MHz). The effect of this detuning can be seen in figure 7.12.

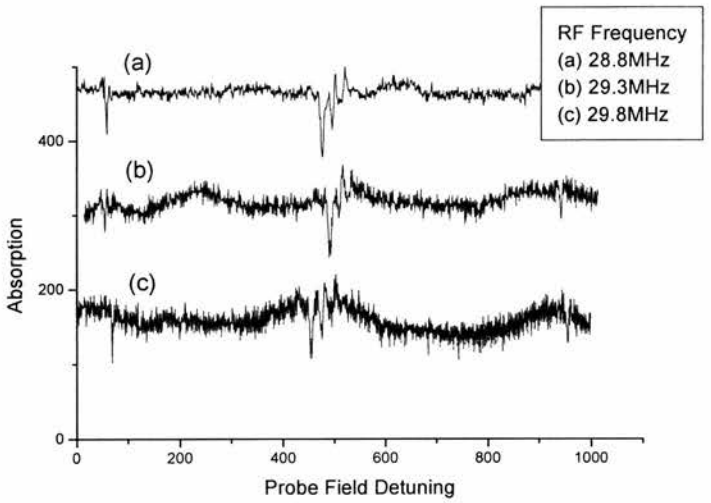

Figure 7.12 (i) RF-modulated probe absorption traces with different frequencies of RF field. In each of the figures 7.12(i) – (v) the frequency of the RF field is 28.8MHz, i.e. resonant with the F=4 – F=3 hyperfine level in the $5D_{5/2}$ state, in the first trace (a) as a reference. In (b) the frequency is 29.3MHz and in (c) 29.8MHz.

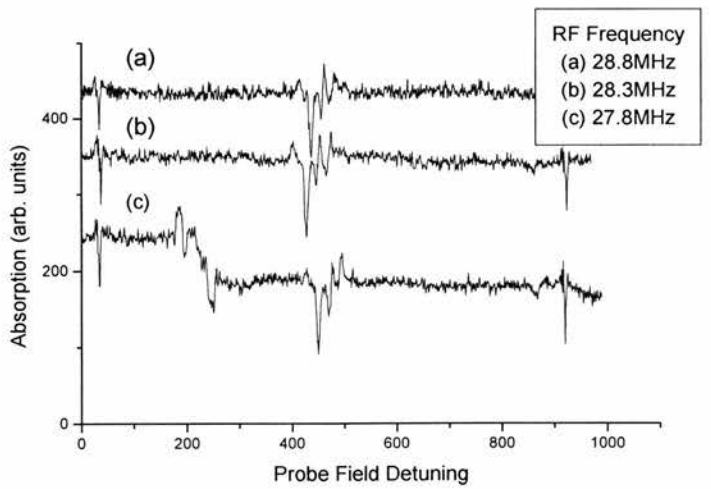

Figure 7.12 (ii) RF-modulated probe absorption traces with different frequencies of RF field. In (b) the frequency is 28.3MHz and in (c) 27.8MHz.

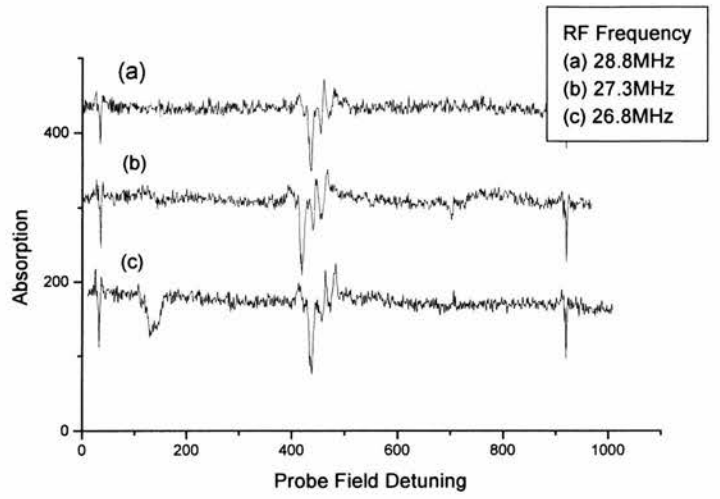

Figure 7.12 (iii) RF-modulated probe absorption traces with different frequencies of RF field. In (b) the frequency is 27.3MHz and in (c) 26.8MHz.

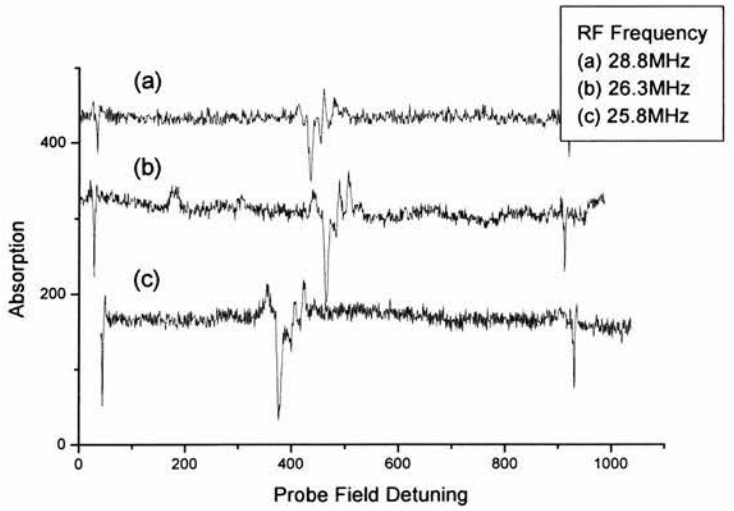

Figure 7.12 (iv) RF-modulated probe absorption traces with different frequencies of RF field. In (b) the frequency is 26.3MHz and in (c) 25.8MHz.

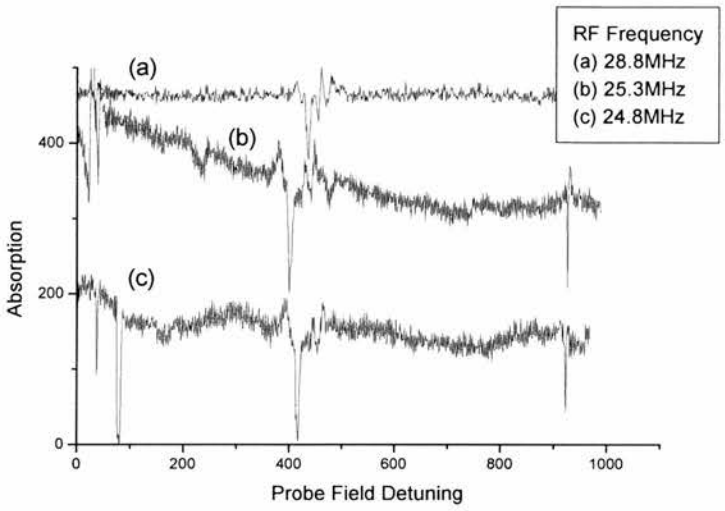

Figure 7.12 (v) RF-modulated probe absorption traces with different frequencies of RF field. In (b) the frequency is 25.3MHz and in (c) 24.8MHz.

7.2.3 Discussion

To allow more accurate modelling of the situation we need to consider exactly how the rf field is applied through the cell, thus allowing us to estimate the RF field Rabi frequency. We can make an estimate of the amount of B-field we can generate in our coils using the Helmholz coil equation and some rough estimations:

$$|B| = \frac{\mu_0 N I r_1^2}{2}\mathbf{k}\left[\frac{1}{\left(r_1^2 + z_1^2\right)^{3/2}} + \frac{1}{\left[(L - z_1)^2 + r_1^2\right]^{3/2}}\right] \tag{7.2}$$

where r_1 is the coil radius, ~1.25cm, z_1 is half the distance between the coils,~1cm, $L=2z_1$, we make an current estimate, I=4A and the number of coils is 4. Under such a situation the B-field at the centre of the coils is 766μT. This implies a Rabi frequency of ~11MHz. This should be enough, based on modelling to induce a destruction of the EIT on line centre. This is only an estimation however.

So what do we predict should happen and how does this compare with our results? We consider the latter set of experimental result detailed above (the situation with probe and coupling field having the same circular polarisation). The method for calculating the predicted probe absorption trace and rf-modulated trace is outlined in chapter 6. If we take a typical result for the case where the rf field is resonant with the F=4 to F=3 transition, with an rf Rabi frequency of 2.2MHz, then the predicted rf-modulated trace looks like that shown in figure 7.13. This is overlaid with the corresponding experimental trace. The immediate difference between the theory and the experiment is the fact that the experiment shows much broader lines than the theory predicts. This might be because of Doppler broadening, which we have so far neglected, but even with Doppler broadening included the features we predict are still very narrow. This is essentially

because the rf-induced features are very sharp, and are effectively Doppler-free and also presumably because the three photon absorption width is very small. We do see that the theory predicts the positions of two of the dips in the rf-modulated trace very precisely and also their relative magnitudes, so we can make the assumption that our theory points in the right direction, even if it's not predictive of the all the details. Another point is that not all of the dips are predicted by the theory.

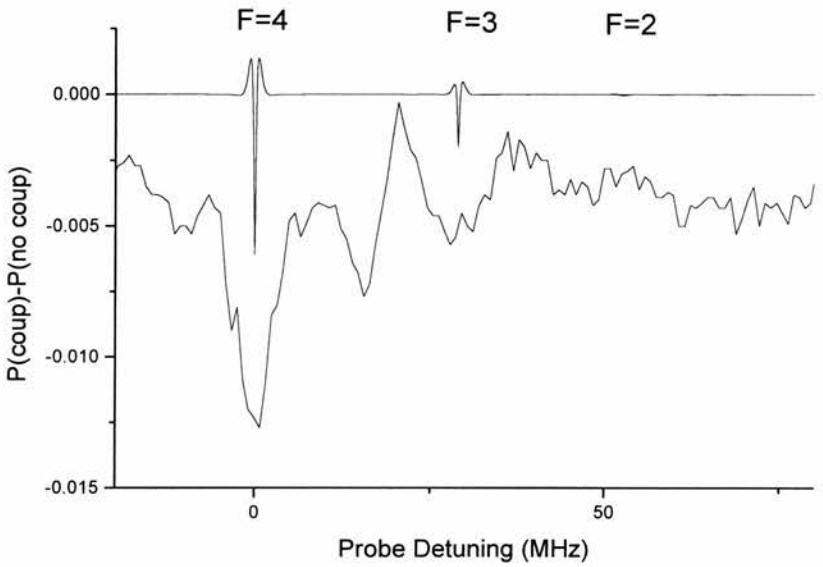

Figure 7.13: *Predicted rf-modulated trace and overlaid experimental trace for an rf frequency of ~29MHz and a rf Rabi frequency of 2.2MHz.*

The traces for the detuned rf cases are shown in figure 7.14 and 7.15. It is fairly obvious that detuning the fields in the model leads to rather fanciful predicted lineshapes. But again they are all narrow features and the experimental traces do not show this structure, or rather, if they do then it has been washed out.

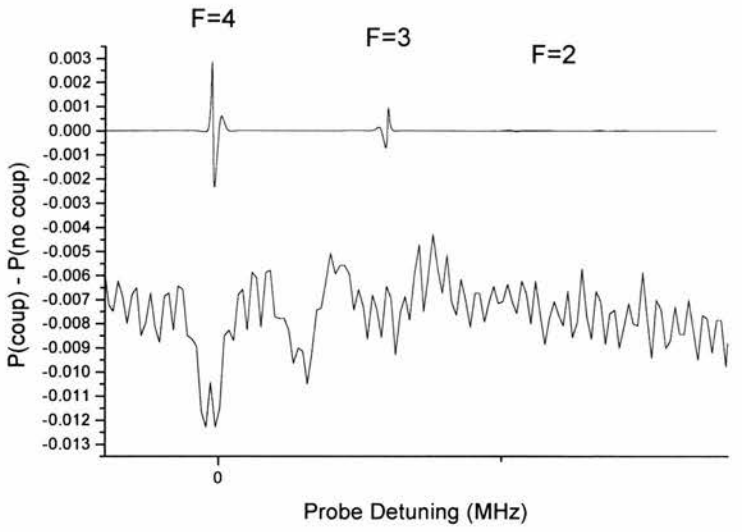

Figure 7.14: *Theoretical and experimental rf-modulated lineshapes for the case where the rf frequency is 30MHz and the rf Rabi frequency (in the theoretical case) is 2.2MHz.*

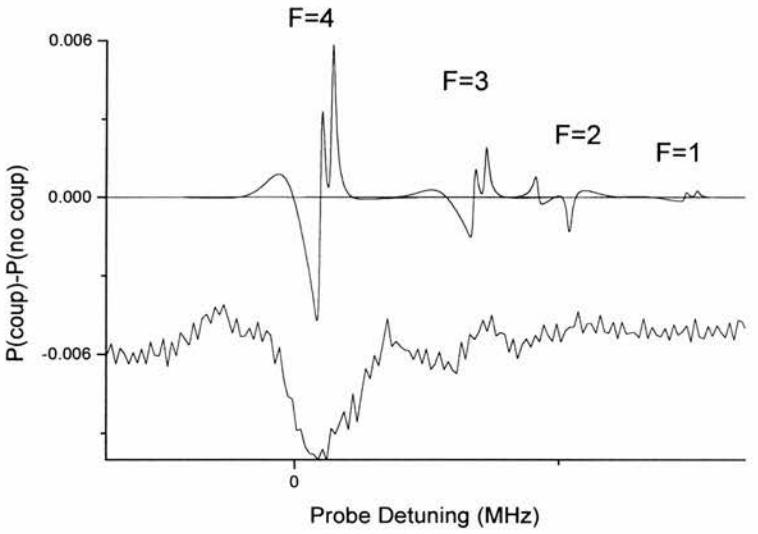

Figure 7.15: *Theoretical and experimental rf-modulated lineshapes for the case where the rf frequency is 23MHz and the rf Rabi frequency (in the theoretical case) is 2.2MHz.*

The obvious reason for the difference between the two sets of experimental results in sections 7.2.1 and 7.2.2 is the difference in polarisation orientations in the two experiments. As shown in chapter 5 polarisation differences affect the EIT profiles. In the three field geometry, however, it complicates matter further. With an extra field coming into play we run the risk of requiring to consider one of the fields as a superposition of fields with differing polarisations. The systems we have considered have the advantage of having no such superpositions, as can be seen in figure 7.16.

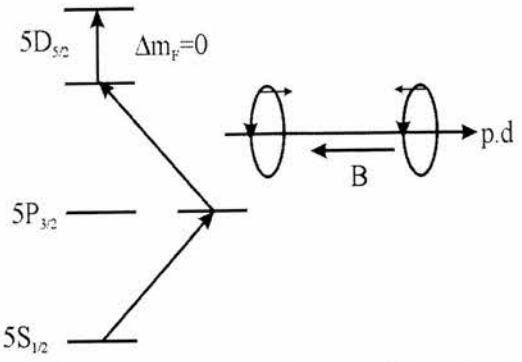

Figure 7.16: *Diagram showing linkage chain for two fields of circularly polarised light followed by a rf field parallel to the propagation direction.*

The two configurations do display marked differences however. This we can attribute to the two photon pathways that are set up within the atom. In the case where we have the opposite circular polarisation the two photon routes result in a atypical EIT profile, which suggests the effect of the rf field will be atypical as well. So we will concentrate on the second case we have examined, that where the probe and coupling field have the same circular polarisation.

First, it is necessary to address the question, what do the rf-modulated traces actually indicate? We verify by direct comparison of probe absorption traces in the presence and absence of the rf field that the sign of the rf-modulated trace indicates a change in the EIT profile, a positive change corresponds to a decrease in probe absorption (bearing in mind how absorption is defined in the EIT graphs above) and a negative change indicates a increase in absorption. This may appear obvious but since we are using phase sensitive detection the trace we see is phase dependent and it is difficult to set the phase without definitively knowing what a negative and positive change relates to. We should also note at this point that the rf-modulated trace will indicate the point on the EIT profile that the rf field has an effect on, so we should not necessarily expect the peaks we see on the rf-modulated trace to match up with the EIT peaks on the straight probe absorption profile, since the rf field is detuned from transitions other than the F=4 to F=3 one.

By examining the figures above (e.g. figures 7.3-7.12) we can state that the application of a rf field modifies the EIT profile. The main problem we face in quantifying this is the fact that it is hard to discern any appreciable effect on the straight probe absorption profile itself. If we initially look at a four level system, then we would expect the EIT to be destroyed on line centre by application of a rf field as shown in figure 6.2. Obviously we do not see the sharp destructive feature we expect, rather a reduction in the amount of EIT over the whole EIT peak. There are potential explanations however. The first is that the coupling laser has a linewidth that is large compared to the rf feature we would expect to see and hence simply washes out the feature. We still see changes in the rf-modulated trace because we are only detecting the probe field that is affected by the rf field itself and hence these features should show through clearly. Another

explanation is that the Doppler broadening effect that we ignored until now that is present in our gas cell washes out any narrow features. Or it could be a combination of both. A less likely reason is that as the rf field is applied to the cell there is a localised heating effect that acts to wash out any sharp resonances. Also a possibility is the fact that the change in absorption that we see is not strictly a destruction of EIT on line centre but a general lowering of the EIT before such an effect takes place, i.e. we do not have enough rf power to induce the effect.

Another problem is that the B-field is non-uniform through the cell and so the actual Rabi frequency experienced by the probe field may be much less than we predicted above. A second factor is the alignment of the B-field within the cell. If the field does not have a near perfect overlap with the optical fields then the full effect of the B-field will not be realised. This alignment however is very difficult to achieve. With the optical it is difficult enough to do with visible beams and pinholes. With an invisible beam it is nigh on impossible, so we have to hope for the best. It does mean however that one, all or a combination of these effects can work against our observing any change in the normal probe absorption, where we would predict one should take place.

7.3 An Alternative Level Structure

It is obvious that the level structure considered above is quite complicated, in particular the way in which the RF field interacts with the hyperfine structure in the $5D_{5/2}$ level is not obvious. Hence interpretation of the experimental results is somewhat complicated as well. We can however envisage a simpler level structure if the upper level of the coupling field transition is less complicated than a D state. Such a manifold is shown in figure 7.17, where the upper level is the $7S_{1/2}$ level.

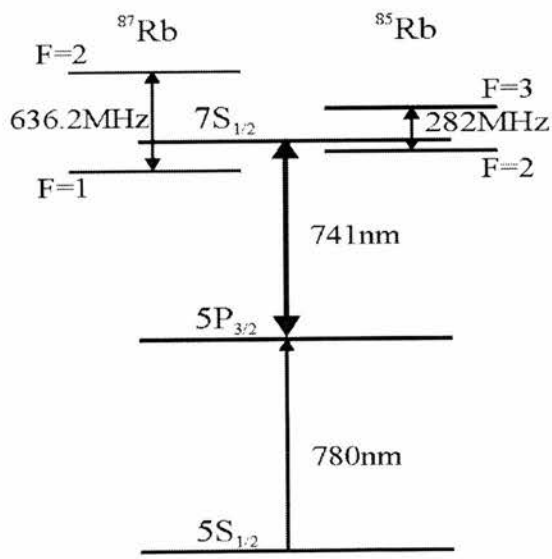

Figure 7.17: *Possible level structure for the observation of rf-manipulation of EIT. The hyperfine structure of the $7S_{1/2}$ level for the two rubidium isotopes is shown.*

EIT can be used to induce birefringence in a medium. This can be understood if a linearly polarised probe field is though of as a superposition of left and right circularly polarised light. Then by applying a circularly polarised coupling field we can see that only one of the superpositions of the probe field will be resonant with the coupling field. The difference in the absorption experienced by the two probe field components leads to the birefringence. This is illustrated in figure 7.18. Not all EIT schemes can experience such birefringence however. The system considered experimentally above, for instance, does not exhibit birefringence due to the hyperfine structure of the $5D_{5/2}$. This is because both superpositions of the probe field will always experience a coupling field, since the largest F number of the $5D_{5/2}$ level exceeds the largest F number of the intermediate level, the $5P_{3/2}$ level.

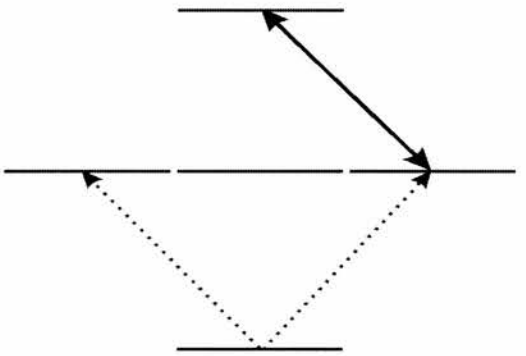

Figure 7.18: *The decomposition of a linearly polarised probe field into two circularly polarised components (dotted lines) will result in induced birefringence in the medium if a circularly polarised coupling field (solid line) is used. The birefringence is a result of the difference in absorption experienced by the two probe field components, i.e. one experiences EIT and the other does not.*

In moving to the $5P_{3/2} - 7S_{1/2}$ transition for the coupling field we allow the F state of the upper level to be greater than that of the lower level and hence we can achieve something like the situation shown in figure 7.18. Birefringence in this system has been demonstrated by Wielandy and Gaeta [4]. As a complement to the experiments described in chapter 5 an attempt was made to observe EIT-induced birefringence [5] in the $5S_{1/2} - 5P_{3/2} - 5D_{5/2}$ system. We did not observe any such effect, as we might expect considering the argument outlined above.

We could gain, not only in birefringence-type experiments by moving to a manifold with a coupling field resonant with the $5P_{3/2} - 7S_{1/2}$ transition but also, potentially, in our rf-induced modification of EIT experiment. Firstly the hyperfine structure of the $7S_{1/2}$ level is much simpler than the $5D_{5/2}$ level and this would make the analysis of the results easier. Also the hyperfine levels are much further apart than in the $5D_{5/2}$ level and this would allow effects associated with individual peaks to be resolved more clearly. The only penalty may be that large amounts of power at the slightly higher frequency of the hyperfine spacing in the $7S_{1/2}$ level may not be as

readily available as they were at 29MHz. But this level structure certainly deserves further investigation.

7.4 EIT with a diode laser probe field

In carrying out our RF induced modification of EIT experiment, as described above, it was found that the theory describing the experiment predicted features with a much narrower linewidth than were actually observed. It was therefore thought that the linewidth of the coupling field may be much greater than previously believed and that linewidth dephasing may be responsible for the discrepancies between theory and experiment. External cavity diode lasers [1, 2] have received much attention of late. They are relatively cheap, widely tuneable and supposedly narrow-linewidth devices. So the EIT experiment was attempted with such a device as the probe field and using the Microlase as the coupling field. As these diodes are used to trap atoms they must have a relatively narrow linewidth compared with the rubidium transitions of interest. Results using a unstabilised ECDL and a unstabilised circulase ECDL (this has a circular ouput beam and has an intrinsic feedback mechanism) are shown in figures 7.19 and 7.20. The unstabilised ECDL trace is shown with the probe laser sitting on the absorption line and the coupling field being scanned, this was done mainly due to the fact that the speed of scan of the diode laser wasn't suitable to observing the EIT. Despite being able to see EIT with the diode it was not possible to observe the hyperfine structure using the ECDL's. The reason for this is that although external cavity diode lasers do have very narrow linewidths, of the order of 100's of kHz, this is only over a very short timescale. Over a timescale of several seconds, during which an EIT trace would be taken, in our experimental configuration the linewidth can rise to, say, 5MHz. At such linewidths we would not expect to see the hyperfine structure with any great clarity. Hence we concluded that the Schwarz laser linewidth was as narrow as we previously thought and that to use diode lasers effectively as EIT probes in a variety of experiments we would need to redesign our experiment. The traces in figure 7.19 and 7.20 do, however, show that good EIT results are readily available with ECDL's, and could be potential replacements for the probe Ti:Sapphire laser in the future, depending on the nature of future experiments.

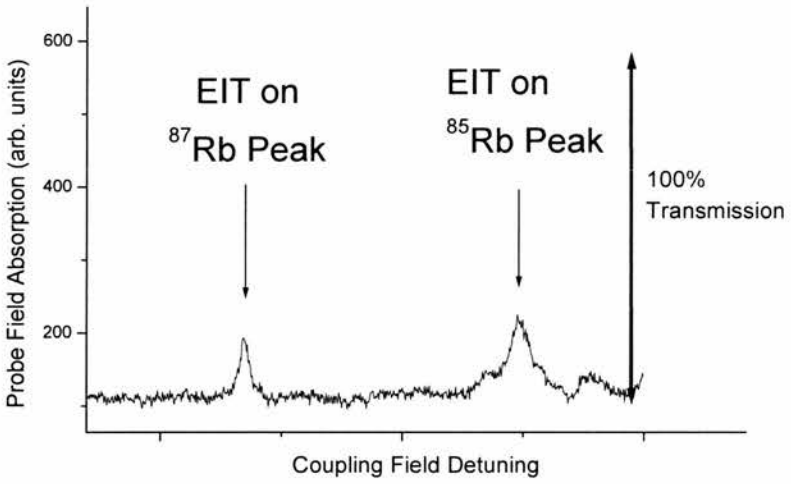

Figure 7.19: *EIT scan with a ECDL as the probe field. In this trace the coupling field is scanned while the probe field is left resonant with its transition. The first peak is EIT on the $^{87}Rb\ 5S_{1/2}$ (F=2) to $5P_{3/2}$ transition and the second peak is EIT on the $^{85}Rb\ 5S_{1/2}$ (F=3) to $5P_{3/2}$ transition. The two peaks show about 20% EIT.*

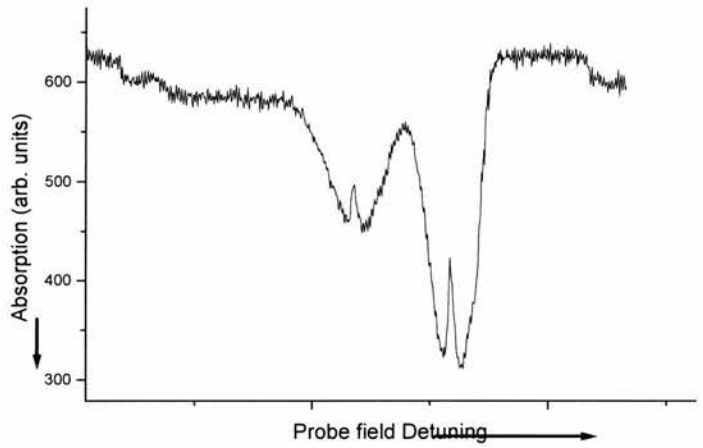

Figure 7.20: *EIT scan with the circulase ECDL as the probe field. Note the steep rise from the second peak compared with the initial slope on the first peak. This is indicative of a slight nonlinearity in the piezo extension that scans the diode cavity. Although the EIT is relatively good, hyperfine structure was unable to be resolved.*

7.5 Conclusions

Although the theory presented here does not give an exact fit to the recorded data we can, nevertheless, get a feel for what is happening. The applied rf field suppresses the EIT profiles to some degree, indicated by the rf-modulated trace. The complications presumably arise due to three factors: firstly the linewidth of the coupling laser acts in some manner either alone or in combination with other factors to broaden out the EIT profiles and hence wash out the sharp rf-induced features, secondly the actual rf field strength that acts on the EIT region is not precisely

determinable and thirdly the complicated level structure masks the straightforward results we would expect. These problems could be negated by application of a much stronger rf field, which would hopefully overcome the broadening that is experienced and potentially show more definitive structure on both the EIT and rf-modulated traces.

It has been shown however that EIT can be manipulated by rf fields. Further study into these processes could lead to the development of a rf-induced lens, outlined in chapter 6. All this would require is the observation of a sharp destructive feature in the straight EIT profile. We could also use this type of system to demonstrate multi-dark states as also examined in chapter 6.

References

[1] **K. B. MacAdam, A. Steinbach and C. Wieman**, "A Narrow-band tunable diode laser system with grating feedback, and a saturated absorption spectrometer for Cs and Rb.," *American Journal of Physics* **60**, 1098-1111 (1992).

[2] **C. E. Wieman and L. Hollberg**, "Using Diode Lasers for Atomic Physics," *Review of Scientific Instruments* **62**, 1-20 (1991).

[3] **W. Weltner Jr**, *Magnetic Atoms and Molecules*. (Dover, New York, 1983).

[4] **S. Wielandy and A. L. Gaeta**, "Coherent control of the polarization of an optical field," *Physical Review Letters* **81**, 3359-3362 (1998).

[5] **F. S. Pavone, G. Bianchini, F. S. Cataliotti, T. W. Hansch and M. Inguscio**, "Birefringence in electromagnetically induced transparency," *Optics Letters* **22**, 736-738 (1997).

Chapter 8

Microwave Induced Transparency in Atomic and Molecular Systems

8.1 Microwave Induced Transparency

As we have seen it is relatively straightforward to establish EIT in a gas cell using lasers as the probe and coupling fields. In all of these experiments an optical field controls the absorption of another optical field – such combinations are readily available in atomic systems. But as the name suggests EIT is not merely confined to the optical regime. In the last chapter we discussed how EIT can be manipulated by non-optical fields, by considering how rf fields could be added to a optical system to perturb the EIT set-up by the optical fields. In this chapter we examine how feasible it is to replace one of the optical fields with a microwave field in atomic systems. It *is* possible to create transparency using a microwave field as the coupling 'laser', or indeed by using both probe and coupling field in some electromagnetic regime other than the optical. In recent years a number of groups have looked at performing Microwave Induced Transparency (MIT) in solids [1, 2]. This has been discussed in Chapter 1 (section 1.3.1). No experimental work has been carried out on MIT in gaseous atoms and yet atoms such as rubidium seem to lend themselves very well to such experiments with their ground state hyperfine structure, which lies in the microwave regime.

8.1.1 Previous Work on M.I.T.

Some theoretical work has been carried out in relation to MIT discussing possible schemes for LWI and EIT in various level systems. Much of the theory regarding microwave effects on EIT is outlined in early EIT and LWI papers. Indeed Scully *et al.* in one of the earliest works in the field [3] describe how a degenerate Λ-quantum beat laser may be made to display inversionless gain when a microwave field is applied between the two lower levels. It is this microwave field that coherently drives the lower states, i.e. without the microwave field no effect is seen. This idea is investigated in more detail by Fearn *et al.* [4]. Blok and Krochik [5] show that inversionless lasing is possible in a three level cascade scheme where the upper two levels are coupled by a high frequency electromagnetic field (e.g. microwaves). They show that such a system exhibits pulsed-mode lasing without inversion and make estimates of the magnetic field strength required to produce such effects. However they take no account of the fact that such a system would require to be Doppler free nor do they relate it to any real atomic system.

More recent work has included the experimental work of Zhao *et al.* in which microwave induced transparency was demonstrated in ruby [1]. This work however is somewhat disputed within the EIT community since the depth of the EIT is not considered to be sufficient to definitively say

that EIT is present. Other work presented by Ham *et al.* [6, 7] has shown transparency in Pr^{3+}:Y_2SiO_5 induced by a rf field. However the authors say that only a small amount of the observed transparency is due to EIT. Similar effects have been observed in a V-type quantum-beat scheme in another Pr^{3+} doped crystal in which a rf field drives the upper two-levels [8]. A recent experimental twist in the tale has been demonstrated by an Italian group [9] in which they use a coherent population trapping Λ scheme to generate microwaves on the electric dipole forbidden transition. The gas cell in which the lasers interact with the caesium is placed inside a microwave cavity to enhance the effect and powers of 100fW are observed. Here the coherence generates an oscillating magnetisation on the two ground state levels.

Other recent theoretical work has been carried out by Yelin *et al* [10] in which they discuss inversionless gain in the frequency up-conversion regime i.e. when the probe wavelength is shorter than the coupling field wavelength. This is the case that was investigated in chapter 3. They briefly mention that a natural choice for such a scheme would be one similar to that shown in figure 8.1 where the coupling field is driving a ground state hyperfine level with microwave frequency spacing. Although they concede gain could be observed in such a scheme, 'using intense microwave radiation,' they make no attempt to quantify such parameters. A final theoretical paper indicates potential uses of MIT theory: it considers the possibility of Maser action without inversion in interstellar space [11]. They suggest that some types of methanol masers may be formed by coherent processes – maser emission at one microwave frequency would drive emission in a second frequency. This is the first practical use of microwave induced EIT processes.

In this chapter we address the possibility of MIT in gaseous systems. By considering the case of atomic rubidium we show theoretically that EIT is possible using microwaves as the coupling field. However we also show that such experiments using cw microwave sources are impractical due the extreme microwave powers that are required to induce transparency. We then consider a number of other gaseous systems that may support MIT, i.e. molecules with appropriate rotational-vibrational structure. This review of appropriate molecules leads into the experimental development of an mid-infrared probe source which is outlined in chapter 9.

8.2 Atomic Systems

8.2.1. Theoretical Model

We use for our atomic model the system shown in figure 8.1. Two closely spaced hyperfine split levels, |1> and |2>, are coupled by a microwave field, B. The ground state is coupled to the upper level |3> by an optical probe field, E.

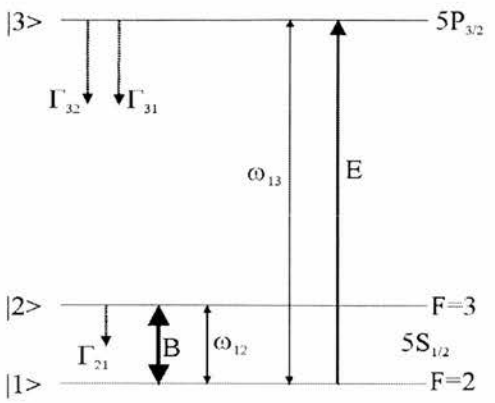

Figure 8.1: *Atomic system under consideration with an electric dipole allowed probe transition and a magnetic dipole allowed coupling transition*

Modelling of this system was carried out using a standard density matrix analysis for a three-level V-scheme with 2 fields and three decays. The equations of motion for this system are given by:

$$\begin{aligned}
\dot{\rho}_{11} &= i\Omega_{12}(\tilde{\rho}_{21}-\tilde{\rho}_{12})+i\Omega_{13}(\tilde{\rho}_{31}-\tilde{\rho}_{13})+\Gamma_{21}\rho_{22}+\Gamma_{31}\rho_{33}\\
\dot{\rho}_{22} &= i\Omega_{12}(\tilde{\rho}_{12}-\tilde{\rho}_{21})-\Gamma_{21}\rho_{22}+\Gamma_{32}\rho_{33}\\
\dot{\rho}_{33} &= i\Omega_{13}(\tilde{\rho}_{13}-\tilde{\rho}_{31})-\Gamma_{31}\rho_{33}-\Gamma_{32}\rho_{33}\\
\dot{\rho}_{12} &= -i(\Delta_{12}-i\gamma_{12})\tilde{\rho}_{12}+i\Omega_{12}(\rho_{22}-\rho_{11})+i\Omega_{13}\tilde{\rho}_{32}\\
\dot{\rho}_{23} &= -i(\Delta_{13}-\Delta_{12}-i\gamma_{23})\tilde{\rho}_{23}+i\Omega_{12}\tilde{\rho}_{13}-i\Omega_{13}\tilde{\rho}_{21}\\
\dot{\rho}_{13} &= -i(\Delta_{13}-i\gamma_{13})\tilde{\rho}_{13}+i\Omega_{13}(\rho_{33}-\rho_{11})+i\Omega_{12}\tilde{\rho}_{23}
\end{aligned} \qquad (8.1a\text{-}f)$$

where the subscripts refer to the level structure shown in figure 8.1 and $\tilde{\rho}_{ij}$ is a substitution used to remove the optical frequency oscillations of ρ_{ij} in the steady state. The Rabi frequencies of the coupling and probe fields are given by $\Omega_{12}=\frac{\mu_{12}B}{\hbar}$ and $\Omega_{13}=\frac{\mu_{13}E}{\hbar}$ where B and E are the magnetic and electric field strengths and μ_{ij} are the magnetic and electric transition dipole matrix elements respectively. We work in a Doppler broadened system (e.g. a gas cell) with the detunings defined as:

$$\Delta_{13}=\omega_1-\omega_{13}-k_1V_z \qquad (8.2a)$$

$$\Delta_{12}=\omega_2-\omega_{12}-k_2V_z \qquad (8.2b)$$

with ω_1 and ω_2 denoting the angular frequencies of the coupling electric field and probe magnetic field respectively, ω_{13} and ω_{12} are the transition frequencies for the V-scheme levels (figure 8.1) . The wavevectors of the two fields are defined as $k_i=2\pi n/\lambda_i$ and V_z is the atomic velocity along the cell length. The decay rates from level *i* to *j* are given by Γ_{ij}. The coherence decay rates, γ_{ij} are given by:

$$\gamma_{12}=\frac{1}{2}\Gamma_{21} \qquad (8.3a)$$

$$\gamma_{13} = \frac{1}{2}(\Gamma_{31} + \Gamma_{32}) \tag{8.3b}$$

$$\gamma_{23} = \frac{1}{2}(\Gamma_{31} + \Gamma_{32} + \Gamma_{21}) \tag{8.3c}$$

We assume that no collisional dephasing takes place, i.e. we idealise the system to one that is dephased solely by the natural population decays and the applied incoherent excitation. The decay rate on the microwave transition may be considered to be very small (indeed so small as to be negligible). There will be, however, a finite decay from the upper microwave level, and to model this we introduce a rate Γ_{21} which is very small compared to Γ_{32} and Γ_{31}.
The equations are solved for steady-state conditions then split into nine real simultaneous equations, using properties of the density matrix. These equations are then solved using linear algebra routines, giving the real and imaginary parts of the coherence on each transition, which can be related to the refractive index, absorption and atomic populations in each of the energy levels. Doppler broadening is then taken into account by integrating over the velocity distribution, providing a comprehensive model of the system.

The microwave-optical system of the type being considered is an extreme version of the wavelength mismatch systems we have previously studied [12, 13] in chapter 3. However, in the microwave-optical case we lose the V-scheme advantage [12-14] that occurs when the mismatch is relatively small and previously allowed us to use coupling field Rabi frequencies less than the probe field Doppler width. Hence, we must initially expect the coupling field Rabi frequencies to be higher than may be expected in simple all optical systems. In a microwave coupled scheme, in which Doppler broadening is important, then we can reasonably say that the contribution of the microwaves to the Doppler detuning effect [12-14] is very small, since the microwave wavevector and hence the associated detuning Δ_{12} for a given velocity is very small. So we need only be concerned here with the probe field wavelength, and as we shall see shortly as the wavelength decreases it becomes harder to induce a transparency.

For rubidium in a gas cell at 373K, the Doppler width of the probe field for the case of the 780nm ($5S_{1/2}$-$5P_{3/2}$) transition is approximately 0.56GHz. Therefore we expect no EIT to occur until the coupling field Rabi frequency exceeds this value [15]. This can be seen in figure 8.2 where we have used values of Γ_{ji} as appropriate in rubidium (Γ_{31}=Γ_{32}=6MHz). In order to achieve substantial transparencies we require the coupling field Rabi frequencies to be relatively high (0.48GHz). To achieve such Rabi frequencies with optical sources is relatively easy; to do so with a (rf) magnetic field is much more difficult, as we shall show below.

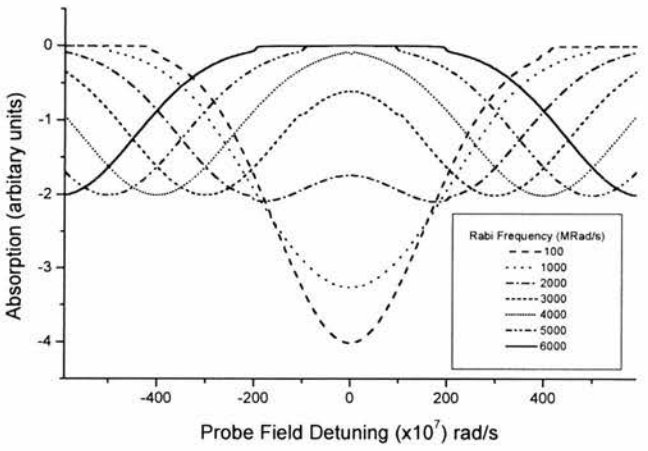

Figure 8.2: *EIT in IR-microwave scheme*

We also consider, for a probe field, the 422nm transition in rubidium ($5S_{1/2}$-$6P_{1/2}$) in order to investigate how further increasing the wavelength mismatch effects the EIT and also to see the difference made by the slower decay rates associated with this transition ($\Gamma_{31}=\Gamma_{32}=1.3$MHz). Previously we have demonstrated EIT on this blue transition using a 780nm-coupling field [16]. The absorption traces for the blue probe are shown in figure 8.3.

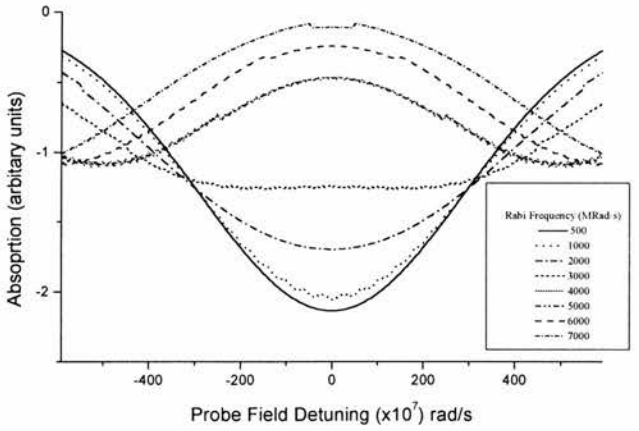

Figure 8.3: *EIT in blue-microwave scheme*

We see, by comparing figures 8.2 and 8.3, that the coupling field power required to induce EIT on the blue transition is greater than that on the infrared transition. This is consistent with a larger wavelength mismatch. In the IR system we need a Rabi frequency of 0.48GHz to induce a 75% transparency, while in the blue system we require a Rabi frequency of 0.64GHz for a similar transparency. As we will show below, this indicates a dramatic difference in the amount of microwave power required for each of the two cases.

8.2.2. Magnetic Dipoles, Cavities and Rabi Frequencies

The fundamental difference between the atomic systems so far described and those seen in previous experiments [17, 18] is that the coupling field is not electric dipole allowed but magnetic dipole allowed. Since magnetic dipoles are much weaker than electric dipoles this has serious implications for the power requirements of the microwave field. It seems sensible that the gas cell containing the rubidium should be placed inside a cavity in order to enhance the microwave field. We can therefore derive an expression that relates the incident microwave power to the on axis B-field inside the cavity. This will then allow us to relate the incident power to the microwave Rabi frequency, Ω_μ. We can relate Ω_μ to the B-field in the following way [19]: since the ground state of rubidium has L=0 and S=1/2, J=1/2 then

$$\Omega_1 = \frac{\mu_B |B_z|}{\hbar}, \tag{8.4}$$

where μ_B is the Bohr magneton. Hence the expression for the magnetic field related Rabi frequency is similar in form to the Rabi frequency for an electric field. It is now possible to calculate the B-field for a given Rabi frequency.

Now, by assuming that the cell is within a microwave cavity we can derive a simple expression for the average B field:

The Q of a cavity is related to the energy stored in the cavity by:

$$Q = \frac{\omega \times EnergyStored}{PowerDissipated}. \tag{8.5}$$

So for a cavity of volume V the stored energy per unit volume is given by:

$$SE = \frac{Q \times PowerDissipated}{\omega V} \tag{8.6}$$

Equating this to the well known energy density equation:

$$SE = \frac{1}{2}\frac{B^2}{\mu_0}, \tag{8.7}$$

gives us:

$$B = \sqrt{\frac{2\mu_0 \times Q \times P}{\omega V}}. \tag{8.8}$$

We may combine equations (8.4) and (8.8) to get a relation between microwave power and Rabi frequency (assuming our average B equal to the magnitude of B_z):

$$P_1 = \frac{1}{2}\frac{\hbar^2 \omega V \Omega_1^2}{\mu_0 \mu_B^2 Q} \tag{8.9}$$

Equation (8.9) allows us estimate the power required to induce transparencies of varying degrees by relating equation (8.9) to our previous modelling of the microwave – optical system (figure 8.4). It is seen that the powers involved for even relatively small transparencies are extremely high, for example to obtain a Rabi frequency of 0.48GHz requires a power in excess of 1MW, indicating that microwave induced transparency is impractical using a weak magnetic dipole transition.

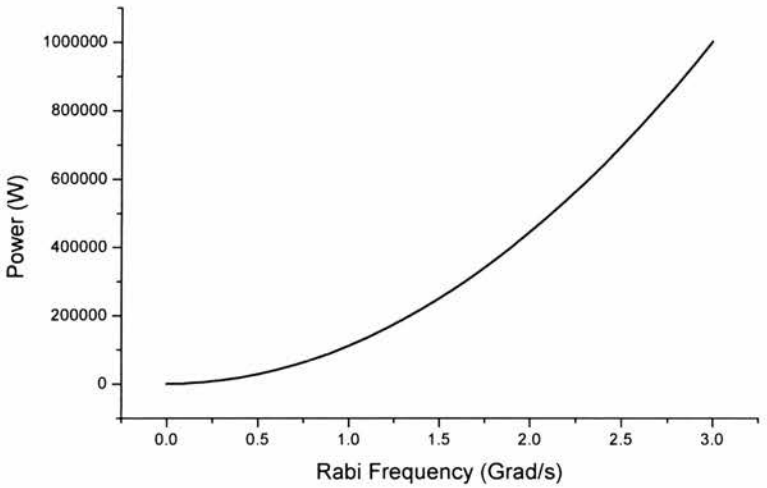

Figure 8.4: *Power requirements for the magnetic dipole case. Parameters are cavity Q=400, cavity radius is 2.8cm and cavity length is 5.7cm. The coupling frequency is 8.83GHz.*

By looking at a previous experiment we can check our estimations based on the above simple arguments. In 1985 R.P. Frueholz and J.C. Camparo performed experiments [19] concerned with Adiabatic Rapid Passage (ARP) in rubidium. Using a rubidium cell in a TE_{011} microwave cavity of Q=400 and with a radius of 2.8cm and a length of 5.7cm, they measured an induced Rabi frequency of approximately 1.5kHz on the 6.835GHz transition in the Rb^{87} ground state using 8mW of microwave power input into the cavity. They measured this power to produce a on axis magnetic field of approximately 3-4mG. For similar parameters our simple model gives approximately 10mG. Thus our power estimation can be seen to reasonably correct.

We also note that the power required to induce transparency scales with frequency. This therefore indicates that any sort of coherent effects will be harder to achieve at microwave frequencies than in the rf regime we considered in the previous chapter.

8.3. Molecular Type Systems

If transparency is unlikely to be induced in atomic schemes using a microwave-coupling field, can we find other systems where there is a possibility of MIT? We now consider schemes, with appropriate transitions in the microwave and optical/infrared regions, that have electric dipole allowed microwave transitions. Such schemes can be found in molecular rather than atomic gases. Some work on EIT in molecules has been carried out before [20]. Bergmann and colleagues recently observed EIT in nitrogen oxide as a by-product of their work on Stimulated Adiabatic Rapid Passage (STIRAP). All such previous work has been solely concerned with optical fields and STIRAP is a pulsed laser phenomenon.

In order to allow a comparison with the V-type scheme described in 8.2.1 we will replace the magnetic dipole allowed transition with an electric dipole allowed transition. We will conclude with a brief look at more specific examples.

By replacing the magnetic dipole with an electric one we modify some of the parameters presented in 8.2.1. The coupling field Rabi frequency becomes: $\Omega_{12} = \frac{\mu_{12} E_c}{\hbar}$, where E_c is the coupling field strength; μ_{12} will no longer be equal to μ_B, and the stored energy density in terms of the electric field may be written:

$$SE = \frac{1}{2}\varepsilon_0 E^2 \tag{8.10}$$

rather than the expression given in equation (8.7). We take the magnitude of the electric dipole moment of the coupling field from an estimate based on the molecule OCS (Carbonyl Sulphide), which was the molecule used in the original Autler-Townes experiment [21]. The transition electric dipole moment of a fixed axis rotator is given by $\mu_m / 2\pi$ where μ_m is the molecular electric dipole moment [22]. In OCS μ_m is 0.7D.

By following a similar argument to that for the magnetic field case we derive an equation that relates power to Rabi frequency in the electric field case:

$$P_2 = \frac{2\pi^2 \hbar^2 \omega \varepsilon_0 V \Omega_{12}^2}{Q \mu_m^2} \tag{8.11}$$

The ratio of P_1/P_2 from (8.11) and (8.9) is hence

$$\frac{P_1}{P_2} = \frac{c^2}{4\pi^2}\left(\frac{\mu_m}{\mu_B}\right)^2 \tag{8.12}$$

For the case when the molecular dipole moment μ_m is equal to 1D, we obtain

$$\frac{P_1}{P_2} \approx 290 \tag{8.16}$$

So, for example, if the power in the magnetic case is 5MW then in the electric dipole case the power required is ≈ 17kW.

So we find that the powers required in an electric dipole scheme compared to that in a similar magnetic dipole scheme are several order of magnitudes less.

8.4. Possible Molecular Schemes

We now examine some possible candidates for MIT experiments. Our criteria, in the first instance, are that they have appropriate microwave transitions coupled with an associated optical/infrared transition. We draw some of our information from infrared-microwave double resonance spectroscopy [23]. The main problem with molecules is both their complicated level structure compared to atoms, and the lack of detailed information in the literature about specific molecular parameters. In a small part this is due to lack of laser sources in the mid-infrared where much of the vibration transitions lie in molecules. We however would hope to investigate such transitions in an EIT type experiment utilising broadly tuneable mid-infrared OPOs [24, 25].

8.4.1 Methanol

Methanol has a number of fundamental bands of vibration, including the ν_2 band at around 3.3microns [26]. A possible V-scheme for this molecule is shown in figure 8.5. The microwaves couple between the K=1E and K=2E sublevels of the J=4 level and have a frequency of 12.47 GHz. The molecular dipole moment of methanol is 1.4D – i.e. large enough that we would hope to be able to induce transparency on this line.

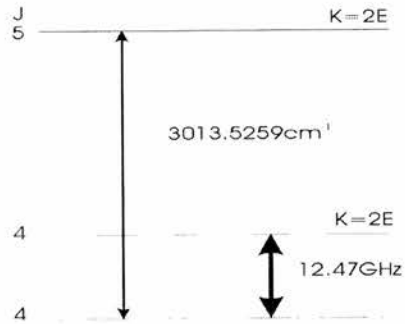

Figure 8.5: *V-Scheme in Methanol*

Methanol has previously been used in studies of dynamic Stark splitting [27]. In 1988 Henningsen and Petersen performed an infrared-microwave double-resonance experiment in methanol. Using microwave fields at around 9 and 10 GHz and infrared radiation at 9.3 – 11.9 microns they demonstrated that dynamic Stark splitting took place in methanol vapour. The interesting thing to note is that (despite a little ambiguity) the microwave line is split by the infrared field and not vice versa, as we would wish. This is an important reminder that in a

microwave-optical EIT experiment the strength of the optical dipole moment will be much larger than that of the microwave transition dipole moment. So if the optical field is made too large unwanted effects will begin to appear. Also of note is the fact that coherent effects are readily observable in molecular systems and can be observed despite the complicated structure of the molecules under study.

8.4.2 Formaldehyde

Initial work on the microwave spectrum of formaldehyde began in the 1940s and 1950s when both experimental [28] and theoretical [29] studies were published. It was found that formaldehyde had a number of lines in the 7-72 GHz region. Coupling this with earlier studies of the infrared bands of the molecule in the 1930s [30, 31], which exist around 3.5-microns (and 1-2-microns), makes formaldehyde an interesting possibility as the molecule for EIT experiments. Unfortunately there is a lack of assigned infrared spectral information. What makes formaldehyde particularly interesting is a series of experiments carried out by Takami and Shimoda [32-35]. In a review of saturation spectroscopy [36] Letokhov remarks that, 'They managed to observe a narrow resonance splitting of the vibrational molecular transition caused by the dynamic Stark effect in a strong microwave field at the rotational transition'. This is exactly what we would wish to do, split the infrared (vibrational) line using a strong microwave field. More importantly this experiment is carried out in the 3.5-micron band with a 72GHz coupling field (see figure 8.6).

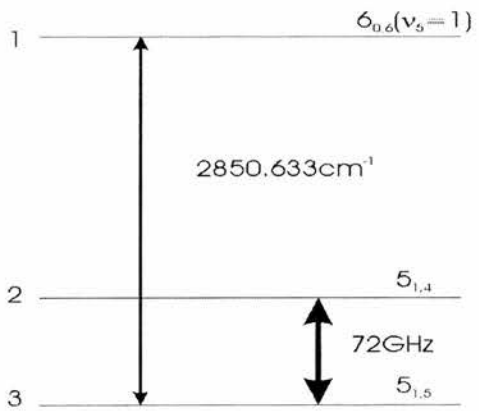

Figure 8.6: *V-Scheme in formaldehyde*

Unfortunately the papers referred to by Letokhov [23, 35] detailing Takami and Shimoda's experiments on formaldehyde are less forthcoming about any dynamic Stark splitting. They observe anomalous lineshape effects, which they could not account for using their standard theory, merely commenting that, "The observed lineshapes are explained by the effect of the resonance modulation due to strong resonant microwaves, although its theoretical calculation would be difficult". These anomalous lineshape effects may have been caused by dynamic Stark splitting but could be due to other effects. Nonetheless their experiment remains of great interest. These two examples have concentrated on probe transitions in the mid to far infrared. Obviously molecules have a wealth of structure and probe transitions in the visible or lower wavelength

regimes may be found. We restrict ourselves to infrared transitions due our immediate experimental experience.

8.4.3 Ammonia

Ammonia is an unusual molecule in that it has vibrational transitions in the microwave regime. This occurs due to its inversion symmetry. This is where the nitrogen atom vibrates about a potential barrier. It does this at a rate that puts its energy levels in the microwave regime. This simplifies its spectral characteristics somewhat. Ammonia has a number of microwave lines that are well-studied [37] It has four fundamental bands in the infrared with a strong parallel band at about 2.99-microns [38]. These can be assigned reasonably straightforwardly with the microwave transitions using experimental data [39].

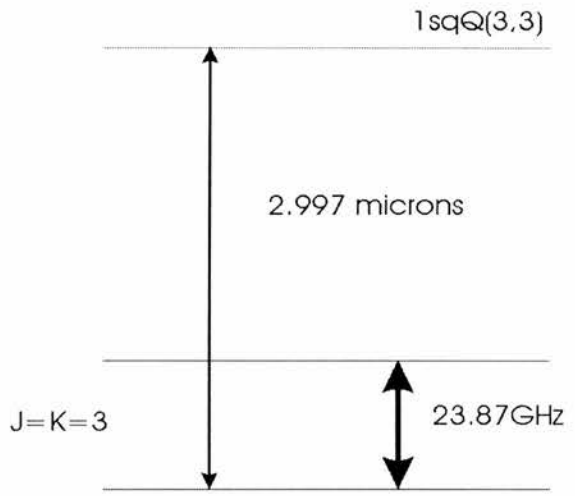

Figure 8.7: *V-scheme in ammonia*

Using these assignments appropriate transitions can be identified and one such suitable transition is that which uses a coupling field or 23.87GHz on the original maser line [40] in the J=K=3 state. This line is linked to suitable probe fields around 3 microns, as shown in figure 8.7. Other considerations include the Doppler width in ammonia at this wavelength (2.1 $Grads^{-1}$ at 100°C) which affects the amount we have to Rabi split the transition and how far we require the probe laser to be scanned. Ammonia has a reasonably large electric molecular dipole moment of 1.4D [41].

8.4.4 Carbonyl Sulphide (OCS)

Since the Autler-Townes experiment [21] was carried out in OCS it is also an interesting candidate in our investigation. OCS is a relatively simple molecule being a triatomic linear chain. Its rotational (microwave) spectrum was extensively studied throughout the 1940s and 1950s [42-45] and as such is well known (figure 8.8).

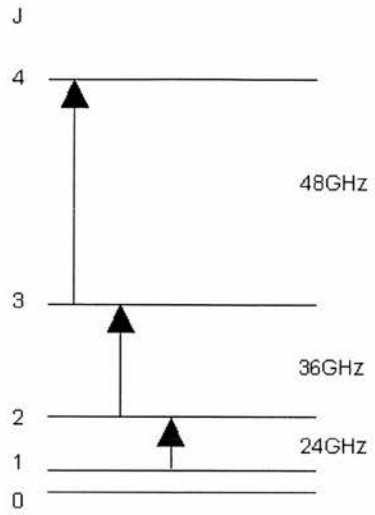

Figure 8.8: *Rotational spectrum of OCS.*

The spectral characteristics are slightly different for the various isotopes of the molecule. The fact that the microwave lines are relatively simple in nature is an obvious benefit if we were to carry out an experiment in OCS. The problem with OCS arises when we look at the vibrational (infrared) spectrum. The fundamental vibrational bands are at 4.81 microns, 11.6 microns and 19 microns [37] and although we have evidence that there exists a 3 micron absorption band (an overtone band) [46], there seem to be no direct references to it in the literature. The assumption is that it is little studied and therefore we can not assign any microwave lines to such a band. Such data does exist for other overtone bands [47] and if further data comes to light then OCS may be a viable molecule for our test bed experiment. Possibilities do exist for other transitions however; in particular the overtone bands around 5 microns. The 4.81-micron fundamental band also remains an interesting possibility.

Another factor in the feasibility assessment of the molecule is the dipole moment. We can compare this, roughly, with the dipole moment on the coupling transition ($5P_{3/2}$ -> $5S_{1/2}$) used in previous experiments in rubidium. A simple calculation [48, 49] gives this moment as 7.53 Debye. The molecule dipole moment (not the transition dipole moment) of OCS is roughly 0.7 D. The detailed calculation of transition moments requires a very complicated quantum mechanical treatment [22] and is not discussed further here. The specific transition moments of OCS are expected to be less than the molecular moment. How much less is obviously an important question and will be dealt with when we consider power requirements below.

The ladder-type level structure of OCS may be interesting for observation of the type of effects described in chapter 6. Although EIT effects are of less interest in the microwave/rf regime (i.e. when the probe field is in this regimes) they can act as testing grounds for the optical arena. A similar type of experiment to that carried out by Autler and Townes [21] could be used to demonstrate multiple dark states via coherent excitation in a N-Level cascade. Indeed the ideal

type of system for observing such effects would be any linear oscillator type system with its ladder of energy levels.

8.4.5 Others

Other molecules have been briefly looked at, which may be of interest in the future. These include NO_2 [50, 51] and thioformaldehyde (H_2CS) [52-54], which have transitions in the visible and SO2 [55], which has transitions in the UV. Another molecule of interest is NO [56] which, as discussed above, has been used in an EIT experiment. It could be possible to induce transparency on a UV line with a mid-infrared laser (around 5 microns) [57] and this and other schemes in NO may be of practical interest in the future.

8.5 Practicalities

Even in molecular systems, it seems, we would need a large amount of microwave power to induce any sort of transparency. It pay be possible to do this however. With careful experimental design, the correct choice of molecule and, for instance, a very high Q cavity, microwave induced EIT in molecular systems could be realisable. However as pointed out above many of the optical transition lines in molecules (suitable for the probe transition) lie in the infrared region. This means that for any chance of observing EIT in these regions we require a probe source. This by necessity, in the cw regime, means a narrow linewidth, frequency stable and highly tuneable (e.g. scannable) source. These are not readily available in the infrared. The development of such a source is described in the next chapter. The initial idea was to carry out a MIT experiment in ammonia, using the level scheme shown in figure 8.7. To achieve this we would require a high Q microwave cavity. This cavity would have to be very small (of the order of $1cm^3$), in order to excite the appropriate E-field mode. This would make plumbing of vacuum equipment to such a cavity difficult and would also result in only a small amount of ammonia being available to absorb the probe field. This would make the detection of any EIT more difficult. Also pressure broadening effects in the ammonia would have to be taken into account. All these factors make an MIT experiment in a molecule a difficult undertaking. With enough care and attention though, it should be possible. So far this experiment has not been carried out.

8.6 Conclusions

We have shown that microwave induced transparency is possible in simple atomic systems where the microwaves couple into the hyperfine ground state of such an atom with an optical field forming a V-scheme. By taking Rb^{85} as an example we have demonstrated that large amounts of microwave power are required to achieve even small amounts of transparency. This is because the hyperfine levels are not electric dipole allowed but, much more weakly, magnetic dipole allowed.

By replacing the magnetic dipole allowed transition in our model with an electric dipole transition it is possible to see that that transparency is much more attainable by up to two orders of magnitude. Such ground state transitions are unavailable in atoms. They do, however, exist in molecules. We have illustrated this fact with a number of examples, methanol, formaldehyde and

ammonia. So we conclude that while microwave induced transparency is practically unfeasible in atomic systems it may be more readily achieved in molecules with appropriate transitions.

Acknowledgements
The work in this chapter relating to molecules was made considerably easier by suggestions from Professor Geoffrey Duxbery of Strathclyde University for which I'd like to thank him.

References

[1] **Y. Zhao, C. K. Wu, B. S. Ham, M. K. Kim and E. Awad**, "Microwave induced transparency in ruby," *Physical Review Letters* **79**, 641-644 (1997).

[2] **B. S. Ham, M. S. Shahriar and P. R. Hemmer**, "Radio-frequency-induced optical gain in Pr3+:Y2SiO5," *Journal of the Optical Society of America B-Optical Physics* **15**, 1541-1544 (1998).

[3] **M. O. Scully, S. Y. Zhu and A. Gavrielides**, "Degenerate quantum-beat laser - lasing without inversion and inversion without lasing," *Physical Review Letters* **62**, 2813-2816 (1989).

[4] **H. Fearn, C. Keitel, M. O. Scully and S. Y. Zhu**, "Lasing without inversion in a simple-model of a 3-level laser with microwave coupling," *Optics Communications* **87**, 323-330 (1992).

[5] **V. R. Blok and G. M. Krochik**, "Theory of lasers without inversion," *Physical Review A* **41**, 1517-1525 (1990).

[6] **B. S. Ham, P. R. Hemmer and M. S. Shahriar**, "Efficient electromagnetically induced transparency in a rare-earth doped crystal," *Optics Communications* **144**, 227-230 (1997).

[7] **B. S. Ham, M. S. Shahriar, M. K. Kim and P. R. Hemmer**, "Frequency-selective time-domain optical data storage by electromagnetically induced transparency in a rare-earth-doped solid," *Optics Letters* **22**, 1849-1851 (1997).

[8] **K. Yamamoto, K. Ichimura and N. Gemma**, "Enhanced and reduced absorptions via quantum interference: Solid system driven by a rf field," *Physical Review A* **58**, 2460-2466 (1998).

[9] **A. Godone, F. Levi and J. Vanier**, "Coherent microwave emission in cesium under coherent population trapping," *Physical Review A* **59**, R12-R15 (1999).

[10] **S. F. Yelin, M. D. Lukin, M. O. Scully and P. Mandel**, "Gain without inversion in the frequency up-conversion regime," *Physical Review A* **57**, 3858-3868 (1998).

[11] **H. P. Liu and J. Sun**, "Maser action without inversion in interstellar space," *Optics Communications* **150**, 153-157 (1998).

[12] **S. Shepherd, D. J. Fulton and M. H. Dunn**, "Wavelength dependence of coherently induced transparency in a Doppler-broadened cascade medium," *Physical Review A* **54**, 5394-5399 (1996).

[13] **J. R. Boon, E. Zekou, D. McGloin and M. H. Dunn**, "Comparison of wavelength dependence in cascade-, Lambda-, and Vee-type schemes for electromagnetically induced transparency," *Physical Review A* **59**, 4675-4684 (1999).

[14] **J. R. Boon, E. Zekou, D. McGloin and M. H. Dunn**, "Prediction of inversionless gain in a mismatched Doppler-broadened medium," *Physical Review A* **58**, 2560-2566 (1998).

[15] **S. E. Harris, J. E. Field and A. Imamoglu**, "Nonlinear optical processes using electromagnetically induced transparency," *Physical Review Letters* **64**, 1107-1110 (1990).

[16] **J. R. Boon, E. Zekou, D. J. Fulton and M. H. Dunn**, "Experimental observation of a coherently induced transparency on a blue probe in a Doppler-broadened mismatched V-type system," *Physical Review A* **57**, 1323-1328 (1998).

[17] **K. J. Boller, A. Imamoglu and S. E. Harris**, "Observation of electromagnetically induced transparency," *Physical Review Letters* **66**, 2593-2596 (1991).

[18] **D. J. Fulton, S. Shepherd, R. R. Moseley, B. D. Sinclair and M. H. Dunn**, "Continuous-wave electromagnetically induced transparency - a comparison of v-system, lambda-system, and cascade systems," *Physical Review A* **52**, 2302-2311 (1995).

[19] **R. P. Frueholz and J. C. Camparo**, "Microwave field-strength measurement in a rubidium clock cavity via adiabatic rapid passage," *Journal of Applied Physics* **57**, 704-708 (1985).

[20] **K. Bergmann, H. Theuer and B. W. Shore**, "Coherent population transfer among quantum states of atoms and molecules," *Reviews of Modern Physics* **70**, 1003-1025 (1998).

[21] **S. H. Autler and C. H. Townes**, "Stark Effect in Rapidly Varying Fields," *Physical Review* **100**, 703 (1955).

[22] **J. D. Greybeal**, *Molecular Spectroscopy*. (McGraw-Hill International Editions, Singapore, 1988).

[23] **K. Shimoda**, *Double-Resonance Spectroscopy of Molecules by means of Lasers*. in *Laser Spectroscopy of Atoms and Molecules* H. Walther, Eds. (Springer-Verlag, Berlin, 1976).

[24] **K. Schneider, P. Kramper, S. Schiller and T. Mlynek**, "Toward an optical synthesizer: A single-frequency parametric oscillator using periodically poled LiNbO3," *Optics Letters* **22**, 1293-1295 (1997).

[25] **D. J. M. Stothard, M. Ebrahimzadeh and M. H. Dunn**, "Low-pump-threshold continuous-wave singly resonant optical parametric oscillator," *Optics Letters* **23**, 1895-1897 (1998).

[26] **L.-H. Xu, X. Wang, T. J. Cronin, D. S. Perry, G. T. Fraser and A. S. Pine**, "Sub-Doppler Infrared Spectra and Torsion-Rotation Energy Manifold of Methanol in the CH-Stretch Fundamental Region," *Journal of Molecular Spectroscopy* **185**, 158-172 (1997).

[27] **J. O. Henningsen and J. C. Petersen**, "Infrared-microwave double resonance in methanol: coherent effects and molecular parameters," *Journal of the Optical Society of America B-Optical Physics* **5**, 1845-1857 (1988).

[28] **J. K. Bragg and A. H. Sharbaugh**, "Microwave Spectrum of Formaldehyde," *Physical Review* **75**, 1774-1775 (1949).

[29] **R. B. Lawrance and M. W. P. Strandberg**, "Centrifugal Distortion in Asymmetric Top Molecules. I. Ordinary Formaldehyde $H_2C^{12}O$," *Physical Review* **83**, 363-369 (1951).

[30] **H. N. Nielsen**, "The Infrared Absorption Spectrum of Formaldehyde. Part I.," *Physical Review* **46**, 117-121 (1934).

[31] **J. R. Patty and H. N. Nielsen**, "The Absorption by Formaldehyde Vapor in the Infrared," *Physical Review* **39**, 957-966 (1932).

[32] **K. Sakurai, K. Uehara, M. Takami and K. Shimoda**, "Stark Effect of Vibration-Rotation Lines of Formaldehyde Observed by a 3.5micron Laser," *Journal of the Physical Society of Japan* **23**, 103-109 (1967).

[33] **K. Shimoda and M. Takami**, "Pressure Dependence of Infrared-microwave Double Resonance in Formaldehyde," *Optics Communications* **4**, 388-391 (1972).

[34] **M. Takami and K. Shimoda**, "Double Resonance of the 3.5micron He-Xe Laser Radiation and Millimeter Waves in H_2CO," *Japanese Journal of Applied Physics* **10**, 658 (1971).

[35] **M. Takami and K. Shimoda**, "Infrared-Microwave Double Resonance in H_2CO with a Zeeman Tuned 3.5micron He-Xe Laser," *Japanese Journal of Applied Physics* **11**, 1648-1656 (1972).

[36] **V. S. Letokhov and V. P. Chebotayev**, *Nonlinear Laser Spectroscopy*. (Springer-Verlag, Berlin, 1977).

[37] **C. H. Townes and A. L. Schawlow**, *Microwave Spectroscopy*. (McGraw-Hill, London, 1955).

[38] **G. Herzberg**, *Infrared and Raman Spectra*. (Van Nostrand Reinhold Company, New York, 1945).

[39] **V. N. Markov, A. S. Pine, G. Buffa and O. Tarrini**, "Self Broadening in the υ_1 Band of NH_3," *Journal of Quantitative Spectroscopy & Radiative Transfer* **50**, 167-178 (1993).

[40] **J. P. Gordan, H. J. Zeiger and C. H. Townes**, "The Maser - New type of microwave amplifier, frequency standard and spectrometer," *Physical Review* **99**, 1264-1274 (1955).

[41] **M. D. Marshall, K. Can Izgi and J. S. Muenter**, "IR-Microwave Double Resonance Studies of Tunneling Frequencies in the υ_1 and υ_3 States of Ammonia," *Journal of Molecular Spectroscopy* **183**, 234-239 (1997).

[42] **T. W. Dakin, W. E. Good and D. K. Coles**, "Resolution of a Rotantional Line of the OCS Molecule and its Stark Effect," *Physical Review* **70**, 560 (1946).

[43] **M. W. P. Strandberg, T. Wentink Jr and R. L. Kyhl**, "Rotaional Absorption Spectrum of OCS," *Physical Review* **75**, 270 (1949).

[44] **R. G. Shulman and C. H. Townes**, "Molecular Dipole Moments and Stark Effects II. Stark Effects in OCS," *Physical Review* **77**, 500 (1950).

[45] **C. H. Townes, A. N. Holden and F. R. Merritt**, "Microwave Spectra of some Linear XYZ Molecule," *Physical Review* **74**, 1113 (1948).

[46] **D. A. Andrews, F. G. Hurtubise and H. Kraessig**, "The presence of Monothiocarbonate substituents in cellulose xanthates," *Canadian Journal of Chemistry* **38**, 1381 (1960).

[47] **K. Tanaka, H. Ito, K. Harada and T. Tanaka**, "CO2 and CO laser microwave double resonance spectroscopy of OCS: Precise measurement of dipole moment and polarizability anisotropy," *Journal of Chemical Physics* **80**, 5893 (1984).

[48] **B. W. Shore**, *The Theory of Coherent Atomic Excitation*. (Wiley, New York, 1990).

[49] **R. Louden**, *The Quantum Theory of Light*. (2nd ed.) (OUP, Oxford, 1983).

[50] **K. K. Lehmann**, "Microwave detected, microwave-optical double resonance spectra of NO2: A test of Hardwick's ergodicity conjecture," *Journal of Chemical Physics* **83**, 3290 (1985).

[51] **F. Bylicki and H. G. Weber**, "Optical-Radio Frequency Two-Photon Transitions in the Double Resonance Spectrum of NO_2," *Physics Letters A* **82A**, 456 (1981).

[52] **J. C. Petersen, D. A. Ramsey and T. Amando**, "Microwave-Optical Double Resonance in the A^1A_2 Excited State of Thioformaldehyde,," *Chemical Physics Letters* **103**, 266 (1984).

[53] **D. J. Clouthier and D. A. Ramsey**, "The Spectroscopy of Formaldehyde and Thioformaldehyde," *Ann. Rev. Phys. Chem.* **34**, 31 (1983).

[54] **D. A. Ramsey**, "Microwave-Optical Double Resonance and Intermodulated Fluorescence Studies of Thioformaldehdye," *Journal of the Chinese Chemical Society* **44**, 93 (1997).

[55] **J. C. D. Brand and R. Nanes**, "The 3400-3000 Å Absorption of Sulfur Dioxide," *Journal of Molecular Spectroscopy* **46**, 194 (1973).

[56] **A. Kuhn, S. Steuerwald and K. Bergmann**, "Coherent population transfer in NO with pulsed lasers: the consequences of hyperfine structure, Doppler broadening and electromagnetically induced absorption," *European Physical Journal D* **1**, 57-70 (1998).

[57] **K. Bergmann**, *personal communication*

Chapter 9

A mid-infrared probe for EIT experiments

9.1 A Quantum Optical Probe

Chapter 8 examined the possibility of microwave induced transparency in molecules. The molecules we examined had probe transitions predominately in the mid-infrared region of the electromagnetic spectrum. This is generally true for molecules due to their vibrational band structure [1]. To perform any such EIT experiment in a molecular gas we would require a probe field at such wavelengths. But the mere existence of a laser to deliver mid-infrared light is not enough, it must also be single frequency and highly tuneable. A commercial source with these properties is not widely available, and is probably a state of the art device itself with attendant problems, e.g. the cooling to liquid nitrogen temperature of a lead salt laser diode. So it was decided that a new probe source would be built utilising a novel optical parametric oscillator (OPO) design. This allows both a suitable probe for EIT experiments in the mid-infrared and a robust spectroscopic tool to be developed.

In this chapter a brief review of basic OPO theory is presented along with a more detailed account of the type of OPO employed here, the pump-enhanced OPO. Cavity design of such an OPO is covered along with experimental results showing tuning and threshold data. The completed device is notable for a number of reasons. It demonstrates the lowest threshold for a pump-enhanced OPO so far recorded along with the longest coarse tuning range. The smooth tuning in excess of 10GHz in the idler field is also the longest so far reported in the literature for this type of device.

9.2 Optical Parametric Oscillator Basics

An OPO is a nonlinear optical device. At normal, low, light intensities normal media will allow light to pass through with the wavelength unchanged. This is the so-called linear regime, where the polarisation produced by the medium is linearly proportional to the applied electric field, and light of one wavelength is not converted into light of another wavelength. If however the light is very intense, for example from a laser, then the story may be very different. In the linear regime the induced polarisation **P** of a medium subject to an electric field **E** is given by:

$$\mathbf{P} = \varepsilon_0 \chi^{(1)} \mathbf{E} \tag{9.1}$$

where $\chi^{(1)}$ is the linear susceptibility of the medium and as we have seen in equation (2.23) it gives rise to the refractive index and absorptive properties of the medium (as well as the birefringence), i.e.

$$\chi^{(1)} = \chi'^{(1)} + i\chi''^{(1)} \tag{9.2}$$

The real part of the susceptibility is related to the refractive index and the imaginary part to the absorption. In the nonlinear regime where the applied field strength is comparable to the intra-atomic electric field then a linear relationship between **P** and **E** is no longer valid and we must use a power series expansion of the field:

$$\mathbf{P} = \varepsilon_0 \left[\chi^{(1)}\mathbf{E} + \chi^{(2)}\mathbf{E}^2 + \chi^{(3)}\mathbf{E}^3 + \ldots \right] \tag{9.3}$$

where $\chi^{(2)}$ and $\chi^{(3)}$ are the second and third order susceptibilities of the medium. These give rise to nonlinear effects such as second harmonic generation (SHG), sum frequency mixing (SFM) and difference frequency mixing (DFM), which are second order effects, and third harmonic generation (THG), self-phase modulation (SPM) and the Kerr effect, which are third order effects. As the order of the effects increases the magnitude of the effects go down, so it is harder to produce the third harmonic than it is the second harmonic of a particular frequency. It is the effects of the second term in equation (9.3) that will be of interest to us here.

Thus if we have two optical frequencies ω_1 and ω_2 inside a nonlinear medium then we see that the second term in (9.3) yields a polarisation at the sum or difference frequency ω_3

$$\begin{aligned} P_{\omega_3} &= \varepsilon_0 \chi^{(2)} E_1 \cos(\omega_1 t) E_2 \cos(\omega_2 t) \\ &= \frac{1}{2} \varepsilon_0 \chi^{(2)} E_1 E_2 \left[\cos((\omega_1 + \omega_2)t) + \cos((\omega_1 - \omega_2)t) \right] \end{aligned} \tag{9.4}$$

It is such wave mixing processes that are the basis for all nonlinear effects.

The OPO process is one by which higher energy light is changed into light of a lower energy. This implies conservation of energy:

$$\hbar\omega_p = \hbar\omega_s + \hbar\omega_i \tag{9.5}$$

where the subscripts *p*, *s* and *i* stand for pump, signal and idler respectively. Thus the OPO process will take light at the pump energy and change it into light at the lower energies of the signal wavelength and idler wavelength, shown in figure 9.1. The ratio in which the signal and idler wavelengths are generated is governed by momentum conservation (termed the *phase matching conditions*) [2]:

$$k_p n_p = k_s n_s + k_i n_i \tag{9.6}$$

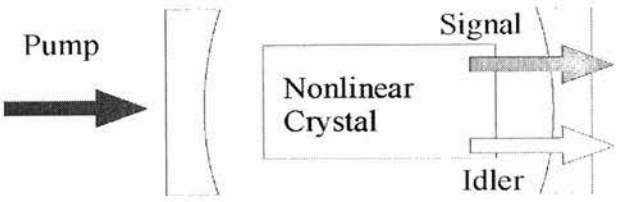

$$\omega_p = \omega_s + \omega_i$$

Figure 9.1: *Basic OPO. A pump field at frequency ω_p is converted via the nonlinear material into two fields of lower frequencies, termed the signal and idler fields.*

However as the light fields propagate through the crystal their differing refractive indices will cause them to move out of phase with each other. The relative phase of the waves will determine the efficiency at which the OPO process (down-conversion from high-energy pump photons to lower energy signal and idler photons) takes place. Through a length of crystal the pump phase will alternatively lead and then lag behind the phase of the other two waves and in doing so will initially down-convert power to the signal and idler but will latterly have power back-converted to the pump. These competing effects determine the gain of the OPO in a single pass. The efficiency of the process is proportional to $\mathrm{sinc}^2(\Delta kL/2)$ where L is the crystal length and $\Delta k = k_p - k_s - k_i$. Hence we require $\Delta k \approx 0$ for high efficiency.

The phase matching conditions can be achieved in a number of ways, namely angle tuning of the crystal, temperature tuning of the crystal and tuning of the pump laser wavelength. Thus it is possible to tune an OPO through a wide wavelength range. More recently however a new method for phase-matching has been demonstrated, that of *quasi-phase-matching* [3]. In this process the phases of the waves can vary along their propagation directions without the back-conversion problem discussed above. This is achieved by periodically flipping the crystal nonlinearity. If the nonlinearity is flipped at the right point i.e. as the pump moves from leading the signal and idler phases to begin to lag them then equation (9.6) need not be satisfied, instead the following equation governs phase-matching:

$$\Delta k - \frac{2\pi m}{\Lambda} = 0 \tag{9.7}$$

where the reversal period is given by Λ and the integer m is called the order of the quasi-phase match process. The reversal period is given by:

$$\Lambda = 2ml_c \tag{9.10}$$

where l_c is the so-called coherence length of the nonlinear crystal and is the distance in the crystal in which the pump phase leads that of the signal and idler fields.

The process ensures that power is always converted from the pump to the signal and idler fields, effectively 're-phasing' the fields after each period reversal. For a given reversal period the

cumulative gain will only be large for a given idler-signal ratio, hence the period must be chosen with a specific wavelength conversion process in mind. Materials that have this periodic structure are called periodically poled materials (the 'poled' part refers to the process by which the materials are manufactured). Hence for instance we refer to periodically poled lithium niobate (PPLN) to describe a lithium niobate crystal that has undergone the poling process.

9.2.1 The Singly Resonant OPO

If a nonlinear crystal is placed within a optical cavity we can create an optical oscillator at the signal or idler frequency provided the parametric gain exceeds the cavity loss. We can design the cavity in a number of ways, either to resonate the signal field creating a singly resonant OPO (SRO), or we can resonate both the signal and idler fields creating doubly resonant OPO (DRO). It is also possible to resonate all three fields, but this is not common, and to resonate the pump and signal fields creating a pump-enhanced OPO, which we deal with below.

The main advantage of a DRO over a SRO is that the threshold of DRO should be far lower than in a SRO, however a price is paid in by the fact that the DRO cavity becomes over-constrained. For instance is it much harder to tune a DRO cavity, as both the signal and idler fields must be kept on resonance for the device to operate.

A recently developed SRO [4] acts as a both as a good illustration as to how an SRO functions but also as a comparative device to the pump-enhanced OPO described below. The SRO cavity geometry is shown in figure 9.2. The device is pumped by a 924nm, 2.5W tuneable diode MOPA (Master-Oscillator Power Amplifier) and has a 1.9W threshold. Pumping at 2.25W produces an idler output (at 2.1μm) of 200mW. The linewidth of the idler is less than 5MHz and the device can be tuned through an impressive 56GHz. The tuning is via pump tuning and is possible as a result of the intracavity etalon clamping the signal frequency. So as the pump field is tuned all the tuning will go into the idler field (as a result of equation (9.5)). This type of behaviour cannot be found in a normal, single cavity, pump-enhanced OPO since if the pump is tuned, the cavity length must be altered to keep the pump field resonant. As we will see this dramatically limits the tuning in such a device.

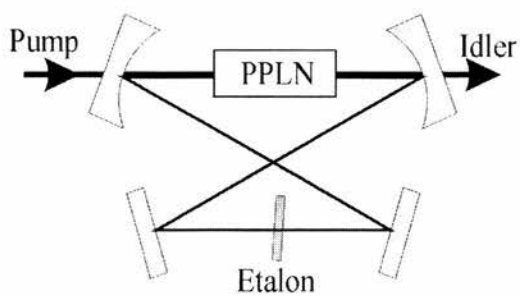

Figure 9.2: *SRO device (Klein et al) capable of producing a widely tuneable idler ~56GHz. The intracavity etalon suppresses the signal field tuning as the pump field is tuned. It is the signal field that is incident on all four mirrors.*

9.3 The Pump-Enhanced OPO

Within a SRO only the signal field is resonated meaning that large pump powers are required to drive the device above resonance. For many OPO applications this may prove to be a problem, for instance field metrology could not be carried out if you required a 5W argon-ion equivalent laser to pump the OPO. This problem may be circumvented by using a DRO-type device, the pump-enhanced OPO [5]. In a pump-enhanced SRO (PE-SRO) both the signal field and the pump field are resonated. This relaxes the constraint that a high power pump must be used as the pump can be resonantly enhanced within the OPO cavity itself to provide a large intracavity pump field. A typical pump-enhanced OPO cavity is shown in figure 9.3.

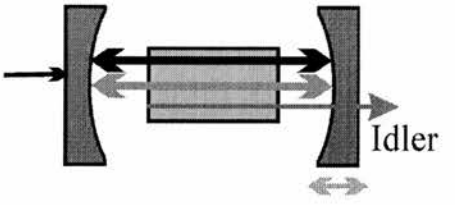

Figure 9.3: *Typical pump-enhanced OPO cavity. The signal and pump fields are resonant within the cavity, while the idler is not (i.e it is single pass).*

We can treat the pump enhanced OPO as shown in figure 9.4 [6].

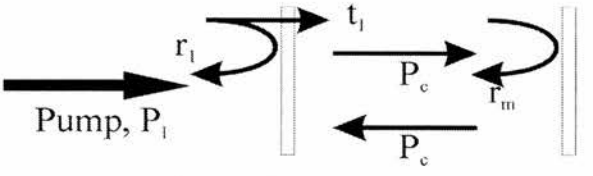

Figure 9.4: *Schematic for a pump-enhanced OPO.*

We assume that all the mirrors, other than the input mirror, can be treated as a single entity with an effective reflectivity r. We also assume that the pump field is constant throughout the cavity (not strictly true since the pump field will be absorbed by the crystal). The input mirror has a reflectivity of r_1 and transmission t_1. The effective transmission of the nonlinear crystal is t but this excludes the nonlinear loss per round trip, which is given by t_{opo}. The dynamic fractional non-linear loss, due to down-conversion is:

$$\eta_{opo} = 1 - t_{opo} \tag{9.11}$$

If we then define:

$$r_m = t t_{opo} r \tag{9.12}$$

Then the resonant pump-enhancement in the cavity is given by:

$$\frac{P_c}{P_I} = \frac{t_1}{\left(1-\sqrt{r_1 r_m}\right)^2} \tag{9.13}$$

where P_c is the circulating intracavity power. Now at and above threshold P_c is clamped at the threshold value given by:

$$OPO_{gain} = OPO_{loss} \tag{9.14}$$

Thus:

$$\kappa P_{cc} = \beta_{opo} \tag{9.15}$$

where P_{cc} is the clamped value of P_c and β_{opo} is the round trip loss of the resonated wave (e.g. the signal) in the OPO. The constant κ is a parameter that depends on the pump focussing and the value of d_{eff} etc. Thus:

$$P_{cc} = \frac{\beta_{opo}}{\kappa} \tag{9.16}$$

In equation (9.13) all the parameters are fixed other than t_{opo} (and hence η_{opo}), the down-conversion influence on the effective transmission. Hence solving (9.13) for t_{opo} gives you the downcoverted power, P_{DC} using:

$$P_{DC} = \eta_{opo} P_{cc} = \left(1 - t_{opo}\right) P_{cc} \tag{9.17}$$

Thus we have the following for the down-converted power:

$$P_{DC} = \frac{\beta_{opo}}{\kappa}\left[1 - \frac{1}{r_1 rt}\left[1 - \sqrt{\frac{t_1 \kappa P_I}{\beta_{opo}}}\right]^2\right] \tag{9.18}$$

Or alternatively:

$$P_{DC} = P_{cc}\left[1 - \frac{1}{r_1 rt}\left[1 - \sqrt{\frac{t_1 P_I}{P_{cc}}}\right]^2\right] \tag{9.19}$$

If we assume a perfect input mirror (one with no transmission loss):

$$r_1 + t_1 = 1 \tag{9.20}$$

and then evaluate:

$$\frac{\partial P_{DC}}{\partial r_1} = 0 \tag{9.21}$$

to determine the optimum down-conversion and optimum mirror transmission to achieve such a down-conversion. This gives:

$$t_1^{opt} = \frac{\kappa P_I}{\beta_{opo}} = \frac{P_I}{P_{cc}} \tag{9.22}$$

under which condition:

$$P_{DC}^{opt} = P_{cc}\left[1 - \frac{1}{rt}\left[1 - \frac{P_I}{P_{cc}}\right]\right] \tag{9.23}$$

Hence we see that under the condition rt=1 the optimum down-converted power equals the pump input power, i.e. 100% down-conversion (idler+signal). This condition imples that there is no parasitic loss from of the pump field from the cavity. Real systems will have these losses, so a more realistic value of rt is one where rt<1. Also note that for equation (9.23), P_{cc} should be calculated from equation (9.16), in terms of the OPO parameters κ and β_{opo}.

We can also express the down-converted power (and more specifically the down-converted idler power) in terms of t_1 and other cavity losses, which we denote, for the moment, as V. We use equation (9.13) to find the value of P_{cc} and writing $r_1 = 1-t_1$ and $r_m = 1-V$ and substitute these values into equation (9.23) to find:

$$P_{DC(i)} = \frac{\lambda_p}{\lambda_i}\frac{t_1 P_{th}}{\left(1-\sqrt{(1-t_1)(1-V)}\right)^2}\left[1 - \frac{1}{(1-t_1)(1-V)}\left[1 - \sqrt{\frac{P_I}{P_{th}}}\left(1-\sqrt{(1-t_1)(1-V)}\right)\right]^2\right] \tag{9.24}$$

where the value P_{th} is the external pump threshold. Note the value V is calculated assuming the OPO cavity is operating below threshold, in which case $t_{opo}=1$ and hence $r_m=rt$. The factor λ_p/λ_i is to calculate the fraction of the down-converted power in the idler field. The value of V can be calculated by a measurement of the cavity finesse, hence knowing t_1:

$$V = \frac{2\pi}{\Im} - t_1 \tag{9.25}$$

where $\Im$ is the cavity finesse. So assuming that t_1=5% and V=0.2% we can plot the expected idler power as a function of input power for a measured threshold value of 35mW. We assume a pump wavelength of 820nm and an idler wavelength of 2.85μm. This is shown in figure 9.5.

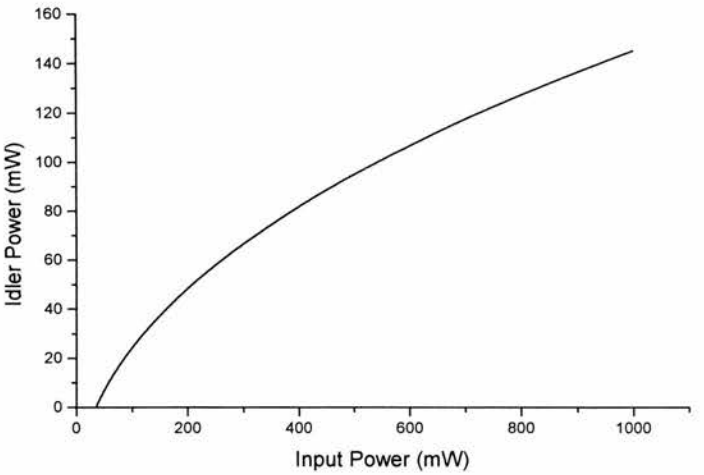

Figure 9.5: *Down-converted idler output power as a function of input pump power. Input mirror transmission is 5%, other cavity losses are 0.8% and OPO threshold is 35mW.*

9.3.1 Tuning Limitations in PE-OPOs

As mentioned above the single cavity pump enhanced OPO suffers from tuning limitations. The problem is the way in which the signal field tunes with the pump field. The signal and idler tuning relations are given by:

$$\Delta\upsilon_s = \frac{\upsilon_s}{\upsilon_p}\Delta\upsilon_p \tag{9.26a}$$

$$\Delta\upsilon_i = \frac{\upsilon i}{\upsilon_p}\Delta\upsilon_p \tag{9.26b}$$

This holds in the absence of mode-hops. We can therefore say that if the centre of the phase-match bandwidth is independent of the pump tuning then we expect a mode-hop of the signal if

$$\left|\frac{\upsilon_s}{\upsilon_p}\Delta\upsilon_p\right| \geq FSR \tag{9.27}$$

where FSR is the free spectral range of the signal cavity. Hence the tuning range of the idler field is given by:

$$\Delta\upsilon_i = \frac{\upsilon_i}{\upsilon_s} \times FSR \tag{9.28}$$

In fact the situation is somewhat worse than this as the phase-match bandwidth does in fact tune with pump frequency, governed by:

$$\Delta\upsilon_s = \frac{\partial\upsilon_s}{\partial\upsilon_p}\Delta\upsilon_p \tag{9.29}$$

where $\partial\upsilon_s/\partial\upsilon_p$ is calculated from:

$$n_p\upsilon_p = n_s\upsilon_s + n_i(\upsilon_p - \upsilon_s) + c/\Lambda \tag{9.30}$$

which is a modified form of equation (9.7). So the condition for observing a mode-hop is now:

$$\left|\left(\frac{\upsilon_s}{\upsilon_p} - \frac{\partial\upsilon_s}{\partial\upsilon_p}\Delta\upsilon_p\right)\right| \geq FSR \tag{9.31}$$

The term in brackets is generally non-zero, as illustrated in figure 9.6, and hence several mode-hops occur in the signal as the pump is scanned through one FSR.

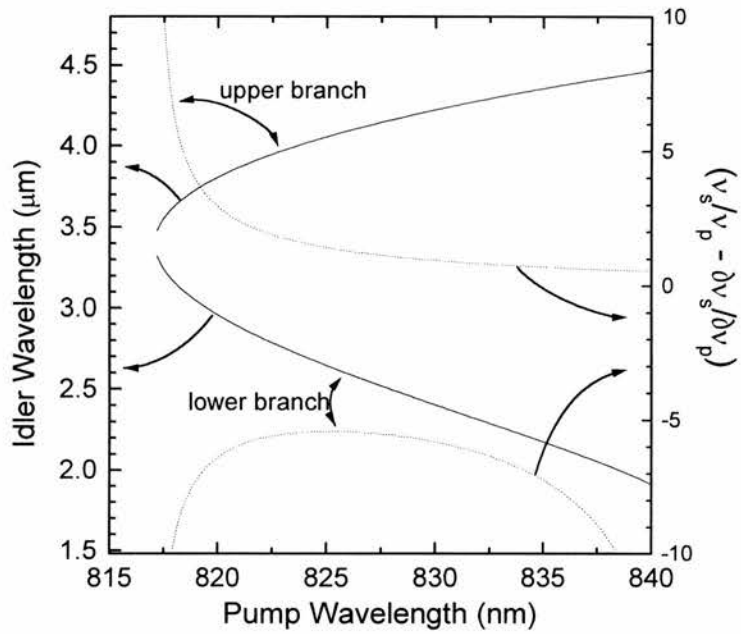

Figure 9.6: *Predicted idler tuning rate and signal mode-hop rate (right-hand axis) from equation (9.31) for PPLN with a grating period of Λ=22.0μm and a temperature of 150°C*

This behaviour is shown in figure 9.7. For the purpose of this example we assume that the ratio $\upsilon_p : \upsilon_s : \upsilon_i = 3:2:1$ and that we are working in a region where the phase-match bandwidth tunes though twice the value of the pump tuning and in the opposite direction, i.e. the RHS of (9.29) is equal to $2\,\Delta\upsilon_p$. In this case if the signal field tunes through 2/8 of the pump FSR then the pump will have moved through 3/8 of the pump FSR, from (9.26a) and the idler moves through 1/8 of the pump FSR. The phase-match bandwidth then moves through 6/8 of a pump FSR. Putting these numbers into (9.27) we see that the mode-hop condition is satisfied and therefore the signal field mode-hops. It mode hops in the opposite direction to that of the pump so as to track the peak

of the phase-match bandwidth. This process then repeats. The idler meanwhile will mode-hop when the signal mode-hops. If the tuning in this situation is smooth what we have is essentially a systematic, 'snapshot' tuneability. We not, however, have a smooth tuneable light source. In fact in can be seen that in the single cavity device, the signal cannot tune more than the FSR of the pump cavity. This therefore imposes a severe limitation on the single cavity's usefulness as a spectroscopic source.

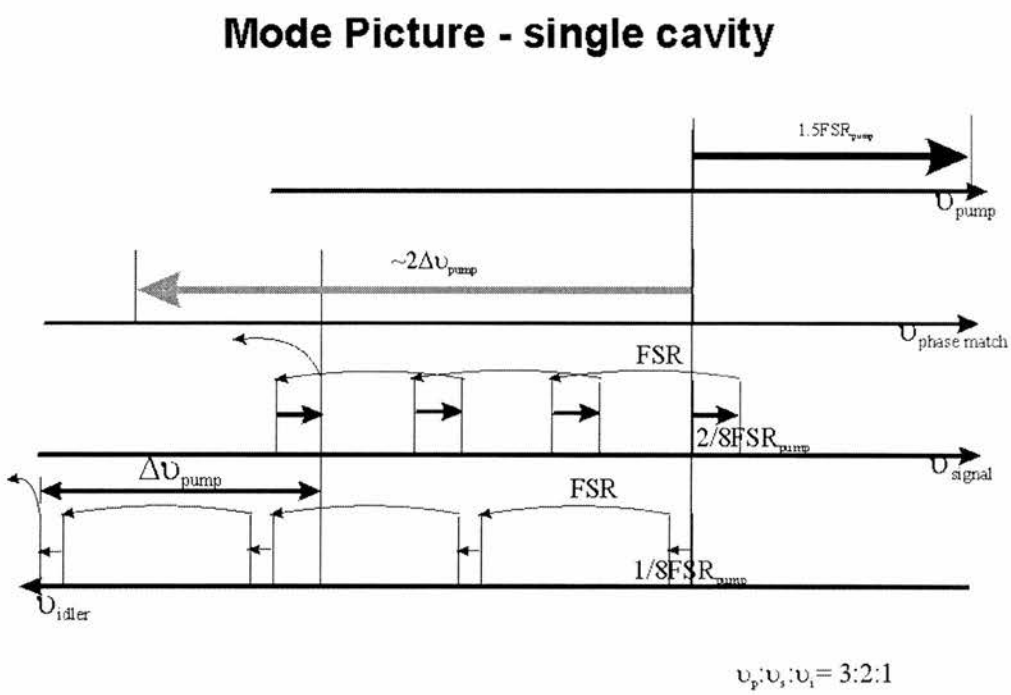

Figure 9.7: *Mode picture in the single cavity case. The smoothing tuning of the pump results the tuning of the signal field of only a fraction of the pump free spectral range before a mode-hop occurs. The peak of the phase-match bandwidth moves in the opposite direction to that of the pump and signal. Note that the idler axis is drawn in an opposite sense to that of the other axes, hence it too moves in the same direction of as the signal.*

We can however solve such problems by moving to a split cavity geometry, shown in figure 9.8. We consider two different tuning schemes. The first, which will be experimentally demonstrated in section 9.4, achieves extended tuning over the single cavity OPO by clamping the tuning of the signal by use of an intracavity etalon. The signal resonating in its own cavity allows the pump and signal fields to be controlled independently. Hence in this case, $\Delta\nu_s=0$ and therefore $\Delta\nu_i=\Delta\nu_p$. This situation is shown in figure 9.9. Immediately we see that our tuning range limitation is lifted. Potentially, using the Microlase Ti:Sapphire as a pump source, we have a idler field that is tuneable over a 40GHz range.

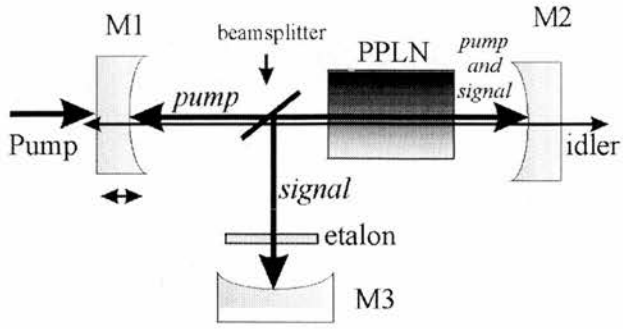

Figure 9.8: *Pump-enhanced OPO, split cavity design. The pump and signal cavities can be independently controlled.*

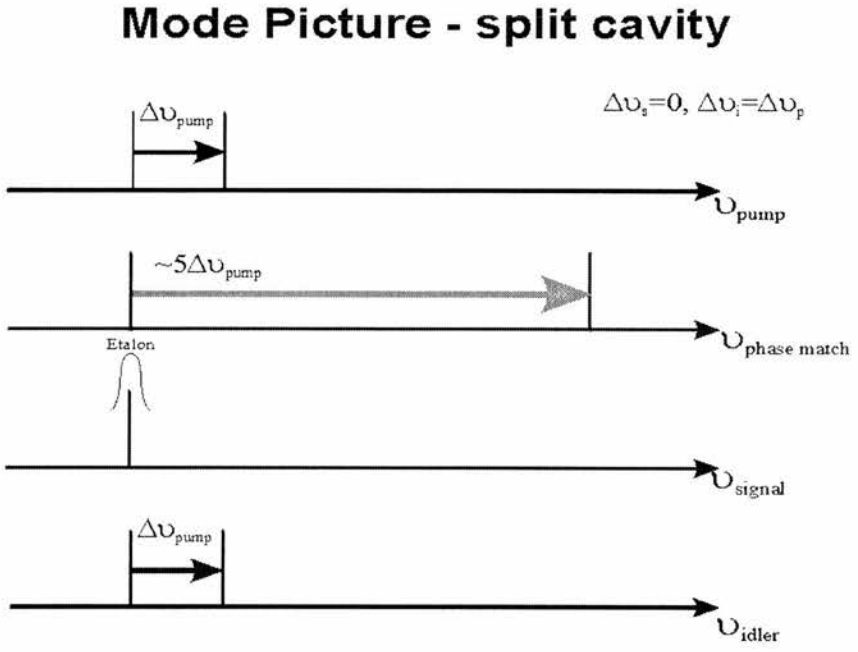

Figure 9.9: *Cavity mode-picture in the split-cavity case with an etalon in the signal cavity to suppress signal mode-hops. In this case the suppression of the signal field means that all the pump tuning is transferred to the idler.*

The second method of tuning is even more promising. As we have seen from figure 9.6, the peak of the phase-match bandwidth moves with pump tuning, but what if we make the signal field track this peak? In this case the idler tuning is given by:

$$\Delta\upsilon_i = \left(1 - \frac{\partial\upsilon_s}{\partial\upsilon_p}\right)\Delta\upsilon_p \tag{9.32}$$

This can be significantly larger than the pump field tuning, as envisaged in figure 9.10, and could offer idler tuning ranges of >100GHz without a mode-hop. Also, this allows the use of pump sources with small tuning ranges to produce large idler tuning ranges, which has the added benefit of relaxing constraints on the pump source itself. We also note that since the peak of the phase-match bandwidth can move a long way (in the case shown in figure 9.10, 5 times the

distance that the pump tunes) and we make the signal field track this, if we can extract some of the signal we may have a useful near-infrared tuneable source as well.

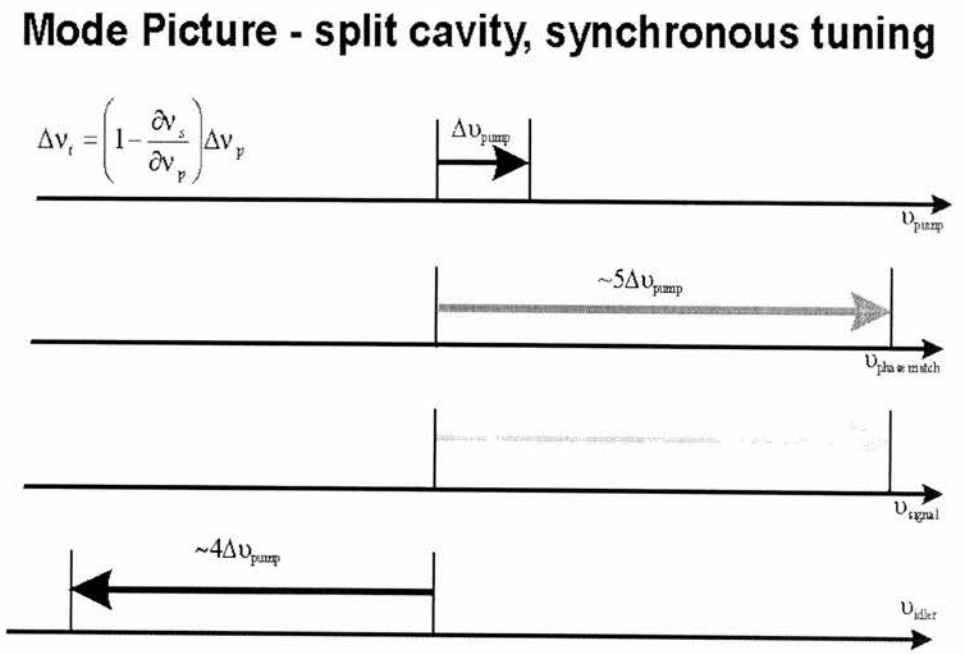

Figure 9.10: *Mode picture in the pump-enhanced OPO with a split cavity and synchronous tuning. The signal cavity is tuned to track the peak of the phase-match bandwidth, hence a small amount of pump tuning can result in a large amount of idler tuning.*

By using either of these tuning schemes we can overcome the intrinsic tuning limitations of a single cavity PE-OPO. Indeed we can significantly enhance the tuning ranges we observe and in doing so move the device in a regime where it becomes genuinely useful as a spectroscopic and quantum optical probe source.

9.4 Experimental Cavity Geometries

The two experimental cavities under study are shown in figure 9.11. We examine the properties of the single cavity device to allow us to compare and contrast with the dual cavity OPO. The device is pumped at around 820nm and this corresponds to a signal field around 1.1μm. In the dual cavity device the pump and signal fields resonate with separate cavities which are separated using a dichroic beamsplitter.

Mirror M1, the input mirror, was coated to give 5% transmission for the pump, to be highly reflecting (HR>99.7%) for the signal and highly transmitting to idler wavelengths near 3μm (HT>95%). The back mirror, M2, was coated to be HR (>99.8%) for both the pump and signal wavelengths and HT (>99%) for the idler. In the dual cavity device the beam-splitter was HR (>99.7%) at the signal and HT at the pump (>99.5%) and idler (>95%). The other signal cavity mirror, M3, was coated to be HR (>99.7%) at the signal and HT (>90%) at the pump. Mirror M2 has a radius of curvature of 25mm and M1 and M3 have radii of curvature 50mm and 75mm

respectively. Each cavity was arranged to give roughly confocal focussing in the 19mm long PPLN crystal.

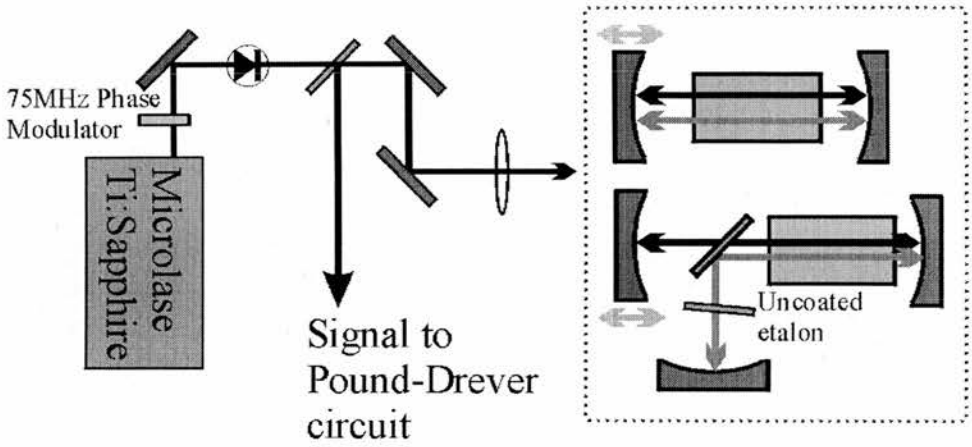

Figure 9.11: *Experimental set-up showing the two cavity configurations under consideration, the single cavity and dual cavity devices.*

The PPLN crystal itself has eight poled grating periods ranging from Λ=21.0μm to 22.4μm in 0.2μm steps. The two end facets of the crystal, through which the pump field enters and exits, were antireflection coated for the pump, signal and idler fields. The residual reflectivities were <0.2% at 820nm, <0.2% at 1100nm and <0.5% at the idler wavelength of 3μm. The crystal was heated to above 130°C to avoid photorefractive damage in a servo-controlled oven. The phase-matching curve for PPLN, for the 22.0μm grating at 150°C is shown in figure 9.12. We can now more clearly see how the value of $\partial\upsilon_s/\partial\upsilon_p$ can affect the tuning of the dual cavity OPO. At 820nm:

$$\frac{\partial\upsilon_s}{\partial\upsilon_p} = 6.5 \text{ or } \frac{\partial\upsilon_s}{\partial\upsilon_p} = -2 \tag{9.33}$$

and hence we can now see how such large tuning ranges are possible in the dual cavity device.

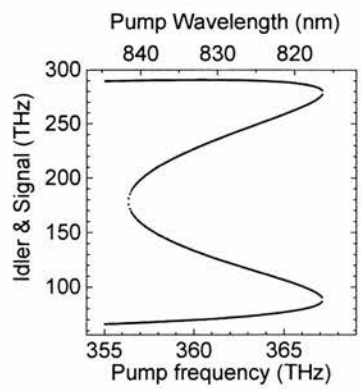

Figure 9.12: *Phase matching curve for grating period, Λ=22μm at 150°C in PPLN.*

We can estimate the pump cavity enhancement using equation (9.13) where t_1 is the transmission of the input coupler and is equal to $1-r_1$, V takes into account other cavity losses and can be calculated from equation (9.25). V is equal to $1-r_m$. For the single-cavity OPO we estimated a pump-enhancement factor of ~55, while for the dual cavity OPO the enhancement was ~45.

The enhancement cavities are kept on resonance by a Pound-Drever-Hall [7, 8] method, with a phase modulation of 75MHz.

9.5 Experimental Results.

As mentioned above it is possible to tune the OPO via a combination of pump wavelength tuning, crystal temperature variation and changing the crystal grating period. In figure 9.13 the idler tuning as a function of crystal temperature is plotted for each grating period, both for a pump wavelength of 820nm and 850nm. The solid lines indicate the theoretical values we would expect based on the appropriate Sellmeier relations [9]. The idler was produced in two separate ranges of 2.71μm to 3.26μm and from 4.07μm to 5.26μm. At wavelengths greater than about 4.5μm experience strong absorption in the PPLN crystal and as such the OPO performance at such wavelengths was quite poor. The corresponding signal tuning range was 1.01μm to 1.18μm, which was limited by the coating bandwidths of the PPLN crystal. The dual cavity OPO did not operate in the long idler wavelength region due to extra cavity losses introduced by the beamsplitter.

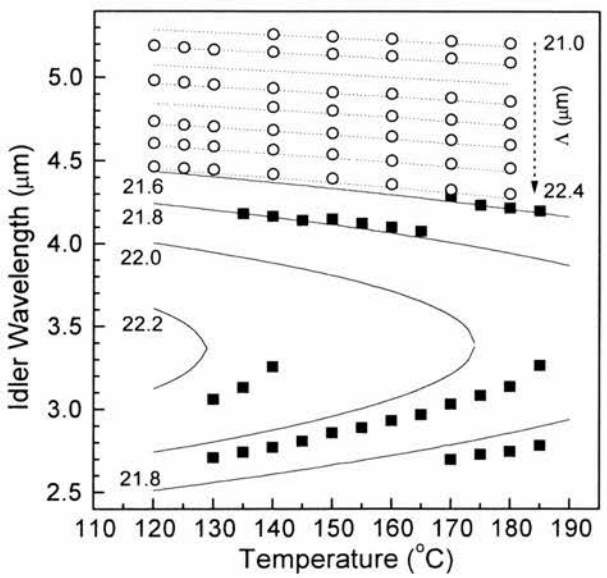

Figure 9.13: *Idler tuning as a function of crystal temperature. The dotted lines and circles are for λ_p = 850nm and the squares and solid line for λ_p = 820nm. The grating period is given by the figures on the right of the top set of curves and the left of the bottom set.*

In the single cavity OPO we measured a lower threshold of ~35mW at an idler wavelength of 3μm. Over the range of the idler tuning the threshold was typically near 100mW, except for long idler wavelengths, >4μm, where the threshold rose up to ~500mW at 5μm. This is mainly due to increasing losses at the corresponding signal wavelengths. If we take these losses into account by dividing the measured threshold by the signal cavity loss then we find that the threshold is more constant, with the threshold rising by a factor of ~2 at 5μm. This is in good agreement with a previous theoretical study of cw PPLN SROs in the presence of strong idler absorption [10]. These results are plotted in figure 9.14. Thresholds in the dual cavity are higher than in the single cavity OPO due to increased signal and pump cavity losses, with a minimum threshold of 100mW for a pump wavelength of 820nm and an idler wavelength of 2.85μm.

At a maximum pump power of 750mW with a 3μm idler, a one-way idler power of 16mW was measured. Taking into account the 35% transmission loss of the output coupler at 3μm this corresponds to a total downconverted power of 180mW.

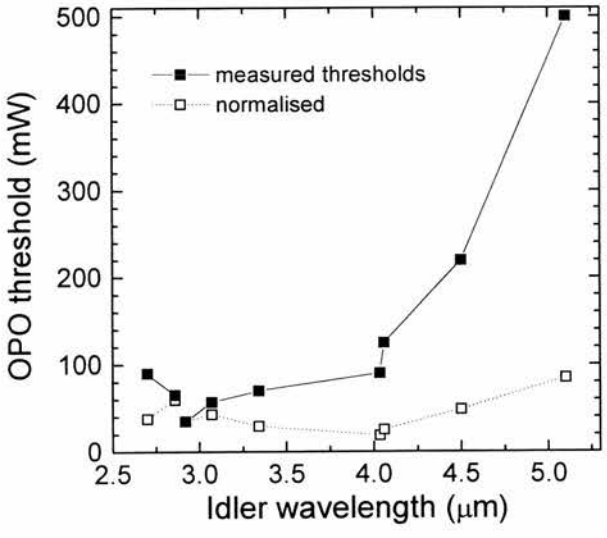

Figurer 9.14: *Measured thresholds for a range of idler wavelengths (solid line). The dashed lines are calculated thresholds with signal cavity losses taken into account.*

To control the mode-hopping in the dual cavity device an uncoated solid etalon of 115GHz FSR was placed in the signal cavity. As the pump laser was tuned the signal field was monitored using a scanning confocal interferometer of 10GHz FSR and finesse ~200 at 1150nm. The idler field was monitored on a Michelson interferometer of 1.8GHz FSR. The fields were monitored to ensure mode-hop free operation with pump tuning. The output trace from the Michelson interferometer is shown in figure 9.15, as a function of enhancement cavity length, as the pump is tuned through 12.3GHz. Within this range it can be seen that the idler tunes smoothly over a period of 10.8GHz without a mode-hop. In contrast with the dual cavity OPO, the single cavity device would suffer 5 or 6 mode-hops with a pump tuning range of just 2GHz, which agrees well

with the calculated value of seven mode-hops from equation (9.16). When the pump was tuned through 10.8GHz the peak of the gain-bandwidth was separated by ~70GHz (55 signal cavity FSR's) from the resonant signal field without suffering a mode-hop (this is summarised in table 9.1). Hence we demonstrate that the dual cavity approach is by far the more versatile approach.

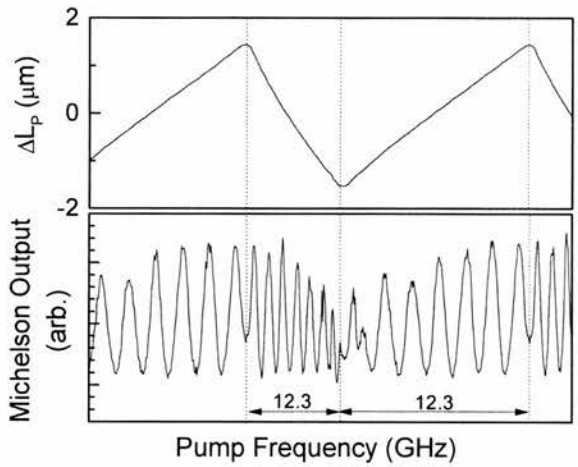

Figure 9.15: *The top trace shows the piezo extension with frequency while the bottom shows the Michelson interferometer output. A slight mode-hop is visible at the beginning of the 12.3GHz pump tuning, hence the idler smoothly tunes through 10.8GHz.*

	Pump	Signal	Idler
λ(nm)	820	1150	2858
FSR (GHz)	1.6	1.3	-
Δν (GHz)	10.8	0	10.8
$\frac{\partial \nu_s}{\partial \nu_p}\Delta\nu_p$	$\approx 70\,\mathrm{GHz} \equiv 55\,\mathrm{FSR_{sig}}$		

Table 9.1: *Summary of PE-OPO tuning characteristics. The FSR range row indicates the FSR of the pump or signal cavity and Δν is the observed tuning range.*

9.6 Ongoing Work

The work in this area is on-going. One of the aims is to produce a pump-enhanced OPO that is able to be pumped by a diode. Recently this has been demonstrated by Lindsey *et al* [11]. As our device has shown the low thresholds of the single cavity device make diode pumping eminently feasible and pumping with a tuneable grating stabilised diode offers the tuning we require for spectroscopic purposes. However the increase in threshold in moving to the dual cavity device makes pumping with these tuneable lasers much more difficult as they only operate at low powers ~70mW. Even with a longer crystal, thresholds are still too high to realistically pump with anything other than a solid state laser. We can potentially reduce the cavity threshold in the dual cavity device by moving to an inline cavity geometry (figure 9.16), in which the signal

cavity sits within the pump cavity. This removes some of the cavity loss by removing the need to have an intracavity beam-splitter. The current goal is to demonstrate a Ti:Sapphire pumped inline synchronously tuned PE-OPO with a view to building a similar diode pumped device.

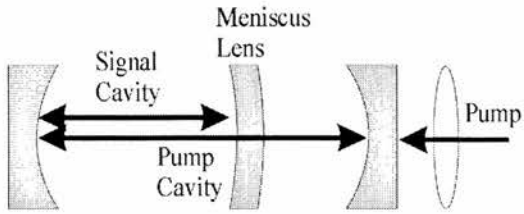

Figure 9.16: *Inline pump-enhanced OPO cavity. The signal cavity is placed within the pump cavity to reduce cavity losses. The removal of one component, in comparison to the dual cavity device, means a reduction in external threshold. Tuning is achieved either by use of an intracavity etalon (not shown) or by simultaneous tuning of both cavities.*

9.7 Conclusions

In this chapter a pump-enhanced optical parametric oscillator capable of over 10GHz of continuous tuning has been developed. At 2.85μm this corresponds to around 30 times the tuning possible in a normal single cavity device [12]. Our OPO also has very low thresholds, a wide idler wavelength coverage and single frequency operation, making it a suitable source for spectroscopy and quantum optics experiments. We have further given an introduction to the pump-enhanced OPO and shown how its tuning range is limited in the single cavity geometry and how the tuning range can be extended by moving to a split cavity device in which the signal field is able to be independently controlled from the pump field.

References

[1] **G. Herzberg**, *Infrared and Raman Spectra.* (Van Nostrand Reinhold Company, New York, 1945).

[2] **J. A. Giordmaine**, "Mixing of light beams in crystals," *Physical Review Letters* **8**, 19-20 (1962).

[3] **M. M. Fejer, G. A. Magel, D. H. Jundt and R. L. Byer**, "Quasi-Phase-Matched Second Harmonic Generation: Tuning and Tolerances," *IEEE Journal of Quantum Electronics* **QE-28**, 2631 (1992).

[4] **M. E. Klein, C. K. Laue, D. H. Lee, K. J. Boller and R. Wallenstein**, "Diode-pumped singly resonant continuous-wave optical parametric oscillator with wide continuous tuning of the near-infrared idler wave," *Optics Letters* **25**, 490-492 (2000).

[5] **G. Robertson, M. J. Padgett and M. H. Dunn**, "Continuous-Wave Singly Resonant Pump-Enhanced Type-Ii Lib3o5 Optical Parametric Oscillator," *Optics Letters* **19**, 1735-1737 (1994).

[6] **M. H. Dunn and M. Ebrahimzadeh**, *Optical Parametric Oscillators.* in *Advances in Lasers and Applications* D. M. Findlayson and B. D. Sinclair, Eds. (IOP Publishing, Bristol, 1999), vol. 52, pp. 61-82.

[7] **R. W. P. Drever**, "Laser Phase and Frequency Stabilisation using an Optical Resonator," *Applied Physics B-Lasers and Optics* **31**, 97 (1983).

[8] **R. V. Pound**, "Electronic Frequency Stabilisation of Microwave Oscillation," *Review of Scientific Instruments* **17**, 490 (1946).

[9] **D. H. Jundt**, "Temperature-dependent Sellmeier equation for the index of refraction ne in congruent lithium niobate," *Optics Letters* **22**, 1553 (1997).

[10] **D. D. Lowenthal**, "CW periodically poled LiNbO3 optical parametric oscillator model with strong idler absorption," *IEEE Journal of Quantum Electronics* **34**, 1356-1366 (1998).

[11] **I. D. Lindsay, C. Petridis, M. Ebrahimzadeh and M. H. Dunn**, *personal communication* (2000).

[12] **K. Schneider, P. Kramper, S. Schiller and J. Mlynek**, "Toward an optical synthesizer: a single-frequency parametric oscillator using periodically-poled LiNbO3," *Optics Letters* **22**, 1293 (1997).

Chapter 10

Conclusions and Further Work

10.1 Conclusions

The overall theme of this work has been to investigate how EIT is affected by either changing the fields involved (probe or coupling) in some way, or by introducing new fields to perturb the existing EIT conditions in some fashion. In changing the fields we have explored the consequences of the probe and coupling fields having different wavelengths (chapter 3), have taken this to the limit of having a microwave coupling field (chapter 8), and have looked at the role of polarisation (chapter 5) and laser linewidths (chapter 4). Power requirements associated with microwave-induced EIT have led us to evaluate the possibility of EIT in molecules and hence develop an OPO, that remains the best in the world of its type (longest tuning range), with scope for development (chapter 9). With regard to the perturbation of EIT resonances we have paid particular attention to how non-optical fields affect EIT and have shown that rf can be used to yield a number of interesting manipulative effects on EIT resonances (chapters 6 and 7).

In chapter 3 we investigated the effect of having probe and coupling fields with differing wavelengths, a situation we refer to as the mismatched wavelength case. We firstly looked at a comparison of the amount of EIT we observe in each of the 3 level systems, with Doppler broadening included [1]. We found that in the case of interest for inversionless lasing, i.e. that of a shorter probe wavelength than coupling field wavelength, the Vee-scheme offered the best EIT. This is due to the nature of the two photon process in the Vee scheme, which is instrumental in EIT and is weaker in the Vee-scheme than in the lambda and cascade schemes. This fact means that, in the Doppler broadened regime, Autler-Townes components of high velocity group atoms that would normally (in the cascade and lambda systems) act to mask EIT on resonance do not obscure the EIT. The Vee-scheme therefore has a natural advantage over its other two counterparts.

Then assuming this Vee-scheme advantage we examined the possibility of achieving inversionless gain in a Doppler-broadened mismatched system [2]. We found that gains of up to 8% were attainable in such systems (using atomic parameters based on rubidium), which should be great enough to observe inversionless lasing. Hence we predict that the EIT observed by Boon *et al* [3] is an indicator that gain may be observed on the $5S_{1/2} - 6P_{1/2}$ 422nm line in rubidium controlled by a 780nm coupling field.

In chapter 4 we examined what effect introducing lasers with finite linewidths had on EIT in a Vee-scheme. We found that the coupling and probe fields can have linewidths greater than the

homogenous linewidth of the probe transition with EIT still visible. In the main the observation of EIT was dependent on the coupling field Rabi frequency. So long as this was large enough, the 'washing out' effect that an increased linewidth would cause can be circumvented. The fact that what are almost incoherent fields can be used in the observation of EIT indicates that we may be able to use truly incoherent fields to observe EIT, which would be particularly useful for EIT experiments where there are no laser sources to act as a probe field. We have briefly described an atomic beam experiment, in which the probe field would be in the X-ray regime (50nm), which could make use of this fact.

We have also investigated the possibility of observing inversionless gain in a system with finite linewidths. We have shown the observation of inversionless gain is dependent on the strength of the coupling field Rabi frequency. A larger coupling field should be enough to offset any increase in coupling field linewidth.

The effect that laser polarisation has on the strength of EIT was investigated in chapter 5. By examining the nature of the two-photon process in determining the magnitude of the EIT we can predict the relative heights of the EIT peaks in our experiment [4]. We also see that there are preferred polarisation orientations for the observation of EIT and that these directly determine the two photon probabilities for reaching the upper coupling field level (in the considered cascade scheme). We find that having the probe and coupling fields with the same circular polarisation (as experienced by atoms in the cell) leads to the greatest amount of EIT.

We then further examine two-photon effects in a four level Vee-scheme and show that two-photon absorption can be inhibited in such a scheme via a strong control field. This inhibition is due to interference between dressed states, as shown in section 5.7.3.1. Further examination of this four level system shows that by doubly driving the probe transition with two strong fields multiple dark regions can be produced. These multi dark states can be used to engineer atomic responses [5]. Again by considering the system in the dressed state basis (and via Autler-Townes splittings) we can see that the system properties are due to the interplay between the splitting of the upper probe level and the splitting of the lower probe level. Since these can be independently controlled, via the two control lasers, the system can be made to display a number of potentially useful effects. Also it should be relatively simple to find an atomic system to experimentally verify our predictions, indeed we propose a system found in atomic rubidium. The main problem in such an experiment would be optical pumping due to the strong field resonant with a ground state transition.

The control of optical fields by rf fields is seriously considered in chapters 6, 7 and 8. In chapter 6 we investigate how rf fields may be used to destroy EIT in multilevel cascade schemes [6]. We find that ladder schemes with an even number of states which have N-1 applied fields will display absorption on line centre. Systems with an odd number of levels and N-1 fields, however, will display EIT on line centre. If, for instance, we consider a 4 level system then we would

expect to see two-dark states either side of an on-resonance absorption. Hence, the EIT on line centre is destroyed by a three photon interference effect. If we take the upper transition in this four level scheme to be an rf field then we can conceivably control the optical field properties with an rf field. An example of such a phenomena would be a rf controlled optical lens. How such a scheme would work, taking advantage of electromagnetically induced focussing [7], is shown in section 6.3.2. We also investigate how EIT in multi-ladder schemes affects the refractive index of such a medium. We show that such media display areas of higher dispersion than normal EIT and so may be useful in the production of slow light [8] and applications of phaseonium [5, 9].

In chapter 7 we experimentally show how some of the rf-induced effects discussed in chapter 6 can be realised experimentally. We perform an experiment in rubidium in which a rf field is coupled into one of the hyperfine transitions of the upper coupling field level. It is found that the EIT resonances are manipulated by the rf field, i.e. they are partially destroyed. These experiments will require further work to show definitive results. Suggestions for how this may be achieved are outlined in section 10.2 below.

Chapter 8 is a brief overview of why microwave induced transparency is 'hard'. We find that since the appropriate transitions in atoms for coupling via a microwave field are magnetic dipole transitions, and hence very weak, large amounts of microwave power are required to induce any significant transparency [10]. Thus these types of experiments are impractical. If the transitions were electric dipole allowed then experiments may be practical but to find such transitions we would have to move to molecules. The difficulties of observing EIT in molecules are numerous and make an MIT experiment feasible, but difficult. We outline a number of potential molecules that could be used for such an experiment, including formaldehyde and ammonia.

Since molecules, by and large, have numerous transitions in the mid-infrared and rather less in the optical regime, in order to perform such an MIT experiment one would require a mid-infrared source suitable for quantum optical experiments. The development of such a source, a pump-enhanced optical parameter oscillator was outlined in chapter 9. This OPO was narrow linewidth, frequency stable, low threshold (~30mW), widely tunable (2.71 to 3.26μm and 4.07 to 5.26μm) and finely tuneable (~12GHz) [11]. The OPO employed a novel dual cavity device, based on PPLN, to provide the fine tuning and as such is a state of the art OPO which should be suitable as a EIT probe field. At time of writing this device is undergoing further development.

The work described above has, in context, addressed some outstanding issues in the EIT literature, namely the viability of MIT in gaseous atomic systems and the role of polarisation in EIT experiments. We have further advanced knowledge in the field in our explorations of multilevel cascade schemes, the role of rf induced EIT effects in rubidium and the nature of EIT in wavelength mismatched situations.

10.2 Future Work

So where will we go tomorrow? A number of interesting avenues open up on consideration of the work covered here. Firstly based on the work in chapter 3, it should be possible to design a proof of principle blue inversionless laser. In order to achieve this we would have to develop a incoherent pump source. De Jong *et al* [12] have reported seeing inversionless gain on this line, although their results still seem to be a little dubious, but our modelling predicts that AWI is possible and that enough gain should be achievable to observe LWI. This would be a interesting and significant experiment.

Leading from the work in chapter 4, in which we propose EIT with incoherent sources, we could look in the first instance to use a incoherent probe source at 780nm to observe EIT. We could then look to the double atomic beam-type experiment outlined in section 4.3.

The work on rf control of optical fields has obvious potential for further improvement. With a view to producing a rf controlled optical lens, the theory behind the 6 level system with 3 applied fields requires improvement, which would then allow the experiment to be improved. If we could see near complete destruction of EIT on a given peak, we could potentially build an ultra finely controlled optical lens, based on EIF. We could look to produce multi-dark states in rubidium and explore their properties, or go one step beyond what we have considered in detail here and produce phaseonium type material, and begin a detailed study of the refractive index properties of such media. It is in the refractive index properties of these media that current interest lies. The dispersion evident in systems with multi-dark states could lead to improved production of slow light, or allow slower light to be produced more easily. It may also be of interest in the production of anomalous dispersion regions capable of allowing negative group velocities [13].

A MIT experiment in molecules is possible but would require further consideration. To carry out such an experiment is a long undertaking (probably a PhD in itself) and would produce work that was ground breaking but not necessarily work that would lead to new avenues of research. That's not to say that EIT in molecules is a uninteresting area of study. Harris' group has discussed possible sub-femtosecond pulse production via EIT effects in molecules [14-16] and so EIT in molecules (without the microwaves) may provide interesting future research directions. Overall one of the significant things to come from this work and the general work in the field over the past few years is the fact that we (the EIT community as a whole) are beginning to examine the properties of multilevel systems. These can yield a number of interesting properties, including the multi-dark states, high dispersion regions, linewidth narrowing effects and two-photon inhibition effects that we have discussed here among others. Further consideration of the properties of such systems is a definite area of future research.

To conclude this thesis, allow me to digress a little. As the last PhD student in the EIT group for the time being I would like to paint a slightly more ambitious picture of the research that could be

carried out here in the years ahead should work in this field continue. The biggest area of interest in the field at the moment is probably slow light. A number of theoretical proposals about the properties of slow light are already published, with no doubt more to follow. The verification of some of these properties could be one aim, as could the prediction of further properties. Slow light is however best achieved in an atom trap (no Doppler broadening and other advantages [17]) or BEC (Bose-Einstein Condensate). So one would need one of them!

Perhaps the most exciting proposal related to EIT in recent times is the potential production of an optical black hole [18]. This proposal is again a very difficult experiment to carry out, but has potentially ground breaking consequences, namely the study of black holes in the lab. Production of such black hole would be science on the same level as the production of a Bose-Einstein condensate, in my opinion. Work toward such an experiment would no doubt produce very interesting science in its own right, both theoretically and experimentally. For instance, an initial experiment could be to explore the drag that a moving gas has on light interacting with it. Other work in this area could include how Laguerre-Gaussian beams behave in EIT experiments and the production of optical vortices in gas cells. Also explorations of Aharonov-Bohm type experiments using EIT and the probing of new types of forces on atoms [19] could be a spin off experiment. A very recent experiment by Turukhin *et al* [20]in which slow light has been observed in a solid for the first time opens a further realistic possibility of observing an optical black hole. Since an effective vortex can be created within a solid by rotating it, solids seem a natural medium for this type of experiment. But to observe EIT in solids they have to be cooled, to near liquid helium temperatures, so the step from slow light to optical black hole is not an easy one.

Given the time and money, the black hole experiment is the one I would go for. I am sure even if it was not feasible experimentally that it would generate lots of new experimental and theoretical work that would be both relevant and exciting.

Maybe, one day, I will be witness to an optical black hole sitting in a little bunch of rubidium atoms sitting on my old optical table. The challenge is laid, to those that follow.

References

[1] **J. R. Boon, E. Zekou, D. McGloin and M. H. Dunn**, "Comparison of wavelength dependence in cascade-, Lambda-, and Vee-type schemes for electromagnetically induced transparency," *Physical Review A* **59**, 4675-4684 (1999).

[2] **J. R. Boon, E. Zekou, D. McGloin and M. H. Dunn**, "Prediction of inversionless gain in a mismatched Doppler-broadened medium," *Physical Review A* **58**, 2560-2566 (1998).

[3] **J. R. Boon, E. Zekou, D. J. Fulton and M. H. Dunn**, "Experimental observation of a coherently induced transparency on a blue probe in a Doppler-broadened mismatched V-type system," *Physical Review A* **57**, 1323-1328 (1998).

[4] **D. McGloin, M. H. Dunn and D. J. Fulton**, "Polarisation Effects in Electromagnetically Induced Transparency," *Physical Review A (In Press)* **62**, (2000).

[5] **M. D. Lukin, S. F. Yelin, M. Fleischhauer and M. O. Scully**, "Quantum interference effects induced by interacting dark resonances," *Physical Review A* **60**, 3225-3228 (1999).

[6] **D. McGloin, D. J. Fulton and M. H. Dunn**, "Electromagnetically Induced Transparency in N-Level Cascade Schemes," **Submitted**, (2000).

[7] **R. R. Moseley, S. Shepherd, D. J. Fulton, B. D. Sinclair and M. H. Dunn**, "Spatial consequences of electromagnetically induced transparency - observation of electromagnetically induced focusing," *Physical Review Letters* **74**, 670-673 (1995).

[8] **L. V. Hau, S. E. Harris, Z. Dutton and C. H. Behroozi**, "Light speed reduction to 17 metres per second in an ultracold atomic gas," *Nature* **397**, 594-598 (1999).

[9] **M. D. Lukin, S. F. Yelin, A. S. Zibrov and M. O. Scully**, "Enhancement of refractive index with quantum coherence: An overview," *Laser Physics* **9**, 759-772 (1999).

[10] **D. McGloin and M. H. Dunn**, "Simple theory of microwave induced transparency in atomic and molecular systems," *Journal of Modern Optics* **47**, 1887-1897 (2000).

[11] **G. A. Turnbull, D. McGloin, I. D. Lindsay, M. Ebrahimzadeh and M. H. Dunn**, "Extended mode-hop-free tuning by use of a dual-cavity, pump-enhanced optical parametric oscillator," *Optics Letters* **25**, 341-343 (2000).

[12] **F. B. deJong**, *Lasing without inversion*, thesis, University of Amsterdam (1998).

[13] **A. M. Akulshin, S. Barreiro and A. Lezama**, "Steep anomalous dispersion in coherently prepared Rb vapor," *Physical Review Letters* **83**, 4277-4280 (1999).

[14] **S. E. Harris and A. V. Sokolov**, "Broadband spectral generation with refractive index control," *Physical Review A* **55**, R4019-R4022 (1997).

[15] **S. E. Harris and A. V. Sokolov**, "Subfemtosecond pulse generation by molecular modulation," *Physical Review Letters* **81**, 2894-2897 (1998).

[16] **A. V. Sokolov, D. D. Yavuz and S. E. Harris**, "Subfemtosecond pulse generation by rotational molecular modulation," *Optics Letters* **24**, 557-559 (1999).

[17] **S. E. Harris and L. V. Hau**, "Nonlinear optics at low light levels," *Physical Review Letters* **82**, 4611-4614 (1999).

[18] **U. Leonhardt and P. Piwnicki**, "Relativistic effects of light in moving media with extremely low group velocity," *Physical Review Letters* **84**, 822-825 (2000).

[19] **U. Leonhardt**, *personal communication* (2000).

[20] **A. V. Turukhin, J. A. Musser, V. S. Sudarshanam, M. S. Shahriar and P. R. Hemmer**, First Observation of Ultraslow Group Velocity of Light in a Solid, quant-ph/0010009

Appendix A

Six Level Cascade Scheme Density Matrix

A.1 Six Level Density Matrix

The six level density matrix used in calculations in chapters 5, 6 and 7 is listed here. By setting the coupling field strengths to zero on unused transitions the matrix can be used for calculations involving systems with less than six levels.

The matrix is rather large and is printed on the next three pages. The convention is as follows:

The matrix row for ρ_{11} is eliminated and hence is not included, so the first matrix row is that for ρ_{22}. The next row is for ρ_{33} and so on until ρ_{66}. The next row after this is for ρ_{12}^{r} and then for ρ_{13}^{r} etc until ρ_{56}^{r} (where j is never less than i, so no elements of the type ρ_{32}^{r} exist) then the rows are for the imaginary parts, e.g. ρ_{12}^{i} ..... ρ_{34}^{i} ..... ρ_{56}^{i}. This complete defines the density matrix. The solution of the matrix can be found by solving the equation:

$$A.x=b \tag{A.1}$$

Where A is the density matrix and b is the solution vector, whose elements are all zero expect the one in the row corresponding to ρ_{12}^{i} whose value is $-\Omega_{12}$.

L :=

$$
\begin{pmatrix}
\Gamma_{21} & -\Gamma_{32} & -\Gamma_{42} & -\Gamma_{52} & -\Gamma_{62} & 0 & 0 & 0 & 0 & \\
0 & \Gamma_{32} & -\Gamma_{43} & -\Gamma_{53} & -\Gamma_{63} & 0 & 0 & 0 & 0 & \\
0 & 0 & \Gamma_{42}+\Gamma_{43} & -\Gamma_{54} & -\Gamma_{64} & 0 & 0 & 0 & 0 & \\
0 & 0 & 0 & \Gamma_{52}+\Gamma_{53}+\Gamma_{54} & -\Gamma_{65} & 0 & 0 & 0 & 0 & \\
0 & 0 & 0 & 0 & \Gamma_{62}+\Gamma_{63}+\Gamma_{64}+\Gamma_{65} & 0 & 0 & 0 & 0 & \\
0 & 0 & 0 & 0 & 0 & \gamma_{12} & 0 & 0 & 0 & \\
0 & 0 & 0 & 0 & 0 & 0 & \gamma_{13} & 0 & 0 & \\
0 & 0 & 0 & 0 & 0 & 0 & 0 & \gamma_{14} & 0 & \\
0 & 0 & 0 & 0 & 0 & 0 & 0 & 0 & \gamma_{15} & \\
0 & 0 & 0 & 0 & 0 & 0 & 0 & 0 & 0 & \\
0 & 0 & 0 & 0 & 0 & 0 & 0 & 0 & 0 & \\
0 & 0 & 0 & 0 & 0 & 0 & 0 & 0 & 0 & \\
0 & 0 & 0 & 0 & 0 & 0 & 0 & 0 & 0 & \\
0 & 0 & 0 & 0 & 0 & 0 & 0 & 0 & 0 & \\
0 & 0 & 0 & 0 & 0 & 0 & 0 & 0 & 0 & \\
0 & 0 & 0 & 0 & 0 & 0 & 0 & 0 & 0 & \\
0 & 0 & 0 & 0 & 0 & 0 & 0 & 0 & 0 & \\
0 & 0 & 0 & 0 & 0 & 0 & 0 & 0 & 0 & \\
0 & 0 & 0 & 0 & 0 & 0 & 0 & 0 & 0 & \\
0 & 0 & 0 & 0 & 0 & 0 & 0 & 0 & 0 & \\
-2\Omega_{12} & -\Omega_{12} & -\Omega_{12} & -\Omega_{12} & -\Omega_{12} & \Delta_{12} & \Omega_{23} & 0 & 0 & \\
0 & 0 & 0 & 0 & 0 & \Omega_{23} & \Delta_{12}+\Delta_{23} & \Omega_{34} & 0 & \\
0 & 0 & 0 & 0 & 0 & 0 & \Omega_{34} & \Delta_{12}+\Delta_{23}+\Delta_{34} & \Omega_{45} & \\
0 & 0 & 0 & 0 & 0 & 0 & 0 & \Omega_{45} & \Delta_{12}+\Delta_{23}+\Delta_{34}+\Delta_{45} & \\
0 & 0 & 0 & 0 & 0 & 0 & 0 & 0 & \Omega_{56} & \Delta_{12}+\Delta_{23}+ \\
\Omega_{23} & -\Omega_{23} & 0 & 0 & 0 & 0 & -\Omega_{12} & 0 & 0 & \\
0 & 0 & 0 & 0 & 0 & 0 & 0 & -\Omega_{12} & 0 & \\
0 & 0 & 0 & 0 & 0 & 0 & 0 & 0 & -\Omega_{12} & \\
0 & 0 & 0 & 0 & 0 & 0 & 0 & 0 & 0 & \\
0 & \Omega_{34} & -\Omega_{34} & 0 & 0 & 0 & 0 & 0 & 0 & \\
0 & 0 & 0 & 0 & 0 & 0 & 0 & 0 & 0 & \\
0 & 0 & 0 & 0 & 0 & 0 & 0 & 0 & 0 & \\
0 & 0 & \Omega_{45} & -\Omega_{45} & 0 & 0 & 0 & 0 & 0 & \\
0 & 0 & 0 & 0 & 0 & 0 & 0 & 0 & 0 & \\
0 & 0 & 0 & \Omega_{56} & -\Omega_{56} & 0 & 0 & 0 & 0 &
\end{pmatrix}
$$

$$
\begin{pmatrix}
0 & 0 & 0 & 0 & 0 & 0 & 0 & 0 & 0 & 0 & 0 & 2\Omega_{12} & 0 & 0 & 0 & 0 & -2\Omega_{23} \\
0 & 0 & 0 & 0 & 0 & 0 & 0 & 0 & 0 & 0 & 0 & 0 & 0 & 0 & 0 & 0 & 2\Omega_{23} \\
0 & 0 & 0 & 0 & 0 & 0 & 0 & 0 & 0 & 0 & 0 & 0 & 0 & 0 & 0 & 0 & 0 \\
0 & 0 & 0 & 0 & 0 & 0 & 0 & 0 & 0 & 0 & 0 & 0 & 0 & 0 & 0 & 0 & 0 \\
0 & 0 & 0 & 0 & 0 & 0 & 0 & 0 & 0 & 0 & 0 & 0 & 0 & 0 & 0 & 0 & 0 \\
0 & 0 & 0 & 0 & 0 & 0 & 0 & 0 & 0 & 0 & 0 & -\Delta_{12} & -\Omega_{23} & 0 & 0 & 0 & 0 \\
0 & 0 & 0 & 0 & 0 & 0 & 0 & 0 & 0 & 0 & 0 & -\Omega_{23} & -(\Delta_{12}+\Delta_{23}) & -\Omega_{34} & 0 & 0 & \Omega_{12} \\
0 & 0 & 0 & 0 & 0 & 0 & 0 & 0 & 0 & 0 & 0 & 0 & -\Omega_{34} & -(\Delta_{12}+\Delta_{23}+\Delta_{34}) & -\Omega_{45} & 0 & 0 \\
0 & 0 & 0 & 0 & 0 & 0 & 0 & 0 & 0 & 0 & 0 & 0 & 0 & -\Omega_{45} & -(\Delta_{12}+\Delta_{23}+\Delta_{34}+\Delta_{45}) & -\Omega_{56} & 0 \\
\gamma_{16} & 0 & 0 & 0 & 0 & 0 & 0 & 0 & 0 & 0 & 0 & 0 & 0 & 0 & -\Omega_{56} & -(\Delta_{12}+\Delta_{23}+\Delta_{34}+\Delta_{45}+\Delta_{56}) & 0 \\
0 & \gamma_{23} & 0 & 0 & 0 & 0 & 0 & 0 & 0 & 0 & 0 & 0 & \Omega_{12} & 0 & 0 & 0 & -\Delta_{23} \\
0 & 0 & \gamma_{24} & 0 & 0 & 0 & 0 & 0 & 0 & 0 & 0 & 0 & 0 & \Omega_{12} & 0 & 0 & -\Omega_{34} \\
0 & 0 & 0 & \gamma_{25} & 0 & 0 & 0 & 0 & 0 & 0 & 0 & 0 & 0 & 0 & \Omega_{12} & 0 & 0 \\
0 & 0 & 0 & 0 & \gamma_{26} & 0 & 0 & 0 & 0 & 0 & 0 & 0 & 0 & 0 & 0 & \Omega_{12} & 0 \\
0 & 0 & 0 & 0 & 0 & \gamma_{34} & 0 & 0 & 0 & 0 & 0 & 0 & 0 & 0 & 0 & 0 & 0 \\
0 & 0 & 0 & 0 & 0 & 0 & \gamma_{35} & 0 & 0 & 0 & 0 & 0 & 0 & 0 & 0 & 0 & 0 \\
0 & 0 & 0 & 0 & 0 & 0 & 0 & \gamma_{36} & 0 & 0 & 0 & 0 & 0 & 0 & 0 & 0 & 0 \\
0 & 0 & 0 & 0 & 0 & 0 & 0 & 0 & \gamma_{45} & 0 & 0 & 0 & 0 & 0 & 0 & 0 & 0 \\
0 & 0 & 0 & 0 & 0 & 0 & 0 & 0 & 0 & \gamma_{46} & 0 & 0 & 0 & 0 & 0 & 0 & 0 \\
0 & 0 & 0 & 0 & 0 & 0 & 0 & 0 & 0 & 0 & \gamma_{56} & 0 & 0 & 0 & 0 & 0 & 0 \\
0 & 0 & 0 & 0 & 0 & 0 & 0 & 0 & 0 & 0 & 0 & \gamma_{12} & 0 & 0 & 0 & 0 & 0 \\
0 & -\Omega_{12} & 0 & 0 & 0 & 0 & 0 & 0 & 0 & 0 & 0 & 0 & \gamma_{13} & 0 & 0 & 0 & 0 \\
0 & 0 & -\Omega_{12} & 0 & 0 & 0 & 0 & 0 & 0 & 0 & 0 & 0 & 0 & \gamma_{14} & 0 & 0 & 0 \\
\Omega_{56} & 0 & 0 & -\Omega_{12} & 0 & 0 & 0 & 0 & 0 & 0 & 0 & 0 & 0 & 0 & \gamma_{15} & 0 & 0 \\
+\Delta_{34}+\Delta_{45}+\Delta_{56} & 0 & 0 & 0 & -\Omega_{12} & 0 & 0 & 0 & 0 & 0 & 0 & 0 & 0 & 0 & 0 & \gamma_{16} & 0 \\
0 & \Delta_{23} & \Omega_{34} & 0 & 0 & 0 & 0 & 0 & 0 & 0 & 0 & 0 & 0 & 0 & 0 & 0 & \gamma_{23} \\
0 & \Omega_{34} & \Delta_{23}+\Delta_{34} & \Omega_{45} & 0 & -\Omega_{23} & 0 & 0 & 0 & 0 & 0 & 0 & 0 & 0 & 0 & 0 & 0 \\
0 & 0 & \Omega_{45} & \Delta_{23}+\Delta_{34}+\Delta_{45} & \Omega_{56} & 0 & -\Omega_{23} & 0 & 0 & 0 & 0 & 0 & 0 & 0 & 0 & 0 & 0 \\
-\Omega_{12} & 0 & 0 & \Omega_{56} & \Delta_{23}+\Delta_{34}+\Delta_{45}+\Delta_{56} & 0 & 0 & -\Omega_{23} & 0 & 0 & 0 & 0 & 0 & 0 & 0 & 0 & 0 \\
0 & 0 & -\Omega_{23} & 0 & 0 & \Delta_{34} & \Omega_{45} & 0 & 0 & 0 & 0 & 0 & 0 & 0 & 0 & 0 & 0 \\
0 & 0 & 0 & -\Omega_{23} & 0 & \Omega_{45} & \Delta_{34}+\Delta_{45} & \Omega_{56} & -\Omega_{34} & 0 & 0 & 0 & 0 & 0 & 0 & 0 & 0 \\
0 & 0 & 0 & 0 & -\Omega_{23} & 0 & \Omega_{56} & \Delta_{34}+\Delta_{45}+\Delta_{56} & 0 & -\Omega_{34} & 0 & 0 & 0 & 0 & 0 & 0 & 0 \\
0 & 0 & 0 & 0 & 0 & 0 & -\Omega_{34} & 0 & \Delta_{45} & \Omega_{56} & 0 & 0 & 0 & 0 & 0 & 0 & 0 \\
0 & 0 & 0 & 0 & 0 & 0 & 0 & -\Omega_{34} & \Omega_{56} & \Delta_{45}+\Delta_{56} & -\Omega_{45} & 0 & 0 & 0 & 0 & 0 & 0 \\
0 & 0 & 0 & 0 & 0 & 0 & 0 & 0 & 0 & -\Omega_{45} & \Delta_{56} & 0 & 0 & 0 & 0 & 0 & 0
\end{pmatrix}
$$

$$
\begin{bmatrix}
0 & 0 & 0 & 0 & 0 & 0 & 0 & 0 & 0 \\
0 & 0 & 0 & -2\Omega_{34} & 0 & 0 & 0 & 0 & 0 \\
0 & 0 & 0 & 2\Omega_{34} & 0 & 0 & -2\Omega_{45} & 0 & 0 \\
0 & 0 & 0 & 0 & 0 & 0 & 2\Omega_{45} & 0 & -2\Omega_{56} \\
0 & 0 & 0 & 0 & 0 & 0 & 0 & 0 & 2\Omega_{56} \\
0 & 0 & 0 & 0 & 0 & 0 & 0 & 0 & 0 \\
0 & 0 & 0 & 0 & 0 & 0 & 0 & 0 & 0 \\
\Omega_{12} & 0 & 0 & 0 & 0 & 0 & 0 & 0 & 0 \\
0 & \Omega_{12} & 0 & 0 & 0 & 0 & 0 & 0 & 0 \\
0 & 0 & \Omega_{12} & 0 & 0 & 0 & 0 & 0 & 0 \\
-\Omega_{34} & 0 & 0 & 0 & 0 & 0 & 0 & 0 & 0 \\
-(\Delta_{23}+\Delta_{34}) & -\Omega_{45} & 0 & \Omega_{23} & 0 & 0 & 0 & 0 & 0 \\
-\Omega_{45} & -(\Delta_{23}+\Delta_{34}+\Delta_{45}) & -\Omega_{56} & 0 & \Omega_{23} & 0 & 0 & 0 & 0 \\
0 & -\Omega_{56} & -(\Delta_{23}+\Delta_{34}+\Delta_{45}+\Delta_{56}) & 0 & 0 & \Omega_{23} & 0 & 0 & 0 \\
\Omega_{23} & 0 & 0 & -\Delta_{34} & -\Omega_{45} & 0 & 0 & 0 & 0 \\
0 & \Omega_{23} & 0 & -\Omega_{45} & -(\Delta_{34}+\Delta_{45}) & -\Omega_{56} & \Omega_{34} & 0 & 0 \\
0 & 0 & \Omega_{23} & 0 & -\Omega_{56} & -(\Delta_{34}+\Delta_{45}+\Delta_{56}) & 0 & \Omega_{34} & 0 \\
0 & 0 & 0 & 0 & \Omega_{34} & 0 & -\Delta_{45} & -\Omega_{56} & 0 \\
0 & 0 & 0 & 0 & 0 & \Omega_{34} & -\Omega_{56} & -(\Delta_{45}+\Delta_{56}) & \Omega_{45} \\
0 & 0 & 0 & 0 & 0 & 0 & 0 & \Omega_{45} & -\Delta_{56} \\
0 & 0 & 0 & 0 & 0 & 0 & 0 & 0 & 0 \\
0 & 0 & 0 & 0 & 0 & 0 & 0 & 0 & 0 \\
0 & 0 & 0 & 0 & 0 & 0 & 0 & 0 & 0 \\
0 & 0 & 0 & 0 & 0 & 0 & 0 & 0 & 0 \\
0 & 0 & 0 & 0 & 0 & 0 & 0 & 0 & 0 \\
0 & 0 & 0 & 0 & 0 & 0 & 0 & 0 & 0 \\
\gamma_{24} & 0 & 0 & 0 & 0 & 0 & 0 & 0 & 0 \\
0 & \gamma_{25} & 0 & 0 & 0 & 0 & 0 & 0 & 0 \\
0 & 0 & \gamma_{26} & 0 & 0 & 0 & 0 & 0 & 0 \\
0 & 0 & 0 & \gamma_{34} & 0 & 0 & 0 & 0 & 0 \\
0 & 0 & 0 & 0 & \gamma_{35} & 0 & 0 & 0 & 0 \\
0 & 0 & 0 & 0 & 0 & \gamma_{36} & 0 & 0 & 0 \\
0 & 0 & 0 & 0 & 0 & 0 & \gamma_{45} & 0 & 0 \\
0 & 0 & 0 & 0 & 0 & 0 & 0 & \gamma_{46} & 0 \\
0 & 0 & 0 & 0 & 0 & 0 & 0 & 0 & \gamma_{56}
\end{bmatrix}
$$

Appendix B

Journal Publications and Conference Proceedings

B.1 Journal Publications

1. *Electromagnetically Induced Transparency in N-Level Cascade Schemes*
   D. McGloin, D.J. Fulton and M.H. Dunn
   (Accepted Opt. Comm)
   See Chapter 6

2. *Polarisation Effects in Electromagnetically Induced Transparency*
   D. McGloin, M.H. Dunn and D.J. Fulton
   (Phys. Rev. A **62** 053802 (2000))
   See Chapter 5

3. *Extended mode-hop-free tuning using a dual-cavity, pump-enhanced optical parametric oscillator*
   G.A. Turnbull, D. McGloin, I.D. Lindsay, M. Ebrahimzadeh and M.H. Dunn
   (Opt. Lett. **25** no.5 341-343 (2000))
   See Chapter 9

4. *Simple Theory of Microwave Induced Transparency in Atomic and Molecular Systems*
   D. McGloin and M.H. Dunn
   (J. Mod. Opt. **47** no.11 1887-1897 (2000))
   See Chapter 8

5. *Comparison of wavelength dependence in Cascade, Lambda and Vee-type schemes for electromagnetically induced transparency*
   J.R.Boon, E.Zekou, D.McGloin and M.H.Dunn
   (Phys. Rev. A **59**, 4675-4684 (1999))
   See Chapter 3

6. *Prediction of inversionless gain in a mismatched Doppler-broadened medium*
   J.R.Boon, E.Zekou, D.McGloin and M.H.Dunn
   (Phys. Rev. A **58**, 2560-2566 (1998)
   See Chapter 3

B.2 Conference Presentations

CLEO/Europe-IQEC 2000, Nice, France

1. Radio Frequency Field Manipulation of Electromagnetically Induced Transparency
   D. McGloin, G.A.Turnbull and M.H. Dunn
   (IQEC 2000)
   See Chapter 7

2. Methods for extending mode-hop-free tuning using a dual-cavity, pump-enhanced optical parametric oscillator
   D. McGloin, G.A.Turnbull, I.D. Lindsay, M.Ebrahimzadeh and M.H. Dunn
   (CLEO/Europe 2000)
   See Chapter 9

CLEO/QELS 2000, San Francisco, USA

3. Extended mode-hop-free tuning using a dual-cavity, pump-enhanced optical parametric oscillator
G.A. Turnbull, D. McGloin, I.D. Lindsay, M.Ebrahimzadeh and M.H. Dunn
(CLEO 2000)
See Chapter 9

4. Electromagnetically Induced Focussing Effects in Four Level Media
D. McGloin, G.A. Turnbull and M.H. Dunn
(QELS 2000)
See Chapter 6

QEP14, 1999, Manchester, UK

5. A Widely Tuneable, Split Cavity, Pump-Enhanced Optical Parametric Oscillator
G.A. Turnbull, D. McGloin, I.D. Linsay, M. Ebrahimzadeh and M.H. Dunn
(Quantum Electronics and Photonics 14)
See Chapter 9

6. Laser linewidth effects in a 3-level V-scheme for amplification without inversion and electromagnetically induced transparency
D. McGloin and M.H. Dunn
(Quantum Electronics and Photonics 14)
See Chapter 4

7. Practical aspects of microwave induced transparency in atomic and molecular systems
D. McGloin and M.H. Dunn
(Quantum Electronics and Photonics 14)
See Chapter 8

IQEC 1998, San Francisco, USA

8. A study of inversionless gain in mismatched, Doppler broadened systems
J.Boon, E.Zekou, D.McGloin and M.H.Dunn
(Paper QWK6, IQEC '98 San Francisco, Technical Digest p143)
See Chapter 3

B.3 Unrefereed Papers

9. Progress in Electromagnetically Induced Transparency and Inversionless gain in Doppler-Broadened Mismatched Systems
D. McGloin, J.R. Boon, E. Zekou and M.H. Dunn
(LEOS Meeting, St. Andrews, November 1998)

10. Progress in Electromagnetically Induced Transparency and Inversionless gain in Doppler-Broadened Mismatched Systems
D. McGloin, J.R. Boon, E. Zekou and M.H. Dunn
(Scottish Universities Summer School in Physics 52 : Advances and Applications in Lasers, St. Andrews 1998)